IMPROVED ZEOLITE BUILDERS FOR DETERGENTS

A Thesis
submitted for the degree of
Doctor of Philosophy of the
University of London

by

Vincent Charles Mole

August 1989

The Physical Chemistry Laboratories,
Department of Chemistry,
Imperial College of Science and Technology,
London.
SW7 2AY.

Dedicated, with much appreciation, to my parents

Acknowledgments

I would like to sincerely thank the following people without whom this thesis would not have been possible and to whom I am deeply indebted.

Professor L. V. C. Rees for his supervision and constant support, help, encouragement and advice throughout my studies.

The Wolfson Foundation, who funded the first year of my research.

Procter and Gamble and the S.E.R.C. who funded the remaining two years.

My parents for their support and for providing additional funding when necessary.

Dr. N. Kermode at the Procter and Gamble Newcastle Technical Centre for his supervision, help and advice.

The staff of the Newcastle Technical Centre for their help, especially Gordon Peters, Joan Muir, Christine Addison, Barry Stoddart, Brian Jeffreys and Bev, Jack and Jim in Lab 13W.

Dr. I. S. Kerr at Imperial College for his help with the X-Ray analysis.

Mike Haddon at Imperial College for his help and advice on atomic absorption analysis.

Chris Groombridge and David Butler at Royal Holloway and Bedford New College for their help with the solid state NMR.

Ian Drummond at Imperial College for his help with the particle size analysis.

Jeff Tucker and John Hooper at Imperial College for their help.

Professor R. P. Townsend for his helpful discussions on the theory of ion exchange.

Peter Graham for proof reading this tome.

Past and present members of the "Coffee Club" for their constant help, support advice and friendship, especially (and in no particular order), Edward Lee, Dave Kier, Peter Graham, Adrian Hughes, Andy Franks, Brian Bennett, Colin Butler, Robin Richards, Prem Sagoo, Judith Taylor, Eric Coker, Andy McAleer, Lesley Belcher, Neil Van den Begin, Oscar Soonieus and Efi Dima.

The members of the British Zeolite Association for providing four interesting and enjoyable conferences.

All my friends and colleagues in London for their support, help and friendship, especially (again in no particular order), Andy Dengel, Andy White, Angie Morris, Sandy Monaghan, Jim Mulligan, Bryan Driscoll, Katy Brown, Lyndon While, Andy Marks, Julia Dines, Paul Savage, Ged O'Shea, Debbie Dobson, Luiza Antonioni and Tom Wright.

Finally, I am deeply indebted to Dr. C. J. Adams at Unilever Research (Port Sunlight) for providing me with the impetus to get off my backside and complete this thesis. I must also thank all my friends and colleagues at Port Sunlight for their support and encouragement.

Contents

List of Figures

Chapter Four - The Ion Exchange Characteristics of Aluminosilicate Gels

Chapter Five - Aluminosilicate Gels as Detergent Builders

List of Tables

Chapter Five - Aluminosilicate Gels as Detergent Builders

Symbols and Abbreviations

The following symbols and abbreviations have been used in the text that follows:

a_i	the activity of ion or component i in the solution phase
$\overline{a}_i$	the activity of ion or component i in the zeolite phase
AFS	Air Filter Soil
$Ca_{(s)}$	the cation equivalent fraction of calcium in the solution phase
$Ca_{(z)}$	the cation equivalent fraction of calcium in the zeolite phase
CPM	Counts Per Minute (radioactivity)
DMO	Dirty Motor Oil
D4R	Double 4 Ring
D6R	Double 6 Ring
E_i	the cation equivalent fraction of ion i in the solution phase
$\overline{E}_i$	the cation equivalent fraction of ion i in the zeolite phase
EDTA	Ethylene DiamineTetra-Acetic acid
ETC	European Technical Centre
f_i	the activity coefficient of ion i in the zeolite phase
g_i	the Gaines and Thomas zeolite phase activity coefficient for ion i
GPR	General Purpose Reagent (BDH)
h_i	the Hogfeldt activity coefficient for ion i in the zeolite phase
I	the ionic strength
IEC	Ion Exchange Capacity
IR	Infra Red

K_a	the thermodynamic equilibrium constant for ion exchange
K_c	the corrected selectivity coefficient (Kielland coefficient) for ion exchange
K_g	the corrected selectivity coefficient (Gaines and Thomas)
K_m	the mass action quotient for ion exchange
K_v	the corrected selectivity coefficient (Bonner et al)
m_s^i	the molality of ion i in the solution phase
M_s^i	the molarity of ion i in the solution phase
MAS-NMR	Magic Angle Spinning Nuclear Magnetic Resonance
$Mg_{(s)}$	the cation equivalent fraction of magnesium in the solution phase
$Mg_{(z)}$	the cation equivalent fraction of magnesium in the zeolite phase
N	solution normality
n_i	the number of moles of ion or component i
NTA	Nitrilo Tri-Acetic acid
NTC	Newcastle Technical Centre
PAA	PolyAcrylic Acid
R	the gas constant (8.31441 J K^{-1} Mol^{-1})
SBU	Secondary Building Unit
SEM	Scanning Electron Microscopy
STPP	Sodium Tri-PolyPhosphate
S4R	Single 4 Ring
S6R	Single 6 Ring
S8R	Single 8 Ring
T	the absolute temperature (K)
T	also used to denote a tetrahedral silicon or aluminium atom, as in TO_4 or T-O
TAED	Tetra Acetyl Ethylene Diamine (a bleach precursor widely used in detergent formulations)

$\overline{X}_i$	the cation mole fraction of ion i (Bonner et al) in the zeolite phase
$\overline{X}_i'$	the mole fraction of ion i (Hogfeldt) in the zeolite phase
XRD	X-Ray Diffraction
z_i	the charge on ion i
ΔG^θ	the standard Gibbs free energy change for a reaction
γ_i	the mean ionic activity coefficient for ion i
$\gamma_{\pm AY}$	the mean activity coefficient for the electrolyte $A_{z_y}Y_{z_a}$
μ_i	the chemical potential of cation i in the solution phase
$\overline{\mu}_i$	the chemical potential of cation i in the zeolite phase
μ_i^θ	the standard chemical potential of cation i in the solution phase
$\overline{\mu}_i^\theta$	the standard chemical potential of cation i in the zeolite phase

Summary

Modern detergent formulations usually contain a detergent builder, the function of which is to remove calcium and magnesium ions from the wash solution. These ions, and other polyvalent cations, are commonly present in household water supplies and may cause a reduction in detergent performance.

Until recently, sodium tripolyphosphate (STPP) has been the most widely used detergent builder. However, the presence of phosphates in domestic, industrial and agricultural wastes gives rise to the eutrophication (choking by plant and algal life) of slow moving and still inland waterways. As a result, the use of phosphates in detergents is strictly controlled or even banned in many parts of the world.

The detergent industry has, therefore, had to develop alternative detergent builders. The most successful of these have been the zeolites, particularly zeolite A. Zeolite X has also been proposed as a detergent builder, but has not yet achieved large scale success.

The zeolites are, at present, the best alternative to the phosphate builders, but their performance does not match that of STPP. In particular, their magnesium binding characteristics are poor. In the time scale of a wash cycle, zeolite A, for instance, removes little or none of the magnesium initially present. This is due to the large hydration sphere of magnesium ions in aqueous solution. Hydrated magnesium ions must lose much of their water before they are able to enter the channel system of a zeolite and, as a result the kinetics of the ion exchange reaction are slow.

Amorphous aluminosilicate gels have also been proposed as detergent builders. Although these materials have a lower ion exchange capacity than the zeolites, they have more open framework structures which should allow hydrated magnesium ions to enter more easily. This thesis examines the use of aluminosilicate gels as detergent builders.

Amorphous aluminosilicate gels have been obtained from the synthesis of zeolite A and the synthesis of zeolite X. These have been characterised by a variety of techniques. Their ion exchange properties have been determined and

compared to those of the crystalline zeolites A and X. Finally, these materials have been tested as detergent builders in detergent formulations and their performance compared with that of zeolites A and X and STPP.

Chapter One

Introduction

1.1 Zeolites

Zeolites are hydrated aluminosilicates containing cations of group I or group II metals, particularly sodium, potassium, calcium, magnesium, strontium and barium. The term "zeolite" means "boiling stone" and refers to the frothy mass which can result when a zeolite is fused in a blowpipe.

Zeolites are framework aluminosilicates formed from SiO_4^{4-} and AlO_4^{5-} tetrahedra (the primary building units) which are joined by the sharing of all oxygens. The framework encloses a system of regular channels and cavities which usually contain water and cations. Zeolites may be regarded as defect forms of silica, $(SiO_2)_n$, in which silicon atoms are replaced by aluminium atoms. Each substitution of aluminium for silicon introduces a net negative charge onto the framework. This charge is counterbalanced by the presence of an equivalent number of cations within the channels and cavities of the zeolite. Since the Si-O and Al-O bond lengths are very similar (0.163nm and 0.173nm respectively), there is very little internal strain within the zeolite framework.

Zeolites may be represented by the following empirical formula:

$$M_pD_q.Al_{(p+2q)}.Si_r.O_{(2p+4q+2r)}.sH_2O$$

where M and D represent monovalent and divalent cations respectively. Since these ions counterbalance the charge due to the presence of aluminium in the framework, the aluminium content is given by (p+2q).

The structural formula of a zeolite is usually written in terms of the crystallographic unit cell:

$$M_pD_q[(AlO_2)_{(p+2q)}(SiO_2)_r].sH_2O$$

the portion within the square brackets represents the framework contents of a unit cell. Lowenstein's rule[1] forbids the sharing of a single oxygen atom by

more than one aluminium and, hence, the minimum theoretical silicon to aluminium ratio is unity. This requires that r must always be equal to or greater than (p+2q). It has been reported[2] that molecules of $NaAlO_2$ can be occluded, giving rise to compositional anomalies. These occluded molecules are not, however part of the framework structure. The complete sharing of all the oxygens requires that the number of framework oxygens per unit cell is given by (2p+4q+2r).

Smith[3] proposed a definition for a zeolite as "an aluminosilicate with a framework structure enclosing cavities occupied by large cations and water molecules, both of which have considerable freedom of movement, permitting ion exchange and reversible dehydration". It would probably be more correct to add that they are tectosilicates, that is that the (Si+Al):O ratio is 1:2, since materials which exhibit the characteristic properties of zeolites may not have the framework structure.

There are two other common aluminosilicate materials. These are the feldspars and feldspathoids. Feldspars have compact frameworks consisting of crosslinked "double crankshaft" chains of $(Si,Al)O_4$ tetrahedra. They do not exhibit ion exchange properties. Zeolites and feldspathoids have more open structures. The cavities of feldspathoids may contain cations and, in some cases, anions. Some synthetic varieties also contain water and such materials may fall within the definition of zeolites since they may exhibit ion exchange properties and show limited adsorption/desorption of water vapour.

Thirty-seven types of natural zeolite have been found, the first being Stilbite, discovered by the Swedish mineralogist Cronstedt[4] in 1756. There are also about 100 types of synthetic zeolite[5-7]. Some synthetic zeolites have no natural counterparts. Zeolites X and Y, for example have the same framework topology as natural Faujasite, but zeolites A, L, Losod and Rho have no natural analogues. Many zeolites, both natural and synthetic, have little practical significance, but the remainder are used in a wide variety of applications (section 1.5).

1.2 Zeolite Synthesis

Early attempts to synthesise zeolites were made by mineralogists and geologists keen to learn more about the natural formation of these minerals.

Geological evidence suggests that natural zeolite formation includes the following genetic types:

1. Crystals resulting from hydrothermal or hot spring activity involving reactions between solutions and basaltic lava flows.

2. Deposits formed from volcanic sediments in closed alkaline and saline lake systems.

3. Similar formations from open freshwater lake or groundwater systems acting on volcanic sediments.

4. Deposits formed from volcanic materials in alkaline soils.

5. Deposits resulting from hydrothermal or low temperature alteration of marine sediments.

6. Formations resulting from low-grade burial metamorphism.

Attempts to synthesise zeolites under hydrothermal conditions began with the synthesis of quartz, reported by Schaufhautle in 1845. In 1862, St. Clair Deville reported the synthesis of Levynite by heating aqueous solutions of potassium silicate in glass tubes at 170°C[8], and the synthesis of Analcime was reported by de Schulten in 1882[9]. These early experiments were based upon then current ideas of the natural formation of zeolites from basaltic rocks. Consequently, they were usually carried out at temperatures in excess of 200°C and at elevated pressures. It was not until the late 1940's and early 1950's that Barrer[10,11] and later Milton and his colleagues at Union Carbide[12,13] reported a new method of zeolite synthesis in which reactive starting materials were used at low temperatures. This new approach to zeolite synthesis was consistent with the formation of natural zeolites in marine sediments on ocean floors.

Zeolites are synthesised under hydrothermal conditions, that is in reactant systems containing substantial quantities of water. In laboratory syntheses, an alumina source, a silica source and a base are mixed, generally producing an amorphous aluminosilicate gel from which the zeolite crystallises. A considerable variety of sources of alumina, silica and base have been used[14].

Different reactions may result if any of these are varied because, in many reactions, nucleation is governed by kinetic rather than thermodynamic considerations[15].

Zeolite synthesis is an extremely complex process involving polymerisation-depolymerisation reactions, solution-precipitation reactions nucleation-crystallisation reactions and other complex phenomena encountered in aqueous colloidal dispersions[16]. The type of zeolite that crystallises depends not only on the usual thermodynamic variables of reactant composition, temperature and pressure, but also on a number of other factors which include[17]:

1. The role of OH^- as a mineralising catalyst.

2. The structure directing effects of cations.

3. The use of organic bases.

4. Structure directing effects of anions other than OH^-.

5. The role of added salts.

6. History dependent effects such as:

   a) The ripening period of the reaction mixture.

   b) Agitation of the reaction mixture during zeolite crystallisation.

   c) The physical and chemical nature of the reactants.

   d) The order in which reactants are mixed.

It is not, therefore, surprising that mixtures of several zeolite phases often result.

In alkaline sodium aluminate solutions, $Al(OH)_4^-$ is the important anion, although other anionic species exist[18,19]. The evidence suggests that polymeric or colloidal oxyaluminium anions do not exist. In alkaline silicate solutions, however, polymeric anions are common[20,21]. The degree of this polymerisation

depends on the concentrations of silicate and free alkali. Mononuclear species such as $Si(OH)_4$, $SiO(OH)_3^-$ and $SiO_2(OH)_2^{2-}$ have also been found to exist, especially in dilute solutions. It is worth noting that, in alkaline solutions, both aluminium and silicon exist in four fold co-ordination with respect to oxygen and that this co-ordination is preserved in the tectosilicates which only crystallise under alkaline conditions.

When alkaline silicate and aluminate solutions are mixed a gel phase usually precipitates because of the strong interactions between silicate and aluminate. This gel phase preferentially incorporates alumina so that the SiO_2/Al_2O_3 ratio is higher in the solution phase. The precipitation of this gel and its subsequent conversion to a crystalline zeolite is an example of Ostwald's rule of successive transformations. The gel is the first product of the interaction between silicate and aluminate. It is metastable and as the reaction proceeds is consumed by dissolution and precipitation as a zeolite or other crystalline phase. According to Ostwald's rule, the first formed phase is always thermodynamically less stable than that which subsequently replaces it. Thus, a sequence of growth and replacement reactions can occur, always in the direction of increasing thermodynamic stability. It is, therefore possible that the first formed crystals may themselves be replaced by a more stable product which may, in turn, also be replaced.

The detailed mechanism of zeolite crystallisation is not well understood. Formation of the amorphous aluminosilicate gel is followed by an induction period during which nucleation takes place. The length of this induction period depends on temperature, gel composition and the origin of the reactants. This is followed by a period of rapid crystal growth which ends when the nutrients begin to become exhausted and crystal growth becomes difficult to maintain. If the reaction is allowed to continue, dissolution of the first formed zeolite phase (or phases) may occur, accompanied by the appearance of a new crystalline phase (Figure 1.1).

The crystallisation of zeolites from reactive gels requires that the disordered gel phase is converted to a more ordered, but metastable, zeolite phase. A single mechanism for this process is not known, but both solid and liquid phase crystallisation mechanisms have been proposed. Zhadanov[23] suggested a quasi-equilibrium between solid and liquid phases in which nucleation and crystal growth occur in the liquid phase. The solid gel phase acts as a nutrient

by continuous dissolution, dissolved species being transported to the crystal nuclei in the solution. This mechanism is consistent with the homogeneous crystallisation mechanism originally proposed by Kerr[24] and later supported by Ciric[25].

Figure 1.1. Zeolite Crystallisation as a Function of Time

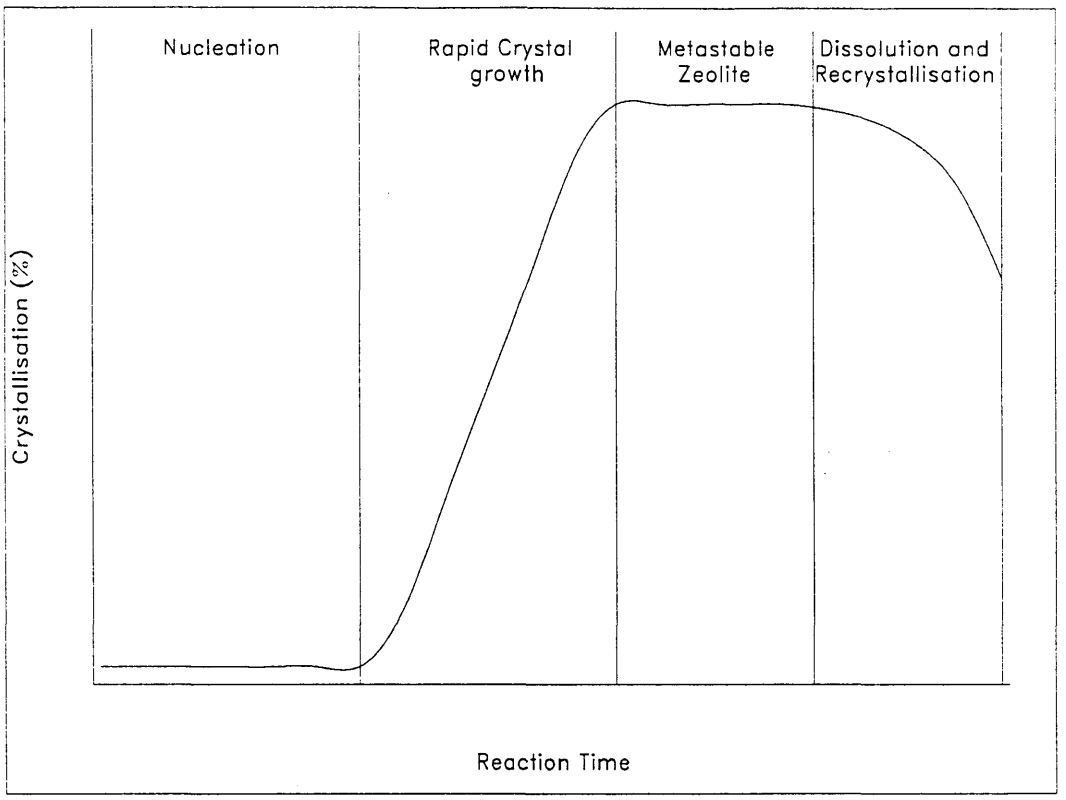

The gel structure is produced by the polymerisation of aluminate and polysilicate anions. It is amorphous and of high simplexity according to the simplexity principle proposed by Goldsmith[26]. Simplexity is defined as disorder, structural simplicity or high entropy and the ease of crystallisation is related to the structural simplexity. The aluminosilicate gel is of higher simplexity and higher entropy than its crystalline product. The growth of zeolite crystals requires the formation of a nucleus and this principle favours the formation of a nucleus of high simplexity, for instance the nucleus of a metastable zeolite phase. The composition and structure of the gel phase is governed by the size and structure of the polymerising species and, therefore, gelation controls nucleation. The size and charge of hydrated cationic species in solution may also affect the nucleation process. Cations are known to have an effect on silicate and, probably aluminate, species in solution[27]. Figure 1.2 shows a

schematic version of this proposed mechanism for zeolite crystallisation[28]. Hydroxyl ions (OH^-) depolymerise the gel structure producing soluble aluminosilicate species. The hydrated cation then acts as a template for the formation of nuclei with the ordered structure of a zeolite. Sodium, for example, which co-ordinates to more water molecules in aqueous solution and hence has a greater effective radius than potassium, produces zeolites with more open structures.

Figure 1.2. A Proposed Mechanism for Zeolite Crystallisation

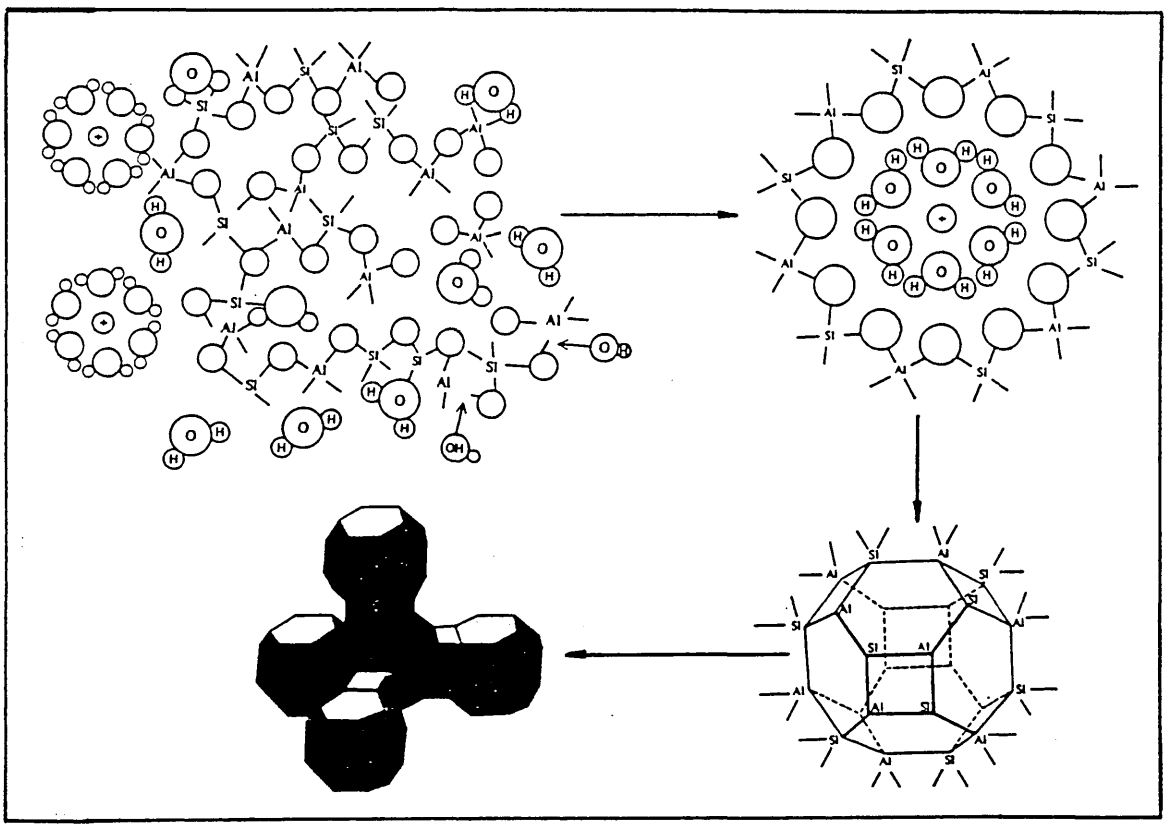

A mechanism involving crystallisation in the solid phase through a re-ordering of the aluminosilicate framework has also been proposed. Khatami and Flanigen[29] observed crystallisation of zeolite X in the absence of any liquid phase. Flanigen[16] proposed a mechanism involving a re-ordering of the hydrogel to a crystalline phase by surface diffusion in the absence of liquid phase transport. Phosphorescence and Raman spectroscopy have been used to study the growth of zeolites from gels, but the results have been conflicting. McNicol et al[30,31] observed no changes in the liquid phase and proposed a solid phase mechanism involving condensation of hydroxylated Si-Al tetrahedra. Guth et

al[32,33] and Angell and Flank[34] found evidence to suggest the presence of soluble aluminosilicate species and ^{29}Si NMR data appears to support this finding[35-37].

Most workers tend to support the solution transport mechanism, although Zhadanov[23] noted the many common elements of both approaches. Derouane et al[38,39] concluded that both mechanisms are important depending on the silica source and the gel composition. It has been suggested that a further understanding of zeolite crystallisation may be obtained by treating such systems as unstable aqueous colloidal dispersions, where the importance of the solid-liquid interface and the diffusional layer are well recognised.

1.3 The Synthesis of Zeolites A and X

Zeolites A and X both crystallise from the four component system Na_2O-SiO_2-Al_2O_3-H_2O. Typically, aqueous solutions of sodium aluminate, sodium silicate and sodium hydroxide are used to prepare the gel. By this relatively simple method, six synthetic zeolites (A, P, R, S, X and Y) have been crystallised. Reaction mixtures using colloidal silica sol or amorphous silica may allow the synthesis of additional zeolites. In addition, the feldspathoids Hydroxycancrinite and Basic or Hydroxy- Sodalite may also crystallise from this system. The relationship between starting gel composition and the synthetic product is illustrated by reaction diagrams of the type shown in Figures 1.3 and 1.4. In Figure 1.3, anhydrous gel compositions are plotted on a mole percent basis using triangular co-ordinates. Rectangular co-ordinates may also be used as illustrated by Figure 1.4, taking the molar ratios Na_2O/SiO_2, SiO_2/Al_2O_3 or H_2O/Na_2O as co-ordinates.

In the synthesis of zeolite A, typical reaction compositions produce a product with an SiO_2/Al_2O_3 molar ratio of 2. High silica forms have been prepared, either by using gels of high silica and sodium hydroxide content or by partial replacement of the alkali metal with the organic Tetra-Methyl Ammonium (TMA) cation. Zeolite A has been synthesised at a variety of temperatures in the range 25 to 150°C and with reaction times between 14 days and 2.5 hours. Zeolite A is a metastable phase and, if left in contact with the mother liquor ($\approx$ 1M NaOH) after crystallisation, conversion to zeolite P occurs. However, if the mother liquor contains a large excess of sodium hydroxide, zeolite A is converted to the feldspathoid Hydroxysodalite.

Figure 1.3. Reaction Composition Diagrams for the system Na_2O-SiO_2-Al_2O_3-H_2O

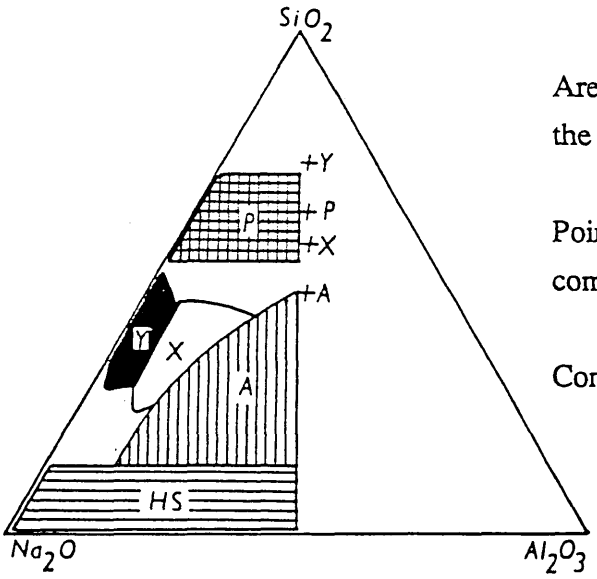

Areas indicate compositions yielding the designated zeolite.

Points (marked +) indicate typical zeolite compositions

Conditions: 100°C
Sodium silicate as SiO_2 source
H_2O 90 - 98 mole %

Figure 1.4. Typical Gel Compositions for Zeolite Synthesis in the System Na_2O-SiO_2-Al_2O_3-H_2O

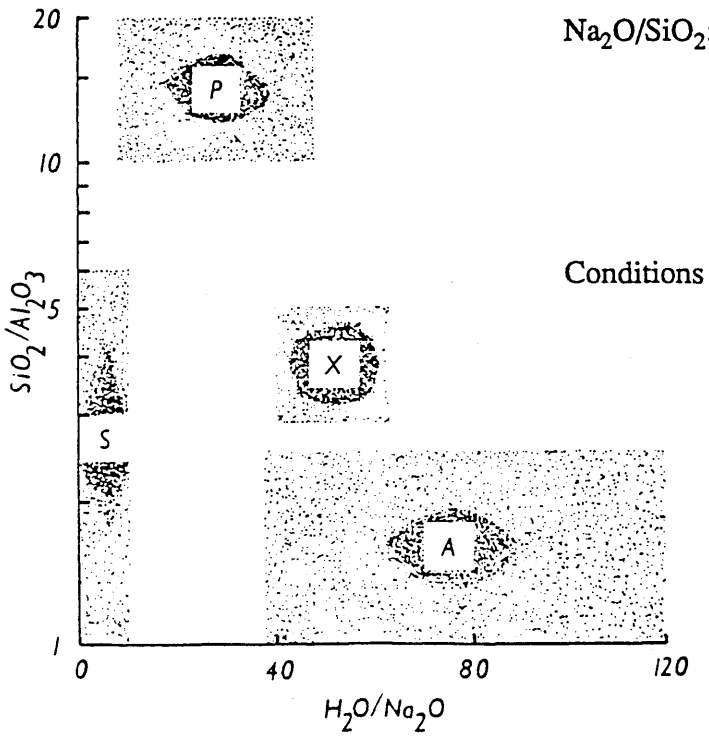

Na_2O/SiO_2: 0.38 - 0.61 for zeolite P
1.20 - 1.50 for zeolite X
0.80 - 3.00 for zeolite A

Conditions as Figure 1.3.

Zeolite X has been synthesised at temperatures between 25 and 120°C, with a wide range of reaction times. Like zeolite A, zeolite X appears to be metastable with respect to zeolite P. Typically, zeolite X crystallises with an SiO_2/Al_2O_3 ratio between 2 and 3, although the low silica forms have proved troublesome to synthesise because of the co-crystallisation of zeolite A. Tatic and Drzaj[40] recently reported the synthesis of zeolite X with an SiO_2/Al_2O_3 ratio between 2.04 and 2.12. Their investigations included a study of the effect of variations in the reaction ratios on the crystalline product. An increase in the SiO_2/Al_2O_3 ratio favoured the crystallisation of zeolite X over zeolite A, as did an increase in the H_2O/Na_2O ratio. Increasing Na_2O/SiO_2 ratios, however, gave traces of zeolite A in the final product. The boundary conditions for the formation of zeolite X were found to be SiO_2/Al_2O_3 above 2.5, Na_2O/SiO_2 above 1.8 and H_2O/Na_2O above 70. The effect of temperature was also studied. The temperature at which a zeolite crystallises depends on the framework density, more porous zeolites crystallising at lower temperatures. Pure zeolite X crystallised below 70°C. Zeolite A co-crystallised at higher temperatures.

1.4 Zeolite Structures

The fundamental building units from which zeolites are constructed are the $(Si,Al)O_4$ tetrahedra which, when linked in three dimensions by the common sharing of all oxygens, produce the frameworks characteristic of zeolites. Silica, $(SiO_2)_n$, exists in 17 different crystalline forms and the substitution of Al^{3+} for silicon produces a framework of the composition $[(Al_xSi_{1-x})O_2]^{x-}$. The ions P^{5+}, Ga^{3+} and Ge^{4+} can also exist in four fold co-ordination and may indeed be substituted into zeolite type structures. Over 35 zeolite framework structures are known to exist and an almost infinite number are possible because of the variety of ways in which tetrahedra can link (by the common sharing of oxygen) to form polynuclear complexes.

Zeolites can be classified into groups according to common features of their aluminosilicate framework structures. Classification schemes have been proposed by Smith[3], Fischer and Meier[41,42] and Breck[43]. Zeolite structures can be described in terms of the secondary building units (SBUs), which are structural subunits consisting of specific arrays of tetrahedra. The Si-Al distribution is neglected. There are 8 SBUs (Figure 1.5), although an additional one, the 5-Ring, should also be included. It has been suggested that, during

synthesis, the SBUs are formed first, then assembled into crystalline zeolites. This, however, seems unnecessarily complex and unlikely. An alternative method for describing zeolite structures is in terms of polyhedral units (Figure 1.6). Zeolite structures may also be described in terms of sheets or chains of tetrahedra.

Figure 1.5 The Secondary Building Units of Zeolite Structures

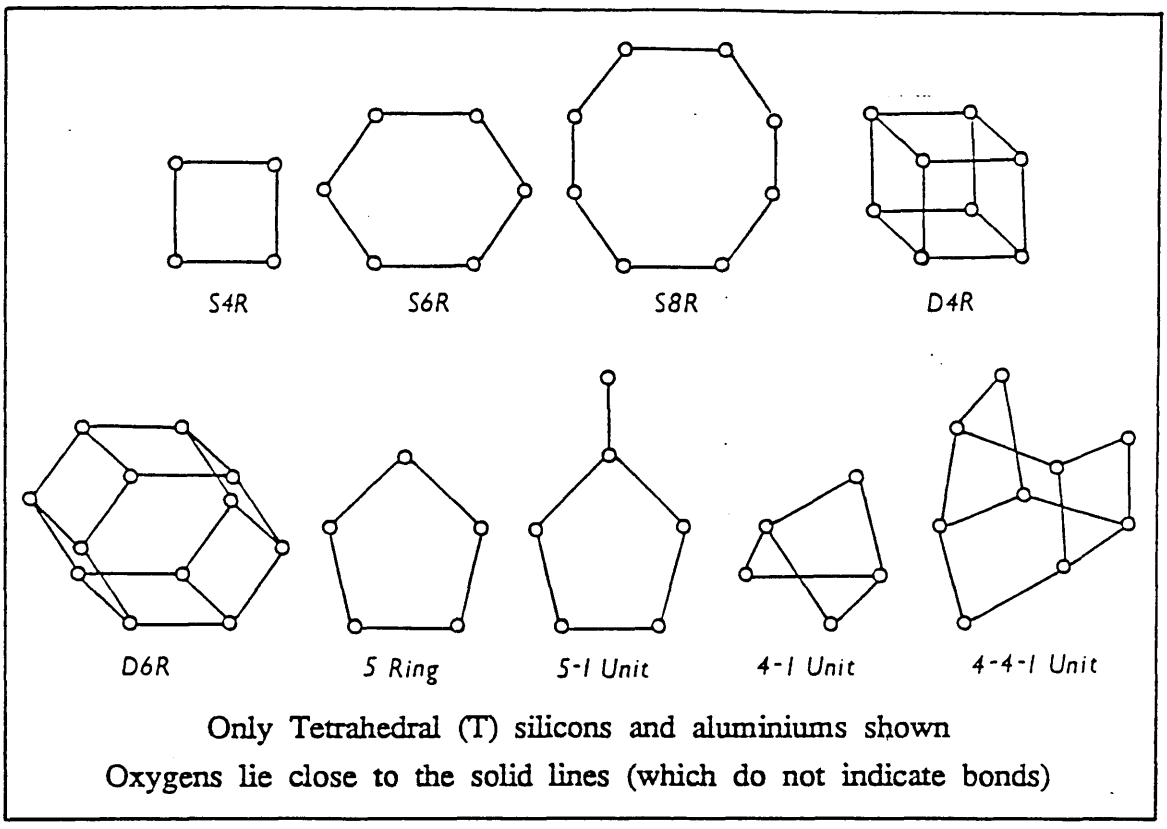

Only Tetrahedral (T) silicons and aluminiums shown
Oxygens lie close to the solid lines (which do not indicate bonds)

The structure of zeolite A (Figure 1.7) can be described in terms of D4R units and truncated octahedra (β-cages) which contain 24 tetrahedra. D4R units placed at the centre of each edge of a cube of side 12.3Å generate a truncated octahedron at each corner. Each of these octahedra enclose a cavity, the β-cage, of free diameter 6.6Å. At the centre of the cube there is a truncated cuboctahedron, the α-cage, of free diameter 11.4Å. The rigorous alteration of aluminium and silicon required by Lowenstein's rule, produces a crystallographic unit cell of 24.6Å containing 192 tetrahedra. It is, however, often more convenient to use the pseudo-cell of 12.3Å which contains 12 tetrahedra, 27 water molecules and 12 sodium ions. In hydrated zeolite A, eight of these sodium ions are located near the centre of the 6-Rings, displaced slightly inside the α-cages[44]. This position is known as site I. The remaining sodium ions are associated with water molecules in the 8-Rings (site II).

Figure 1.6. The Polyhedral Complexes of Zeolite Structures

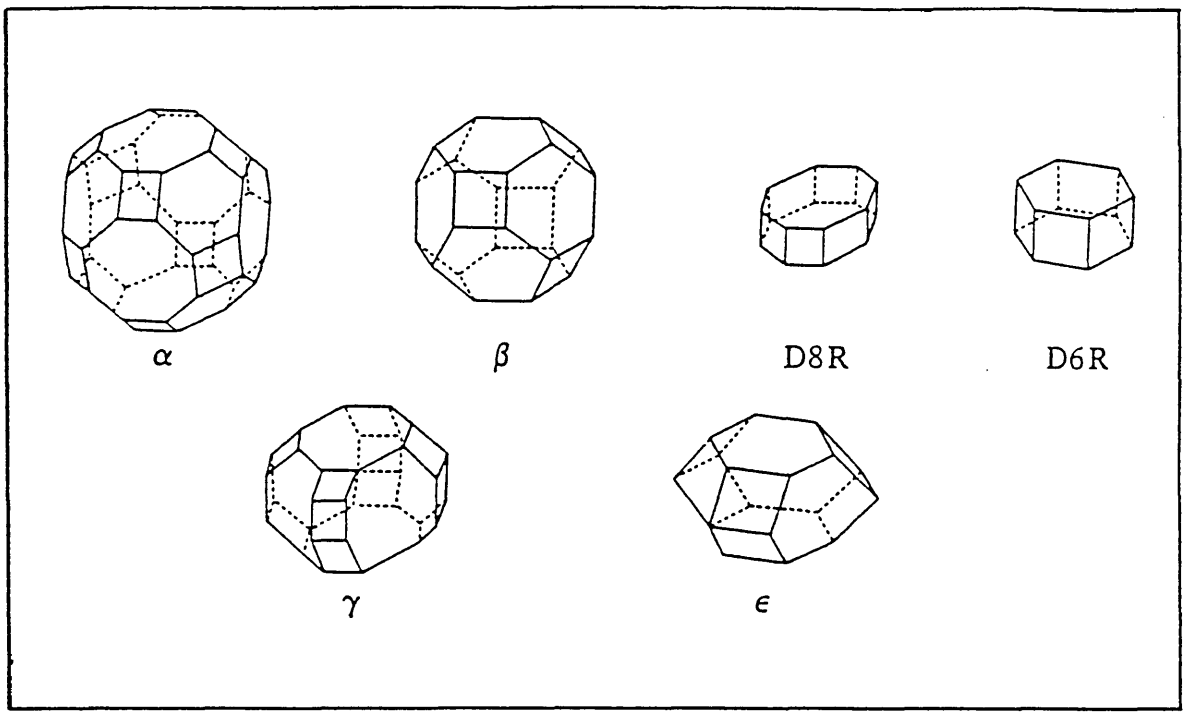

Figure 1.7. The Structure of Zeolite A

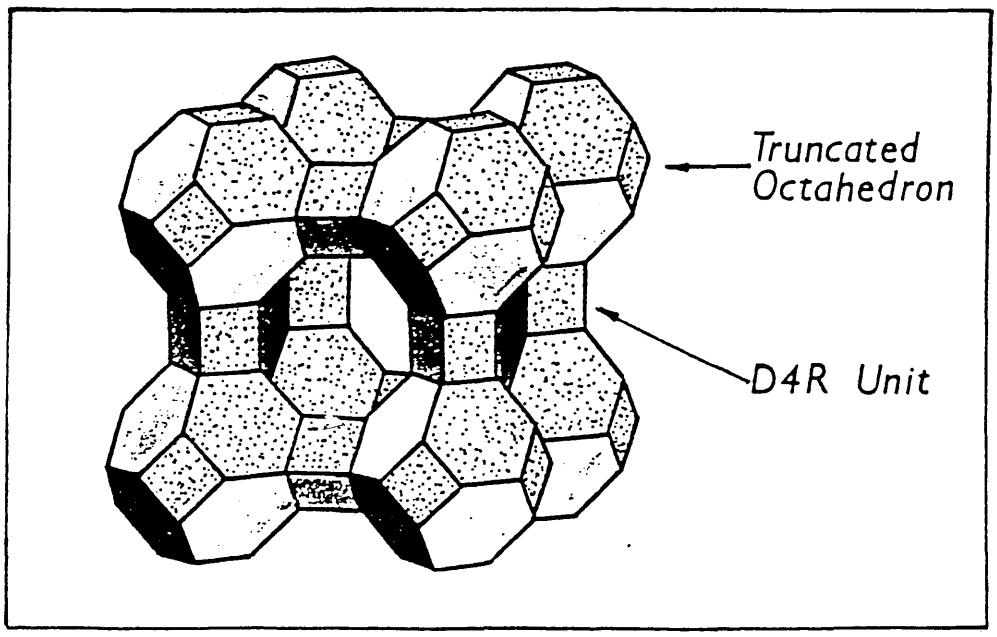

In dehydrated zeolite A, eight sodium ions (Na_I) are displaced 0.4Å into the α-cage from the centre of the 6-Rings[45,46]. Three sodium ions (Na_{II}) are located in the 8-Rings, about 1.2Å from the centre[46]. The remaining sodium ion (Na_{III}) has been located opposite the 4-Ring.

Zeolite X is topologically similar to the natural zeolite Faujasite, but is a distinct zeolite species with its own characteristic properties. The crystallographic unit cell is cubic with a large cell dimension of nearly 25Å. Each unit cell contains 192 tetrahedra. The framework is remarkably stable and rigid and contains the largest void space of any known zeolite. In dehydrated zeolite X this void volume comprises nearly 50% of the total crystal volume. The aluminosilicate framework is a diamond like array of truncated octahedra linked tetrahedrally via the 6-Rings (Figure 1.8). The linkage between adjacent octahedra is the Double 6-Ring (D6R) or hexagonal prism. The framework structure can also be described in terms of hexagonal prisms.

Figure 1.8. The Structure of Zeolite X

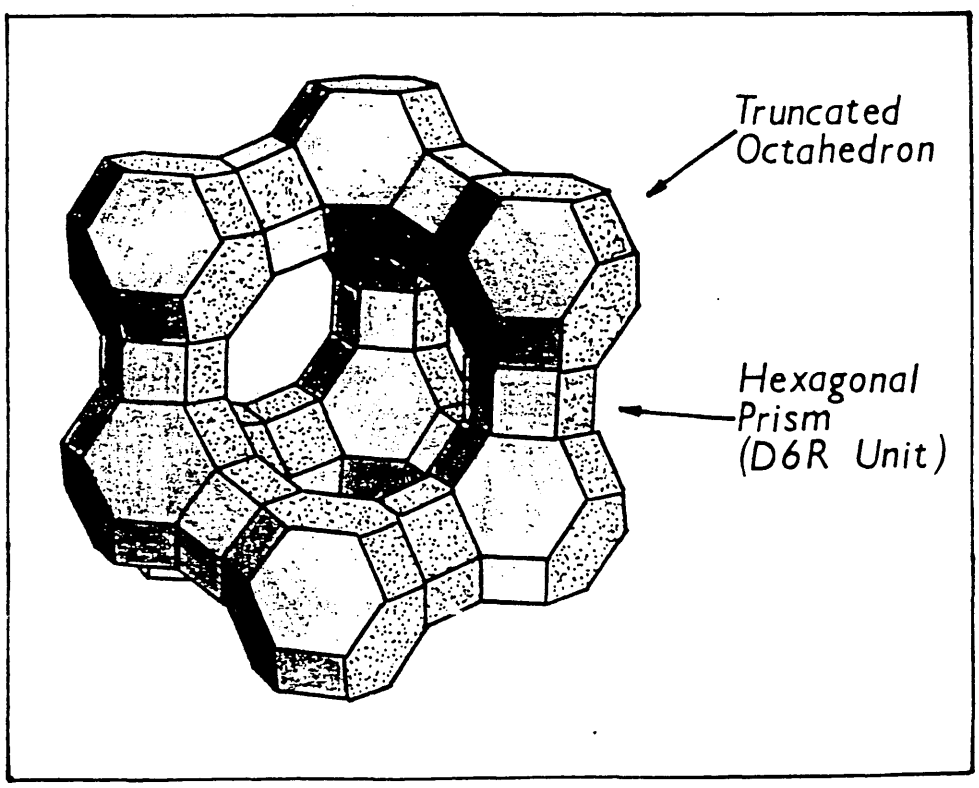

Nine cation sites in the faujasites have been identified and these are summarised in Table 1.1. There is also evidence to suggest that some of the

cations and the water molecules act as a strong electrolyte solution. One study[44] located 48 out of 80 sodium ions in zeolite X in sites I and II, the remainder of the ions being associated with water molecules. A later study[48], assigned sodium ions to sites I, I′ and II.

Table 1.1: Cation Sites in Zeolite X

Site	Position	No./uc
I	Centre of hexagonal prisms	16
I′	In β-cages adjacent to hexagonal prisms	32
U	Centre of β-cages	8
II	In S6R of β-cages	32
II′	Near S6R of site II but inside β-cages	32
II*	Near S6R of site II but inside β-cages	32
III	Against 4-Ring "ribs" of α-cage	48
IV	Centre of α-cage	8
V	In 12-Rings of α-cage	16

1.5 Properties and Applications of Zeolites

Zeolites exhibit three properties of industrial importance. These are the sorption of gases, liquids and vapours, catalytic activity and ion exchange. All zeolites exhibit these properties to varying degrees, but only zeolites A, X, Y, ZSM-5, Chabazite, Clinoptilolite and Mordenite are widely used. Other zeolites that have attracted limited commercial interest include zeolites L, Ω, ZSM-11, Theta-1 (Nu-10), Offretite and Erionite.

The sorption characteristics of zeolites are employed in a variety of applications including the separation of hydrocarbons, the drying of liquids and gases such as air and natural gas, the removal of sulphur from petroleum and the separation of air. Many of these applications rely on the property of molecular sieving which is characteristic of zeolites[49-51]. The channels and cavities of zeolites, and the apertures that permit entry to them, are regular and of fixed dimensions. Thus, molecules that are too large, or of the wrong shape, cannot enter the channel system. This property facilitates separation and by careful

zeolite selection, many different separations may be carried out. The molecular sieving properties of zeolites can be dramatically altered by ion exchange. The cations in a zeolite are accommodated in the channel system, that is in the same spaces that sorbate molecules occupy. Some cations occupy positions adjacent to apertures, thus reducing the effective free diameter of the aperture and controlling the size of molecule that may pass through. However, it is not simply the size of such cations that is important, but also their valence and numbers. Indeed, ion exchange often results in a different cation distribution in the framework, and thus modifies the molecular sieving characteristics accordingly.

Not all separations, however, rely on molecular sieving. The separation of air, for instance, can be effected by Mordenite, Chabazite, calcium-A or Faujasite, all of which permit the entry of both oxygen and nitrogen to their channel systems. Nitrogen is sorbed more strongly than oxygen because it has a quadrupole moment which interacts with the electric field gradient of the framework, enhancing sorption energy. The gas phase becomes oxygen enriched and the sorbed phase is rich in nitrogen[52]. A pressure swing method[53] can be used for small scale oxygen production (25 or 30 tons per day), although on a larger scale liquefaction is more economic.

Zeolite catalysts were first introduced in 1962 after it was realised that certain rare-earth and hydrogen forms possessed cracking activities far in excess of the then conventional silica-alumina catalysts. Zeolite catalysts gave less coking, increased production capacity and improved gasoline yields and they now dominate this market. Faujasite-type zeolites and ZSM-5 are the principal zeolite catalysts. Mordenite is used in some specialist applications, although its one-dimensional channel system is prone to coking. Other zeolites such as L, Ω, Erionite and Offretite also exhibit excellent catalytic activities.

Hydrogen-zeolites contain Bronsted acid sites[54] which can, by proton transfer to occluded hydrocarbons, produce carbonium ions. These reactive species can be involved in polymerisation, isomerisation and cracking reactions. A major advantage of the zeolite catalysts is that their catalytic and molecular sieving properties can be simultaneously harnessed. Since the vast majority of reactive sites lie within the channel system, only those molecules that are permitted to enter will be able to react. Products must be able to diffuse out of the channel system and reaction intermediates must fit within the confines of the zeolite cavities. Thus, zeolites exhibit reactant, intermediate and product selectivity.

Zeolite catalysts can be modified by ion exchange and by the sorption of elements such as sulphur, selenium or tellurium[55,56]. Such modification may increase catalytic activity or alter the product distributions. For example, synthetic zeolites containing transition metal ions are active for the oxidation of hydrogen, carbon monoxide, ethene and ammonia[57].

Ion exchange has already been shown to be important in the regulation of molecular sieving and the production of zeolite catalysts. Direct applications of this property are, however, somewhat limited. Removal of ammonia, as ammonium ions, from municipal, industrial and agricultural wastes can be carried out by Clinoptilolite or Zeolite F. Clinoptilolite can also be used for the removal of long-lived strontium and caesium isotopes from radioactive waste solutions.

Just as zeolites exhibit molecular sieving, an ion sieve effect is also observed. Ag-Analcime or Ag-Sodalite, for instance, readily exchange with sodium ions, but not with caesium ions. Thus, solutions of caesium chloride contaminated with sodium chloride can readily be purified by the reaction:

$$NaCl + Ag\text{-}Zeolite \rightarrow Na\text{-}Zeolite + AgCl\downarrow$$

Lanthanide and actinide isotopes have been separated by exchanging these cations into zeolites X or Y[58]. The ions were then trapped in the sodalite (β) cages by the appropriate heat treatment and exposed to neutron radiation in a nuclear reactor. The (n,γ) reaction produced isotopes one mass unit heavier than the parent ion. On emission of the γ-radiation, the nucleus recoiled dislodging a large proportion of the new isotope from the β-cage to the α-cage. The new isotope was then eluted by ion exchange with solutions containing lithium or calcium ions. Separation factors were high and significant amount of the recoil isotope were concentrated in this way (Szilard - Chalmers Recoil)

By far the most important commercial application of zeolite ion exchange is in water softening. The detergent industry uses large quantities of zeolites as detergent builders and, in tonnage terms, it is the single largest consumer of zeolites. The function of a builder is to remove calcium and magnesium ions from wash solutions. This application of zeolites is the subject of this thesis and is discussed in more detail below.

1.6 Detergents

Synthetic detergents were first produced in Germany during World War I when animal fats were in short supply and could no longer be used for soap production. Modern detergent formulations are complex mixtures of chemicals, including surfactants (actives), builders, fillers, bleaches, buffers, fluorescers and, frequently, enzymes.

Surfactants, so called because they are surface active chemicals, are the most important ingredients and are responsible for the cleansing properties of the formulation. They have amphipathic structures, that is they contain both water soluble (hydrophilic or polar) groups and water insoluble (hydrophobic or non-polar) groups. In aqueous solution, or indeed in other solvents, such molecules are preferentially absorbed at the interface. At high concentrations, micelle formation takes place. There are four main classes of surfactant. These are the anionic detergents, the cationic detergents, the nonionic detergents and the amphoteric detergents[59].

The anionic detergents are by far the largest class of detergents. The detergency of such molecules is vested in the anion, which has to be neutralised in alkaline or basic material before the full detergency is realised. This class of detergents includes the soaps, neutralisation products of natural fats with sodium or potassium hydroxide. The vast majority of the anionic detergents are synthetic sulphated or sulphonated products.

In cationic detergents, the detergency is vested in the cation. Although no neutralisation takes place in the manufacturing process, these materials are effectively neutralised by strong acid. Commonly, they are amino compounds, the most effective being quarternary ammonium salts with one long chain attached to the nitrogen nucleus, or quarternary pyridine based salts. Their detergency is poor compared to that of the anionic and non-ionic detergents and their cost is high. The main uses of these compounds are as fabric softeners, germicides and specialist emulsifiers.

Many of the nonionic detergents are condensation products of ethylene oxide with a hydrophobe. Usually, the hydrophobe is a high molecular weight material with an active hydrogen. Variation in the amount of ethylene oxide used allows the hydrophobe/hydrophile balance, and hence the detergency, to be adjusted to almost any requirements[60].

The final class of surfactants, the amphoterics, are not widely used, but are of interest because they exhibit the properties of both the anionic detergents and the cationic fabric softeners. They generally possess quarternary ammonium and anionic radicals, the anionic usually being a carboxyl, sulphate or sulphonate group.

Detergents may, and often do, contain a mixture of surfactants to allow the performance of the final product to be tailored to the purpose for which it is designed. A heavy duty fabric washing powder, for instance, will contain a different mix of surfactants to a floor washing formulation.

The remaining ingredients in a detergent formulation are added to enhance surfactant performance. Sodium sulphate is often added as a filler, not merely to cheapen the product, but also to make it more convenient to use. Essentially it acts as a diluant which allows the product to be added to the wash solution in easily measurable quantities. It also raises the ionic strength of the wash solution and reduces the interfacial tension between the wash solution and the soil to be removed. Chelating agents such as Ethylene Diamine Tetra-Acetic Acid (EDTA) or Nitrilo Tri-Acetic Acid (NTA) are used to minimise the deleterious effects of polyvalent cations, which may cause stains during the wash, decompose the bleach species or dull the effects of fluorescers. They are not used to control water hardness, which is the function of the detergent builder. Fluorescers are dyestuffs that are absorbed by textiles during the wash, but which are not removed in the rinse cycles. They absorb uv radiation and emit visible light at the blue end of the spectrum, thus making washed fabrics look whiter and brighter. Bleaches, anti-oxidants (to prevent oxidation of fatty acids), pH buffers and perfumes are also widely used in detergent formulations.

1.7 Detergent Builders

An important group of detergent additives, which have not yet been described in any detail are the detergent builders. Builders are added to detergent formulations primarily to control water hardness (primarily due to the presence of Ca^{2+} and Mg^{2+} ions), but which may have other important functions. Detergent manufacturers have long been aware of the need to control water hardness in order to produce adequate cleaning from detergents. It is well known

that divalent ions, particularly the calcium and magnesium ions commonly present in water, have a detrimental effect on the laundering process. Calcium is generally regarded as being more harmful than magnesium, although the differences in effects depend on the fabric, soil and wash conditions.

There are at least two important mechanisms which cause this loss of detergency[62]. The first is the removal of active surfactant from solution as its insoluble calcium or magnesium salt. The second is the deposition of calcium bound and calcium bridged soils. The anionic detergents, particularly the soaps are prone to precipitation, but the non-ionics are more resistant. However, even those products that are resistant to precipitation by water hardness ions require some builder to prevent the deposition of water hardness ions on fabrics, particularly at the sites of body soil stains. For ideal detergent performance, it is recommended that the calcium level is below 10^{-5}M and the magnesium level below 10^{-4}M[61]. Very few natural waters fulfil these requirements.

There is a wide variety of suitable detergent builders[63,64]. These can be divided into three groups, the sequestrant builders (chelating agents) such as sodium tripolyphosphate (STPP), NTA and more recently polyacrylic acid (PAA), precipitant builders such as sodium carbonate and the ion exchange builders such as the zeolites. Until recently, the most successful of these have been the condensed polyphosphates, particularly STPP.

Sodium tripolyphosphate ($Na_5P_3O_{10}$) has the following structure:

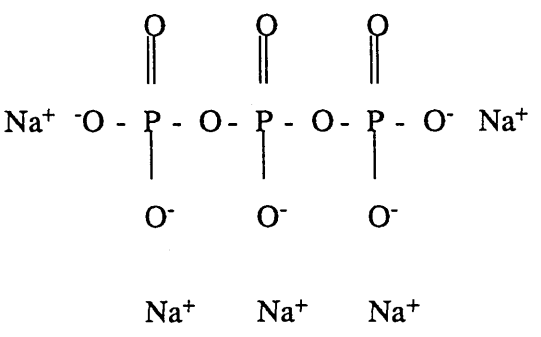

It forms soluble complexes with calcium and magnesium ions:

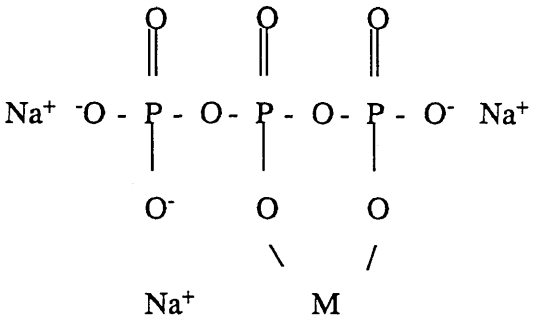

The calcium or magnesium involved in the complex is no longer ionic and is thus effectively removed from solution. Up to two divalent ions can be complexed by each STPP molecule, although the second stability constant is considerably lower than the first.

STPP is not, however, simply a softening agent. It has a number of other important functions which include:

1. Provision of excess basicity to convert sebum fatty acids to effective soaps which assist in the removal of oily and greasy soils.

2. Deflocculation of particulate soils.

3. Buffering of the wash solution in the optimum pH ranges.

4. Decreasing soil redeposition by stabilising dispersed soils.

5. Helping to lower the critical micelle concentration (CMC) of anionic surfactants, thus producing detergency at lower detergent concentrations.

6. Aiding in the spray drying processing of detergent powders.

The use of phosphate builders is not, however, without its drawbacks. In aqueous solution the polyphosphates are hydrolysed to orthophosphates. This reaction is relatively slow at moderate temperatures, but speeds up at higher temperatures. Thus, the polyphosphates may be unsuitable for use in liquid detergents and in detergents designed for use at high temperatures. Additionally, the control of ions other than calcium and magnesium is poor and

many formulations contain additional chelants for this purpose. These are, however, relatively minor problems and the polyphosphates are widely regarded as the best detergent builder so far discovered.

A major problem associated with the polyphosphates is the eutrophication of inland waterways. High levels of phosphates, which are plant nutrients, in natural waters are thought to be responsible for the excessive plant and algal growth which can, eventually, lead to the choking of the waterway. Detergent wastes account for around a quarter of the phosphates found in natural waters, the remainder coming from industrial and agricultural sources. Removal of phosphates at sewage treatment plants is possible, but not widely used, and in countries where the problem is severe, governmental pressure has been applied to detergent manufacturers to reduce, or even remove, phosphates from their formulations.

The detergent industry is, therefore looking for alternative detergent builders. These must meet the following requirements[65]:

1. No degradation of overall detergent performance.

2. Toxicological and ecological safety.

3. Economic feasibility.

4. Large scale production from easily available raw materials.

Ideally such products should also be odourless, essentially non-hygroscopic, free flowing, white, crystalline powders. Inorganic builders, such as zeolites, are potentially the most attractive since there is no dependence on oil as a raw material and there are no problems of biodegradability or possible metabolites.

1.8 The Zeolite Detergent Builders

The use of zeolites as detergent builders initially may seem anomalous since they are insoluble in aqueous solution. Conventional wisdom dictates that the builder should, ideally, form soluble complexes with calcium and magnesium ions. However, zeolites, and in particular zeolite A, have achieved large scale

success, particularly in low phosphate detergents.

Zeolites soften water by ion exchange, harmless sodium ions being exchanged into the wash solution in place of calcium and magnesium ions. A number of zeolites, both natural and synthetic, have been proposed and studied for this application[66]. Natural zeolites have the advantage of being cheap, but may show a significant variation in composition depending on their origin, are often impure and may contain significant quantities of iron, which can give rise to stains during laundering. The synthetic zeolites, although more expensive, can be prepared in pure form and the reaction variables allow control of the crystal size. Particle sizes below 1μm are preferred because the crystals can then pass through fabric meshes and are not trapped, forming encrustations. Additionally, the rate of ion exchange increases as the crystal size decreases thus favouring the smaller crystals.

Zeolite A has particularly advantageous characteristics in the washing process compared to other zeolite types. It has the highest possible theoretical ion exchange capacity (7.04 meq/g or 352mg $CaCO_3$ per g) and, therefore, the greatest weight efficiency. In practice, however, the full exchange capacity is never achieved due to competing sodium ions, although, in fairness, no builder ever achieves its theoretical capacity. Whilst the kinetics of calcium uptake by zeolite A are slower than for STPP, they are perfectly adequate for the purposes and are faster than the precipitant builders such as sodium carbonate. Its calcium binding power is roughly equivalent to that of STPP and it binds to calcium in the presence of surfactants, thus preventing the formation of insoluble calcium salts of anionic detergents[67]. It also assists in the washing process by absorbing various organic soil constituents and by acting as a substrate for the deposition of slightly soluble salts. zeolite A has been shown to be non-toxic and environmentally safe. It does not cause redistribution of heavy metals in the environment as was initially feared and is neither a carcinogen nor a teratogen[68].

There are, however, a number of technical problems associated with the use of zeolites as detergent builders. Formulations containing relatively large proportions of zeolite builder may be difficult to wet. As a result, after dissemination or rinsing into water, the detergent powder may remain unwetted or floating on the surface (the "sawdust" effect) for relatively long periods of time. This delayed detergent activity may cause a serious reduction in

performance, particularly in automatic machines where the full time available in the wash cycle is not used, and the "sawdust" effect may result in considerable loss of detergent. Thus, detergent grade zeolites must have improved wettabilities, that is they must be hydrophilised.

More importantly, Zeolite A alone does not provide equivalent performance to STPP because its magnesium ion control is inadequate. In aqueous solutions, magnesium ions have a large hydration sphere and the hydrated magnesium ion is too large to enter the channels of zeolite A. For ion exchange to take place, some of these water molecules must be lost. Thus, whilst zeolite A exhibits an ion exchange selectivity for magnesium ions over sodium ions, the kinetics of the reaction are slow and, in the timescale of a wash cycle, little or none of the magnesium is removed. Additionally, zeolites are unable to redissolve calcium and magnesium precipitates. Both these problems can be overcome by the addition of low levels of a chelating agent to the formulation in conjunction with the zeolite builder. In the low phosphate detergents, this additional chelating agent is STPP. It is added in considerably lower proportions than in the purely phosphate built detergents, but sufficient STPP must be added so that free STPP remains in the wash solution to carry out its other functions. Other chelating agents are used in the non-phosphate detergents, but here only the sequestering effects of STPP are replaced and the other effects must be achieved by adjusting the formulation.

Zeolite A, despite its problems, has been widely accepted as the most suitable alternative to the phosphate detergent builders. Many patents concerning its use are now in existence[69]. It is usually used in the hydrated form, containing between 10 and 28% water. The preferred form has a water content between 18 and 22%.

Zeolite X has also been proposed as a detergent builder, but has not yet achieved large scale success[70]. It has a lower theoretical ion exchange capacity than zeolite A, but exhibits good selectivity for calcium and magnesium ions. The channel system is controlled by windows 7.4Å in diameter compared with windows of 4.2Å diameter in zeolite A. This more open channel system allows hydrated magnesium ions to exchange more easily. However, unlike zeolite A in which all the exchange sites are readily accessed, some of the exchange sites in zeolite X are less accessible. Admixtures of zeolites A and X have been shown to exhibit a synergistic effect and give improved performance over either of the

pure zeolites. It has been suggested that this effect is due to the better magnesium exchange characteristics of zeolite X. A commercial product (Union Carbide Linde ZB300), which consists of a mixture of detergent grade zeolite A and X, is available[61,71]

The amorphous aluminosilicate gels from which zeolites crystallise (see section 1.3) also show promise as detergent builders. These materials exhibit the property of ion exchange, but unlike the crystalline zeolites, their frameworks are less compact and their channel systems are not of regular dimensions. Exchange of large hydrated cations such as magnesium ions should, therefore, occur more readily in these materials.

The work described in this thesis investigates the synthesis of aluminosilicate gels and their use as detergent builders. Changes in ion exchange selectivities and capacities with respect to crystallisation time will also be analysed to ascertain if these parameters can add to our knowledge of the nucleation and crystal growth process.

1.9 References

1. W. Lowenstein, Am. Mineral., **39**, (1942), 92
2. R. M. Barrer and W. M. Meier, Trans. Farad. Soc., **54**, (1958), 1074
3. J. V. Smith, Am. Mineral Soc. Special Paper, **1**, (1963),281
4. A. F. Cronstedt, Akad. Handl. Stockholm, **17**, (1756), 120
5. D. W. Breck, "Zeolite Molecular Sieves", R. E. Krieger Publ. Co., (1984), 5
6. R. M. Barrer, "Hydrothermal Chemistry of Zeolites", Acad. Press, (1982), 2
7. R. M. Barrer, "Zeolites and Clay Minerals as Sorbents and Molecular Sieves", Acad. Press, (1978), 4
8. H. de St. Clair Deville, Compt. Rend., **54**, (1862), 324
9. G. W. Morey and E. Ingerson, Econ. Geol., **38**, (1937), 607
10. R. M. Barrer, J. Chem. Soc., (1948), 2158
11. R. M. Barrer, J. Chem. Soc., (1948), 127
12. R. M. Milton, U.S. Patent 2,882,243 (1959)
13. R. M. Milton, U.S. Patent 2,882,244 (1959)
14. R. M. Barrer, "Hydrothermal Chemistry of Zeolites", Acad. Press, (1982), 106
15. R. M. Barrer, Proc 6th Int. Zeol. Conf., Butterworths, (1984), 17
16. E. M. Flanigen, "Molecular Sieves", A.C.S. Adv. in Chem. Ser. 121, (1973), 119

17. R. M. Barrer, Zeolites, **1**, (1981), 130
18. J. R. Glastonbury, Chem. and Ind., (1961), 121
19. R. J. Moolenaar, J. C. Evans and L. D. McKeever, J. Phys. Chem., **74**, (1970), 3629
20. J. Aveston, J. Chem. Soc., (1965), 4445
21. R. K. Harris and R. H. Newman, J. Chem. Soc. Farad. Trans. II, **73**, (1977), 1153
22. F. Polak and E. Stobieca, Bull. Acad. Pol. des Sciences, Ser. des Sciences Chim., **26**, (1978), 899
23. S. P. Zhadanov, A.C.S. Adv. in Chem Ser. 101, (1970), 20
24. G. T. Kerr, J. Phys. Chem., **70**, (1966), 1947
25. J. Ciric, J. Colloid Interface Sci., **28**, (1968), 315
26. J. R. Goldsmith, J. Geol., **61**, (1953), 439
27. R. K. Iler, "The Colloid Chemistry of Silica and Silicates", Cornell Univ. Press, Ithaca, New York, (1955), 26-30
28. D. W. Breck, "Zeolite Molecular Sieves", R. E. Krieger Publ. Co., (1984), 341
29. H. Khatami and E. M. Flanigen, Unpublished Work
30. B. D. McNicol, G. T. Pott and K. R. Loos, J. Phys. Chem., **76**, (1972), 3388
31. B. D. McNicol, G. T. Pott, K. R. Loos and N. Mulder, A.C.S. Adv in Chem. Ser. 121, (1973), 152
32. J. L. Guth, P. Caullet and R. Wey, Proc. 5th Int. Zeol. Conf., Heyden, London, (1980), 30
33. J. L. Guth, P. Caullet, P. Jacques and R. Wey, Bull. Soc. Chim. France, **3-4**, (1980), 121
34. C. L. Angell and W. H. Flank, "Molecular Sieves II", A.C.S Symp. Ser. 40, (1977), 194
35. W. E. Dibble, B. H. W. S. de Jong and L. W. Cary, Proc. Int. Symp. Water-Rock Inst., Edmonton, Canada, (1980), 47
36. G. Englehardt, D. Hoebbel, M. Tarmak, A. Samosan and E. Lippmaa, Z. Anorg. Allg. Chem., **484**, (1982), 22
37. S. Ueda, N. Kageyama and M. Koizumi, Proc. 6th Int. Zeol. Conf., Butterworths, (1983), 905
38. E. G. Derouane, S. Detremmerie, Z. Gabelica and N. Blom, Appl. Catal., **1**, (1981), 201
39. Z. Gabelica, N. Blom and E. G. Derouane, Appl. Catal., **5**, (1983), 227
40. M. Tatic and B. Drjaz, "Zeolites: Synthesis, Structure, Technology and Application", Studies in Surf. Sci. and Catal. 24, Elselvier, (1985), 129

41. K. F. Fischer and W. M. Meier, Fortschr. Mineral., **42**, (1965), 50
42. W. M. Meier, "Molecular Sieves", Soc. Chem. Ind., London, (1968), 10
43. D. W. Breck, A.C.S. Adv. in Chem Ser. 101, (1971), 1
44. L. Broussard and D. P. Shoemaker, J. Am. Chem. Soc., **82**, (1960), 1041
45. T. B. Reed and D. W. Breck, J. Am. Chem. Soc., **78**, (1956), 5972
46. J. V. Smith and L. G. Dowell, Z. Krystallogr., **126**, (1968), 135
47. R. Y. Yanagida, A. A. Amaro and K. Seff, J. Phys. Chem., **77**, (1973), 805
48. D. H. Olsen, J. Phys. Chem., **74**, (1970), 2758
49. R. M. Barrer, J. Soc. Chem. Ind., **64**, (1945), 130
50. R. M. Barrer and L. Belchetz, J. Soc. Chem. Ind., **64**, (1945), 131
51. R. M. Barrer, J. Soc. Chem. Ind., **64**, (1945), 133
52. H. A. Stewart and J. L. Heck, Chem. Eng. Prog., **65**, (1969), 78
53. D. W. Breck, "Zeolite Molecular Sieves", R. E. Krieger Publ. Co., (1984), 709
54. P. B. Venuto and P. S. Landis, Adv. Catal., **18**, (1968), 259
55. J. N. Miale and P. B. Weisz, J. Catal., **20**, (1971), 288
56. W. H. Lang, R. J. Mikovsky and A. J. Silvestri, J. Catal., **20**, (1971), 293
57. K. M. Minachev and Y. I. Isakov, A.C.S. Adv. in Chem Ser. 121, (1973), 451
58. D. O. Campbell, A.C.S. Adv. in Chem Ser. 121, (1973), 281
59. A. Davidsohn and B. M. Milwidsky, "Synthetic Detergents", John Wiley, (1978), 11
60. Vaugh, J.A.O.C.S., **29**, (1952), 240
61. J. D. Sherman, A. F. Denny and A. J. Goiffre, Soaps Cosmetics and Chem. Specialities, December, (1978), 33
62. M. K. Nagarajan and H. L. Paine, J.A.O.C.S., **61(9)**, (1984), 1475
63. B. M. Milwidsky, Household and Personal Prods. Ind., November, (1984), 74
64. M. Sittig, "Detergent Manufacture Including Zeolites and Other New Materials", Noyes Data Corp., (1979), 337
65. Y. Yoneyama and K. Ogino, Tenside Detergents, **19(4)**, (1982), 197
66. H. G. Smolka and M. J. Schwuger, Colloid and Polymer Sci., **256**, (1978), 270
67. T. Mukaiyama, H. Nishio and O. Okumura, Proc. 7th Int. Zeol. Conf., Butterworths, (1986), 1017
68. A. Llenado, Proc. 6th Int. Zeol. Conf., Butterworths, (1983), 940
69. M. Sittig, "Detergent Manufacture Including Zeolites and Other New Materials", Noyes Data Corp., (1979), 387-405
70. G. H. Kuhl and H. S. Sherry, Proc. 5th Int. Zeol. Conf., Heyden, London, (1980), 813

71. A. F. Denny, A. J. Goiffre and J. D. Sherman, U.S. Patent 4,094,778 (1978)

Chapter Two

The Theory of Ion Exchange

2.1 Ion Exchange Isotherms

The ion exchange reaction in zeolites may be represented by the following equation:

$$z_a B_{(z)}^{z_b+} + z_b A_{(s)}^{z_a+} \leftrightarrow z_a B_{(s)}^{z_b+} + z_b A_{(z)}^{z_a+} \quad (1)$$

where z_a and z_b are the charges on the ions A and B respectively and the subscripts s and z refer to the solution and zeolite phases. Ion A is commonly referred to as the "ingoing" ion and ion B as the "outgoing" ion.

Equivalent cation fractions in both phases can be defined as follows:

$$E_a = \frac{z_a m_s^a}{z_a m_s^a + z_b m_s^b} \quad (2)$$

$$\bar{E}_a = \frac{\text{No. Equivalents Cation A in Zeolite}}{\text{Total No. Equivalents of Cation in Zeolite}} \quad (3)$$

m_s^a and m_s^b are the respective molalities of ions A and B in the equilibrium solution. The bar is used to indicate the zeolite phase. Similar equations can be written for ion B. Finally:

$$(E_a + E_b) = (\bar{E}_a + \bar{E}_b) = 1 \quad (4)$$

The equivalent cation fraction scale is used to allow for the differing charges which may be present on ions A and B. An ion e xchange isotherm is a plot of E_a as a function of $\bar{E}_a$ at a given solution normality and fixed temperature. An ideal ion exchange obeying the law of mass action produces an isotherm which follows a straight diagonal line (Figure 2.1). No selectivity for either ion is exhibited. However, zeolites usually show selectivity for one of the ions involved in the exchange reaction and the isotherm deviates from this diagonal line. There are five types of isotherm which may be exhibited by zeolites (Figure 2.1)[1]. Curve (a) represents selectivity by the zeolite for the ingoing cation and the isotherm lies below the diagonal line. Curve (b) represents the

opposite case where the selectivity is for the outgoing ion. Sigmoidal isotherms, curve (c), are common for zeolites. Here, the selectivity depends on the degree of exchange and the overall selectivity of the exchange is determined from the sign of the Gibbs free energy change (ΔG^{θ}) of the reaction. Curve (d) demonstrates another common type of isotherm, where the exchange does not go to completion. This effect occurs when some of the sites initially occupied by the outgoing ions are inaccessible to the ingoing ions. This may be due to the sizes of the cations involved or to the charge distribution on the zeolite framework. Finally, curve (e) represents the rare case where hysteresis is observed. This effect is observed, for instance, in potassium-rubidium exchange in Analcime[2] and is explained by the formation of two zeolite phases.

Figure 2.1. Zeolite Ion Exchange Isotherms

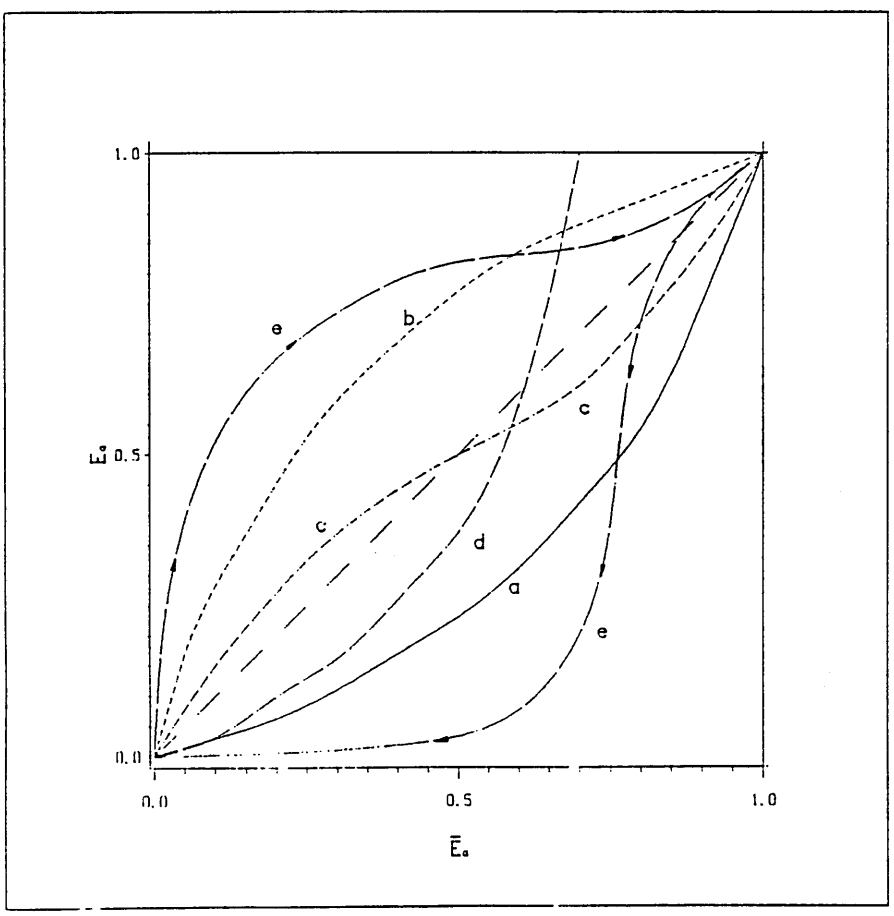

2.2 Factors affecting Ion Exchange

The ion exchange behaviour of zeolites depends on a number of factors which include the following:

1. The size of the ions, both hydrated and dehydrated. This affects not only the diffusion of ions through the zeolite pores, but may also restrict the number of ions that can be accommodated within the zeolite framework.

2. The charge distribution of the framework and the charge on the cation. Charge distributions may be unfavourable for multivalent cations.

3. Total solution normality. This is important because of the "concentration-valency" effect which is discussed in more detail below.

4. The solvent in which exchange takes place. Most work to date has been carried out in aqueous solution, but some work has been done using non-aqueous solvents[3,4].

5. The temperature at which exchange takes place. Ion exchange is an equilibrium reaction and higher temperatures favour the endothermic reaction over the exothermic one.

6. The anion associated with the cation in solution.

7. The structural characteristics of the zeolite.

Factors such as these affect both the kinetics and the thermodynamics of ion exchange in zeolites.

2.3 The Thermodynamics of Ion Exchange

There are three equilibrium constants that are of importance in ion exchange reactions. They can be defined as follows:

$$K_a = \frac{a_B^{z_a} \cdot \overline{a}_A^{z_b}}{a_A^{z_b} \cdot \overline{a}_B^{z_a}} \qquad (5)$$

$$K_c = \frac{a_B^{z_a} \cdot \overline{E}_a^{z_b}}{a_A^{z_b} \cdot \overline{E}_b^{z_b}} \qquad (6)$$

$$K_m = \frac{E_b^{z_a} \cdot \bar{E}_a^{z_b}}{E_a^{z_b} \cdot \bar{E}_b^{z_a}} \tag{7}$$

where a represents the activity of the ions in the solution or zeolite phases. K_a is the thermodynamic equilibrium constant, K_c is the corrected selectivity coefficient, or Kielland coefficient, and K_m is the mass action quotient. The Kielland coefficient may be rewritten:

$$K_c = \frac{\bar{E}_a^{z_b} \cdot (m_s^b)^{z_a} \cdot \gamma_b^{z_a}}{\bar{E}_b^{z_a} \cdot (m_s^a)^{z_b} \cdot \gamma_a^{z_b}} \tag{8}$$

where γ represents the mean ionic activity coefficient of the respective ions in mixed electrolyte solutions. As dilute solutions are usually used, molalities can be replaced by molarities (M):

$$M_s^a = \frac{E_a}{z_a}(z_a m_s^a + z_b m_s^b) = \frac{E_a}{z_a} \cdot N \tag{9}$$

$$M_s^b = \frac{E_b}{z_b}(z_a m_s^a + z_b m_s^b) = \frac{E_b}{z_b} \cdot N \tag{10}$$

where N is the total solution normality. Substituting these expressions into equation (8):

$$K_c = \frac{\bar{E}_a^{z_b} \cdot E_b^{z_a} \cdot \Gamma}{\bar{E}_b^{z_a} \cdot E_a^{z_b} \cdot Q} \tag{11}$$

where:

$$\Gamma = \frac{\gamma_b^{z_a}}{\gamma_a^{z_b}} \tag{12}$$

and:

$$Q = \frac{(z_b)^{z_a} \cdot N^{(z_b - z_a)}}{(z_a)^{z_b}} \tag{13}$$

However, mean ionic activity coefficients, γ_a and γ_b, are for individual ions in solution and as such cannot be evaluated. The mean activity coefficient for an electrolyte $A_{z_y}Y_{z_a}$, which dissociates into the ions A^{z_a+} and Y^{z_y-} in solution can be defined as:

$$\gamma_{\pm AY} = (\gamma_a^{z_y} \cdot \gamma_y^{z_a})^{1/(z_a + z_y)} \tag{14}$$

Similarly for an electrolyte $B_{z_y}Y_{z_b}$:

$$\gamma_{\pm BY} = (\gamma_b^{z_y} \cdot \gamma_y^{z_b})^{1/(z_b+z_y)} \tag{15}$$

If both sides of equation (14) are raised to the power $z_b(z_a + z_y)/z_y$ and both sides of equation (15) to the power $z_a(z_b + z_y)/z_y$, division of the second equation by the first produces:

$$\Gamma = \frac{\gamma_b^{z_a}}{\gamma_a^{z_b}} = \frac{(\gamma_{\pm BY})^{z_a(z_b+z_y)/z_y}}{(\gamma_{\pm AY})^{z_b(z_a+z_y)/z_y}} \tag{16}$$

and the mean activity coefficients, $\gamma_{\pm AY}$ and $\gamma_{\pm BY}$, for mixed electrolyte solutions can be obtained from the literature or measured experimentally.

For a uni-divalent exchange, such as sodium-calcium or sodium-magnesium exchange, involving a divalent ion A and a monovalent ion B, combining equations (11) and (16) produces:

$$K_c = \frac{\bar{E}_a \cdot (E_b)^2}{(\bar{E}_b)^2 \cdot E_a} \cdot 2N \cdot \frac{(\gamma_{\pm BY})^4}{(\gamma_{\pm AY})^3} \tag{17}$$

The dependence of K_c on solution normality according to equation (17) gives rise to the "concentration-valency effect" which has been mentioned previously. It has been shown[6] that the change in Q is greater than the change in Γ and cumulative (i.e. as Q increases, so Γ decreases). Thus, as the total solution concentration is reduced, and since K_c is constant for a fixed $\bar{E}_a$, then $(E_b)^2/E_a$ must increase and consequently, the isotherm appears more selective for the divalent ion.

Equation (5), defining K_a, the thermodynamic equilibrium constant, can be rewritten in terms of activity coefficients:

$$K_a = \frac{\bar{E}_a^b \cdot (m_s^b)^{z_a} \cdot f_a^{z_b} \cdot \gamma_b^{z_a}}{\bar{E}_b^a \cdot (m_s^a)^{z_b} \cdot f_b^{z_a} \cdot \gamma_a^{z_b}} \tag{18}$$

where f represents the activity coefficient of the ion in the zeolite. Substituting from equation (7):

$$K_a = K_c \cdot \frac{f_a^{z_b}}{f_b^{z_a}} \tag{19}$$

In a few cases the ratio f_a/f_b is constant and for those uni-univalent exchanges where Γ is also constant:

$$\frac{\overline{E}_a \cdot E_b}{\overline{E}_b \cdot E_a} = \text{Constant} \qquad (20)$$

Therefore, the selectivity coefficient is independent of degree of exchange and this has been found to be true of a small number of zeolite ion exchanges. These include sodium-lithium, sodium-potassium and sodium-silver exchanges in basic sodalite[2], sodium-thallium in zeolite A[7] and ammonium-rubidium in zeolite Rho[8]. However, this is not generally the case and Kielland[9] found an empirical relationship between zeolite phase activity coefficients and degree of exchange:

$$\log f_a = C\,\overline{E}_b^2$$
$$\log f_b = C\,\overline{E}_a^2 \qquad (21)$$

where C is an empirical constant. Substituting for f_a and f_b in equation (19):

$$\log K_a = \log K_c + C(1 - 2\,\overline{E}_a) \qquad (22)$$

This relationship implies that a plot of log K_c as a function of $\overline{E}_a$ should be a straight line of slope 2C and intercept (log K_a - C). This type of plot is known as a Kielland plot and for exchanges such as sodium-rubidium and sodium- caesium in zeolite A[8], the plot is indeed a straight line of slope 2C. However, in most cases, the Kielland plot is not a straight line.

2.4 The Gaines and Thomas Approach

Gaines and Thomas[10] developed a simplified thermodynamic approach for the evaluation of the solid phase activity coefficients and the thermodynamic equilibrium constant. They confined their considerations to the exchange of a pair of ions (A and B) in a solid of constant exchange capacity. The chemical potentials of the cations in solid and solution phases can be defined as follows:

$$\overline{\mu}_a = \overline{\mu}_a^{\theta} + RT \ln \overline{E}_a . g_a \qquad (23)$$

$$\mu_a = \mu_a^{\theta} + RT \ln \gamma_a.m_s^a \quad (24)$$

$$\bar{\mu}_b = \bar{\mu}_b^{\theta} + RT \ln \bar{E}_b.g_b \quad (25)$$

$$\mu_b = \mu_b^{\theta} + RT \ln \gamma_b.m_s^b \quad (26)$$

where g_a and g_b are the Gaines and Thomas zeolite phase activity coefficients. Gaines and Thomas pointed out that these do not have the character of individual ion activity coefficients, but refer to the combination of these ions with the exchanger in a definite composition of the whole mass. Application of the Gibbs-Duhem equation to the solid phase gives:

$$n_a d\,\bar{\mu}_a + n_b d\,\bar{\mu}_b + n_w d\,\bar{\mu}_w = 0 \quad (27)$$

and, therefore:

$$n_a RT d\ln \bar{E}_a g_a + n_b RT d\ln \bar{E}_b g_b + n_w RT d\ln \bar{a}_w = 0 \quad (28)$$

where n_a, n_b and n_w are the number of moles of ion A, ion B and water respectively and a_w is the activity of the water in the zeolite phase. If each term in equation (28) is multiplied by $z_a z_b / RT(z_a n_a + z_b n_b)$:

$$\frac{z_a n_a}{(z_a n_a + z_b n_b)} z_b d\ln \bar{E}_a g_a + \frac{z_b n_b}{(z_a n_a + z_b n_b)} z_a d\ln \bar{E}_b g_b + \frac{n_w z_a n_b}{(z_a n_a + z_b n_b)} z_b d\ln \bar{a}_w = 0 \quad (29)$$

but for one equivalent:

$$z_a n_a + z_b n_b = 1 \quad (30)$$

$$\frac{z_a n_a}{(z_a n_a + z_b n_b)} = \bar{E}_a \quad (31)$$

$$\frac{z_b n_b}{(z_a n_a + z_b n_b)} = \bar{E}_b \quad (32)$$

and thus:

$$z_b \bar{E}_a d\ln \bar{E}_a g_a + z_a \bar{E}_b d\ln \bar{E}_b g_b + z_a z_b \nu_w d\ln \bar{a}_w = 0 \quad (33)$$

where $\nu_w = n_w/(z_a n_a + z_b n_b)$. If the logarithmic terms are separated:

$$z_b d\,\bar{E}_a + z_a d\,\bar{E}_b + \bar{E}_a d\ln g_a^{z_b} + \bar{E}_b d\ln g_b^{z_a} + z_a z_b \nu_w d\ln \bar{a}_w = 0 \qquad (34)$$

and from equation (19), which defines K_a:

$$\ln K_a = \ln K_c + \ln f_a^{z_b} - \ln f_b^{z_a} \qquad (35)$$

therefore:

$$d\ln K_c + d\ln g_a^{z_b} - d\ln g_b^{z_a} = 0 \qquad (36)$$

Combining equations (34) and (36) and using the fact that $d\,\bar{E}_a = -d\,\bar{E}_b$:

$$d\ln g_a^{z_b} = (z_b - z_a) d\,\bar{E}_b - \bar{E}_b d\ln K_c - z_a z_b \nu_w d\ln \bar{a}_w \qquad (37)$$

$$d\ln g_b^{z_a} = -(z_b - z_a) d\,\bar{E}_a - \bar{E}_a d\ln K_c - z_a z_b \nu_w d\ln \bar{a}_w \qquad (38)$$

To allow a definite integration of these equations, the standard states of the various components must be defined. For the solvent, these are chosen so that the activity of the water in both phases is equal. The chosen reference states for the solid phase are mono-ionic exchanger in equilibrium with an infinitely dilute solution of the respective ion. In the solution phase, standard states are chosen such that ion activities approach the corresponding molalities as the solute concentration approaches zero. Integration of equations (37) and (38) thus gives:

$$\ln g_a^{z_b} = (z_b - z_a)\,\bar{E}_b - \int_{K_{c_1}}^{K_c} \bar{E}_b d\ln K_c \qquad (39)$$

$$\ln g_b^{z_a} = -(z_b - z_a)\,\bar{E}_a - \int_{K_{c_0}}^{K_c} \bar{E}_a d\ln K_c \qquad (40)$$

where:

$K_c = K_{c_1}$ when $\bar{E}_b = 0$

$K_c = K_{c_0}$ when $\bar{E}_a = 0$

The swelling of zeolites is small or insignificant and as ion exchange reactions are normally studied in dilute solutions, the error involved in omitting the water activity terms is negligible.

Substituting for the activity coefficient terms in equation (35):

$$\ln K_a = (z_b - z_a) + \int_0^1 \ln K_c d\,\bar{E}_a \qquad (41)$$

Equations (39) and (40) can be rewritten in more useful terms:

$$\log g_a^{z_b} = 0.4343(z_b - z_a) - \bar{E}_b \log K_c + \int_{\bar{E}_a}^1 \log K_c d\,\bar{E}_a \qquad (42)$$

$$\log g_b^{z_a} = -0.4343(z_b - z_a) + \bar{E}_a \log K_c - \int_0^{\bar{E}_a} \log K_c d\,\bar{E}_a \qquad (43)$$

The integrals required for the evaluation of equations (41), (42) and (43) are obtained from the Kielland plot. They may be determined graphically, or by a least squares method in which a curve is fitted to the experimental data. This curve is represented by a polynomial of the form:

$$\log K_c = C_1 + C_2\,\bar{E}_a + C_3(\bar{E}_a)^2 + C_4(\bar{E}_a)^3 + \ldots \qquad (44)$$

where C_1 to C_4 are constants. Such an expression readily allows evaluation of the required integrals. Having determined the thermodynamic selectivity coefficient for the reaction, K_a, the Gibbs free energy change can be calculated using the following equation:

$$\Delta G^\theta = -\frac{RT}{z_a z_b} \ln K_a \qquad (45)$$

The sign of this change indicates the overall selectivity of the exchange. Negative values indicate overall selectivity for the ingoing ion, ion A. Positive values indicate that the reverse reaction is favoured, that is that the zeolite is selective for the outgoing ion, ion B.

2.5 The Validity of the Gaines and Thomas Approach

The Gaines and Thomas approach has been widely used for studies of ion exchange reactions in zeolites. However, there have been criticisms of this method[12-14].

Equation (19) defines K_a as follows:

$$K_a = K_c \cdot \frac{f_a^{z_b}}{f_b^{z_a}}$$

Clearly, under ideal conditions:

$$f_a = f_b = 1$$

and:

$$K_a = K_c$$

However, from equation (41) we have:

$$\ln K_a = (z_b - z_a) + \int_o^1 \ln K_c d \bar{E}_a$$

From this equation K_a cannot equal K_c unless z_a equals z_b. Equations (19) and (41) are, therefore, mutually exclusive.

Additionally, the solid phase activity coefficients derived using the Gaines and Thomas approach have been criticised. Indeed, Gaines and Thomas noted that these coefficients do not have the character of individual ion activity coefficients[10]. It has been claimed that activity coefficients derived using the cation equivalent fraction scale are "only formal parameters without a strict thermodynamic meaning in themselves"[12]. In particular, it was claimed that these coefficients are "not true activity coefficients because the activity of a component of a mixture does not become equal to its equivalent fraction in the limiting case where Raoult's law is obeyed"[13].

Barrer and Townsend[15-17] have, however, shown these criticisms to be unfounded. Evaluation of the activity coefficients, and subsequently K_a, relies on the application of the Gibbs-Duhem equation:

$$\sum_i n_i d\mu_i = 0 \qquad (46)$$

where n_i is, in this case, the amount of ion i and μ_i is its chemical potential. There are three concentration scales of interest in zeolite ion exchange

reactions. Bonner et al[18] used a cation mole fraction scale in which the mole fraction, $\bar{X}_i$, of ion i was defined as:

$$\bar{X}_i = \frac{n_i}{n_a + n_b} \tag{47}$$

Thus, applying the Gibbs-Duhem equation:

$$\frac{n_a}{n_a + n_b} d\,\bar{\mu}_a + \frac{n_b}{n_a + n_b} d\,\bar{\mu}_b + \frac{n_w}{n_a + n_b} d\,\bar{\mu}_w = 0 \tag{48}$$

and, therefore:

$$\bar{X}_a d\,\bar{\mu}_a + \bar{X}_b d\,\bar{\mu}_b + \frac{n_w}{n_a + n_b} d\,\bar{\mu}_w = 0 \tag{49}$$

Chemical potentials can be defined as:

$$\mu_i = \mu_i^{\theta} + RT \ln a_i \tag{50}$$

and the activity term, a_i, can be expanded:

$$\mu_i = \mu_i^{\theta} + RT \ln X_i f_i \tag{51}$$

Therefore:

$$d\mu_i = RT\, d\ln X_i + RT\, d\ln f_i \tag{52}$$

Substituting into equation (49):

$$\bar{X}_a d\ln \bar{X}_a + \bar{X}_a d\ln f_a + \bar{X}_b d\ln \bar{X}_b + \bar{X}_b d\ln f_b + \frac{n_w}{n_a + n_b} d\ln \bar{a}_w = 0 \tag{53}$$

Since $d\ln \bar{X}_a = d\,\bar{X}_a / \bar{X}_a$, this equation becomes:

$$d\,\bar{X}_a + d\,\bar{X}_b + \bar{X}_a d\ln f_a + \bar{X}_b d\ln f_b + \frac{n_w}{n_a + n_b} d\ln \bar{a}_w = 0 \tag{54}$$

and, by definition:

$$d\,\bar{X}_a + d\,\bar{X}_b = 0 \tag{55}$$

Hence:

$$\bar{X}_a d\ln f_a + \bar{X}_b d\ln f_b + \frac{n_w}{n_a + n_b} d\ln \bar{a}_w = 0 \qquad (56)$$

Hogfeldt[19] also used a mole fraction scale, but unlike the scale used by Bonner et al, the Hogfeldt mole fraction is defined per mole of exchanger. In this case, the ion exchange reaction is written:

$$z_b A_{(s)}^{z_a+} + z_a z_b (B_{(z)}^{z_b+})_{1/z_b} \leftrightarrow z_a B_{(s)}^{z_b+} + z_a z_b (A_{(z)}^{z_a+})_{1/z_a} \qquad (57)$$

and the mole fraction is given by:

$$\text{Mole Fraction (Hogfeldt)} = \bar{X}_i' = \frac{n_{i_{1/z_i}} L}{n_{A_{1/z_i}} L + n_{B_{1/z_i}} L} \qquad (58)$$

where L represents the exchanger. It can be shown that the Hogfeldt mole fraction is numerically equal to the cation equivalent fraction E_i. Thus, applying the Gibbs-Duhem equation:

$$\bar{E}_a d\ln \bar{E}_a + \bar{E}_b d\ln \bar{E}_b + \bar{E}_a d\ln h_a + \bar{E}_b d\ln h_b + \frac{n_w}{n_{A_{1/z_i}L} + n_{B_{1/z_i}L}} d\ln \bar{a}_w = 0 \qquad (59)$$

Where h_a and h_b are the Hogfeldt activity coefficients. Since $d\bar{E}_a + d\bar{E}_b = 0$:

$$\bar{E}_a d\ln h_a + \bar{E}_b d\ln h_b + \frac{n_w}{n_{A_{1/z_i}\,L} + n_{B_{1/z_i}L}} d\ln \bar{a}_w = 0 \qquad (60)$$

Gaines and Thomas, however, applied the Gibbs-Duhem equation to obtain:

$$n_a d\ln \bar{a}_a + n_b d\ln \bar{a}_b + n_w d\ln \bar{a}_w = 0 \qquad (61)$$

where n_a, n_b and n_w are the number of moles of ions A, B and water respectively. The activity terms are, however, expanded on the cation equivalent fraction scale:

$$n_a d\ln \bar{E}_a g_a + n_b d\ln \bar{E}_b g_b + n_w d\ln \bar{a}_w = 0 \qquad (62)$$

It is this confusion of concentration scales that leads to the discrepancy between equations (19) and (41). Multiplication of equation (62) by $z_a z_b/(z_a n_a + z_b n_b)$ gives:

$$z_b d\,\bar{E}_a + z_a d\,\bar{E}_b + z_b\,\bar{E}_a d\ln g_a + z_a\,\bar{E}_b d\ln g_b + z_a z_b \nu_w d\ln \bar{a}_w = 0 \quad (63)$$

where $\nu_w = z_a z_b(z_a n_a + z_b n_b)$ and, except when $z_a = z_b$, then:

$$z_b d\,\bar{E}_a + z_a d\,\bar{E}_b \neq 0 \quad (64)$$

Ideal conditions are defined such that $f_a=f_b=h_a=h_b=g_a=g_b=1$ and thus, under these conditions, both equations (56) and (60) become:

$$d\ln \bar{a}_w = 0 \quad (65)$$

This is the third condition for ideal behaviour. However, under the same conditions, equation (63) becomes:

$$z_b d\,\bar{E}_a + z_a d\,\bar{E}_b + z_a z_b \nu_w d\ln \bar{a}_w = 0 \quad (66)$$

Thus, when using the Gaines and Thomas approach, the third condition for ideality is not equation (65), but:

$$\frac{d\,\bar{E}_a}{d\ln \bar{a}_w} = \frac{-z_a z_b \nu_w}{(z_b - z_a)} \quad (67)$$

and so, equation (41) should, in fact, contain an extra term:

$$\ln K_a = (z_b - z_a) + \int_0^1 \ln K_c d\,\bar{E}_a + \int_x^y \frac{(z_a - z_b)}{z_a z_b} \cdot \frac{d\,\bar{E}_a}{d\ln \bar{a}_w} . d\ln \bar{a}_w \quad (68)$$

Where the limits of the second integral are:

x: $\ln \bar{a}_w = 0$ ($\bar{E}_a = 1$, $I = 0$)

y: $\ln \bar{a}_w = 0$ ($\bar{E}_b = 1$, $I = 0$)

and I is the ionic strength. Under ideal conditions:

$$\int_x^y \frac{(z_a - z_b)}{z_a z_b} \cdot \frac{d\,\bar{E}_a}{d\ln \bar{a}_w} \cdot d\ln \bar{a}_w = (z_a - z_b) \quad (69)$$

and equation (41) becomes:

$$\ln K_a = \int_0^1 \ln K_c d\,\bar{E}_a \tag{70}$$

Equation (41) is, in fact, an approximation which fails under ideal conditions. It is perfectly valid for non-ideal conditions where the second integral may be ignored.

The criticisms regarding the Gaines and Thomas activity coefficients, g_a and g_b, have also been shown to be incorrect by Barrer and Townsend[15], who demonstrated that the approaches used by Gaines and Thomas and by Bonner et al are equally valid and compatible.The standard Gibbs free energy for reaction (1) per equivalent of exchange is given by:

$$\Delta G^\theta = \left(\frac{\bar{\mu}_a^\theta}{z_a} + \frac{\mu_b^\theta}{z_b}\right) - \left(\frac{\bar{\mu}_b^\theta}{z_b} + \frac{\mu_a^\theta}{z_a}\right) \tag{71}$$

and:

$$K_a = e^{-z_a z_b \Delta G^\theta / RT} \tag{72}$$

It therefore follows that if the reference states for solid and solution phases are chosen as before (section 2.3) then the values for ΔG^θ must be the same. The Bonner et al corrected selectivity coefficient, K_v, defines K_a according to the following equation:

$$\ln K_a = \int_0^1 \ln K_v \, d\,\bar{E}_a \tag{73}$$

whereas Gaines and Thomas define K_a as:

$$\ln K_a = (z_a + z_b) + \int_0^1 \ln K_g \, d\,\bar{E}_a \tag{74}$$

K_g being the Gaines and Thomas corrected selectivity coefficient. It follows, therefore, that if both these equations are valid, equations (73) and (74) can be equated to give:

$$\int_0^1 \ln \left(\frac{K_v}{K_g}\right) d\,\bar{E}_a = z_b - z_a \tag{75}$$

K_v and K_g are defined as follows:

$$K_v = \frac{a_b^{z_a} \cdot \bar{X}_a^{z_b}}{a_a^{z_b} \cdot \bar{X}_b^{z_a}} \tag{76}$$

$$K_g = \frac{a_b^{z_a} \cdot \bar{E}_a^{z_b}}{a_a^{z_b} \cdot \bar{E}_b^{z_a}} \tag{77}$$

and therefore:

$$\frac{K_v}{K_g} = \frac{\bar{X}_a^{z_b} \cdot \bar{E}_b^{z_a}}{\bar{X}_b^{z_a} \cdot \bar{E}_a^{z_b}} \tag{78}$$

It can be shown that[15]:

$$\bar{X}_a = \frac{z_b \bar{E}_a}{[z_a + (z_b - z_a) \bar{E}_a]} \tag{79}$$

$$\bar{X}_b = \frac{z_a \bar{E}_b}{[z_b + (z_a - z_b) \bar{E}_b]} \tag{80}$$

and substituting these into equation (78):

$$\frac{K_v}{K_g} = \frac{z_b^{z_b}}{z_a^{z_a}}[z_a + (z_b - z_a) \bar{E}_a]^{(z_a - z_b)} \tag{81}$$

Thus, if both treatments are equally valid, it follows from equations (75) and (81) that:

$$\int_0^1 \ln\left(\frac{z_b^{z_b}}{z_a^{z_a}}\right) d\bar{E}_a + \int_0^1 (z_a - z_b) \ln[z_a + (z_b - z_a) \bar{E}_a] d\bar{E}_a = z_b - z_a \tag{82}$$

The first integral (I_1) is equal to $z_b \ln z_b - z_a \ln z_a$, and the second integral (I_2) gives the standard form:

$$I_2 = \int_{\bar{E}_a=0}^{\bar{E}_a=1} \ln[z_a + (z_b - z_a) \bar{E}_a] d[(z_a + \{z_b - z_a\}) \bar{E}_a]$$

$$= -z_b \ln z_b + z_a \ln z_a + z_a - z_b \tag{83}$$

and therefore:

$$I_1 + I_2 = z_b - z_a \tag{84}$$

This result proves that the two approaches are equally valid and compatible. If the activity coefficients f_a and f_b are to be regarded as being true activity coefficients, so must the coefficients g_a and g_b.

The two sets of activity coefficients can now be related through equations (79) and (80):

$$g_a = \frac{f_a}{z_a}[z_b + (z_a - z_b)\,\bar{X}_a] \tag{85}$$

$$g_b = \frac{f_b}{z_b}[z_a + (z_b - z_a)\,\bar{X}_b] \tag{86}$$

and inspection of these equations shows that for any values of z_a and z_b:

$$\text{Lim}_{\bar{E}_a \to 1}\ g_a = f_a = 1 \tag{87}$$

$$\text{Lim}_{\bar{E}_b \to 1}\ g_b = f_b = 1 \tag{88}$$

Thus, in conclusion, the approach adopted by Gaines and Thomas is perfectly valid and produces activity coefficients which may be regarded as true activity coefficients. Additionally, these activity coefficients may be used in detailed statistical thermodynamic formulations, provided that the concentration scale is consistent with that used by Gaines and Thomas.

2.6 References

1. D. W. Breck, "Zeolite Molecular Sieves", John Wiley and Sons, New York, (1974), 532
2. R. M. Barrrer and J. Falconer, Proc. Roy. Soc. (London), **A236**, (1956), 227
3. D. W. Breck, J. Chem Ed., **41**, (1964), 678
4. P. C. Huang, A. Mizany and J. L. Pauley, J. Chem. Phys., **68**, (1966), 2575
5. F. Helfferich, "Ion Exchange", McGraw Hill, New York, (1962), 166
6. B. Munday, PhD. Thesis, "University of London", (1978)
7. R. M. Barrer, L. V. C. Rees and D. J. Ward, Proc. Roy. Soc., **A273**, (1963), 180
8. S. A. I. Barri, D.I.C. Thesis, "University of London", (1978)
9. J. Kielland, J. Soc. Chem. Ind., **54**, (1935), 232T
10. G. L. Gaines and H. C. Thomas, J. Chem Phys., **21(4)**, (1953), 714
11. R. M. Barrer and J. Klinowski, J. Chem. Soc, Farad. Trans. I, **70**, (1974), 2080

12. G. Sposisto, A.S.A. Spec. Publ., **40**, (1981), 13
13. G. Sposisto and S. V. Mattigod, Clays Clay Miner., **27**, (1979), 125
14. G. Sposisto, "Thermodynamics of Soil Solutions", Oxford Clarendon Press, (1980), 125
15. R. M. Barrer and R. P. Townsend, J. Chem. Soc. Farad. Trans. II, **80**, (1984), 150
16. R. M. Barrer and R. P. Townsend, Zeolites, **5**, (1985), 287
17. R. P. Townsend, Proc 7th Int. Zeolite Conf. (Tokyo), Butterworths, (1986), 273
18. O. D. Bonner, W. J. Argersinger and A. W. Davidson, J. Am. Chem. Soc., **74**, (1952), 1044
19. E. Hogfeldt, Arkiv. for Kemi, **5**, (1953),147

Chapter Three

The Synthesis and Characterisation of Aluminosilicate Gels

3.1 Introduction

Two sets of samples of varying reaction times were prepared using standard techniques for the synthesis of zeolites. One of these sets of samples was based on the synthesis of zeolite A, the other on the synthesis of zeolite X. In the case of the zeolite A synthesis samples, the reaction times ranged from 0 hours to 14 hours. This range was 0 hours to 24 hours for the zeolite X synthesis samples. Thus, both sets of samples included totally amorphous aluminosilicates and crystalline zeolites.

All samples were characterised using the following techniques:

1. Infra-Red (IR) Spectroscopy
2. X-Ray Diffraction (XRD)
3. Scanning Electron Microscopy (SEM)
4. Water Capacity Determination
5. Chemical Analysis
6. Particle Size Analysis
7. Solid State NMR (MAS-NMR)

This chapter describes the synthesis and the characterisation of these materials. For the sake of brevity, each sample has been coded according to its synthetic route (either A or X) and its reaction time. Thus, sample A0 is a sample prepared using a zeolite A synthesis and with a reaction time of 0 hours. Similarly, sample X12 is a zeolite X synthesis sample with a reaction time of 12 hours.

3.2 The Synthesis of Zeolite A Type Aluminosilicate Gels

Aluminosilicate gels based on the synthesis of zeolite A were prepared using a method based on that described by Meise and Schwochow[1]. The molar composition of the reaction mixture was SiO_2/Al_2O_3 = 2.00; Na_2O/SiO_2 = 2.50; H_2O/Na_2O = 40. The aluminium source was a sodium aluminate solution prepared by dissolving aluminium hydroxide (BDH GPR Grade; 86.60g per litre) in boiling sodium hydroxide solution (BDH Analar; 122.0g per litre). The use of sodium aluminate (BDH Lab Reagent) as an aluminium source was avoided because, even when fresh, this material was clearly discoloured and, presumably, contaminated. Silica was provided by a sodium silicate solution prepared from colloidal silica (BDH Lab Reagent; 66.7g per litre) dissolved in sodium hydroxide solution (BDH Analar; 100.0g per litre). Both solutions were filtered before use to remove any undissolved material.

To prepare aluminosilicate gel samples, the sodium aluminate solution (1 litre) was slowly added to the sodium silicate solution (1 litre) in a polythene vessel and the mixture thoroughly stirred until a homogeneous gelatinous white liquid resulted. This was divided equally between ten polythene screw cap bottles which were then placed in an oven at 80°C. Ten samples were prepared by varying the reaction time between 0 and 14 hours. Reaction was terminated by filtration under vacuum followed by thorough washing of the precipitate with distilled deionised water until the pH of the washings fell below pH 8. All samples were then air dried for 24 hours.

It was important to ensure that all samples were obtained in the pure sodium form. After air drying, therefore, each sample was twice exchanged with concentrated sodium chloride solution (BDH Analar; ≈ 1.0M). Excess sodium chloride was removed by washing the samples, until chloride free (acidified silver nitrate test), with distilled deionised water adjusted to pH 10 using sodium hydroxide solution (BDH Analar). If neutral or acidic water is used, it is possible to remove some of the sodium ions from within the framework, these being replaced by hydronium ions. This hydronium ion exchange is readily demonstrated by mixing sodium zeolites with untreated distilled deionised water. In the cases of both zeolite A and zeolite X, the pH of the water rapidly rises to around pH 10 as hydronium ion migrate to the zeolite phase. Finally, all samples were dried in an oven at 40-50°C. Higher temperatures were not used to avoid possible thermal degradation of the gel samples.

3.3 The Synthesis of Zeolite X Type Aluminosilicate Gels

Aluminosilicate gels based on the synthesis of zeolite X were prepared from a reaction mixture of molar composition SiO_2/Al_2O_3 = 3.00; Na_2O/SiO_2 = 1.20; H_2O/Na_2O = 40. Aluminium was provided, as in the synthesis of zeolite A type gels, by dissolving aluminium hydroxide (BDH GPR Grade; 120.40g per litre) in boiling sodium hydroxide solution (BDH Analar; 122.0g per litre). Silica was provided by a sodium silicate solution prepared from colloidal silica (BDH Lab Reagent; 139.1g per litre) dissolved in sodium hydroxide solution (BDH Analar; 100.0g per litre). Both solutions were filtered before use to remove any undissolved material.

The remaining synthesis conditions and sample pretreatment were identical to those for the zeolite A type samples except that the reaction temperature was 90°C and the reaction time ranged from 0 to 24 hours.

3.4 Sample Characterisation

All of the samples were fine white free-flowing powders. Samples with a long reaction time, that is the more crystalline samples, appeared to have finer particles than those with short reaction times, which had a more grainy appearance. It was also clear that the bulk density of the crystalline samples was significantly greater than that of the amorphous samples. This was to be expected in view of the more open frameworks of the amorphous aluminosilicate gels.

3.4a Infra Red Spectroscopy

Infra Red (IR) spectra were obtained for all samples using a Perkin Elmer 457 Grating Infra Red Spectrophotometer. Samples were prepared as caesium iodide discs using a Specac Specadie. Caesium iodide (BDH IR Grade) was used, rather than the more usual potassium bromide, because it allows observation of vibrations down to 250cm^{-1}, whereas potassium bromide "cuts off" at around 400cm^{-1}.

Tables 3.1 and 3.2 give spectral assignments for zeolite A and zeolite X respectively[2,3]. Mid IR vibrations in the zeolites can be divided into two groups, those due to internal linkages and those due to external linkages. Internal linkage vibrations are due to the TO_4 tetrahedra and are common to all zeolites and amorphous aluminosilicates, with small changes, regardless of structure. External linkage vibrations are assigned to linkages of the TO_4 tetrahedra in a particular framework topology. These vibrations depend purely on the type of structure present and are unique to that structure. Thus each zeolite displays a typical IR spectrum suitable, at least, for the identification of a particular zeolite family.

Table 3.1. IR Spectral Assignments for Zeolite A

ν (cm^{-1})	Strength	Assignment
1115	v. weak sh.	Asym. T-O Stretch
1060	v. weak sh.	Asym. T-O Stretch
995	strong	Asym. T-O Stretch
670	v. weak	Sym. T-O Stretch
560	med. strong	Double Rings
470	med.	T-O Bend
380	med. strong	Pore Opening
260	v. weak broad	Pore Opening

v.=very med.=medium sh.=shoulder sym.=symmetric

The exact position of the vibration at around $995cm^{-1}$ has been related to the Si/Al ratio of the sample[4], this peak shifting towards longer wavelengths as the Si/Al ratio decreases. The frequency of bond stretching vibrations varies

inversely with atomic mass and this would suggest that the substitution of aluminium for silicon should result in higher vibrational frequencies. However, vibrational frequencies are also affected by bond force constants. These vary directly with the electronegativity product of the nuclei and inversely with bond length. Aluminium is less electronegative than silicon and the aluminium-oxygen bond is longer than the silicon-oxygen bond. These two factors combine to produce a reduced force constant and correspondingly lower vibrational frequencies. Unfortunately, this band shift is fairly small, and the range of Si/Al ratios observed in the synthetic samples is too small for it to be clearly seen.

Table 3.2. IR Spectral Assignments for Zeolite X

ν (cm^{-1})	Strength	Assignment
1060	med. sh.	Asym. T-O Stretch
980	strong	Asym. T-O Stretch
750	med.	Sym. T-O Stretch
690	weak sh.	Sym. T-O Stretch
670	med.	Sym. T-O Stretch
565	med.	Double Rings
465	med. strong	T-O Bend
406	weak	Pore Opening
365	med.	Pore Opening
250	v. weak broad	Pore Opening

v.=very med.=medium sh.=shoulder sym.=symmetric

IR spectra can also be used to make approximate crystallinity measurements. Coudurier et al[5] and Jansen et al[6] have both reported the use of IR data in the determination of the approximate crystallinity of ZSM-5 samples, but this method can be extended to other zeolite types. The vibration centred around 470cm^{-1} is assigned to a T-O bend and is exhibited by crystalline zeolites and amorphous materials, such as silica, alike. However, the crystalline zeolites, unlike amorphous materials, also exhibit vibrations due to the external linkages. The optical density ratio of one of these external linkage bands to that at 470cm^{-1} can be calculated and is characteristic of the type of zeolite present. These ratios can also be used to assess the approximate crystallinity of the sample, and, indeed, may be useful probes for the presence of crystalline zeolites since, for very small particles, XRD patterns may give erroneous results.

IR spectra for the zeolite A type samples are presented in Figure 3.1. In zeolite A, the external linkage vibrations occur at 560cm^{-1} (double ring vibration), 380cm^{-1} and 260cm^{-1} (both pore opening vibrations). Optical density ratios have been calculated and are presented in Table 3.3. Band A is at 560cm^{-1} and Band B at 380cm^{-1}. The band at 260cm^{-1} was not used in these calculations because it is a weak vibration which lies in the region where caesium iodide cuts off. Band C is the T-O bending vibration at 470cm^{-1} characteristic of all aluminosilicates. Band ratios were calculated using peak areas measured in arbitrary units.

Crystalline zeolite A has an A:C band ratio of 2.01 (± 0.05) and a B:C ratio of 0.75 (± 0.07). Both these ratios are zero for amorphous aluminosilicates (bands A and B are absent). Sample A3 exhibits an A:C ratio of 1.24 and a B:C ratio of 0.47, both of which indicate an approximate crystallinity of 63%. Samples with reaction times longer than three hours appear to be totally crystalline and those with reaction times less than three hours appear to be totally amorphous.

The IR spectrum of a reference sample of zeolite A (Laporte Industries) was also obtained for comparison. The A:C and B:C band ratios for this sample were 2.01 and 0.71 respectively. Samples with a reaction time in excess of three hours exhibited identical IR spectra to this sample suggesting that pure crystalline zeolite A had been formed.

Figure 3.1. IR Spectra of Zeolite A Type Samples

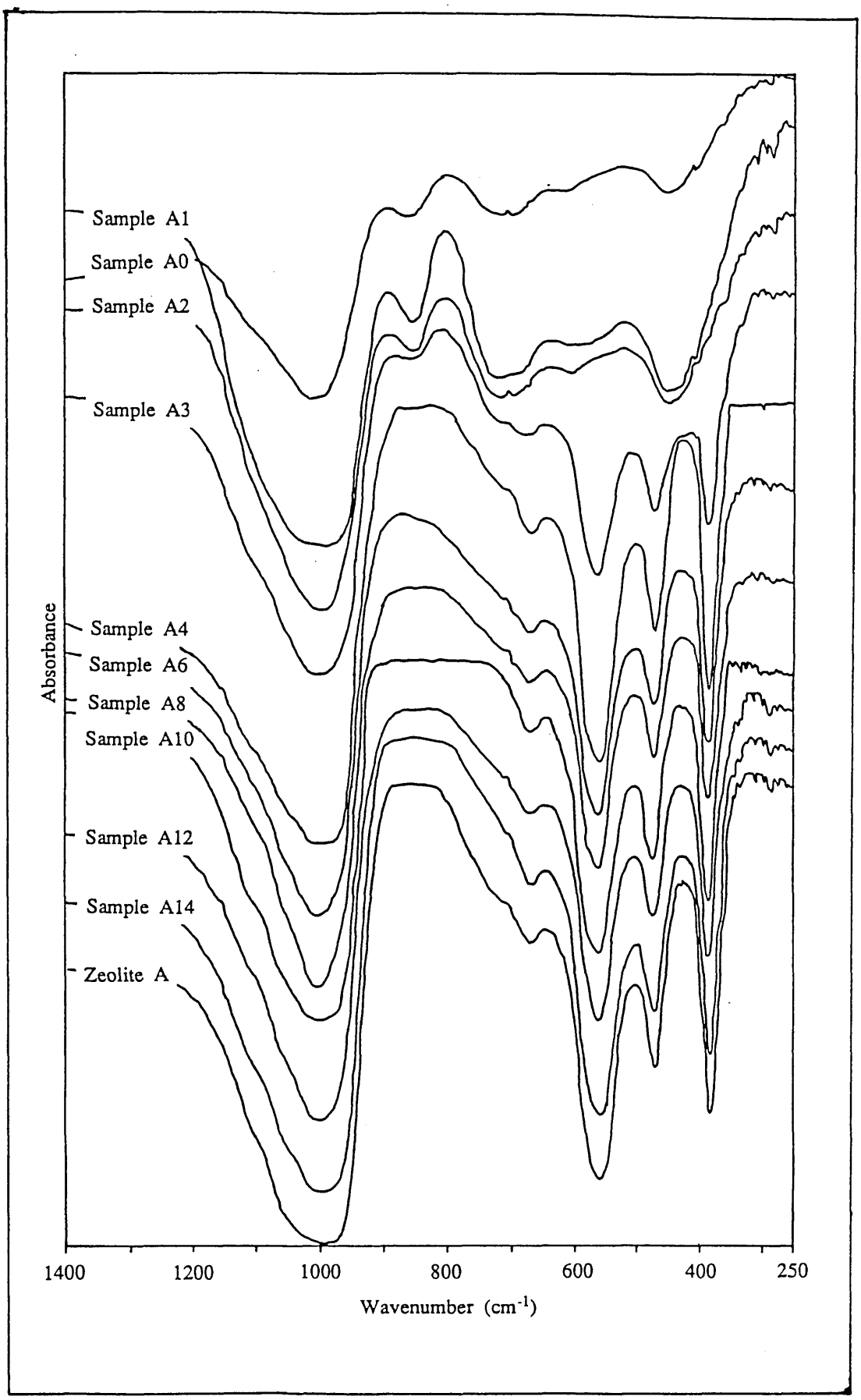

Table 3.3. Approximate Crystallinity Measurements for Zeolite A Type Gels

Sample	Band Areas			Ratios		Crystallinity (%)
	A	B	C	A:C	B:C	
A0	0	0	11.21	0	0	0
A1	0	0	28.06	0	0	0
A2	0	0	17.69	0	0	0
A3	15.92	6.00	12.87	1.24	0.47	63
A4	16.33	5.82	8.10	2.02	0.72	100
A6	16.12	5.67	8.10	1.99	0.70	100
A8	11.75	4.44	5.75	2.04	0.77	100
A10	22.19	8.91	11.34	1.96	0.78	100
A12	15.22	6.09	7.38	2.06	0.82	100
A14	20.48	7.61	10.28	1.99	0.74	100
A(Ref)	20.32	7.22	10.12	2.01	0.71	100

The IR spectra of the zeolite X type samples are shown in figure 3.2. In zeolite X, the external linkage vibrations occur at $565cm^{-1}$ (double ring vibration) and at $406cm^{-1}$, $365cm^{-1}$ and $250cm^{-1}$ (pore opening vibrations). Optical density ratios have also been calculated for these samples and are presented in table 3.4. Band A is at $565cm^{-1}$ and band B is the T-O bending vibration at $465cm^{-1}$. The pore opening vibrations tend to be weak and have not been used in these calculations.

Figure 3.2. IR Spectra of Zeolite X Type Samples

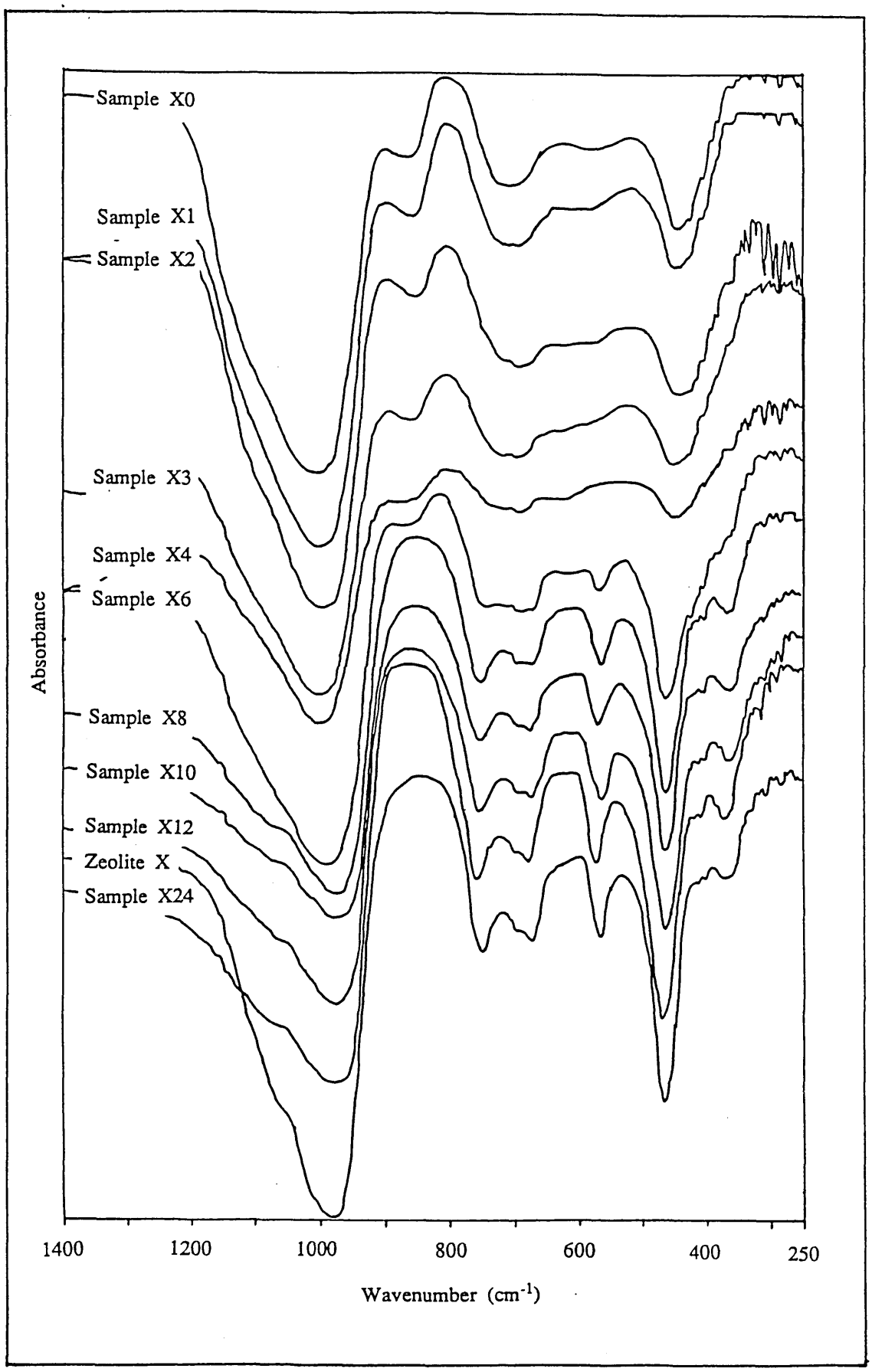

Crystalline zeolite X exhibits an A:B band ratio of 0.51 (± 0.02). Sample X6 shows an optical density ratio of 0.37 which corresponds to an approximate crystallinity of 72%. Samples with a reaction time longer than six hours appear to be totally crystalline whereas those with reaction times less than six hours appear to be amorphous.

A reference sample of zeolite X was also studied for comparison. This exhibits an A:B optical density ratio of 0.49. The IR spectra of samples with a reaction time in excess of six hours are identical to that of this reference sample suggesting that pure crystalline zeolite X has been formed.

Table 3.4. Approximate Crystallinity Measurements for Zeolite X Type Samples

Sample	Band Areas		A:B Ratio	Crystallinity (%)
	A	B		
X0	0	7.24	0	0
X1	0	6.90	0	0
X2	0	9.14	0	0
X3	0	1.80	0	0
X4	0	1.32	0	0
X6	3.00	8.16	0.37	72
X8	4.40	8.80	0.50	100
X10	3.98	7.98	0.50	100
X12	5.40	11.66	0.52	100
X24	7.56	14.43	0.52	100
X(Ref)	5.23	10.71	0.49	100

The IR spectra of the amorphous samples (samples A0 to A2 and samples X0 to X4) appear remarkably similar. They are characterised by broad bands. This is due to the wide variety of chemical environments in which silicon and aluminium atoms exist in these samples. In all cases, the asymmetric T-O stretch is centred around $1000cm^{-1}$. In the zeolite X samples this shifts to lower wavenumbers (longer wavelengths) as zeolite X crystallises suggesting that the aluminosilicate gel has a higher Si/Al ratio than the final crystalline product. In sample X6, for instance, this band is centred at $990cm^{-1}$ and in the remaining crystalline samples (samples X8 to X24) it is centred at $975cm^{-1}$. This is to be expected since the molar Si/Al ratio of the initial gel is higher than that of the final product (section 3.4e). In the synthesis of zeolite A, this band remains centred at around $1000cm^{-1}$ suggesting that the Si/Al ratios of the gel and the crystalline product are similar.

The amorphous samples all exhibit a band centred at around $860cm^{-1}$. This disappears as the zeolite phase crystallises.

3.4b X-Ray Diffraction

Powder X-Ray Diffraction (XRD) patterns were obtained using a Philips 2W 1050 Diffractometer. The radiation source was copper which produces a K_α line at $1.5412 \times 10^{-10}m$. The powder patterns described here were obtained for fully hydrated samples, since partial dehydration affects the intensities[7]. Zeolites A and X have large unit cell constants (12.32Å and 24.93Å respectively) and the X-Ray powder patterns contain many reflections at low diffraction angles. As a result, there is considerable overlap of reflections.

Standard X-Ray data for zeolite A is presented in Table 3.5[7,8] and that for zeolite X is presented in Table 3.6[9,10]. The data includes the Miller Indices (hkl), the spacing (d) and the relative intensity (I).

As has been previously pointed out (section 3.4a), XRD patterns may give unreliable results. If the particle size is small, it may be wrongly concluded that the sample is amorphous. However, the results presented here for both the zeolite A type samples (Figure 3.3) and the zeolite X type samples (Figure 3.4) are supported by the IR data. In the case of the zeolite A type samples, samples A0, A1 and A2 are clearly X-Ray amorphous indicating the absence of crystalline

Figure 3.3 XRD Patterns for Zeolite A Type Samples

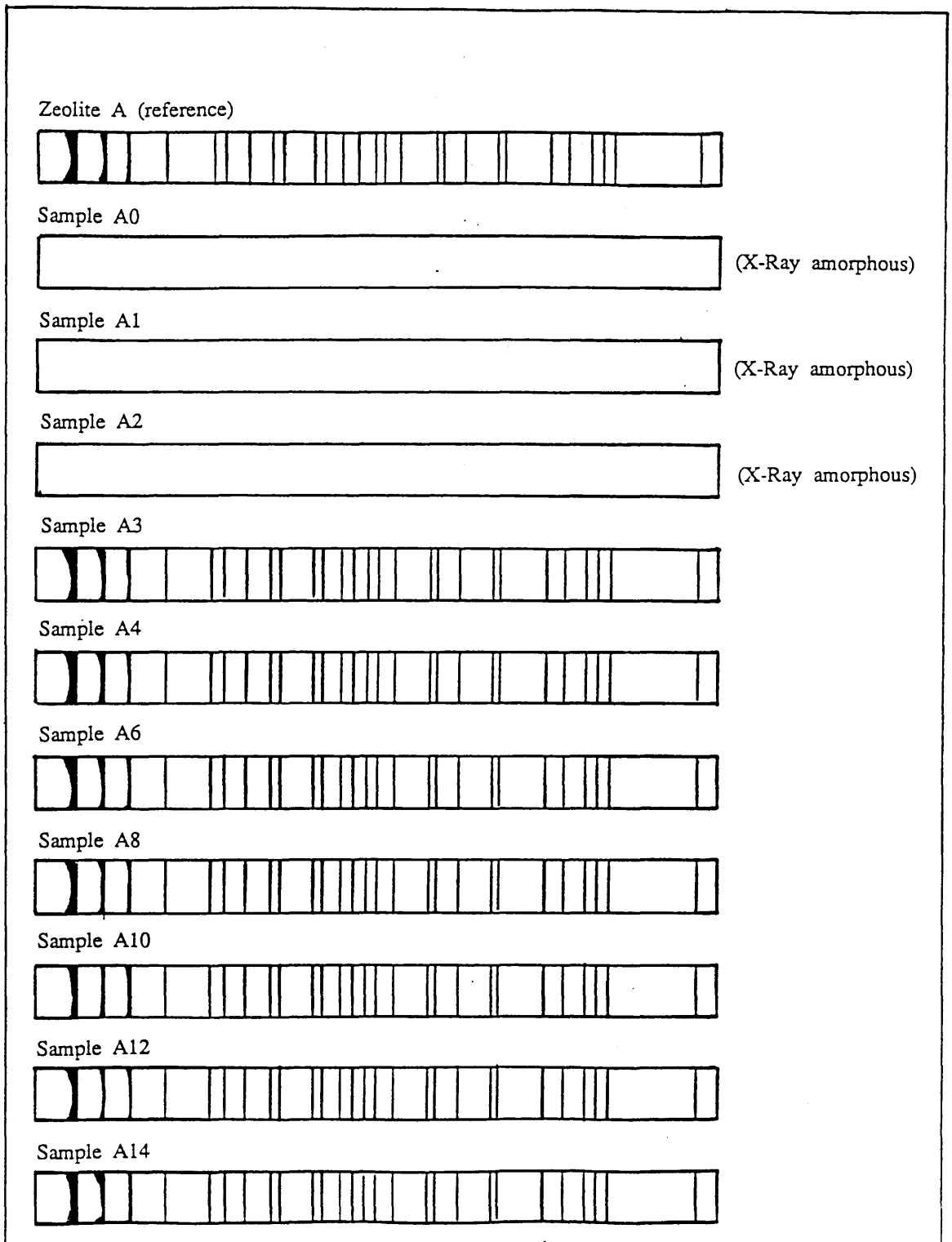

These diagrams show the XRD patterns as obtained on photographic film. Only the most intense bands are shown.

Figure 3.4 XRD Patterns for Zeolite X Type Samples

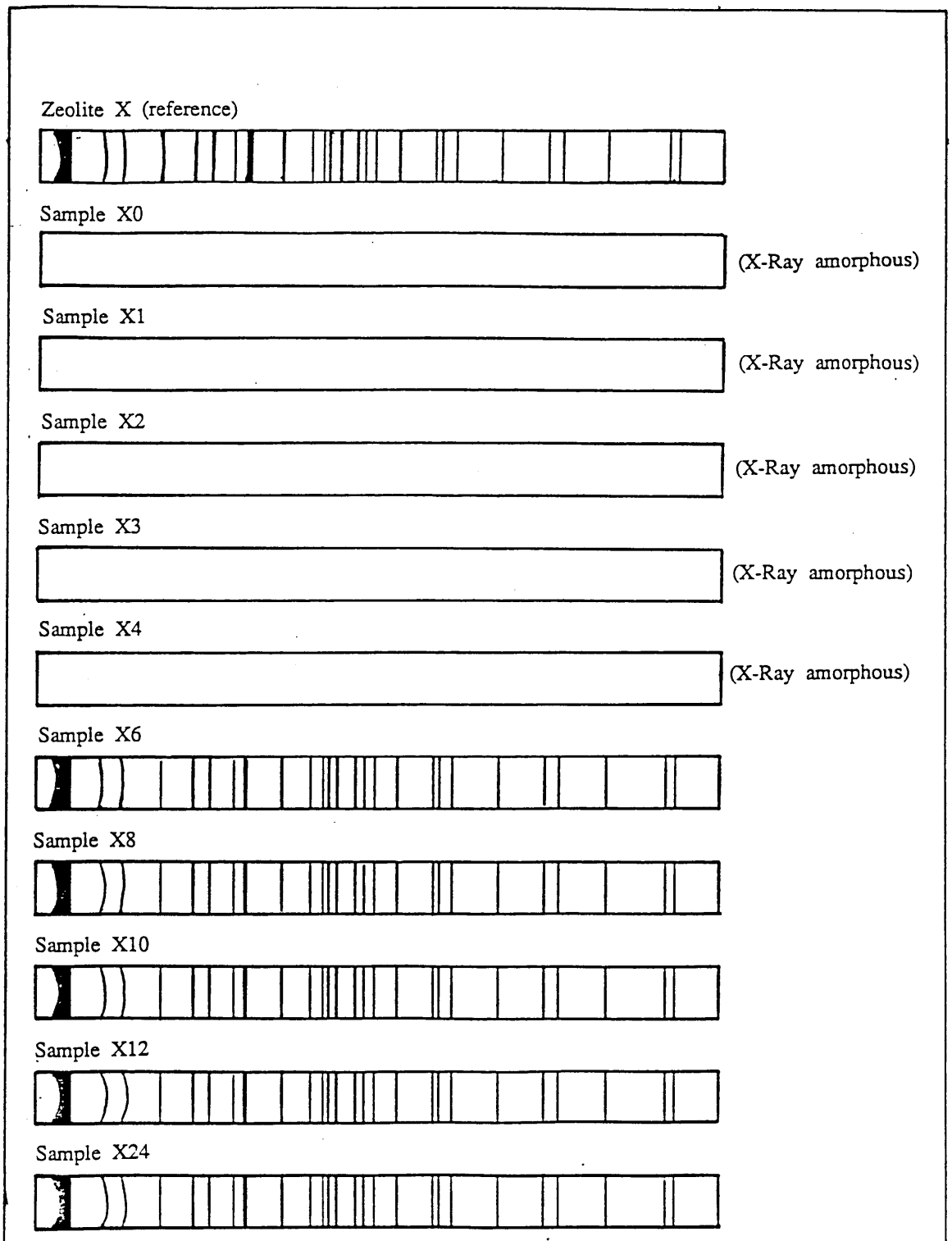

These diagrams show the XRD patterns as obtained on photographic film. Only the most intense bands are shown.

material. Samples with a reaction time of three hours and greater exhibit the characteristc XRD pattern of zeolite A (as compared with a standard zeolite A (Laporte Industries) sample). Similarly for the zeolite X type samples, samples X0, X1, X2, X3 and X4 are X-Ray amorphous. Samples with a reaction time of six hours or more exhibit the characteristic XRD pattern of zeolite X.

Table 3.5. XRD Data for Zeolite A*

hkl	d(Å)	I	hkl	d(Å)	I	hkl	d(Å)	I
100	12.29	100	321	3.293	47	511,333	2.371	3
110	8.71	69	410	2.987	55	520,432	2.289	1
111	7.11	35	411	2.904	9	521	2.249	3
210	5.51	25	420	2.754	12	440	2.177	7
211	5.03	2	421	2.688	4	441,522	2.144	10
220	4.36	6	332	2.626	22	530,433	2.113	3
221,300	4.107	36	422	2.515	5	531	2.083	4
311	3.714	53	430,500	2.464	4	600,442	2.053	9
320	3.417	16						

*$Na_{12}[(AlO_2)_{12}(SiO_2)_{12}].27H_2O$; a=12.32Å

Table 3.6. XRD Data for Zeolite X*

hkl	d(Å)	I	hkl	d(Å)	I	hkl	d(Å)	I
111	14.65	100	620	3.946	4	731,553	3.253	1
220	8.845	18	533	3.808	21	733	3.051	4
311	7.538	12	622	3.765	3	822,660	2.944	9
331	5.731	18	444	3.609	1	751,555	2.885	19
333,551	4.811	5	711,551	3.500	1	840	2.749	8
440	4.419	9	642	3.338	8	911	2.743	2
531	4.226	1						

*Hydrated sodium X (Si/Al=1.25); a=24.93Å

3.4c Scanning Electron Microscopy

Scanning electron microscopy (SEM) was carried out at the Procter and Gamble Newcastle Technical Centre using a JEOL 100CX Temscan. Samples were first mounted onto brass stubs using conducting paint and coated with a thin layer of gold. All samples were examined using a variety of magnifications.

Electron micrographs of the zeolite A type samples are shown in Figures 3.5 to 3.7. Samples A0, A1 and A2 are clearly amorphous and consist of large particles which have a grainy appearance under higher magnifications. A scanning electron micrograph of sample A2 is shown in Figure 3.5. Samples A0 and A1 produced similar micrographs. Sample A3 (Figure 3.6) consists of a mixture of amorphous material, characterised by large grainy particles, and crystalline zeolite A, characterised by small cubic crystals. Samples A4 to A14 (represented by sample A4 in Figure 3.7) all exhibit the characteristic cubic crystals of zeolite A. There is evidence of crystal twinning.

Electron micrographs of the zeolite X type samples are shown in Figures 3.8 to 3.11. Sample X6 (Figures 3.9 and 3.10) consists of a mixture of amorphous material and crystalline zeolite X. All samples with a shorter reaction time (represented by sample X2 in Figure 3.8) are totally amorphous and are again characterised by large particles which have a grainy appearance under higher magnifications. Samples with reaction times longer than six hours (represented by sample X8 in Figure 3.11) consist of crystalline material characteristic of zeolite X. The SEM of sample X8 (Figure 3.11) shows evidence of the presence of a small amount of amorphous material. This is not evident in samples with a longer reaction time.

Figure 3.5. Scanning Electron Micrograph of sample A2 (x20000)

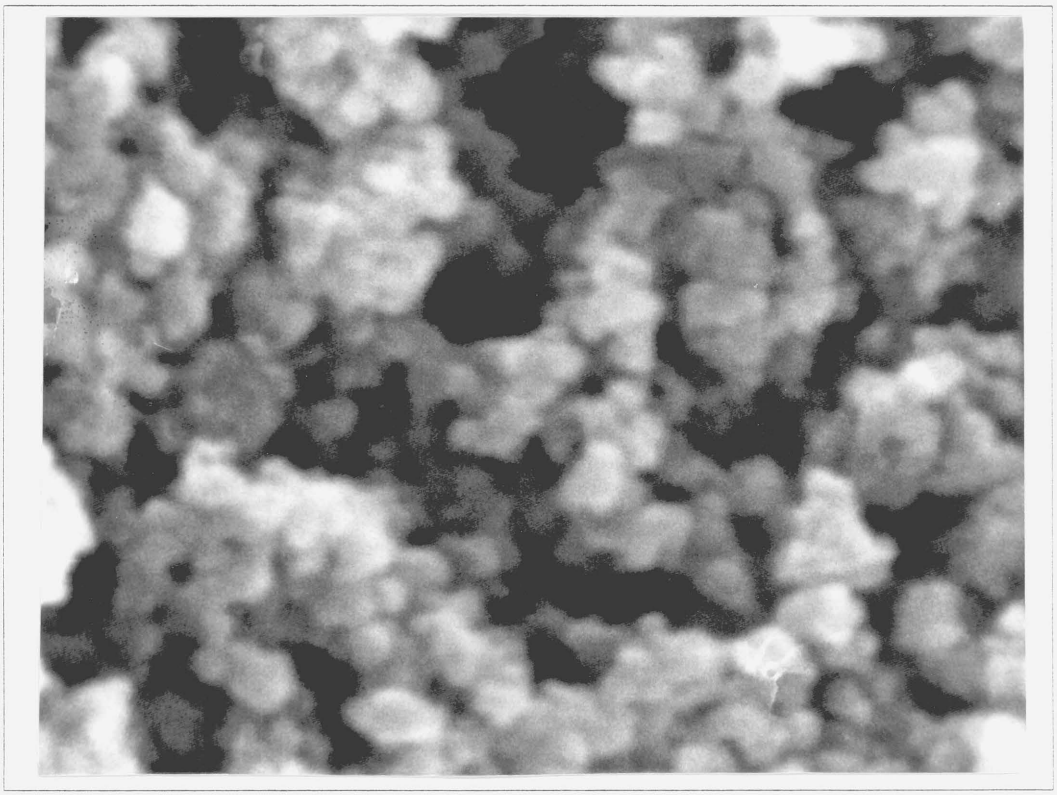

Figure 3.6. Scanning Electron Micrograph of sample A3 (x5000)

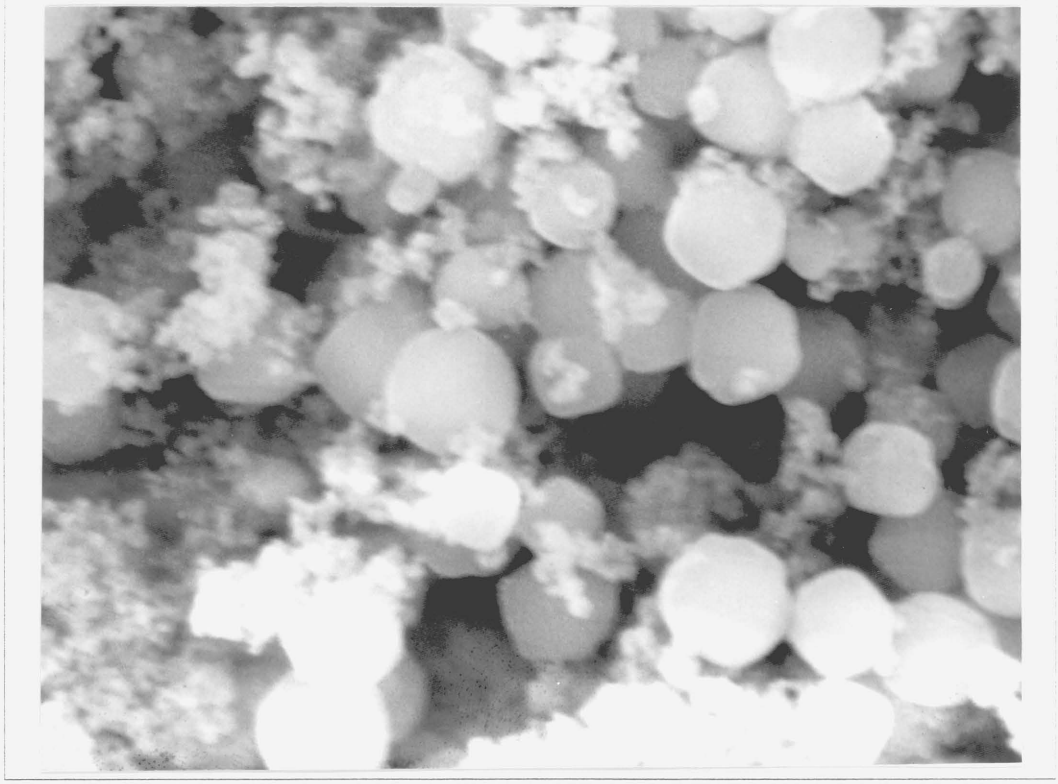

Figure 3.7. Scanning Electron Micrograph of sample A4 (x10000)

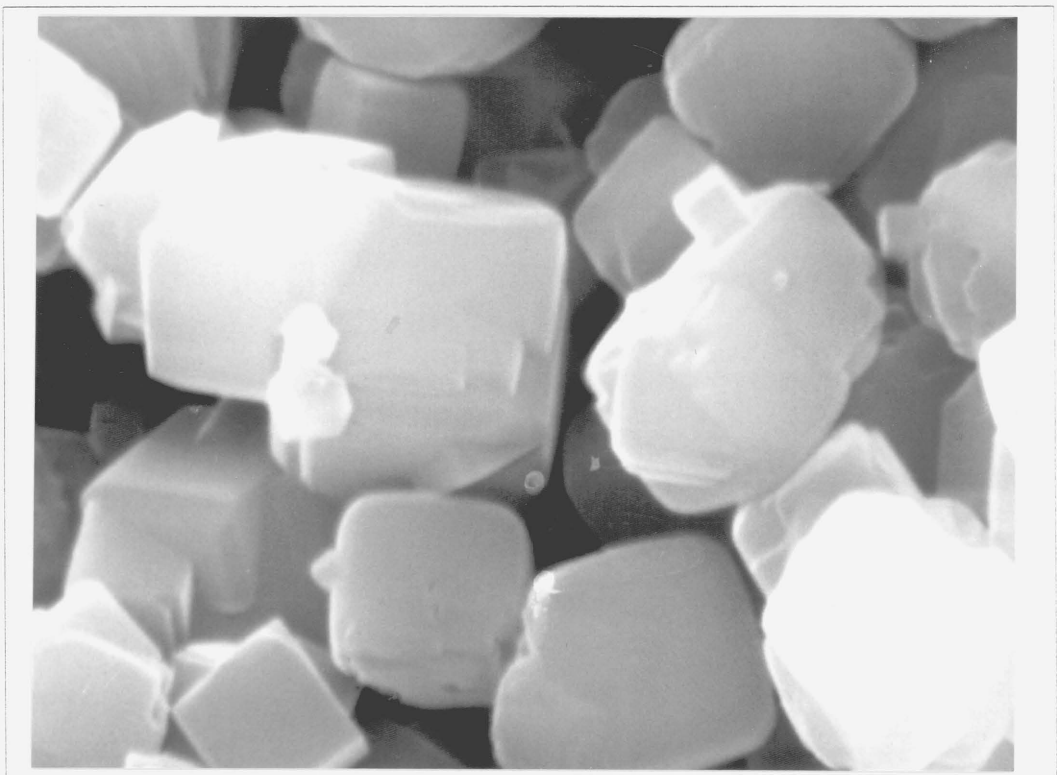

Figure 3.8. Scanning Electron Micrograph of sample X2 (x15000)

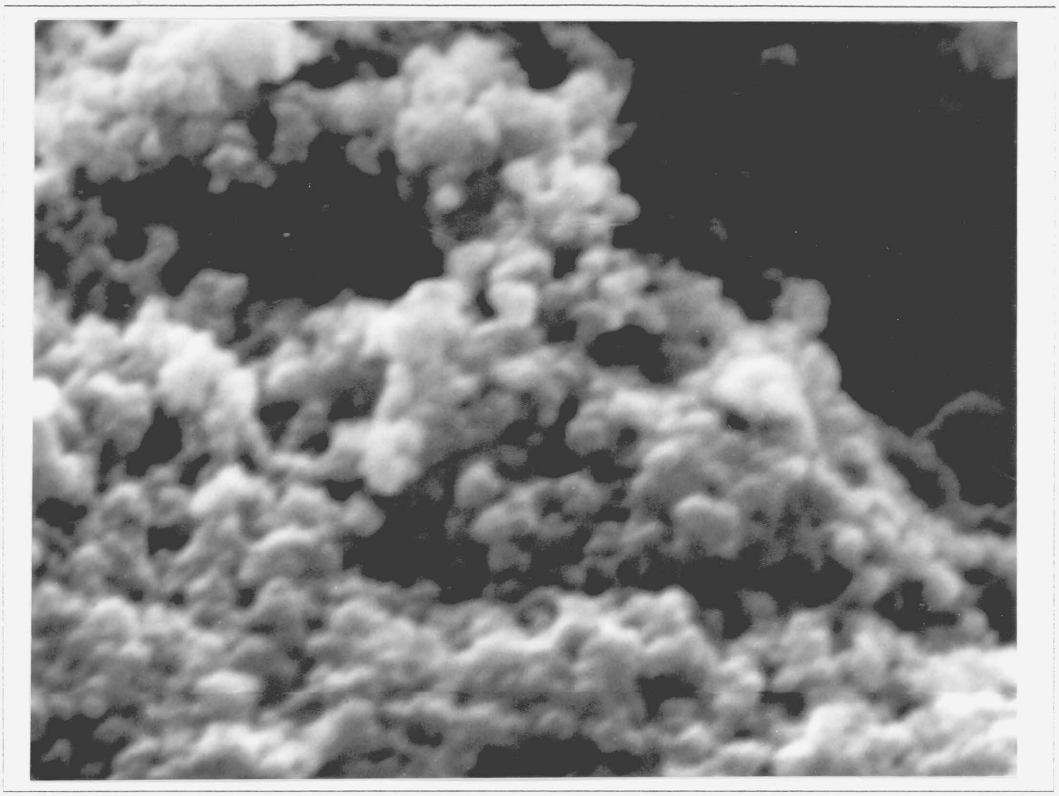

Figure 3.9. Scanning Electron Micrograph of sample X6 (x1500)

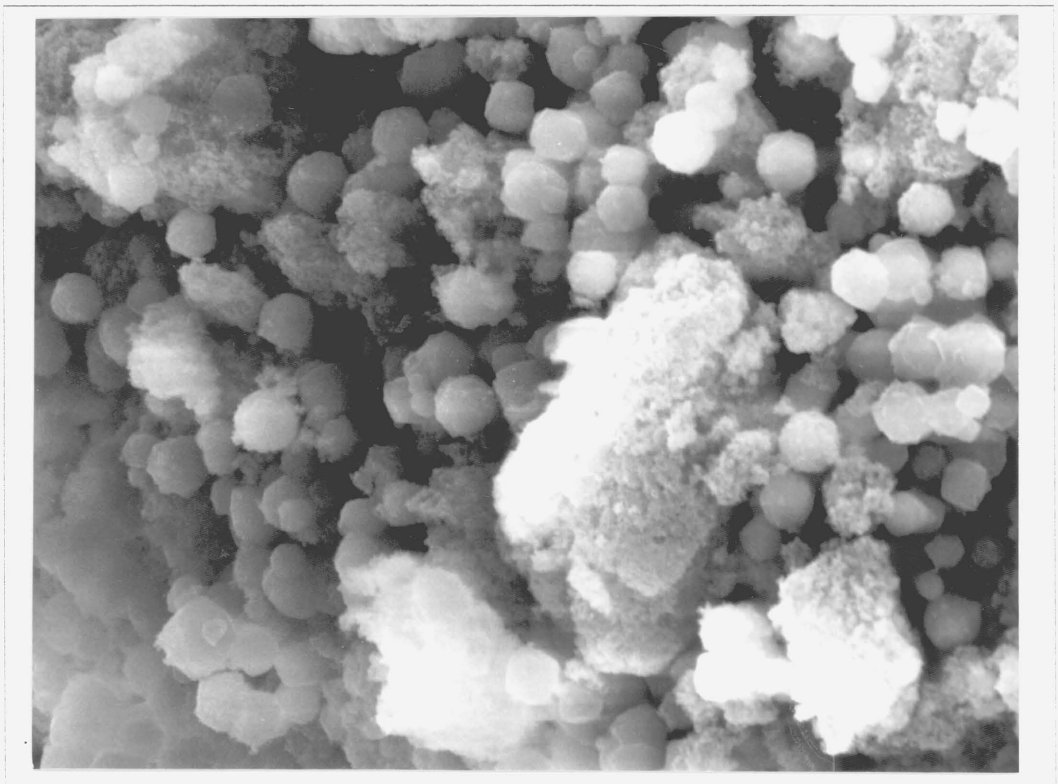

Figure 3.10. Scanning Electron Micrograph of sample X6 (x10000)

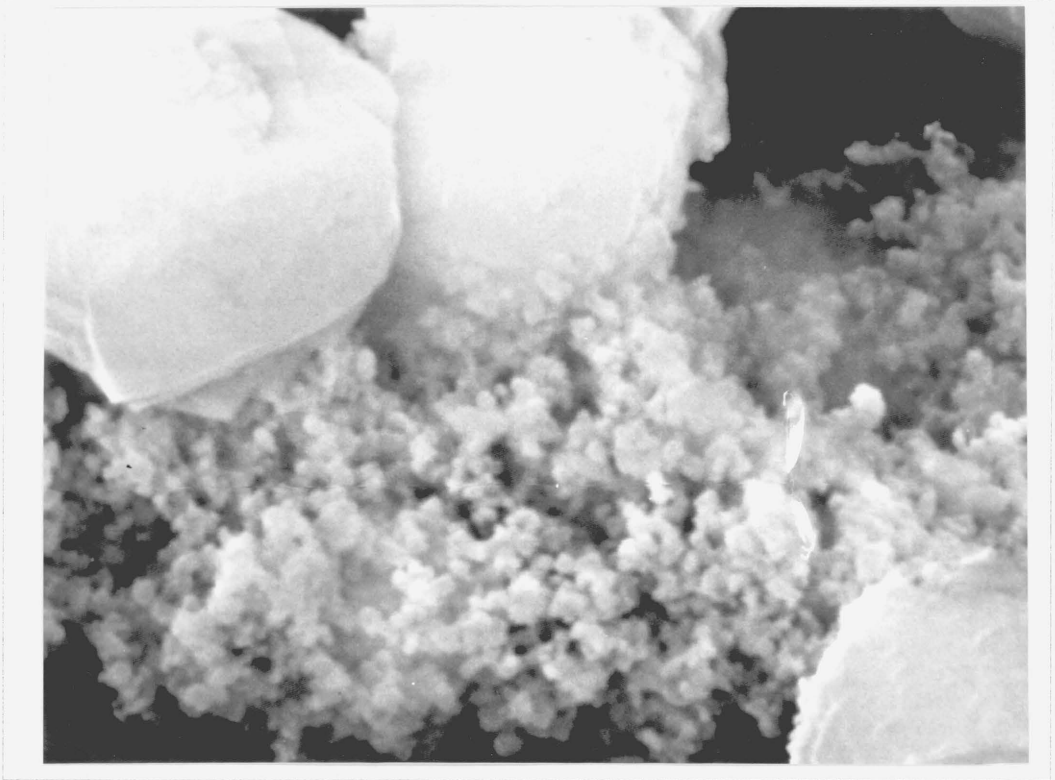

Figure 3.11. Scanning Electron Micrograph of sample X8 (x3500)

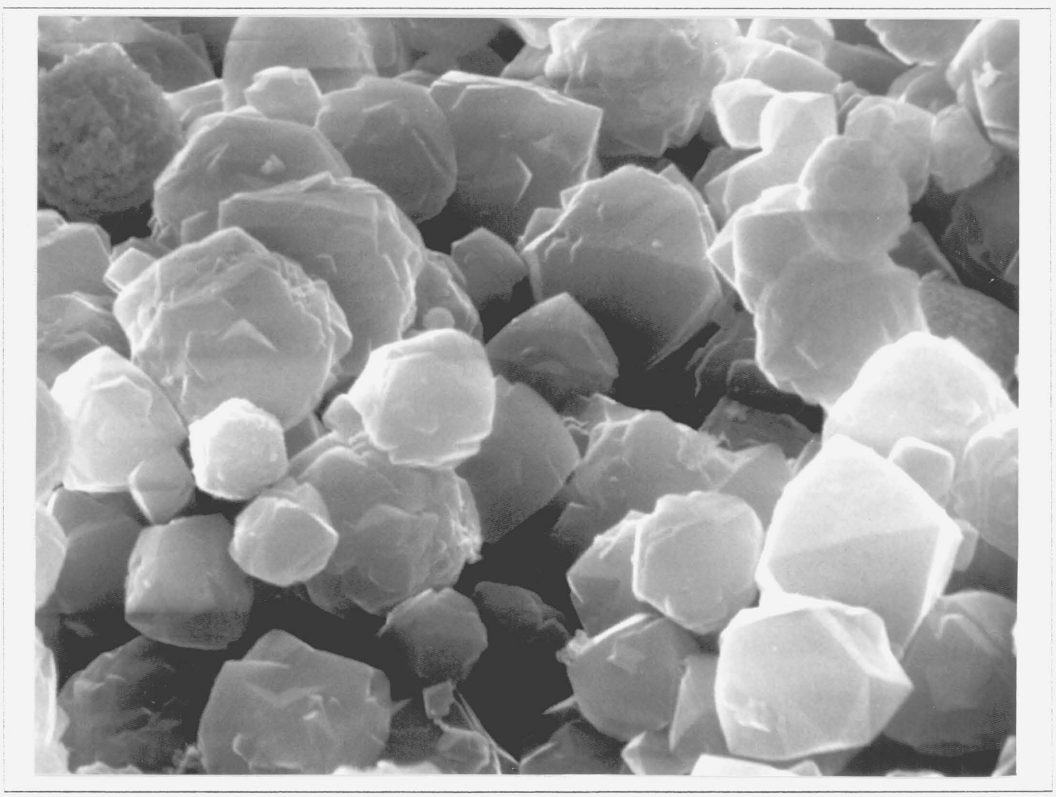

3.4d Water Capacity Determination

The water capacities of all samples were determined by heating them in a furnace at 350°C. Small accurately known weights of each fully hydrated sample were placed in small glass volumetric flasks (5ml). The unstoppered flasks were placed in the furnace overnight and, after cooling in a desiccator over silica gel, were stoppered and reweighed. The observed weight loss was assigned to water loss and was used to calculate water capacities. The dehydrated samples were then re-equilibrated with water vapour in a desiccator over saturated sodium chloride solution. When they had achieved constant weight they were again dehydrated overnight in a furnace at 350°C and the weight loss used to calculate calcined water capacities.

Water capacities for the zeolite A type samples are given in Table 3.7 and are shown in Figure 3.12. The amorphous samples (samples A0, A1 and A2) exhibit high uncalcined water capacities consistent with the more open structures of aluminosilicate gels, but after calcination this water capacity is not achieved. The reason for this is that the amorphous samples are not as thermally stable as the crystalline samples and, under the conditions of dehydration (350°C), structural collapse occurs. The sodium form of zeolite A first shows signs of structural degradation at 660°C and the structure is 50% decomposed at 755°C[11]. The temperature used here is sufficient to dehydrate the samples, but not sufficient to cause structural degradation of the crystalline samples. Calcined water capacities can, therefore be used as a probe for crystalline zeolite A. Sample A3, as expected from the previous data, exhibits a water capacity intermediate between that of the amorphous gel samples and that of the crystalline zeolite A samples. The crystalline samples (samples A4 to A14) exhibit an average water capacity of 21.03 (± 0.29)% and an average calcined water capacity of 20.79 (± 0.29)%.

Table 3.7. Water capacities of Zeolite A Type Samples

Sample	Uncalcined Water Capacity (Wt. %)	Calcined Water Capacity (Wt. %)
A0	27.43	2.53
A1	28.13	2.42
A2	27.55	2.59
A3	22.85	17.09
A4	21.01	20.73
A6	21.12	20.83
A8	20.74	20.51
A10	21.07	20.87
A12	21.28	21.08
A14	20.96	20.73

Water capacities for the zeolite X type samples are presented in Table 3.8 and in figure 3.13. The uncalcined water capacities of the amorphous samples are variable, but, as with the zeolite A type samples, their calcined water capacities are significantly lower due to structural collapse. The pure sodium form of crystalline zeolite X first shows signs of structural degradation at 660°C and is 50% decomposed at 770°C[11].

Figure 3.12. Water Capacities of Zeolite A type Samples

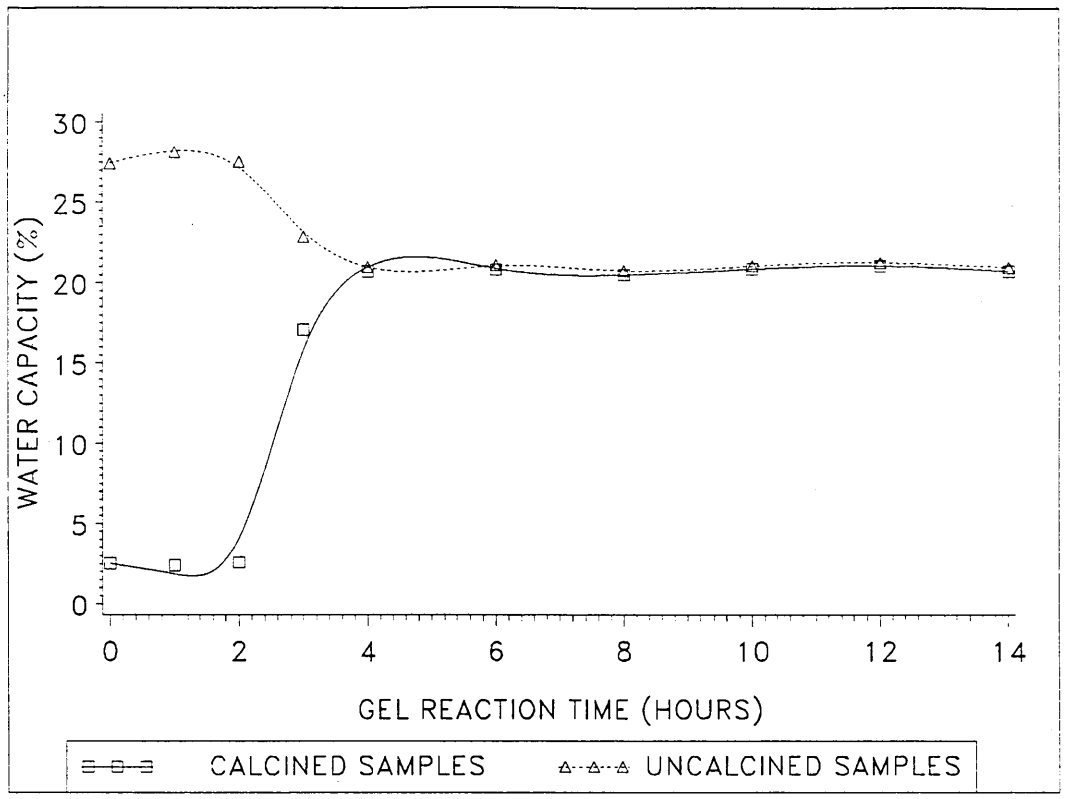

It is interesting to note that the uncalcined water capacities of the amorphous samples (samples X0 to X6) are generally slightly lower than those of the crystalline samples (samples X8 to X24). At first sight, this would appear to suggest that the gel structure is more dense than that of zeolite X. This is clearly not the case, since the bulk density of the gel samples was clearly significantly less than that of the crystalline samples. Alternative explanations are that the gel structure is less hydrophilic than zeolite X or that there are fewer sites available for water vapour sorption. The former explanation seems possible, since the IR data indicates that the Si/Al ratio of the gel samples is higher than that of the crystalline samples. The gel samples would, therefore, be expected to be less hydrophilic than zeolite X.

Table 3.8. Water Capacities of Zeolite X Type Samples

Sample	Uncalcined Water Capacity (Wt. %)	Calcined Water Capacity (Wt. %)
X0	25.54	8.22
X1	24.42	5.68
X2	24.92	4.86
X3	22.50	4.58
X4	21.89	4.65
X6	22.76	13.13
X8	25.23	24.77
X10	25.87	24.73
X12	25.25	25.00
X24	25.43	24.99

Again, calcined water capacities have proved to be a sensitive probe for crystalline zeolite X. As the previous characterisation data would suggest, sample X6 exhibits a calcined water capacity intermediate between that of amorphous aluminosilicate gels and crystalline zeolite X. The crystalline samples exhibit an average uncalcined water capacity of 25.44 (± 0.43)%. On calcination this average is 24.87 (± 0.13)%.

Figure 3.13. Water Capacities of the Zeolite X Type Samples

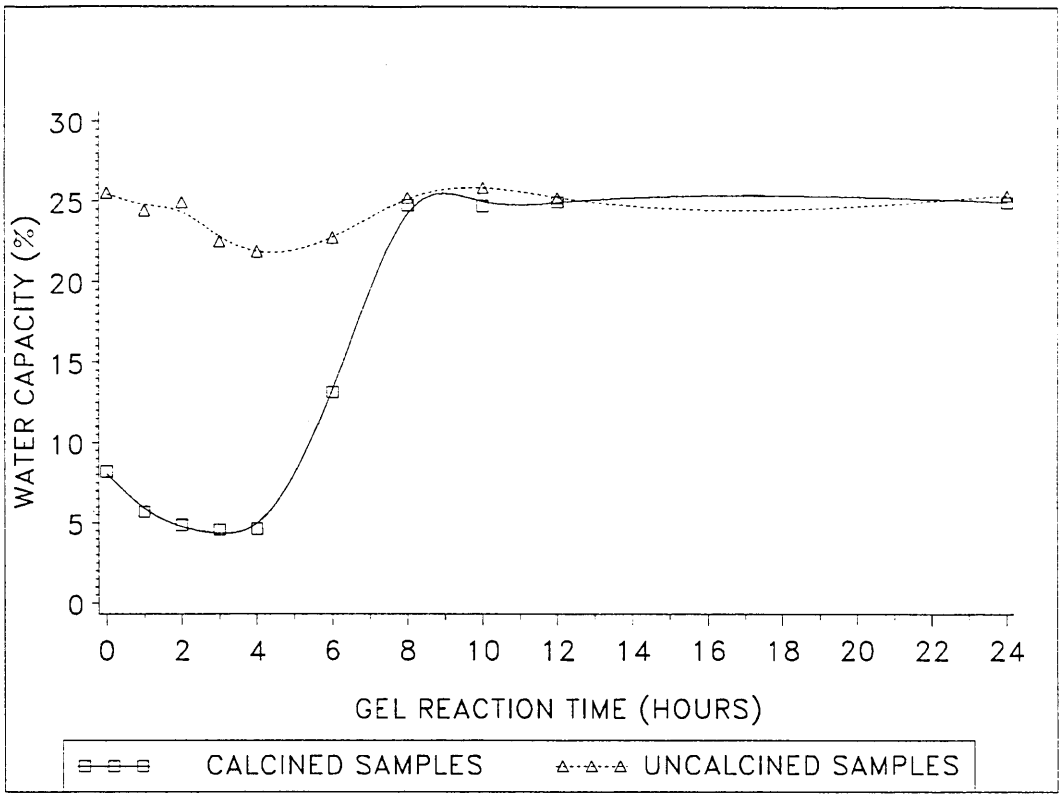

3.4e Chemical Analysis

Chemical analysis was carried out by dissolving samples in a mixture of hydrochloric and hydrofluoric acids. Small amounts of each sample (0.05-0.1g) were accurately weighed into teflon beakers and wetted with distilled deionised water (10ml). Hydrochloric acid (Specific Gravity 1.18; 10ml) was added to this mixture followed by hydrofluoric acid (40% Solution; 1ml). Generally the samples dissolved fairly rapidly, but to ensure complete dissolution, the beakers were covered and left overnight. The resultant solutions were diluted to 100ml with distilled deionised water in plastic volumetric flasks (since hydrofluoric acid attacks glass) and analysed for silicon and aluminium using a Perkin Elmer 2380 Atomic Absorption Spectrophotometer. A radiochemical method was used for sodium analysis (see chapter four).

Both aluminium and silicon are easily ionised in the spectrophotometer flame and, consequently, an ionisation suppressant is required. In this case, 1000ppm Cs^+ was added to each solution (as Caesium chloride; BDH Analar) including blank and standard solutions. In fact, all the alkali metals, because of the ease with which they ionise, are suitable as ionisation suppressants.

Silicon is conventionally analysed from a solution adjusted to pH 5. The solutions prepared here were all in the range pH 1-2. However, this was found to be perfectly adequate for accurate silicon analysis and no adjustment was made to the solution pH. Chemical matrix effects were minimised by ensuring, as far as possible, that all solutions, including blank and standard solutions, contained the same chemical matrix.

The chemical analyses of the zeolite A type samples are presented in Table 3.9. The initial product (sample A0) has an Si/Al ratio of 1.3. Since the Si/Al ratio of the initial reaction mixture was 1.00, the precipitated gel phase is rich in silicon and the liquid phase is rich in dissolved aluminium species. As the reaction proceeds, the Si/Al ratio of the solid phase drops to a value of 1.02 (sample A6). Initially, this decreasing Si/Al ratio may be ascribed to the more rapid dissolution of silicate species from the solid phase. However, as the reaction proceeds, the deposition of crystalline zeolite A, an aluminium rich phase, would also account for this observation. As the reaction proceeds beyond six hours, there are fluctuations in the Si/Al ratio. This may be explained by experimental error in the analysis, although it is also possible that minor variations in the reaction conditions (e.g. temperature or composition) may be responsible. Alternatively, for samples with longer reaction times, further reaction may have taken place. Zeolite A is a metastable phase and recrystallisation to zeolite P is known to occur. Zeolite P has an Si/Al ratio in the range 1.1 to 2.5 and crystallisation of small amounts of this zeolite would lead to an increase in the observed Si/Al ratio. The IR and XRD data from earlier attempts to synthesise both zeolites A and X clearly showed contamination by zeolite P. However, the IR spectra and XRD patterns of these samples indicate that zeolite P is absent, even in sample A14, which has the longest reaction time of the samples synthesised.

The crystalline samples (samples A6 to A14) have an average Si/Al ratio of 1.05 (± 0.04). This corresponds to an average unit cell formula for these samples of $Na_{11.71}[(AlO_2)_{11.71}(SiO_2)_{12.29}].25H_2O$. Unit cell formulae have been calculated for each of the zeolite A type samples using the pseudo-cell of 24 tetrahedra. In the case of the amorphous samples, the unit cell formulae are somewhat meaningless, since the term "unit cell" is a crystallographic term applied to crystalline samples. However, these formulae are useful for the purposes of comparison and it has been suggested that the gel phase in zeolite A synthesis has the structure of crystalline zeolite A without the long range ordering[12].

Sodium to aluminium ratios have also been calculated using the data from chapter four (section 4.2). These are generally close to unity, although for the crystalline samples there does appear to be a slight excess of sodium. This is probably due to experimental error. Octahedral aluminium in the framework does not give rise to a framework charge and the presence of octahedral aluminium should, in theory, be indicated by Na/Al ratios less than unity. These samples would appear to contain little or no octahedral aluminium, but it should be stressed that chemical analysis is not a very sensitive technique for the detection of octahedral aluminium and, indeed may give misleading results if species such as $NaAlO_2$ are present. This apparent absence of octahedrally co-ordinated aluminium is consistent with the view that both silicon and aluminium exist in four fold co-ordination under the conditions of synthesis.

Chemical analysis results for the zeolite X type samples are presented in Table 3.10. For the purposes of comparison, unit cell formulae have again been determined for all samples, including the amorphous gels, using the unit cell of 192 tetrahedra.

The Si/Al ratio of the first formed solid (sample X0) is higher than that of the initial reaction mixture (Si/Al=1.50), suggesting that the solid phase is silicon rich compared to the liquid phase. This is effect is not as marked as in the synthesis of zeolite A. As the reaction proceeds, the Si/Al ratio of the solid phase falls until crystalline zeolite X is produced. The crystalline samples (samples X8 to X24) exhibit an average Si/Al ratio of 1.27 (± 0.02), corresponding to an average unit cell formula for these samples of $Na_{84.58}[(AlO_2)_{84.58}(SiO_2)_{107.42}].254H_2O$. The variation in observed Si/Al ratios is much smaller (± 1.5%) than for the zeolite A type samples and is probably due to experimental error. Again, it is also possible that variation in reaction conditions may have occurred or that further reaction, to zeolite P for instance, may have taken place, but the IR spectra and XRD patterns of the crystalline samples suggest that pure zeolite X has been formed.

Sodium to aluminium ratios have also been determined for these samples and, as with the zeolite A type samples, appear to indicate the presence of little or no octahedral aluminium.

Table 3.9. Chemical Analysis of Zeolite A Type Samples

Sample	Si (mmol/g)	Al (mmol/g)	Na (mmol/g)	H_2O (Wt. %)	Si/Al	Na/Al	Unit Cell Formula
A0	5.76	4.43	4.44	27.43	1.30	1.00	$Na_{10.43}[(AlO_2)_{10.43}(SiO_2)_{13.57}].35H_2O$
A1	5.29	4.59	4.45	28.13	1.15	0.97	$Na_{11.38}[(AlO_2)_{11.73}(SiO_2)_{12.27}].37H_2O$
A2	5.45	4.57	4.31	27.55	1.19	0.94	$Na_{10.30}[(AlO_2)_{10.96}(SiO_2)_{13.04}].35H_2O$
A3	5.30	4.88	5.11	22.85	1.09	1.05	$Na_{11.48}[(AlO_2)_{11.48}(SiO_2)_{12.52}].28H_2O$
A4	5.40	5.12	5.33	21.01	1.05	1.04	$Na_{11.71}[(AlO_2)_{11.71}(SiO_2)_{12.29}].25H_2O$
A6	5.16	5.07	5.34	21.12	1.02	1.05	$Na_{11.88}[(AlO_2)_{11.88}(SiO_2)_{12.12}].25H_2O$
A8	5.30	5.00	5.31	20.74	1.06	1.06	$Na_{11.65}[(AlO_2)_{11.65}(SiO_2)_{12.35}].25H_2O$
A10	5.47	5.02	5.34	21.07	1.09	1.06	$Na_{11.48}[(AlO_2)_{11.48}(SiO_2)_{12.52}].25H_2O$
A12	5.23	5.10	5.33	21.28	1.03	1.04	$Na_{11.82}[(AlO_2)_{11.82}(SiO_2)_{12.18}].25H_2O$
A14	5.30	5.14	5.41	20.96	1.02	1.05	$Na_{11.89}[(AlO_2)_{11.89}(SiO_2)_{12.11}].25H_2O$

Table 3.10. Chemical Analysis of Zeolite X Type Samples

Sample	Si (mmol/g)	Al (mmol/g)	Na (mmol/g)	H_2O (Wt. %)	Si/Al	Na/Al	Unit Cell Formula
X0	6.33	4.12	4.17	25.54	1.54	1.01	$Na_{75.59}[(AlO_2)_{75.59}(SiO_2)_{116.41}].251H_2O$
X1	5.98	4.42	4.53	24.42	1.35	1.02	$Na_{81.70}[(AlO_2)_{81.70}(SiO_2)_{110.30}].239H_2O$
X2	5.98	4.46	4.50	24.92	1.34	1.01	$Na_{82.05}[(AlO_2)_{82.05}(SiO_2)_{109.95}].246H_2O$
X3	5.98	4.48	4.80	22.50	1.33	1.07	$Na_{82.40}[(AlO_2)_{82.40}(SiO_2)_{109.60}].215H_2O$
X4	6.00	4.56	4.78	21.89	1.31	1.05	$Na_{83.12}[(AlO_2)_{83.12}(SiO_2)_{108.88}].208H_2O$
X6	5.98	4.55	4.70	22.76	1.31	1.06	$Na_{83.12}[(AlO_2)_{83.12}(SiO_2)_{108.88}].218H_2O$
X8	5.78	4.54	4.54	25.23	1.27	1.00	$Na_{84.58}[(AlO_2)_{84.58}(SiO_2)_{107.42}].251H_2O$
X10	5.71	4.54	4.43	25.87	1.26	0.98	$Na_{83.26}[(AlO_2)_{83.96}(SiO_2)_{107.04}].259H_2O$
X12	5.62	4.50	4.53	25.25	1.25	1.01	$Na_{85.33}[(AlO_2)_{85.33}(SiO_2)_{106.67}].251H_2O$
X24	5.76	4.46	4.57	25.43	1.29	1.02	$Na_{83.84}[(AlO_2)_{83.84}(SiO_2)_{108.16}].253H_2O$

It is interesting to note that in the IR spectra of the zeolite X type samples, the band centred around 980cm^{-1} shifts to longer wavelengths as the Si/Al ratio decreases. Although there is a similar decrease in Si/Al ratio during the synthesis of zeolite A, this effect is not apparent in the IR spectra of the zeolite A type samples. Here, the corresponding band in the IR spectrum remains fixed at about 1000cm^{-1}. If the position of this band is dependent on the Si/Al ratio of the sample, these results would appear to be contradictory, especially since the crystalline zeolite A samples have a lower Si/Al ratio than the crystalline zeolite X samples. The exact position of this band is not, however, solely controlled by the atomic masses and bond force constants of the vibrating atoms. Structural effects are also important, although this band is assigned to an internal linkage vibration (asymmetric T-O stretch) and their contribution will be small. The dependence of the frequency of this vibration on the Si/Al ratio was originally observed over a wide range of ratios and should be regarded as a trend rather than a general rule.

3.4f Particle Size Analysis

Particle size analysis was carried out using a Malvern Instruments Master Particle Sizer M3.0. The presence of particle aggregates in a sample can give rise to misleading results and, to avoid this problem, each sample, suspended in water, was subject to ultrasonic radiation immediately prior to analysis. This treatment was continued until further exposure to ultrasonic radiation had no effect on the observed particle size distribution.

Particle size distributions for the zeolite A type samples are shown in Figures 3.14 to 3.23. The numbers to the right of each diagram indicate the percentage of the sample in each size band.

The crystalline samples (samples A4 to A14) consisted predominantly of small particles. In each case, over 90% of the sample consisted of particles less than 10.5μm. The size bands 6.4-5.0μm and 5.0-3.9μm were consistently the most heavily populated. Particles smaller than 1.5μm were absent.

Figure 3.14. Particle Size Analysis of Sample A0

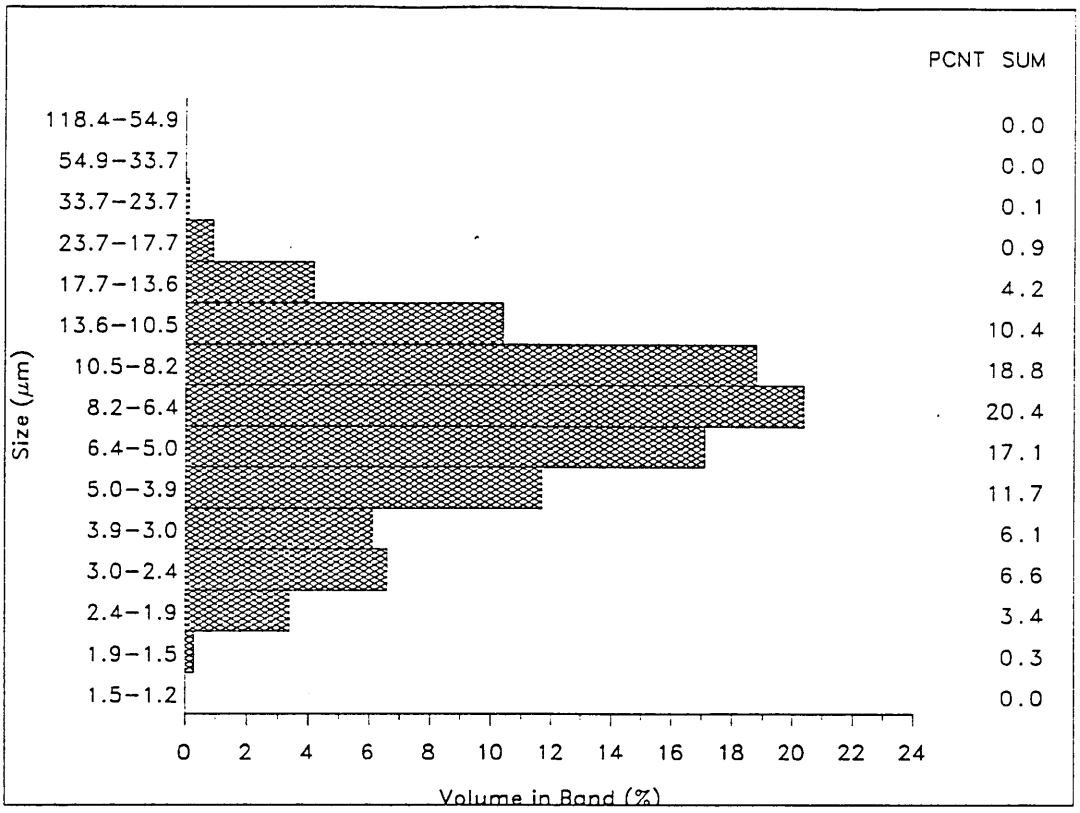

Figure 3.15. Particle Size Analysis of Sample A1

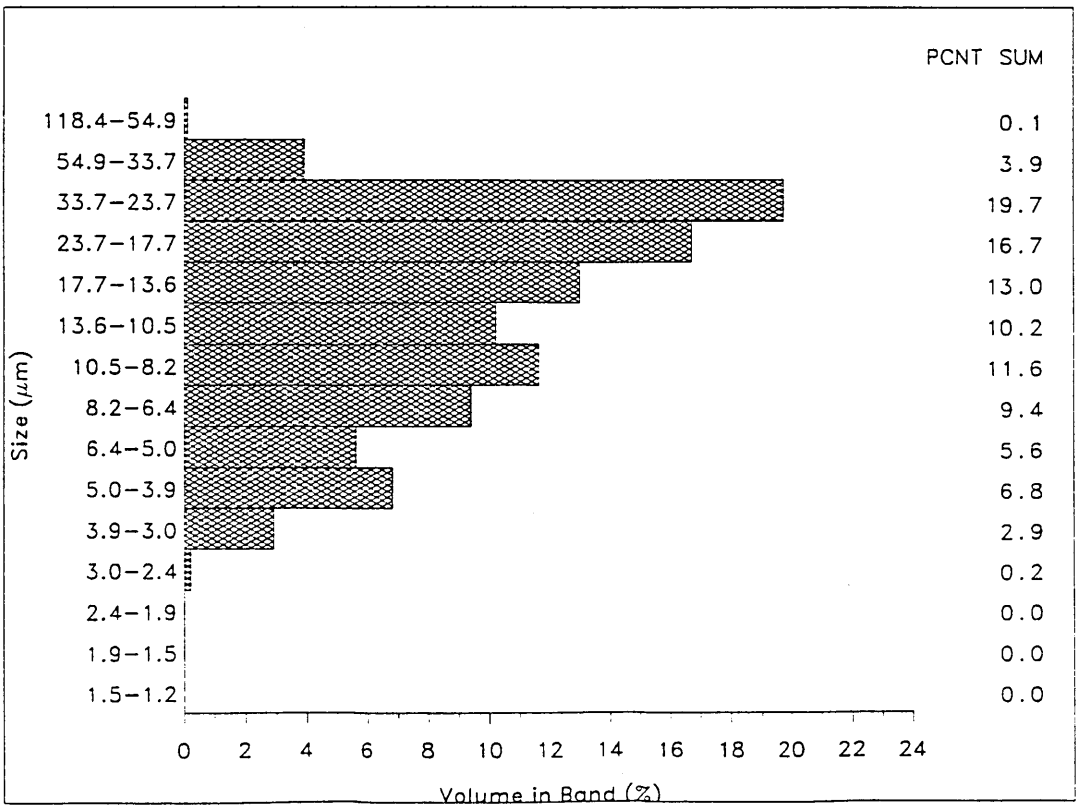

Figure 3.16. Particle Size Analysis of Sample A2

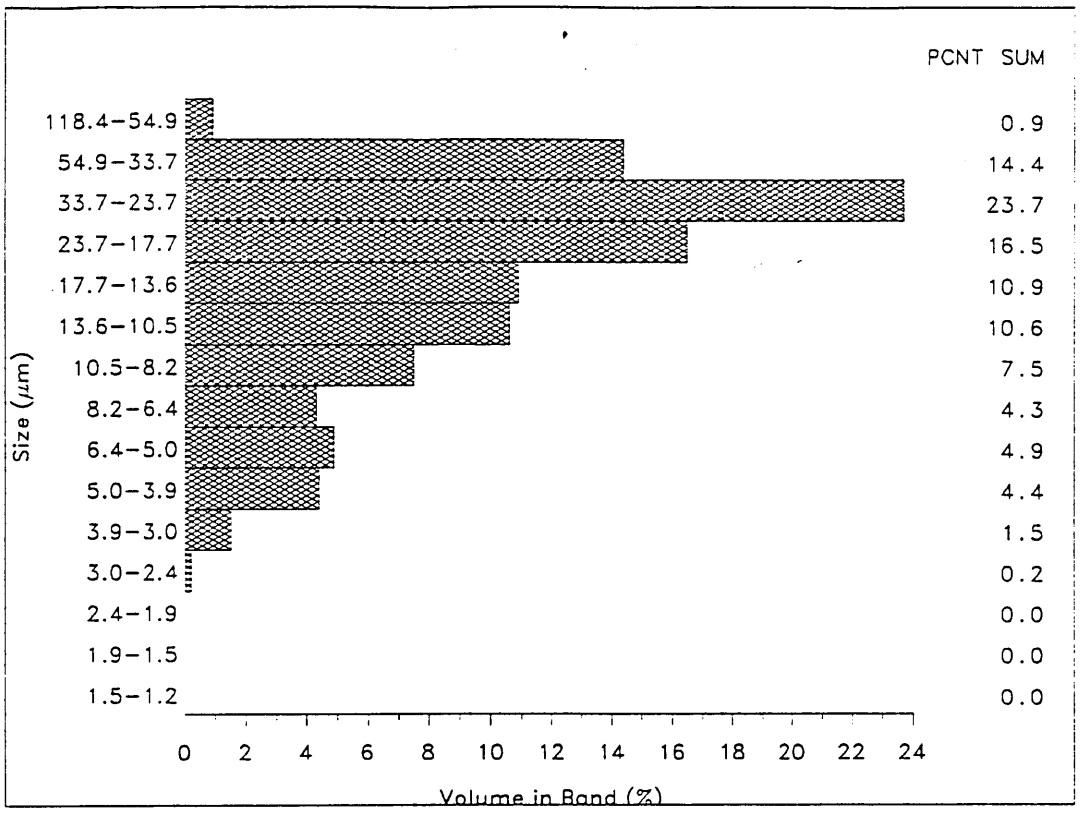

Figure 3.17. Particle Size Analysis of Sample A3

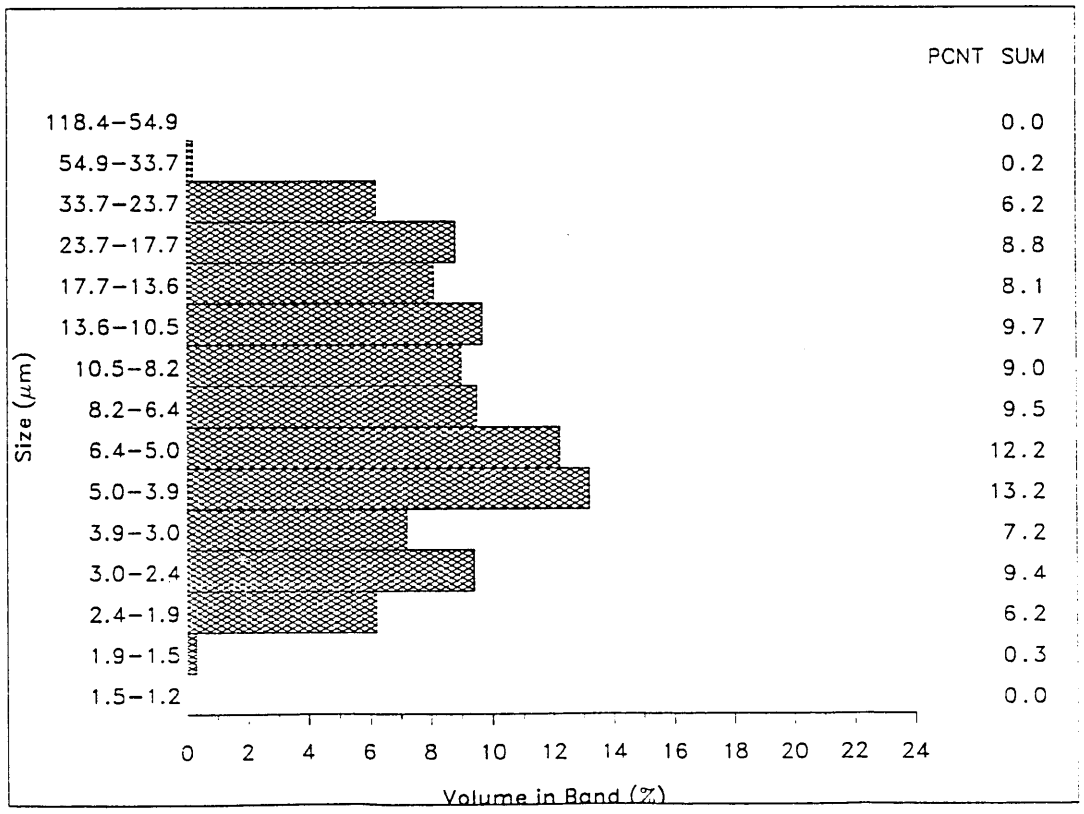

Figure 3.18. Particle Size Analysis of Sample A4

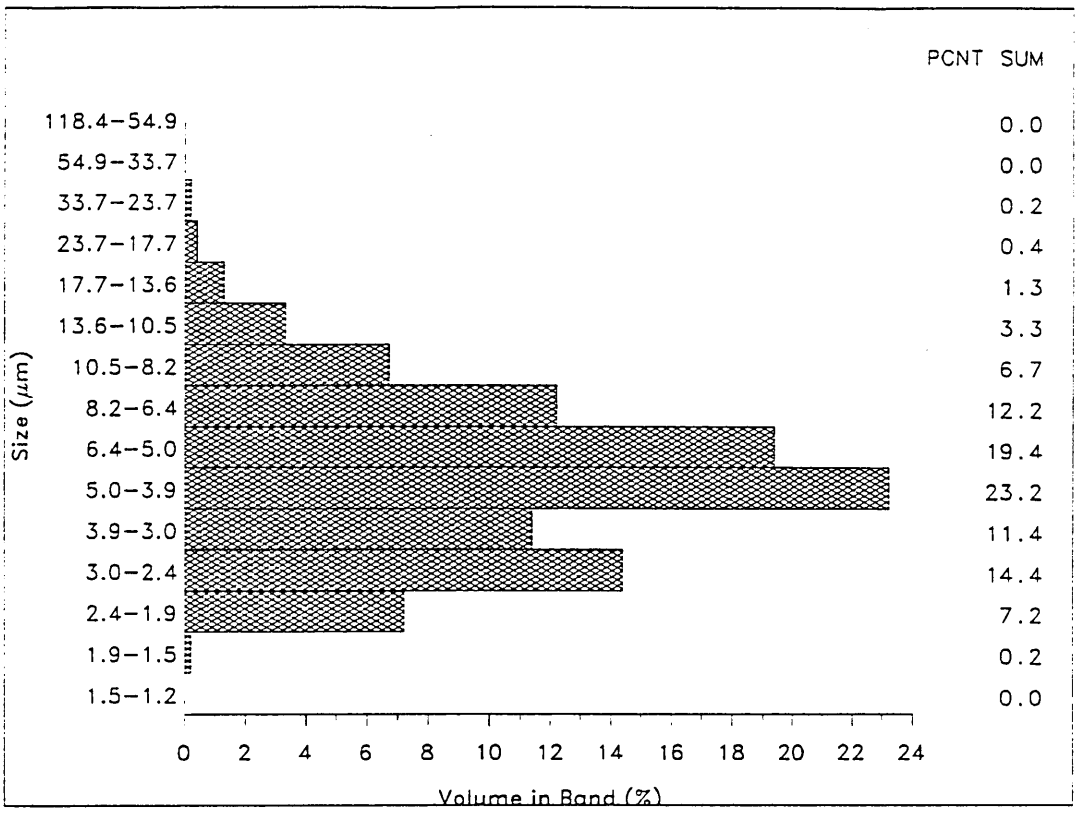

Figure 3.19. Particle Size Analysis of Sample A6

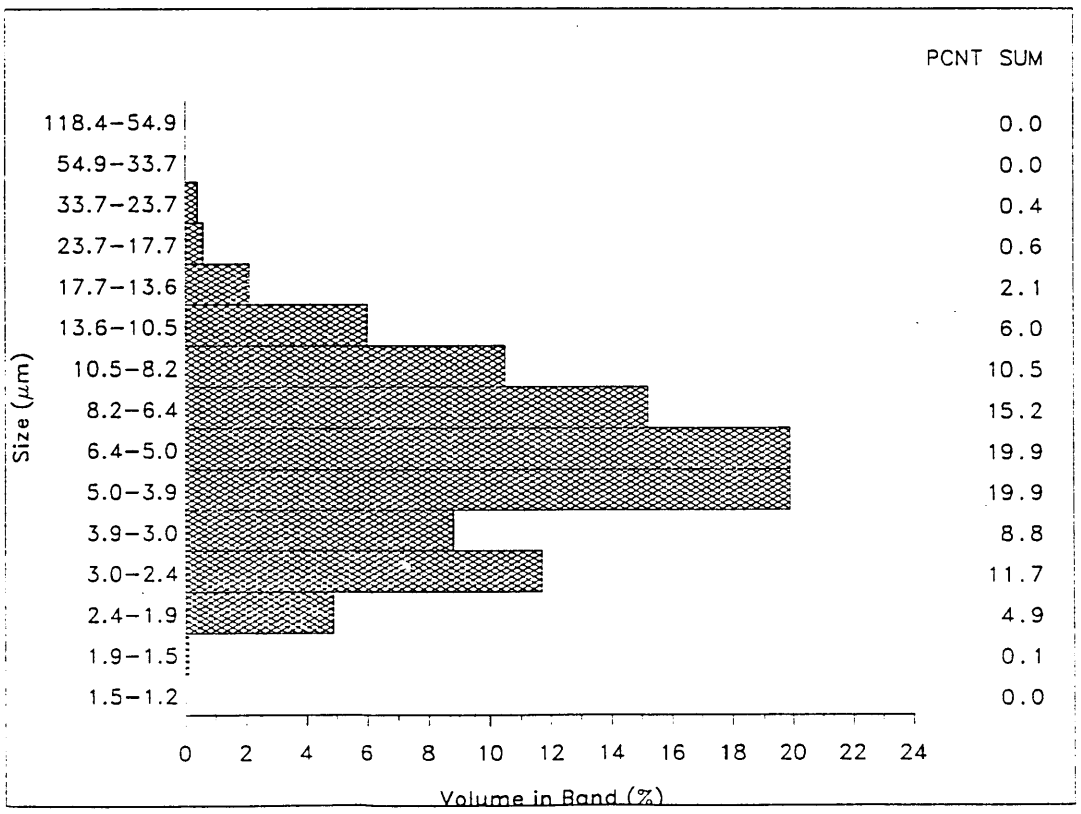

Figure 3.20. Particle Size Analysis of Sample A8

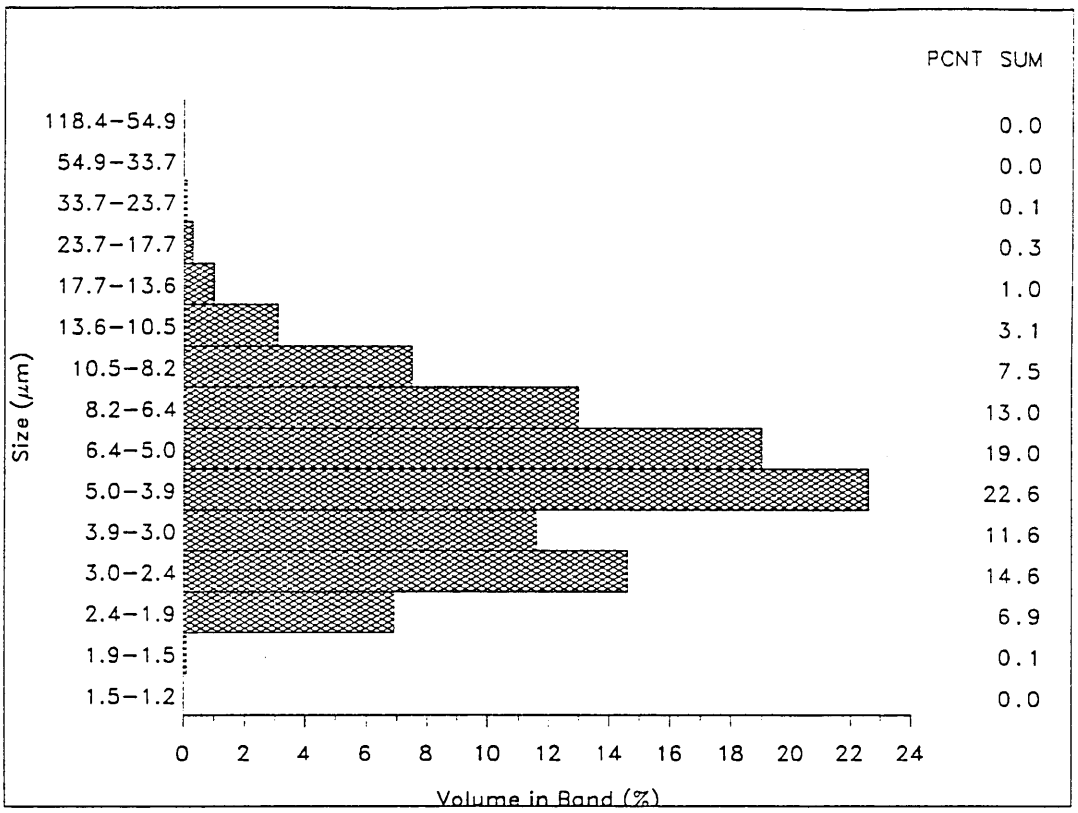

Figure 3.21. Particle Size Analysis of Sample A10

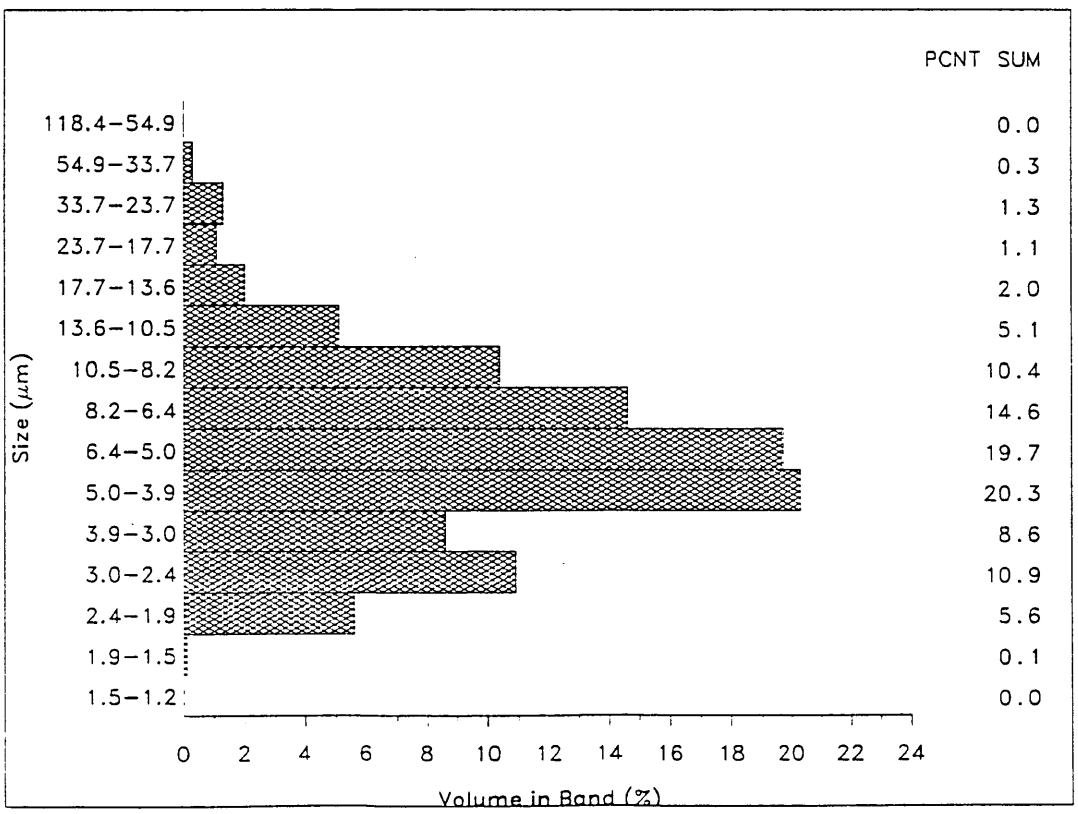

Figure 3.22. Particle Size Analysis of Sample A12

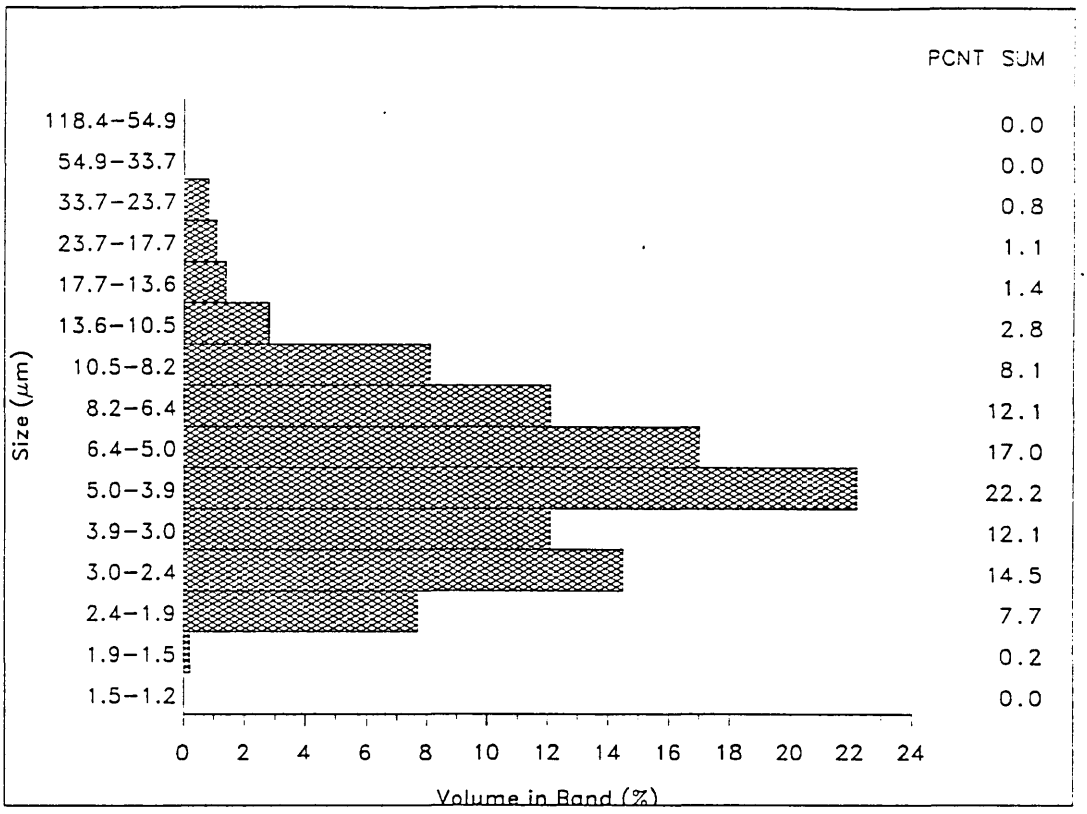

Figure 3.23. Particle Size Analysis of Sample A14

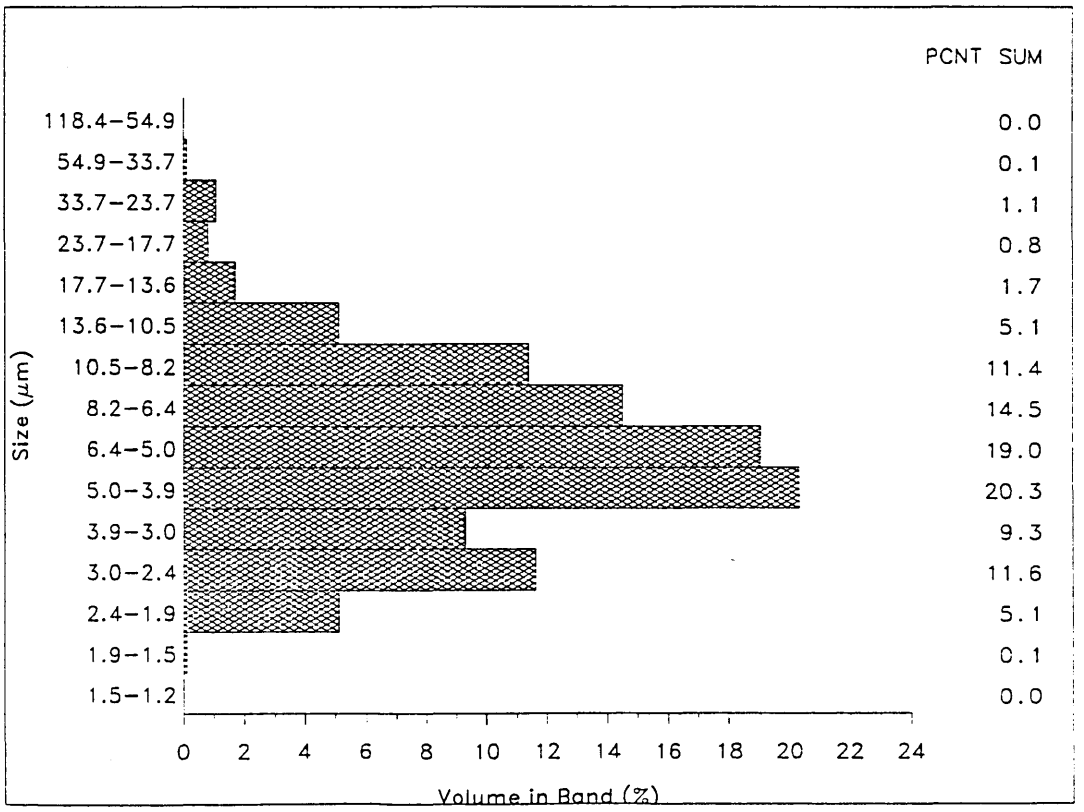

The amorphous samples A1 (Figure 3.15) and A2 (Figure 3.16) were characterised by larger particles. In both cases, over 75% of the sample comprised particles greater than 8.2μm and a significant proportion was in the size bands 33.7-23.7μm and 23.7-17.7μm. Interestingly, sample A0 (Figure 3.14) did not exhibit a similar particle size distribution. Here the majority of the particles (over 75%) were in the range 13.6-3.9μm. This would tend to suggest that the first formed gel in zeolite A synthesis consists of relatively small particles which initially increase in size as the reaction proceeds, then decrease as crystalline zeolite A is formed. Particle size analysis of sample A3 (Figure 3.17) revealed a more or less even distribution of particles in the range 33.7-1.9μm. This is consistent with the view that this sample consisted of a mixture of relatively large amorphous particles and smaller crystals of zeolite A.

Particle size distributions for the zeolite X type samples are shown in Figures 3.24 to 3.33. As with the zeolite A type samples, the amorphous samples X0, X1, X2, X3 and X4 were characterised by a significant proportion of large particles. In these cases, over 50% of the sample comprised particles greater than 17.7μm and particles smaller than 2.4μm were absent. The crystalline samples X8, X10, X12 and X24 exhibited an approximately even distribution of particles in the range 54.9-3.9μm. These results seem to be in conflict with the SEMs of the crystalline samples, which suggested that these samples consisted of small crystals in the approximate range 1-10μm. It would appear that, despite exposure to ultrasonic radiation, these samples still contained aggregates of perhaps three or four crystals. Sample X6, which consisted of a mixture of amorphous and crystalline material, exhibited a particle size distribution intermediate between these two extremes.

Figure 3.24. Particle Size Analysis of Sample X0

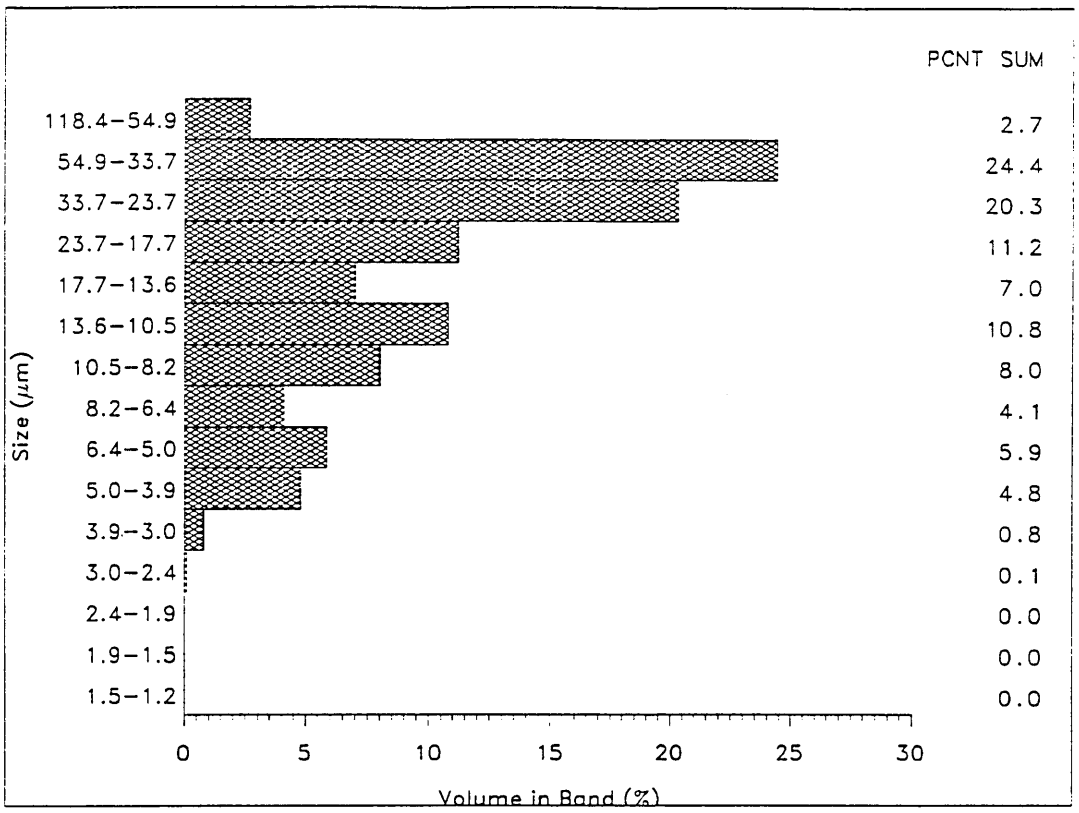

Figure 3.25. Particle Size Analysis of Sample X1

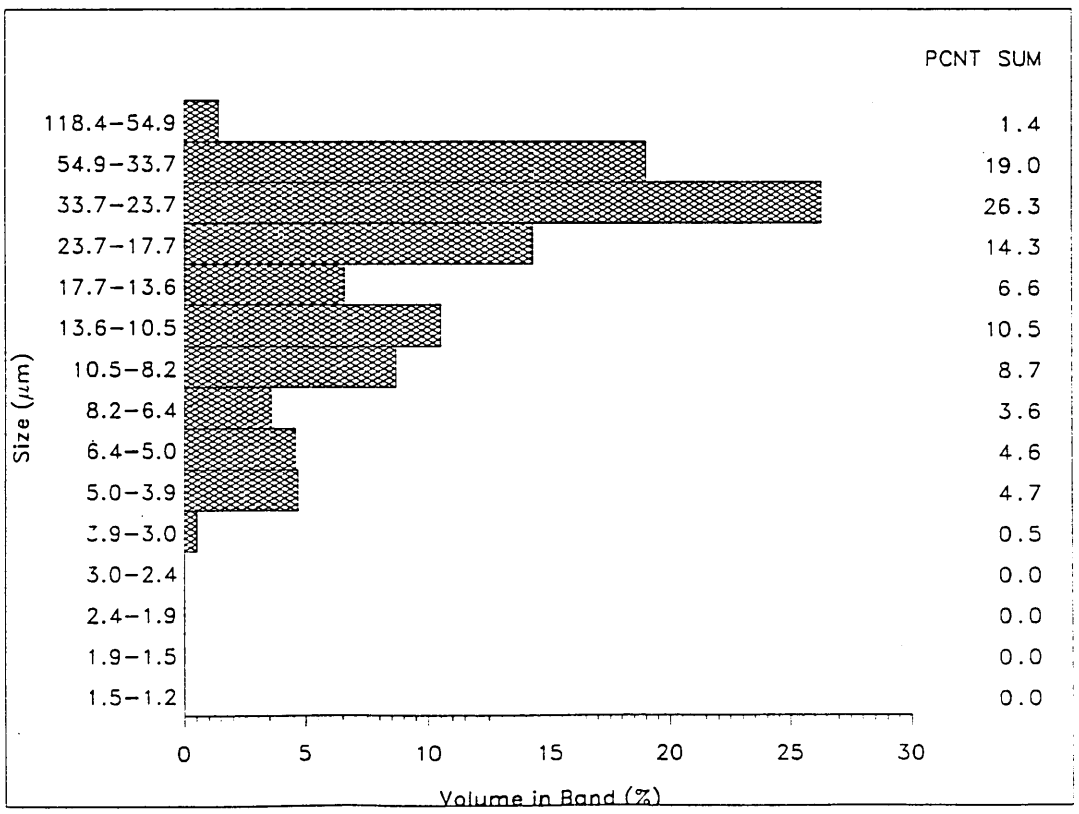

Figure 3.26. Particle Size Analysis of Sample X2

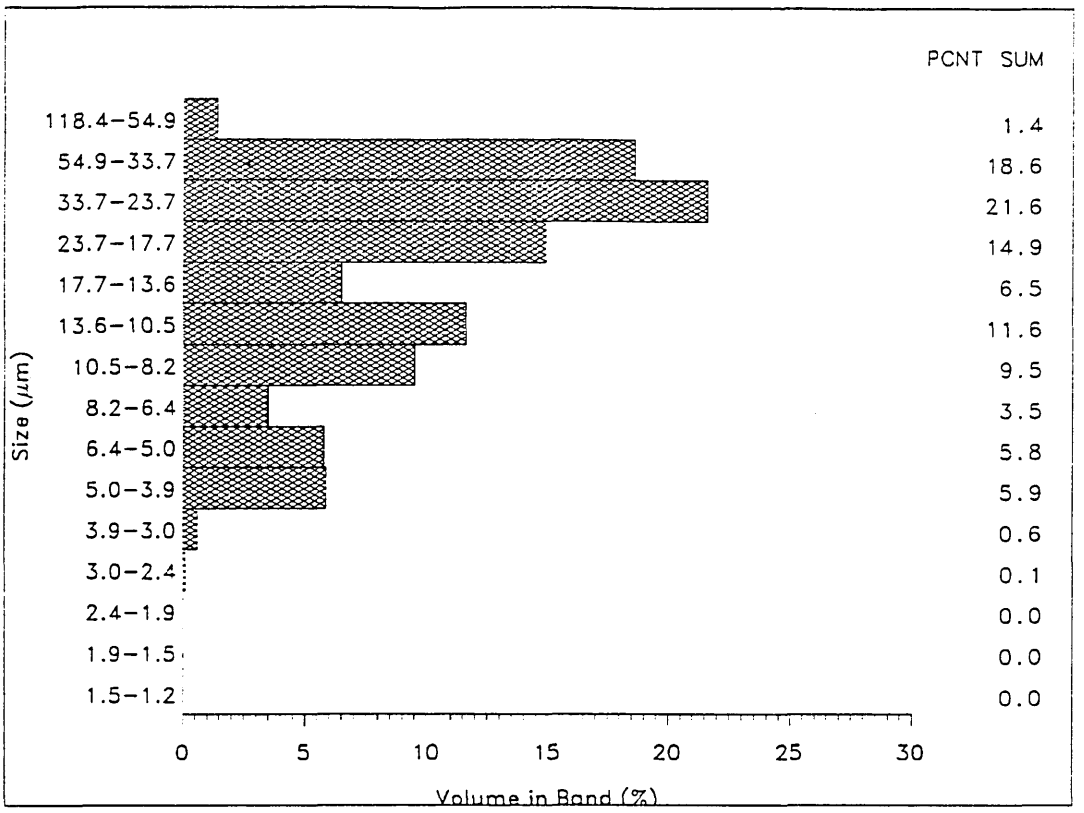

Figure 3.27. Particle Size Analysis of Sample X3

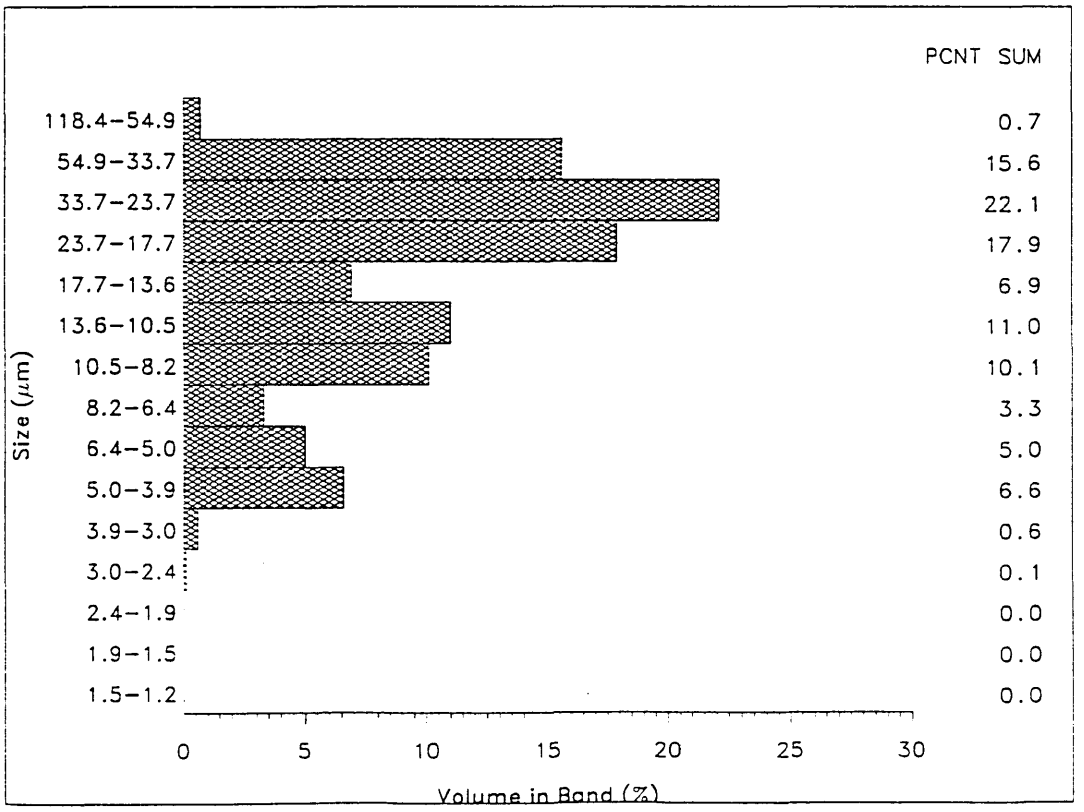

Figure 3.28. Particle Size Analysis of Sample X4

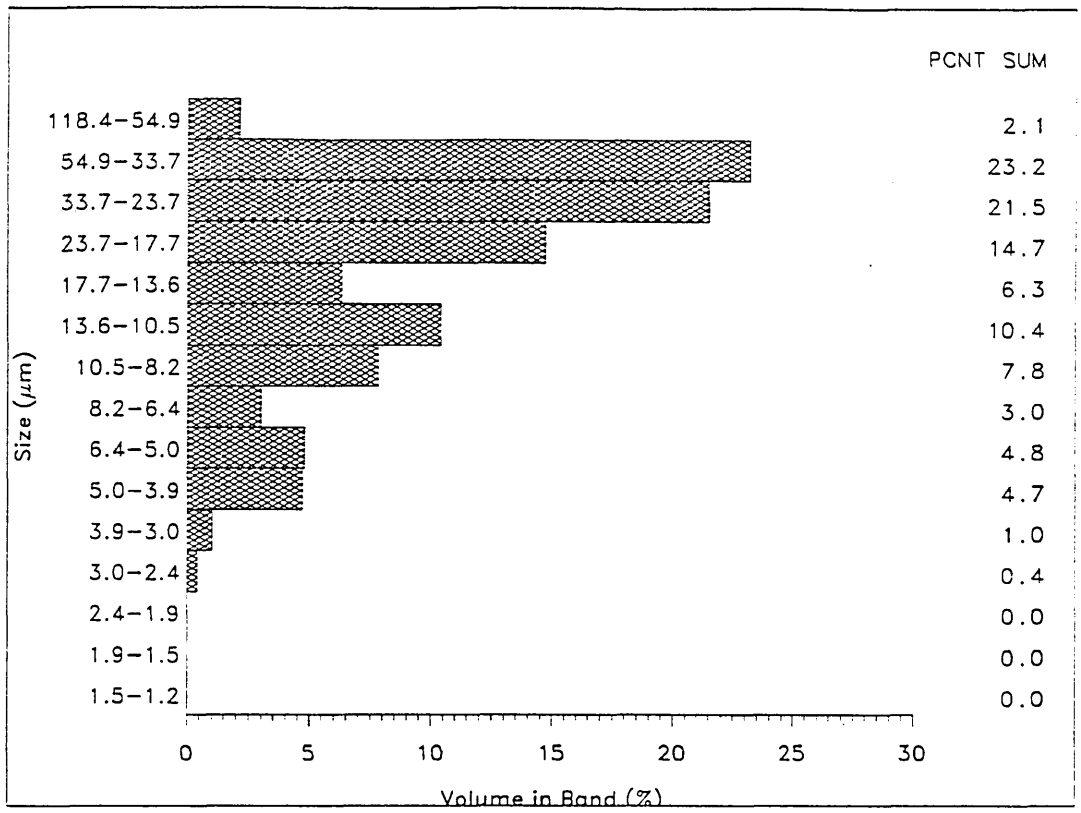

Figure 3.29. Particle Size Analysis of Sample X6

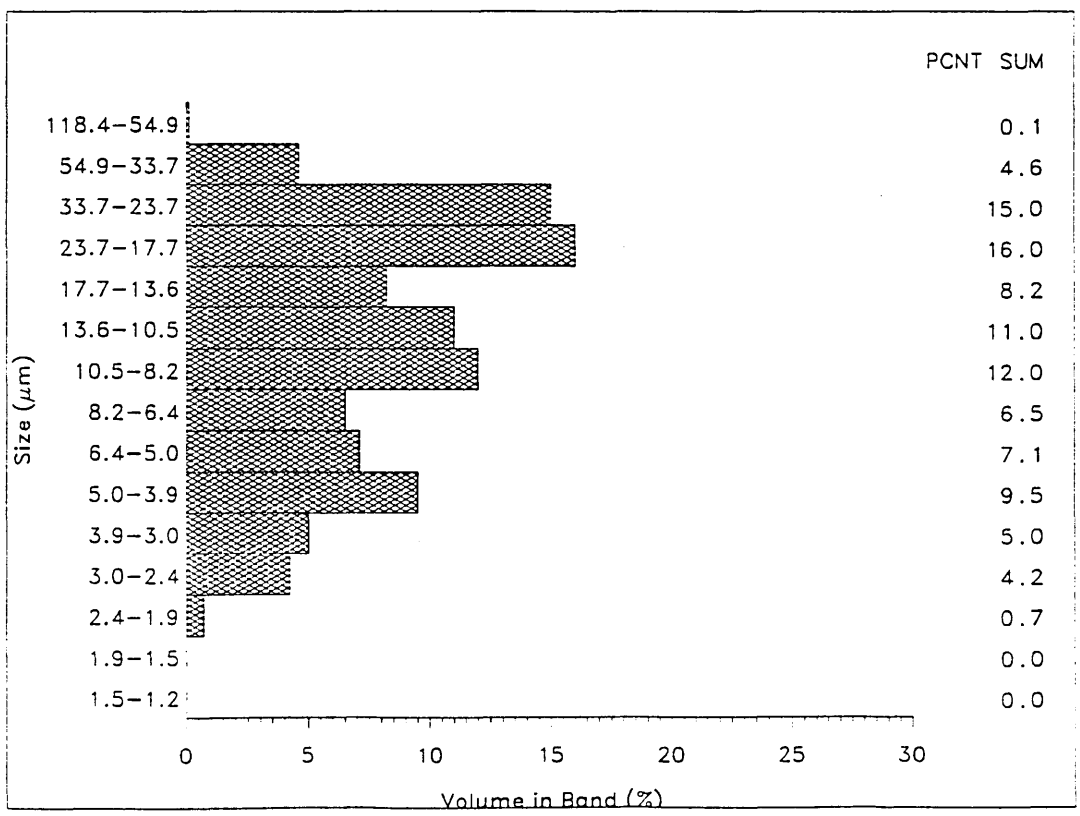

Figure 3.30. Particle Size Analysis of Sample X8

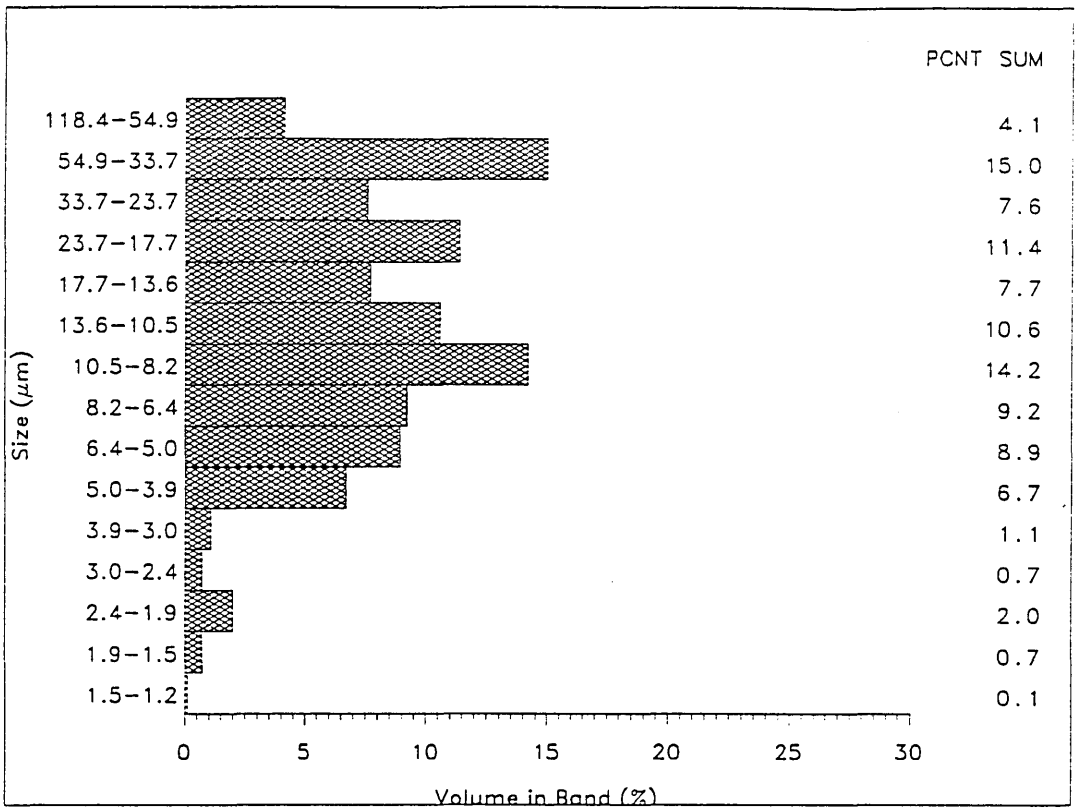

Figure 3.31. Particle Size Analysis of Sample X10

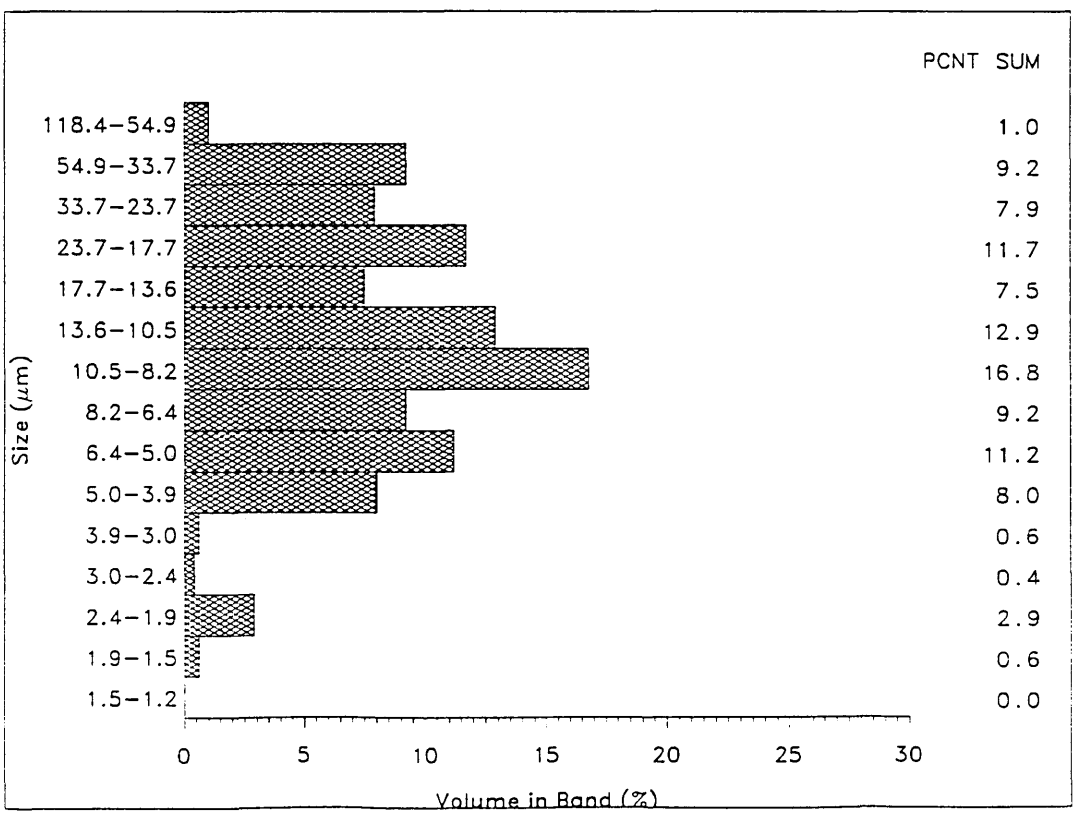

Figure 3.32. Particle Size Analysis of Sample X12

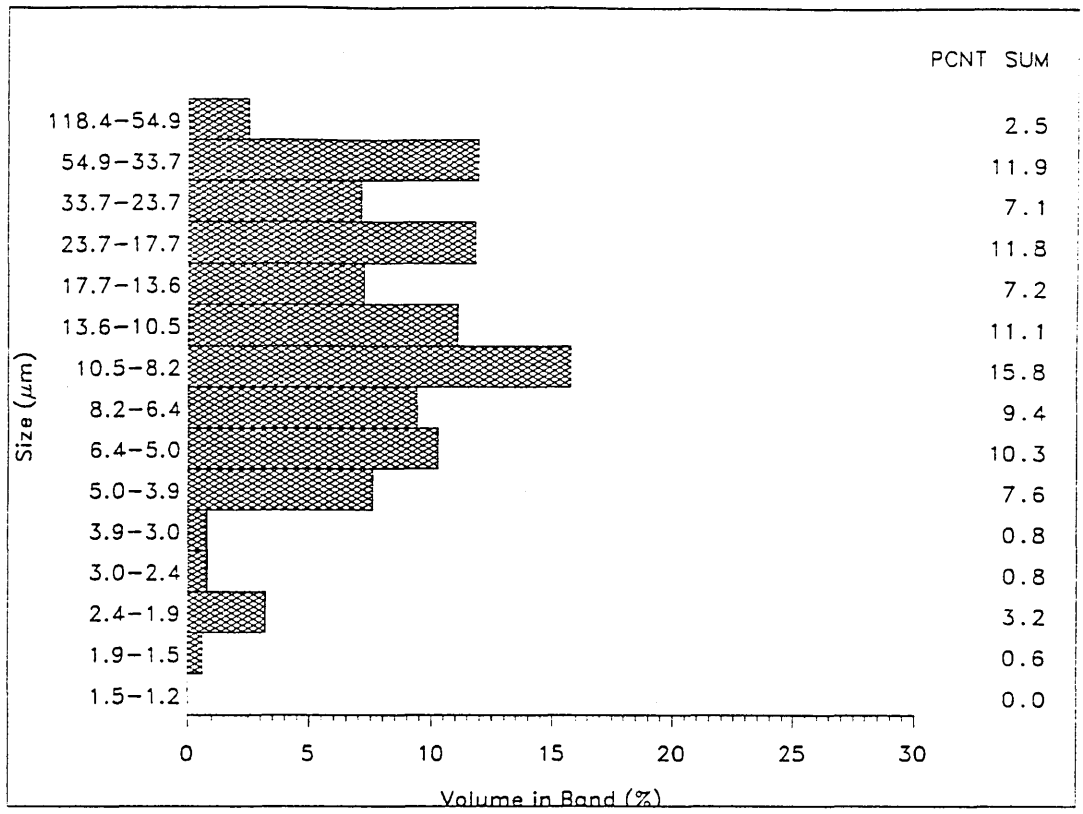

Figure 3.33. Particle Size Analysis of Sample X24

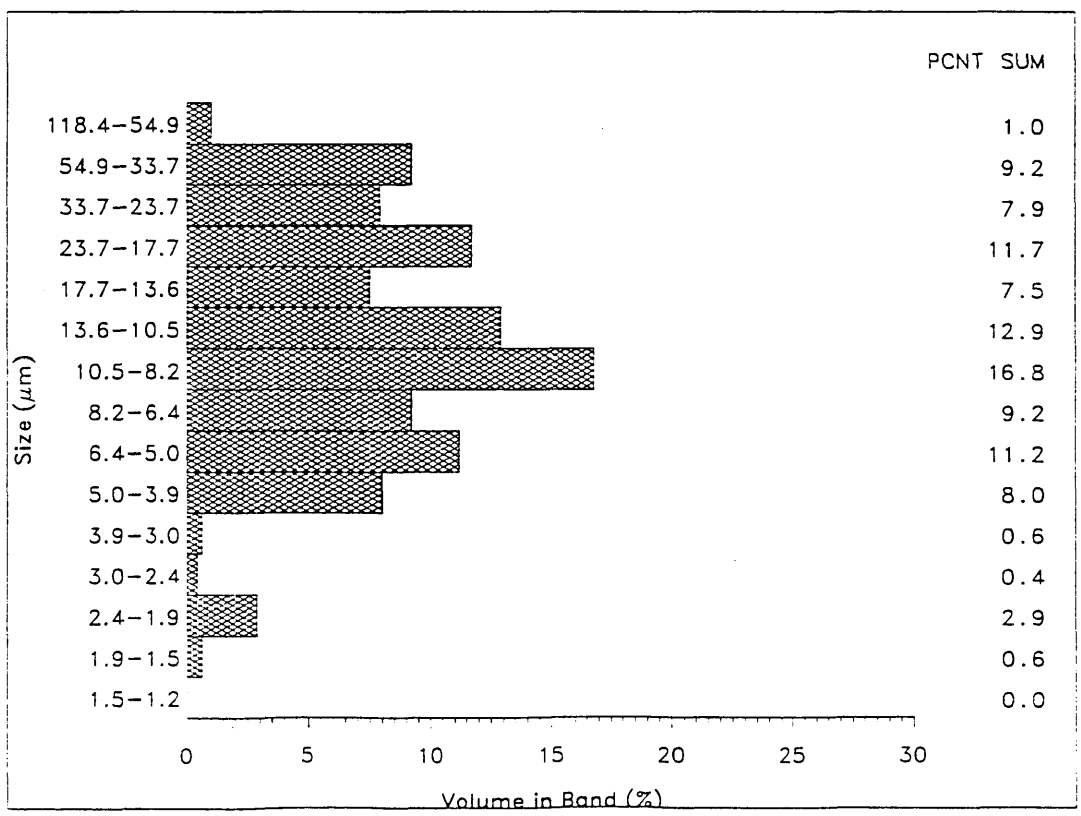

3.4g Solid State NMR

Solid State NMR was carried out at Royal Holloway and Bedford New College (Egham) using a Brucker MSL 300 NMR Spectrometer. ^{29}Si spectra were obtained using a signal frequency of 59.6 MHz and ^{27}Al spectra using a frequency of 78.2 MHz. All samples submitted for analysis were in the hydrated form. I am indebted to both Chris Groombridge and David Butler for their help.

^{27}Al NMR is an extremely useful tool for detecting the presence of octahedral aluminium in zeolitic samples. This method is certainly more reliable than wet chemical techniques and is more sensitive than other available methods such as those based on shifts in aluminium K_β X-ray emission lines or on XPS measurements. Therefore, ^{27}Al NMR were obtained for all amorphous samples to ascertain whether octahedral aluminium was present. In order to detect extraframework octahedral aluminium, acetylacetone (acac) was sorbed onto these samples before analysis.

^{27}Al NMR spectra for samples A0, A1, A2, A3 and A4 are shown in Figures 3.34 to 3.38 respectively. These spectra are dominated by a single symmetrical line. The ^{27}Al chemical shifts of 57.5 to 58.0 ppm are typical of tetrahedrally co-ordinated aluminium bound via oxygen to four silicon atoms, i.e. $Al(OSi)_4$ units[13]. The chemical shift of tetrahedral $Al(OAl)_4$ species is around +75 ppm[14] and, clearly, this species is absent. Octahedral AlO_6 species exhibit a chemical shift of around 0 ppm. There is evidence to suggest the presence of very low levels of octahedral aluminium in samples A0, A1, A3 and A4. Sample A4 is a crystalline sample, and the virtual absence of octahedral aluminium in this sample is not unexpected. The spectrum for sample A2, however, exhibits a much larger peak at a chemical shift of 0.5 ppm. This would appear to indicate the presence of a small, but significant, amount of octahedral aluminium in this sample. It is interesting to note that chemical analysis of this sample indicated a Na/Al ratio of 0.94 and that this can be explained by the presence of octahedrally co-ordinated aluminium species.

Figure 3.34. ^{27}Al NMR Spectrum of Sample A0

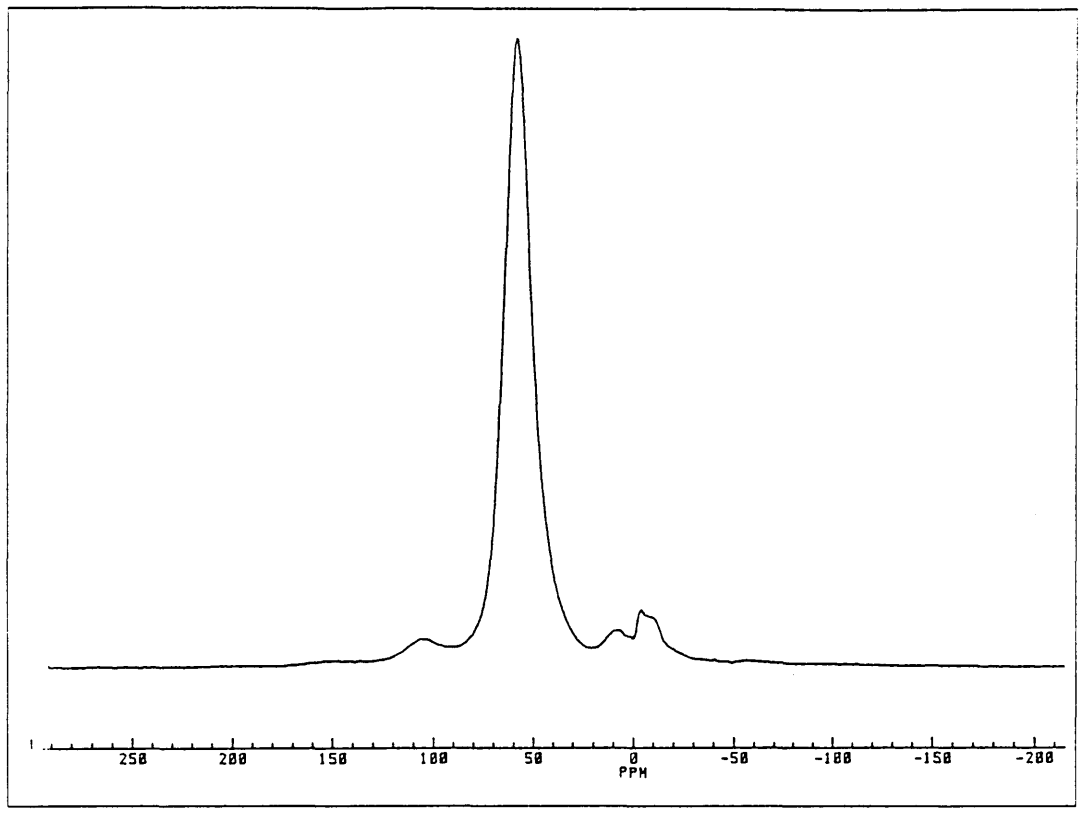

Figure 3.35. ^{27}Al NMR Spectrum of Sample A1

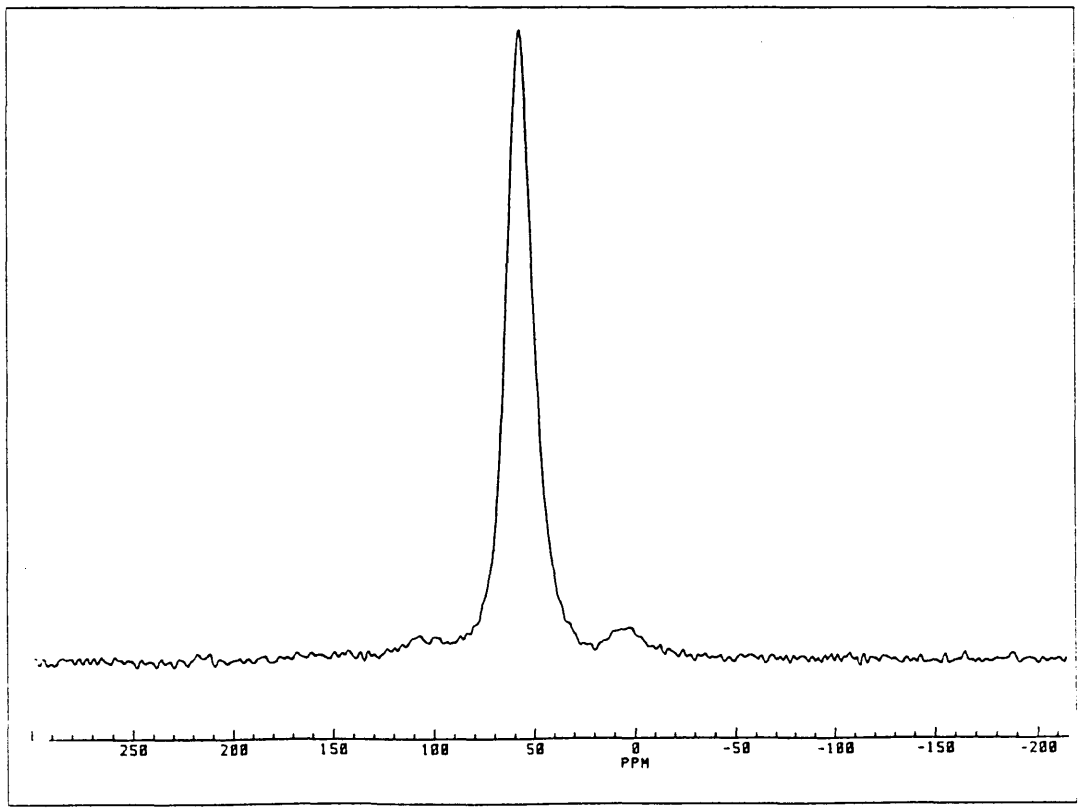

Figure 3.36. ^{27}Al NMR Spectrum of Sample A2

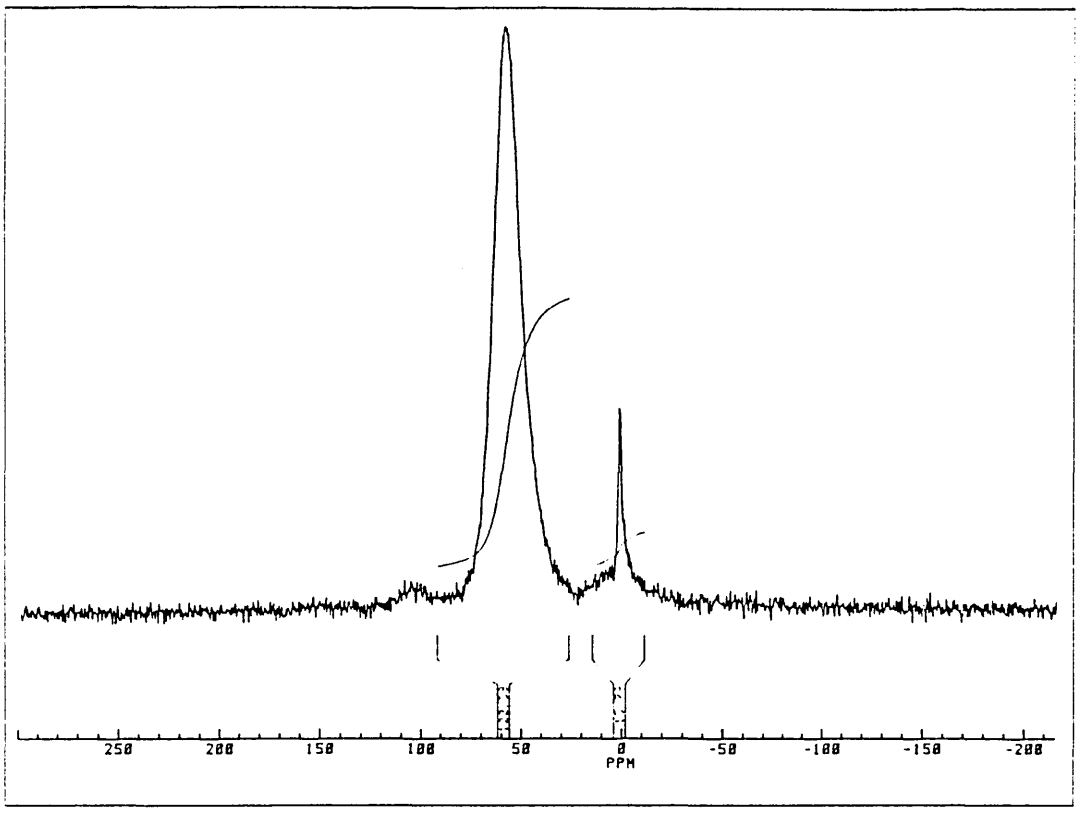

Figure 3.37. ^{27}Al NMR Spectrum of Sample A3

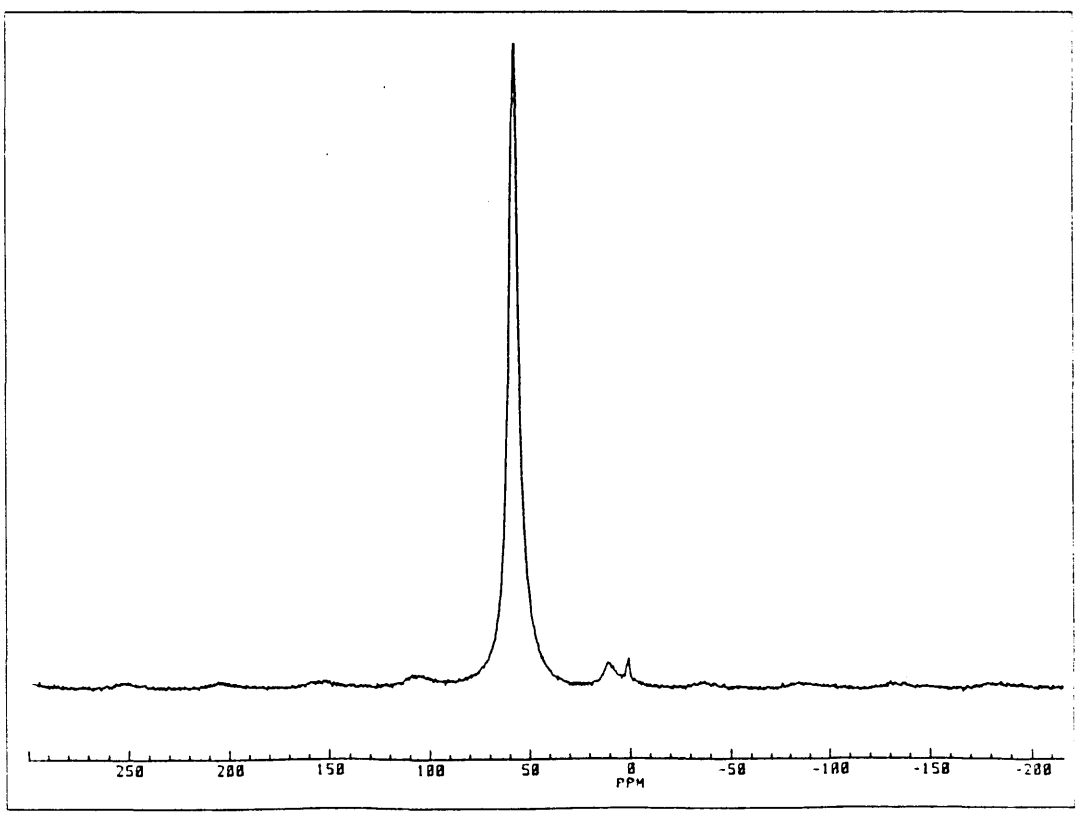

Figure 3.38. ^{27}Al NMR Spectrum of Sample A4

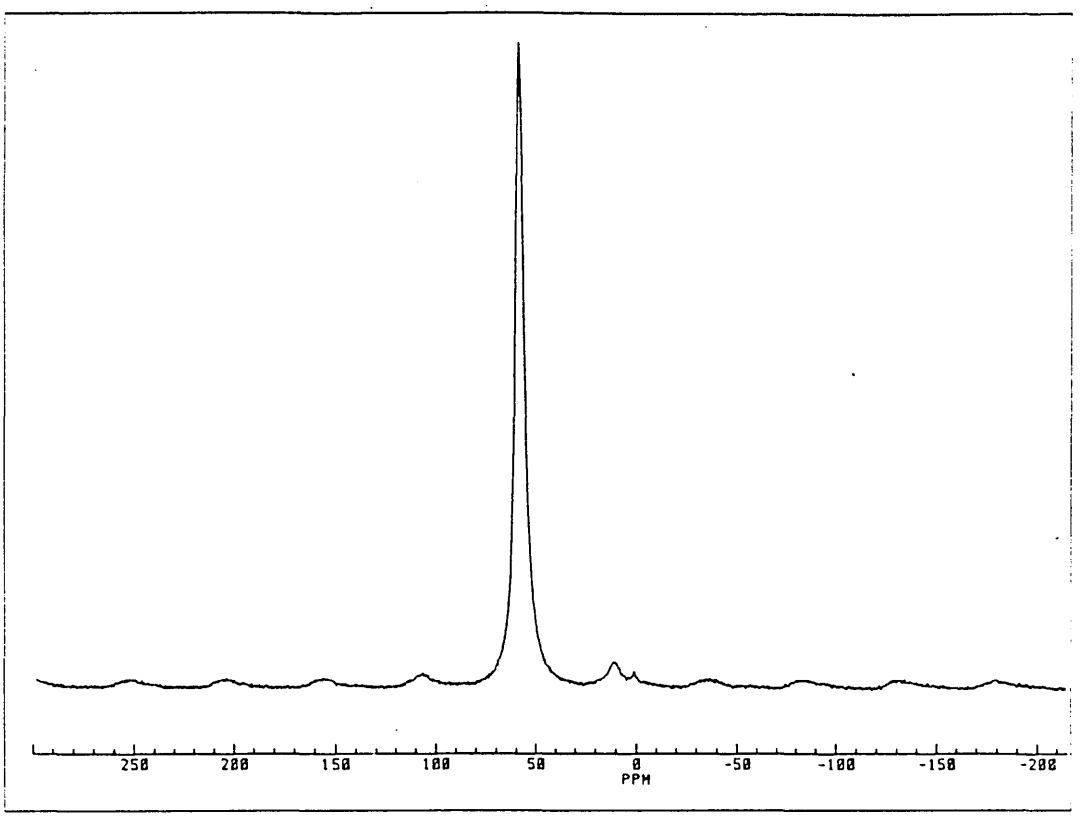

Figure 3.39. ^{27}Al NMR Spectrum of Sample X0

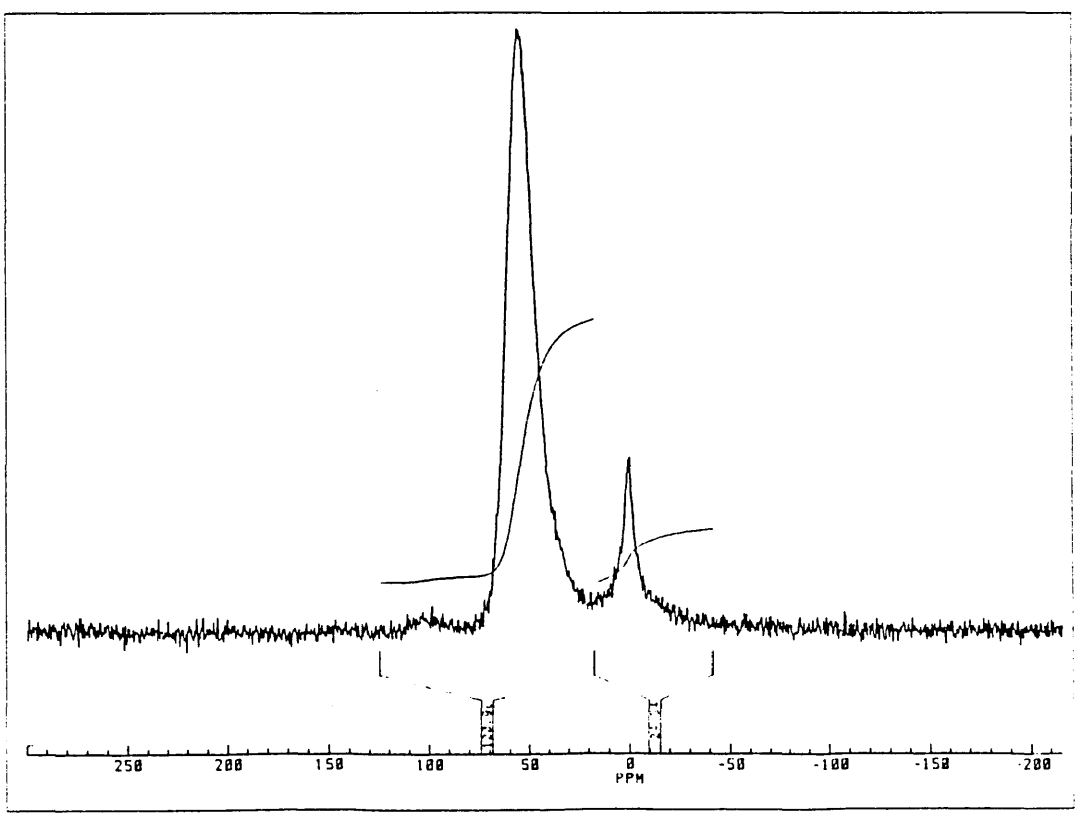

Figure 3.40. ^{27}Al NMR Spectrum of Sample X1

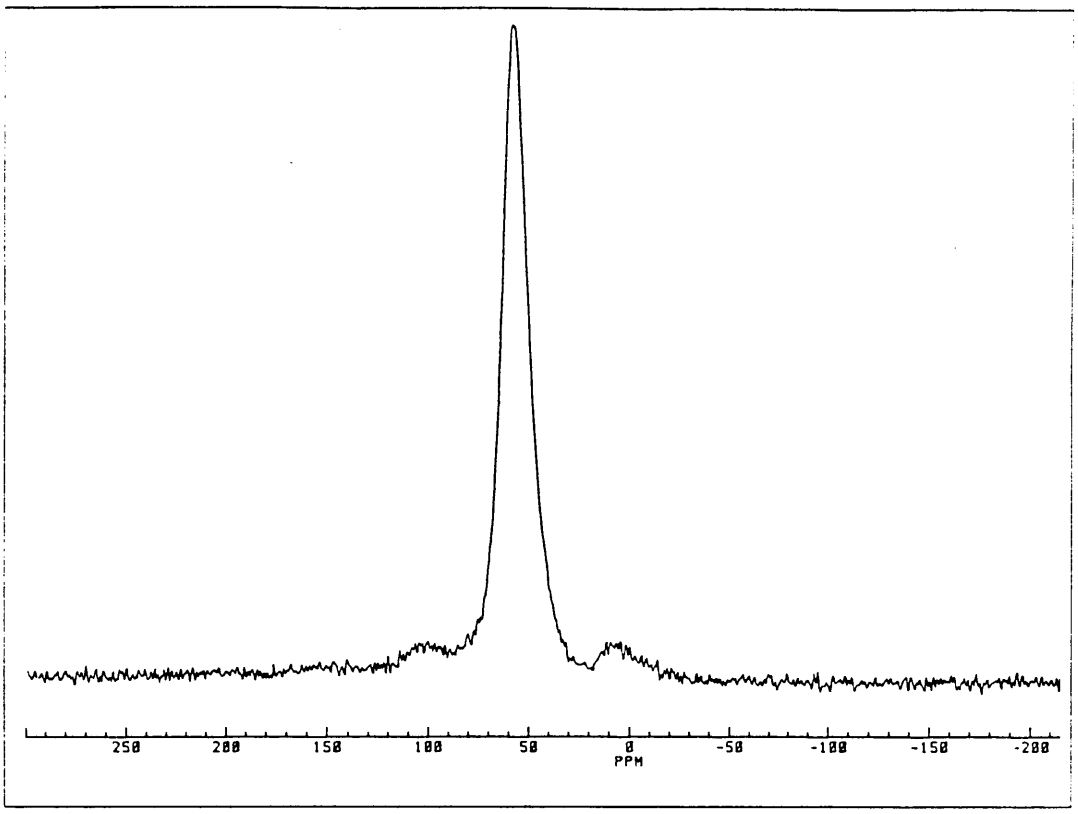

Figure 3.41. ^{27}Al NMR Spectrum of Sample X2

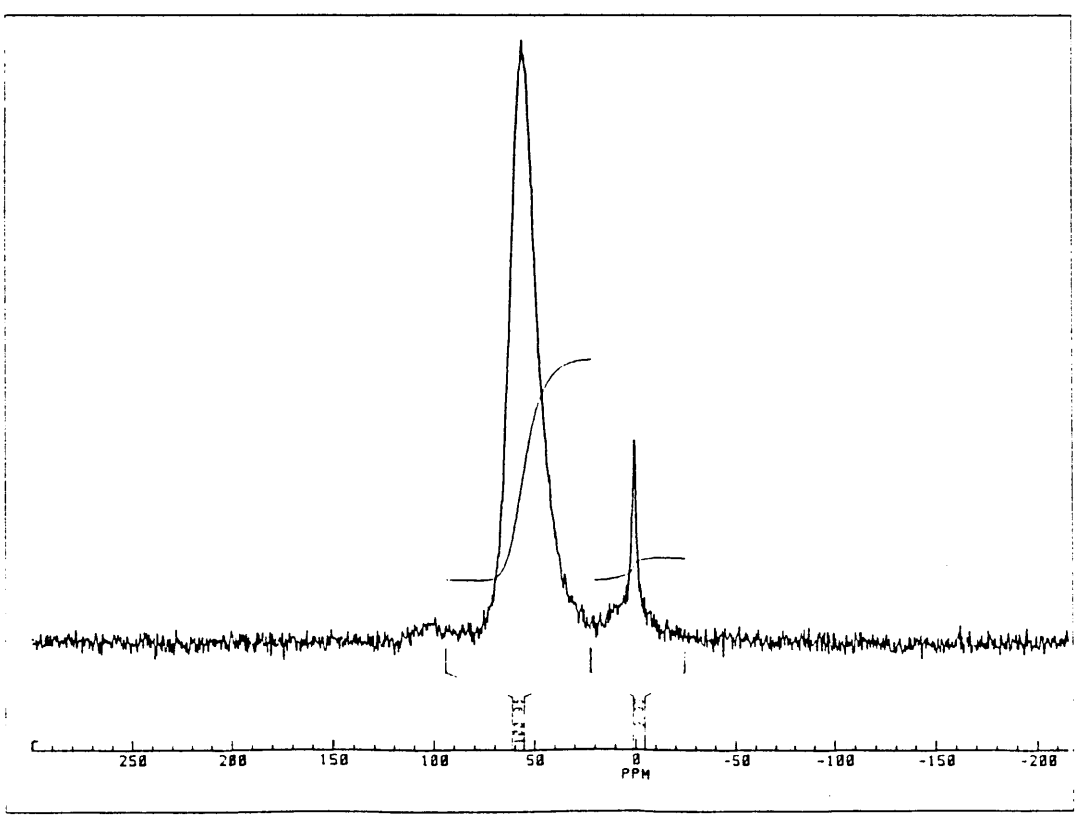

Figure 3.42. ^{27}Al NMR Spectrum of Sample X3

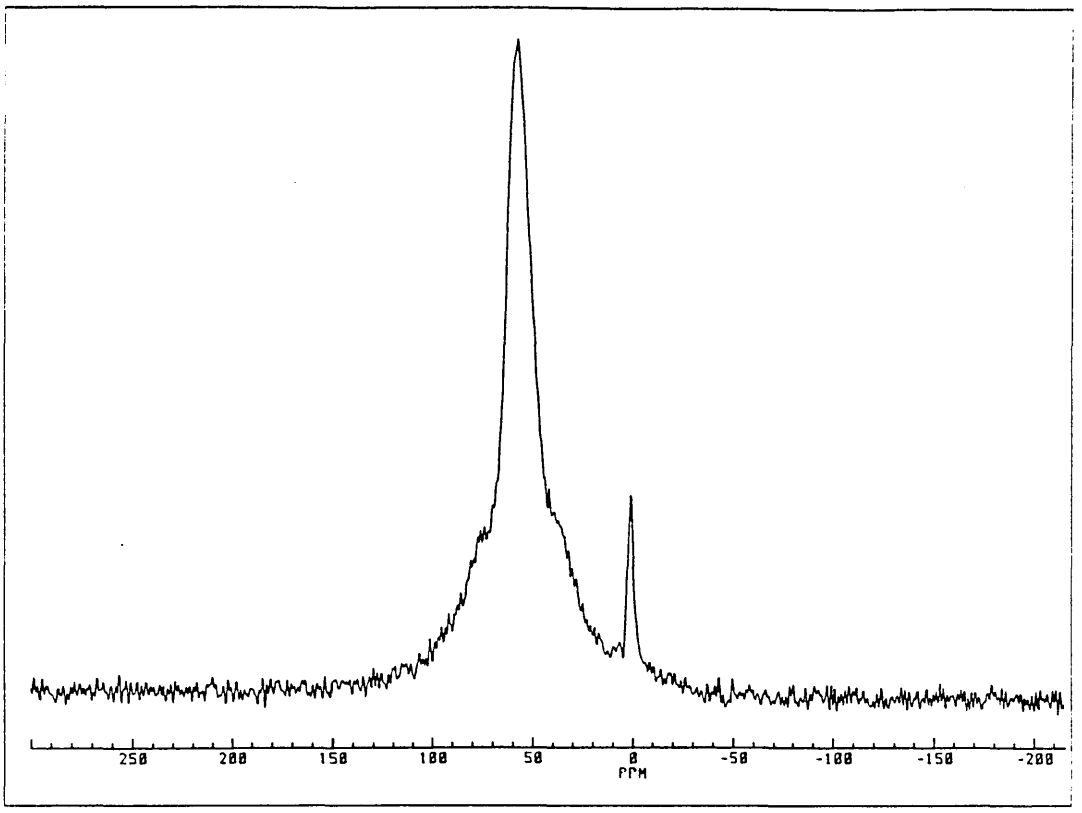

Figure 3.43. ^{27}Al NMR Spectrum of Sample X4

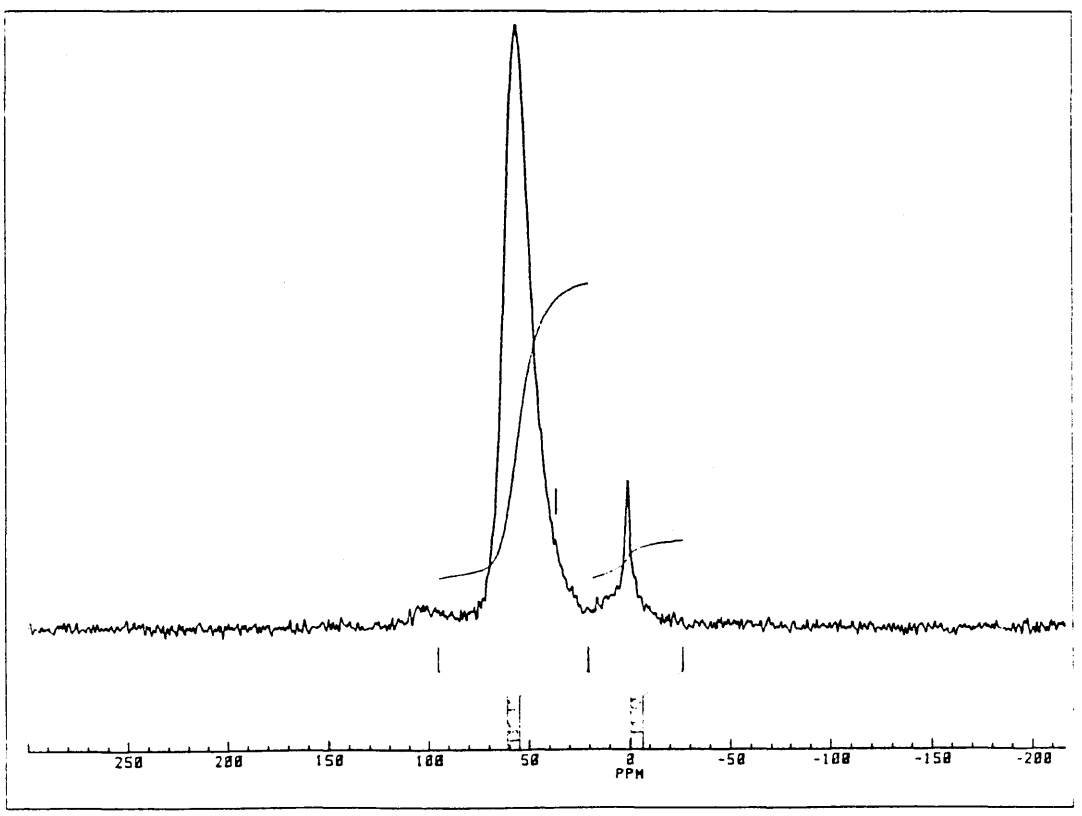

Figure 3.44. ^{27}Al NMR Spectrum of Sample X6

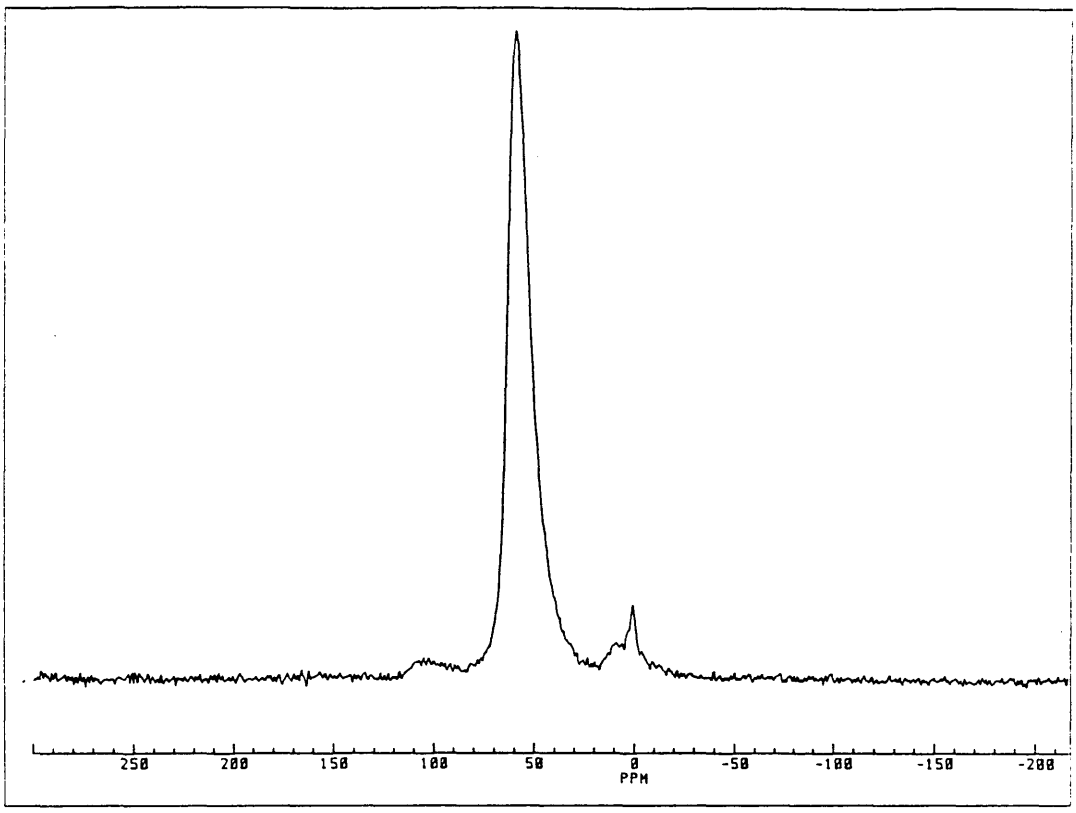

Figure 3.45. ^{27}Al NMR Spectrum of Sample X8

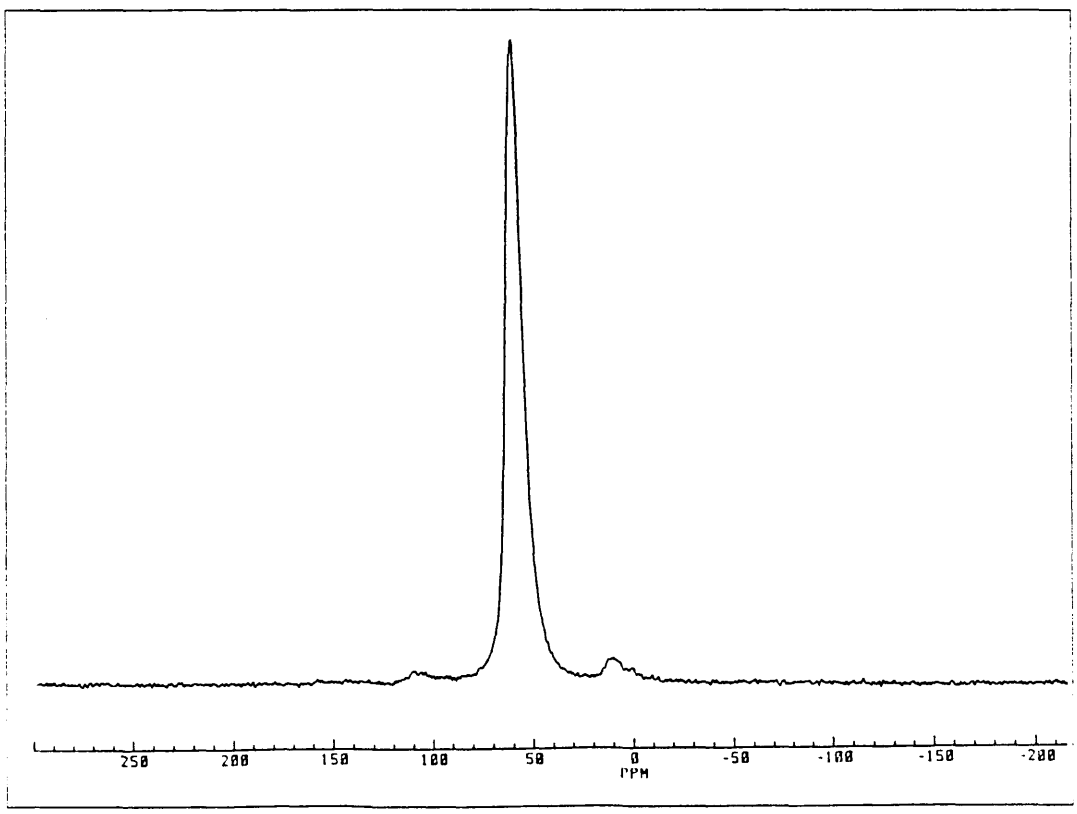

^{27}Al NMR spectra for samples X0, X1, X2, X3, X4, X6 and X8 are shown in Figures 3.39 to 3.45 respectively. Again these spectra are dominated by a symmetrical line with a chemical shift (56 to 59 ppm) typical of tetrahedrally co-ordinated $Al(OSi)_4$ units. Tetrahedral $Al(OAl)_4$ species are absent. With the exception of the amorphous sample X1 and the crystalline sample X8, all the spectra exhibit lines at around 0.5 ppm characteristic of octahedral aluminium species. The absence of octahedral aluminium in sample X8 is not unexpected, and indicates that this sample is, indeed, crystalline zeolite X. The absence of octahedral aluminium from sample X1 is harder to explain, especially since the spectra of the other amorphous samples suggest that the zeolite X type aluminosilicate gels contain octahedrally co-ordinated aluminium, but that this disappears as the reaction proceeds.

Some ^{29}Si NMR spectra were also obtained and these are shown in Figures 3.46 to 3.49. The spectra for both samples A0 (Figure 3.46) and X2 (Figure 3.48) show broad peaks with the peak maxima at chemical shifts of -84.5 ppm and -85.6 ppm respectively. These chemical shifts of around -85 ppm indicate that these amorphous samples consist mainly of $Si(OAl)_4$ units. The signal broadenings are typical of amorphous aluminosilicates[15,16] and are due to the overlapping of peaks with slightly different δ-values. This overlapping arises because of small differences in the structural arrangements of the SiO_4 tetrahedra in the gel skeleton[17].

Sample A14 is a crystalline sample and its ^{29}Si NMR spectrum is shown in Figure 3.47. A single symmetrical peak is seen at a chemical shift of -89.5 ppm. This is typical of $Si(OAl)_4$ units in highly ordered microcrystalline zeolite A. The observed high field shift of the ^{29}Si NMR peak of the $Si(OAl)_4$ units in going from amorphous gel (sample A0) to crystalline zeolite (sample A14) is due to the structure of the zeolite A framework[18]. The presence of this single peak is consistent with Lowenstein's rule[19] and agrees well with the observed Si/Al ratio of this sample of 1.02.

Figure 3.46. ^{29}Si NMR Spectrum of Sample A0

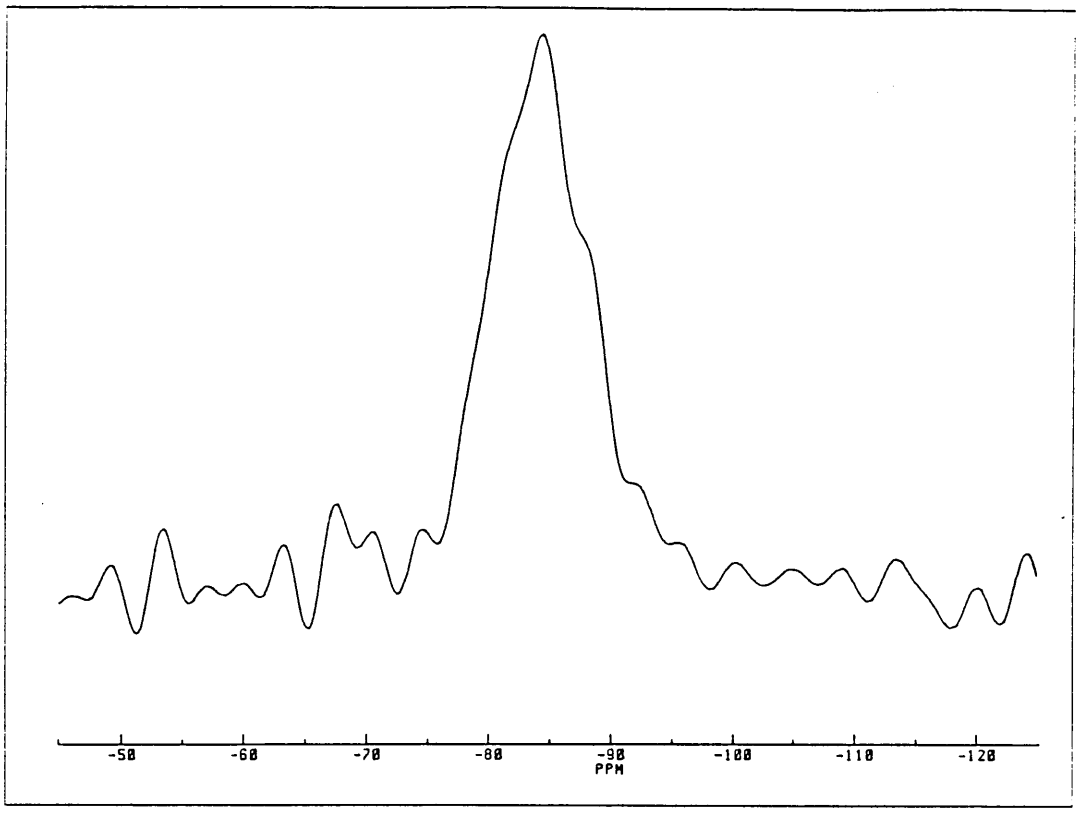

Figure 3.47. ^{29}Si NMR Spectrum of Sample A14

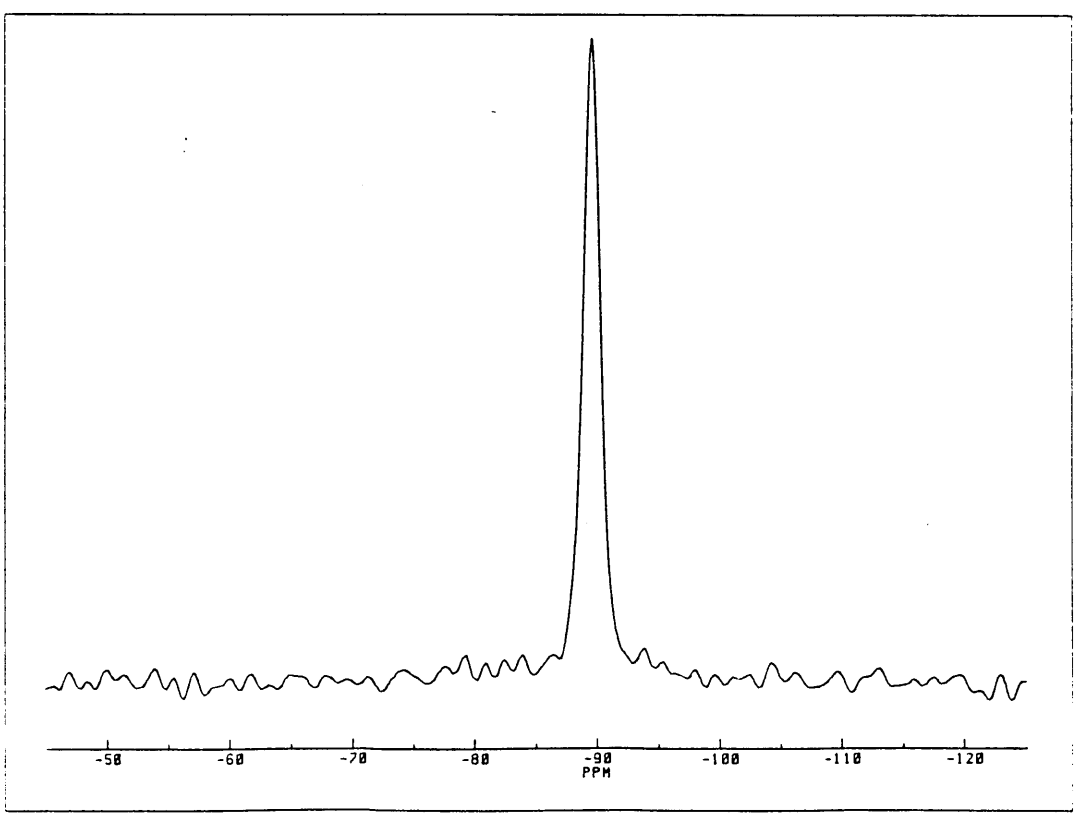

Figure 3.48. ^{29}Si NMR Spectrum of Sample X2

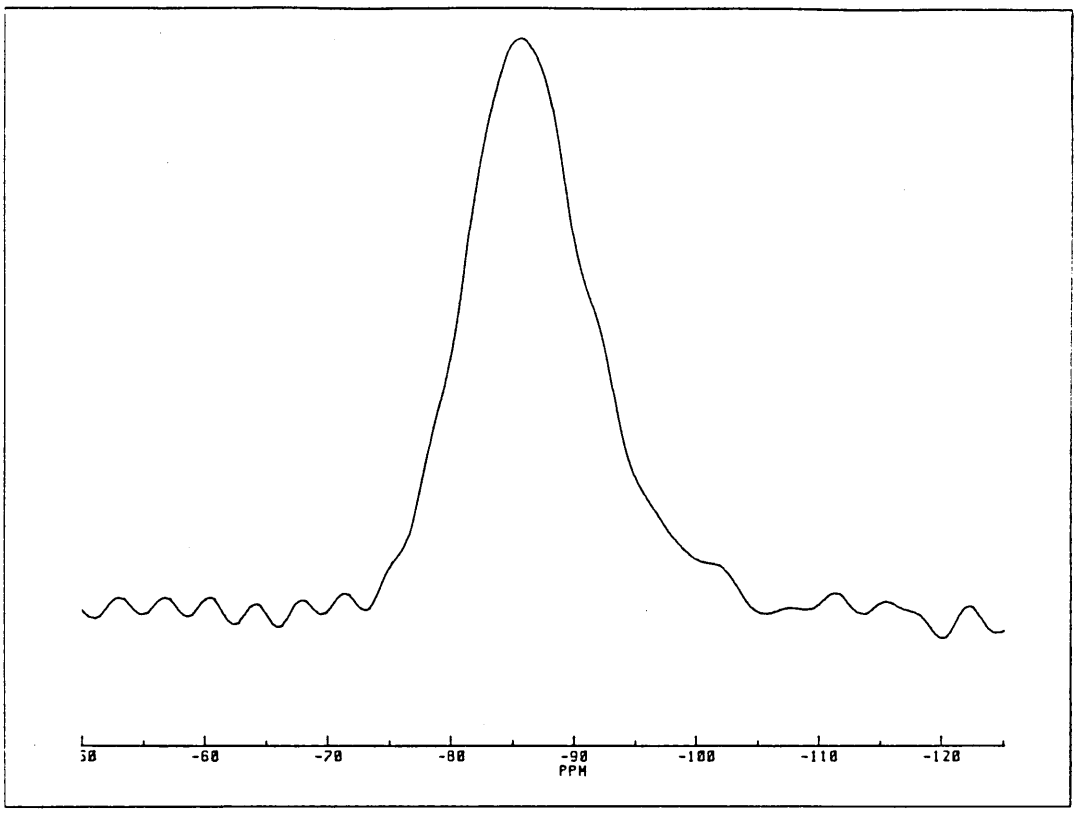

Figure 3.49. ^{29}Si NMR Spectrum of Sample X24

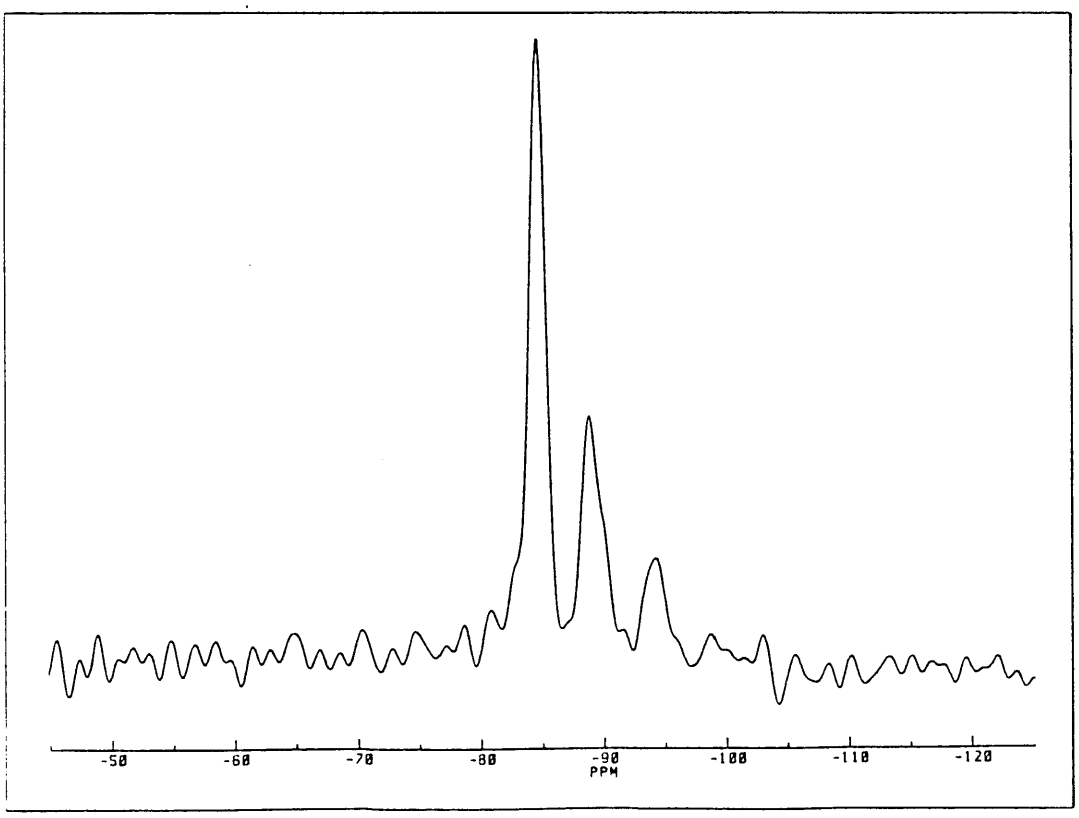

The ^{29}Si NMR spectrum of the crystalline sample X24 is shown in Figure 3.49 and exhibits three major peaks at chemical shifts of -84.6, -88.9 and -94.3 ppm. The largest of these peaks, at -84.6 ppm, is characteristic of $Si(OAl)_4$ units and this indicates a high degree of silicon-aluminium ordering in this sample. The peaks at -88.9 ppm and -94.3 ppm are characteristic of $Si(OAl)_3OSi$ and $Si(OAl)_2(OSi)_2$ units respectively. $SiOAl(OSi)_3$ and $Si(OSi)_4$ units appear to be absent. This is consistent with the observed Si/Al ratio of 1.29 for this sample.

3.5 References

1. F. Meise and F. E. Schwochow, "Molecular Sieves", A. C. S. Adv. in Chem. Ser. 121, (1973), 209
2. D. W. Breck, "Zeolite Molecular Sieves", Robert E. Krieger Publ. Co., (1984), 415-424
3. E. M. Flanigen, H. A. Szymanski and H. Khatami, A. C. S. Adv. in Chem. Ser. 101, (1971), 201
4. R. G. Milkey, Am. Mineralogist, **45**, (1960), 990
5. G. Coudurier, C. Naccache and J. C. Vedrine, J. Chem. Soc. Chem. Comm. 1413, (1982)
6. J. C. Jansen, F. J. Van der Gaag and H. Van Bekkum, Zeolites, **4**, (1984), 369
7. R. M. Milton, U.S. Patent 2,882,243 (1959)
8. D. W. Breck, W. G. Eversole, R. M. Milton, T. B. Reed and T. L. Thomas, J. Am. Chem. Soc., **78**, (1956), 5963
9. R. M. Milton, U.S. Patent 2,882,244 (1959)
10. D. W. Breck and E. M. Flanigen, "Molecular Sieves", Soc. Chem. Ind., London, (1968), 47
11. D. W. Breck, "Zeolite Molecular Sieves", Robert E. Krieger Publ. Co., (1984), 495
12. Y. Tsurata, T. Satoh, T. Yoshida, O. Okumura and S. Ueda, Proc. 7th Int. Conf. Zeolites, Elsevier, Tokyo, (1986), 1001
13. C. A. Fyfe, G. C. Gobi, J. S. Hartman, J. Klinowski and J. M. Thomas, J. Phys. Chem., **86**, (1982), 1247
14. D. Muller, W. Gessner, H. J. Behrens and G. Scheler, Chem. Phys. Lett., **79**, (1981), 59
15. E. Lippmaa, M. Magi, A. Samoson, G. Englehardt and A. R. Grimmer, J. Am. Chem. Soc., **102**, (1980), 4889

16. E. Lippmaa, M. Magi, A. Samoson, M.Tarmak and G. Englehardt, J. Am. Chem. Soc., **103**, (1981), 4992
17. G. Englehardt, B. Fahlke, M. Magi and E. Lippmaa, Zeolites, **3**, (1983), 292
18. J. M. Thomas, C. A. Fyfe, S. Ramdas, J. Klinowski and G. C. Gobbi, J. Phys. Chem., **86**, (1982), 3061
19. W. Lowenstein, Am. Mineral., **39**, (1942), 92

Chapter Four

The Ion Exchange Properties of Aluminosilicate Gels

4.1 Introduction

The ion exchange characteristics of the aluminosilicate gels described in the previous chapter are of crucial importance since they control the detergent builder performance of these materials and, therefore, determine the suitability of such materials as replacements for the phosphate builders.

Cation exchange capacities determine the weight efficiency of zeolite detergent builders. Zeolites with high exchange capacities have a greater weight efficiency than zeolites with low capacities, that is, less zeolite has to be added to the formulation to achieve the same builder performance. Zeolite A, with its 1:1 Si/Al ratio exhibits the maximum theoretical ion exchange capacity and, hence, the highest weight efficiency of the zeolites. This is one of the reasons for the large scale success of this zeolite as a detergent builder. Zeolite X has a lower exchange capacity and, therefore, lower weight efficiency than zeolite A. To compensate for this, higher levels of zeolite X must be used in detergent formulations.

Ion exchange isotherms and their associated Kielland plots demonstrate the selectivity of the zeolite for calcium and magnesium ions over a range of ion uptakes. Zeolite detergent builders must exhibit good selectivity for calcium and magnesium ions, particularly at low $Ca_{(s)}$ and $Mg_{(s)}$ values. Detergency is improved at high ionic strengths and, as a result, detergent formulations frequently contain large quantities of sodium ions. Even the initial fraction of calcium and magnesium ions is low, and zeolites must exhibit the required selectivity under these conditions.

Finally the kinetics of exchange are important because water hardness ions must be removed relatively quickly to prevent reaction with surfactants. Procter and Gamble have defined a minimum acceptable rate of $\approx$ 2 grains per g builder per minute ($\approx$ 0.13g/g builder per minute$\equiv$ 6.5 x 10^{-3} meq Ca^{2+} or 1.1 x 10^{-2} meq Mg^{2+} per g builder per minute)[1]

This chapter describes work carried out to determine the maximum exchange capacities and the selectivities and kinetics of the exchange reactions of the aluminosilicate gels described in the previous chapter.

4.2 Ion Exchange Capacities

Ion exchange capacities were determined radiochemically using ^{22}Na as a tracer ion. The ^{22}Na isotope is a gamma emitter with a half life of 2.6 years and, as such, can not only be used to determine exchange capacities, but also for the determination of ion exchange isotherms and kinetics.

When a solution containing a mixture of ^{22}Na and ^{23}Na ions is allowed to equilibrate with the pure sodium (100% ^{23}Na) form of a zeolite or aluminosilicate gel, an isotopic redistribution takes place. Some of the radioactive ^{22}Na ions partition into the solid phase and, at equilibrium, the ratio of ^{22}Na to ^{23}Na in the solid phase is identical to that in the liquid phase. The relative radioactivities of the two phases can thus be used to calculate the ion exchange capacity of the solid sample.

The natural abundance of the ^{23}Na isotope is 100%. The ^{22}Na isotope is a synthetic isotope prepared by exposing Magnesium (^{24}Mg) to deuterons in a cyclotron. ^{22}Na tagged sodium chloride solutions are prepared by adding small volumes (5-10ml) of a highly dilute solution of $^{22}NaCl$ to concentrated solutions of $^{23}NaCl$ and diluting to the required concentration. The concentration of sodium in the $^{22}NaCl$ solution is sufficiently small to be neglected.

Small, precisely known weights (approximately 0.1g) of the pure sodium forms of the aluminosilicate gel samples were equilibrated with accurately known volumes of ^{22}Na tagged 0.1N sodium chloride (BDH Analar) solution. Sealable plastic tubes were used throughout. Isotopic dilution takes place fairly rapidly, but to ensure complete equilibration, samples were equilibrated for a minimum period of 24 hours. After equilibration, the solid and liquid phases were separated by centrifugation and small accurately known volumes of the liquid (about 5ml) were removed. The radioactivity of these liquid samples was determined using an LKB Wallac 1282 Universal Gamma Counter. Count rates for similar volumes of the original tagged sodium chloride solution were also

determined at the same time. Ion exchange capacities (IECs) were then determined according to the following equation:

$$IEC = \frac{(\text{Ref count} - \text{Liq count}) \times \text{Volume added} \times \text{Conc}^n}{\text{Liq count} \times \text{Sample Wt.}}$$

where:

Ref count = Count rate for original NaCl solution (CPM/ml)

Liq count = Count rate for NaCl solution after equilibration with sample (CPM/ml)

Volume Added = Volume tracer solution added (ml)

$Conc^n$ = Concentration of tracer solution (meq/ml)

Sample wt = Weight of sample (g)

^{22}Na has a relatively long radioactive half life and as sample and reference solutions were counted at the same time, there was no need to make a correction for radioactive decay. The determination of count rates in counts per minute (CPM) per ml provided the necessary correction for differences in volume between sample and reference solutions.

Water capacities were also determined (see section 3.5d) for each sample and, from this data, dehydrated ion exchange capacities were calculated. The dehydrated ion exchange capacity provides a measure of the exchange capacity per unit weight (g) of aluminosilicate framework.

Hydrated and dehydrated ion exchange capacities for the zeolite A type samples are summarised in Table 4.1 and are shown in Figure 4.1. The amorphous aluminosilicate gel samples exhibit lower exchange capacities than their crystalline counterparts, although, because the amorphous samples have higher water capacities, this effect is less marked for the dehydrated ion exchange capacities.

Table 4.1. Ion Exchange Capacities of Zeolite A Type Samples

Sample	Hydrated IEC (meq/g)	Dehydrated IEC (meq/g)
A0	4.441 ± 0.018	6.120
A1	4.446 ± 0.036	6.186
A2	4.310 ± 0.040	5.949
A3	5.113 ± 0.095	6.627
A4	5.333 ± 0.095	6.751
A6	5.336 ± 0.110	6.765
A8	5.315 ± 0.021	6.719
A10	5.345 ± 0.031	6.772
A12	5.326 ± 0.015	6.766
A14	5.384 ± 0.065	6.812

The shape of the plots of ion exchange capacity against gel reaction time for both hydrated and dehydrated samples (Figure 4.1) suggest that such plots can be useful indicators of the presence of crystalline zeolite A. These curves are characterised by an initial period of more or less constant ion exchange capacity followed by a rapid increase then another period of constant ion exchange capacity. This shape is typical of plots of crystallinity versus time for zeolite syntheses. The crystalline samples (A4 to A14) exhibit an average hydrated ion exchange capacity of 5.340 meq/g (±0.044 meq/g). This relatively high ion exchange capacity is characteristic of zeolite A. The non-crystalline samples (A0 to A2) exhibit an lower average capacity of 4.399 meq/g (±0.089 meq/g). As expected from its characterisation data, sample A3 exhibits an exchange capacity (5.113 meq/g) intermediate between these two extremes.

Figure 4.1. Ion Exchange Capacities of the Zeolite A Type Samples

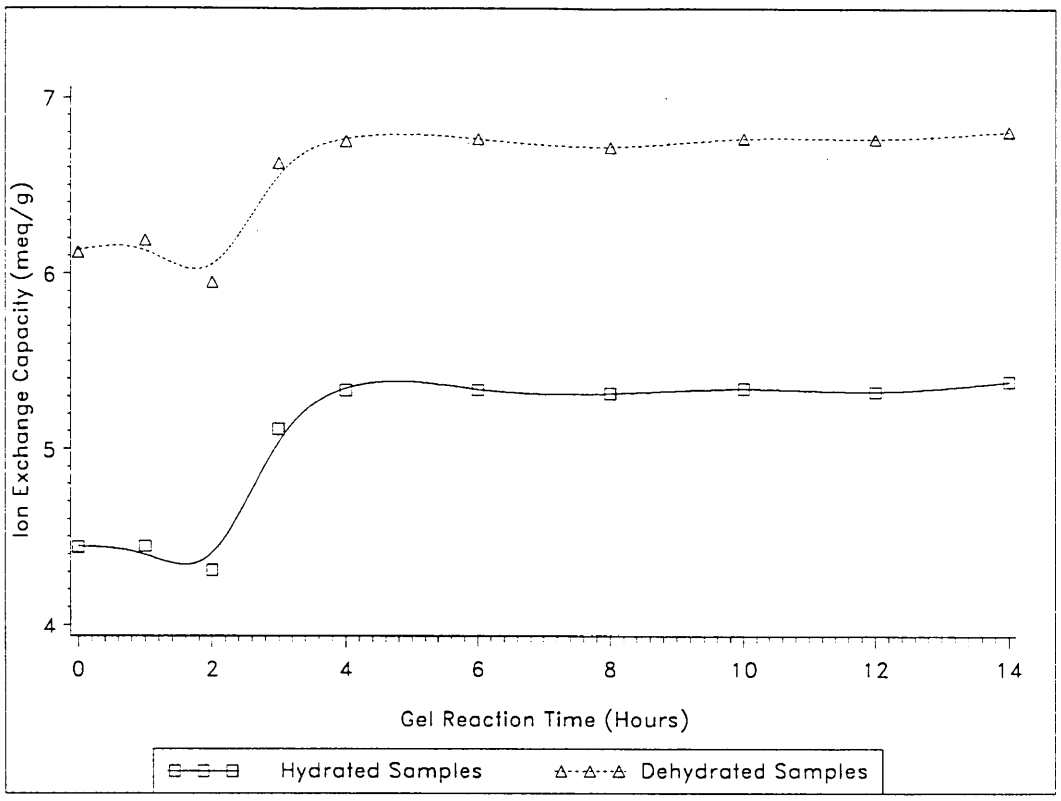

Tsurata et al[2] have carried out similar work in which they investigated the performance of amorphous aluminosilicates (obtained from the synthesis of zeolite A) as detergent builders. Their results correlate extremely well with those presented here, although, under the synthesis conditions that they used, crystalline zeolite A first appeared after approximately one hour and the synthesis reaction was essentially complete in two hours.

Similar results for the zeolite X type samples are presented in Table 4.2 and in Figure 4.2. Here, the hydrated ion exchange capacities show a more complex behaviour than that observed for the zeolite A type samples. The initial amorphous sample (sample X0) exhibits a low hydrated exchange capacity, but, as the reaction time increases, the hydrated ion exchange capacity increases to a maximum (sample X3) and then decreases again as crystalline zeolite X appears. The crystalline samples (samples X8 to X24) show a more or less constant ion exchange capacity. For these samples, the average hydrated ion exchange capacity is 4.518 (± 0.086) meq/g.

The shape of the plot of hydrated ion exchange capacity against gel reaction time for the zeolite X type samples (Figure 4.2) is almost exactly the reverse of the plot of uncalcined water capacity against gel reaction time for these samples (Figure 3.13). This would tend to suggest that the complex behaviour observed for these samples could be explained, at least in part, by their water capacities. The plot of dehydrated ion exchange capacities against gel reaction time (Figure 4.2), apart from the initial sample X0 which exhibits a low ion exchange capacity, follows a straight line at 6.076 (± 0.096) meq/g. Clearly, in the case of zeolite X synthesis, such plots cannot be used to indicate the presence of crystalline zeolite X.

Table 4.2. Ion Exchange Capacities of Zeolite X Type Samples

Sample	Hydrated IEC (meq/g)	Dehydrated IEC (meq/g)
X0	4.170 ± 0.069	5.600
X1	4.530 ± 0.057	5.994
X2	4.500 ± 0.047	5.994
X3	4.798 ± 0.067	6.191
X4	4.782 ± 0.048	6.122
X6	4.699 ± 0.041	6.084
X8	4.538 ± 0.031	6.070
X10	4.432 ± 0.057	5.979
X12	4.533 ± 0.096	6.065
X24	4.568 ± 0.117	6.184

Figure 4.2. Ion Exchange Capacities of the Zeolite X Type Samples

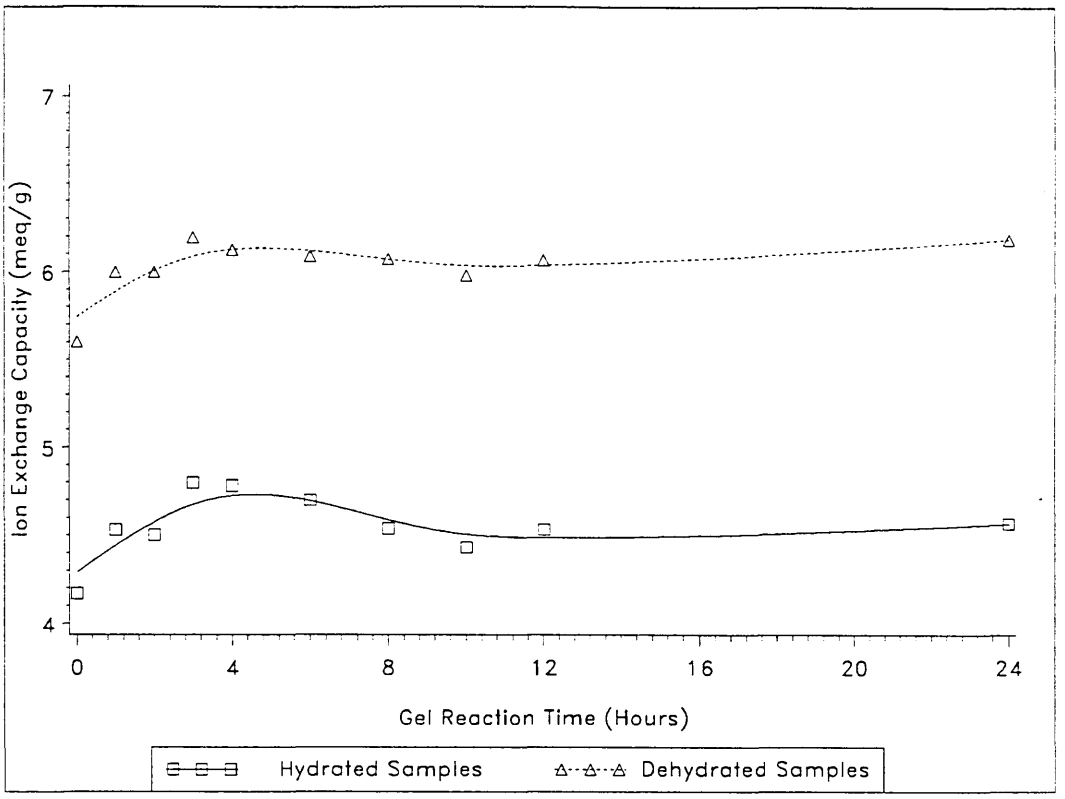

4.3 Ion Exchange Isotherms

Ion exchange isotherms were also determined radiochemically using ^{22}Na as a tracer ion. An accurately known volume of 0.05N calcium or magnesium chloride solution (BDH Analar) was added to a precisely known weight of the pure sodium form of each sample in 15ml plastic centrifuge tubes. To this was added an accurately known volume of ^{22}Na tagged 0.05N sodium chloride solution (BDH Analar). By varying the volumes of calcium or magnesium chloride and sodium chloride solutions, a significant portion of the ion exchange isotherm could be determined.

The equilibration of these samples involved two processes; the isotopic dilution of ^{22}Na and the exchange of calcium or magnesium ions in the solution phase with sodium ions from the zeolite phase. All samples were equilibrated for a week at 25°C to ensure the attainment of equilibrium.

After equilibration, the liquid was separated from the solid by centrifugation and an accurately known volume (about 5ml) of the liquid, together with similar volumes of the original ^{22}Na tagged sodium chloride solution were counted using the LKB Wallac 1282 Universal Gamma Counter. The count rates of sample and reference solutions were then used to calculate isotherm points.

It should be noted that magnesium chloride is only available as the hexahydrate. This salt is hygroscopic and the concentration of solutions prepared from it must be verified. In order to ensure that magnesium chloride solutions were of the correct concentration, EDTA titrations were carried out[5]. Calcium chloride is available as the dihydrate or as the hexahydrate. The hexahydrate is hygroscopic, but the dihydrate is less so. For this reason, only the dihydrate was used to prepare solutions of calcium chloride, although the concentrations of these were also checked by EDTA titration.

This relatively simple method allowed determination of a significant portion of the ion exchange isotherm and limited the amount of radioactive solid that needed to be handled. However, at high $Ca_{(s)}$ and $Mg_{(s)}$ values this method could not be used. Here the change in radioactivity of the solution phase was too small to be conveniently or accurately measured. To overcome this problem, ^{22}Na tagged sodium exchange solids were used.

The pure sodium forms of each sample were first equilibrated with ^{22}Na tagged sodium chloride then washed repeatedly with distilled deionised water adjusted to pH 10 (to prevent the loss of sodium ions from within the framework), dried in an oven at 50°C and finally re-equilibrated with water vapour in a desiccator over saturated sodium chloride solution. The activity of these solids could be determined by counting either the liquid equilibrium solution or the solid phase. Generally, activities were determined from liquid phase count rates. Accurately known weights of these active solids were then equilibrated with precisely known volumes of 0.05N calcium or magnesium chloride solution (BDH Analar)and the isotherm points determined by counting a known volume of the equilibrium solution.

A similar problem existed at low $Ca_{(s)}$ and $Mg_{(s)}$ values. The isotherms were found to be highly selective to calcium and magnesium ions and, at points below $Ca_{(s)}$=0.6 or $Mg_{(s)}$=0.5 the solution concentration of calcium or magnesium

ions was extremely low. Indeed, at points near the origin, the solution concentration of calcium or magnesium could be as low as 10^{-6}M. As a result, the statistical error involved in the radiotracer method was too large to allow accurate determination of these isotherm points. This region of the isotherm was determined using atomic absorption analysis.

Known weights of each sample were equilibrated with solutions containing sodium ions and calcium or magnesium ions exactly as before, except that non-radioactive solutions were used to avoid contaminating the spectrophotometer. Calcium and magnesium ion concentrations in solution were then determined by atomic absorption spectrophotometry.

Despite the low levels of calcium and magnesium in these solutions, many needed dilution to allow accurate analysis using this technique. Chemical matrix effects can be quite important in atomic absorption analysis and it is necessary to minimise these effects as far as possible. Since the isotherm equilibrium solutions were effectively 0.05N sodium chloride containing low levels of calcium or magnesium, all dilutions were carried out with 0.05N sodium chloride solution (BDH Analar), thus keeping constant the chemical matrix from which calcium or magnesium was analysed. Standard and blank solutions were also prepared using 0.05N sodium chloride solution.

The determination of calcium or magnesium in solution by atomic absorption analysis may be subject to interference from phosphorus or aluminium. To overcome this, a stock solution of 5% lanthanum (as lanthanum chloride; BDH Analar) in 25% (v/v) hydrochloric acid was prepared and added to standard, blank and test solutions such that the final concentration of lanthanum was 1% and that of hydrochloric acid was 5%. This concentration of lanthanum was capable of protecting the calcium or magnesium determination from up to 200 ppm phosphorus and 1000 ppm aluminium in the final diluted solution.

Hydronium ion exchange has been shown to occur in some exchanges[3,4], and may give rise to significant errors in determination of the isotherm points. Thus, all solutions were prepared using boiled distilled deionised water since boiling removes dissolved carbon dioxide, raising the pH and reducing the probability of hydronium ion exchange. In addition, a number of points in each isotherm were checked by titrating for calcium or magnesium in the equilibrium isotherm solution. An EDTA titration was used (Solochrome Black 6B as an indicator)[5] for this purpose.

All ion exchange isotherms were determined at a total solution normality of 0.05N and at a constant temperature of 25°C.

Sodium-calcium and sodium-magnesium ion exchange isotherms for the zeolite A type samples are shown in Figures 4.3 and 4.4 respectively. Numerical data is given in appendix 1. Samples A3 to A14 all produced identical isotherms for both sodium-calcium and sodium-magnesium exchange. Thus, only the isotherm for sample A14, that is the sample with the longest reaction time, is shown on these diagrams.

Figure 4.3. Sodium-Calcium Ion Exchange Isotherms for Zeolite A type Samples

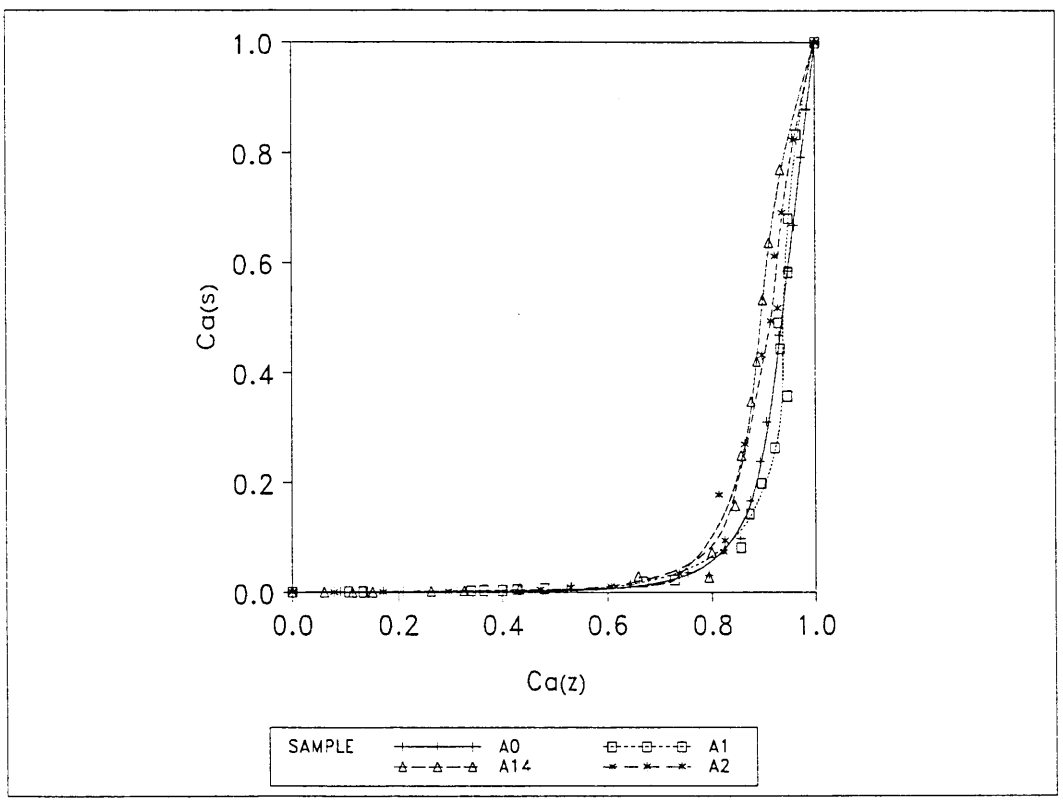

The sodium-calcium isotherms indicate that all of the zeolite A type samples showed good selectivity for the ingoing ion (calcium). There is a change of selectivity with gel reaction time, selectivity for calcium generally increasing with decreasing reaction time. This effect is, however, fairly small. Samples A0 and A1 show very similar isotherms, as do samples A2 and A14. Since sample A2 has been shown to consist purely of amorphous material, it is surprising that it should exhibit a similar isotherm to crystalline zeolite A.

This is also true of sample A3 which contains a significant proportion of amorphous material.

Figure 4.4. Sodium-Magnesium Ion Exchange Isotherms for Zeolite A type Samples

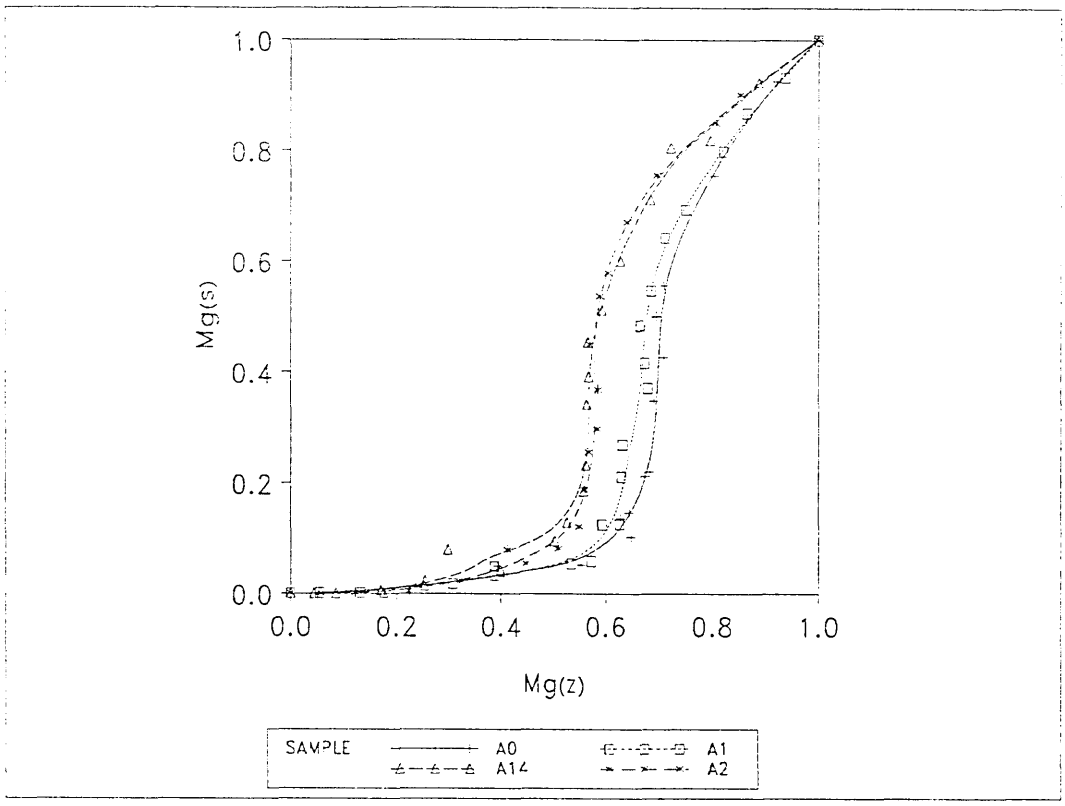

The sodium-magnesium isotherms also indicate that all of the zeolite A type samples show good selectivity for the ingoing ion (magnesium), although the selectivity for magnesium is lower than for calcium, as might be expected. Again there is a decrease in selectivity for magnesium as the gel reaction time [illegible] This effect is more marked than in sodium-calcium exchange. Here there is a clear distinction between samples A0 and A1, although sample A2 still exhibits a similar isotherm to sample A14.

Sodium-calcium and sodium-magnesium isotherms for the zeolite X type samples are shown in Figures 4.5 and 4.6 respectively. Numerical data is also given in appendix 1. Here samples X8 to X24 all produced identical isotherms and only the isotherm for sample X24 is shown. Samples X4 and X6 (not shown) produced identical isotherms, both showing an even lower selectivity than sample X3.

Figure 4.5. Sodium-Calcium Ion Exchange Isotherms for Zeolite X type Samples

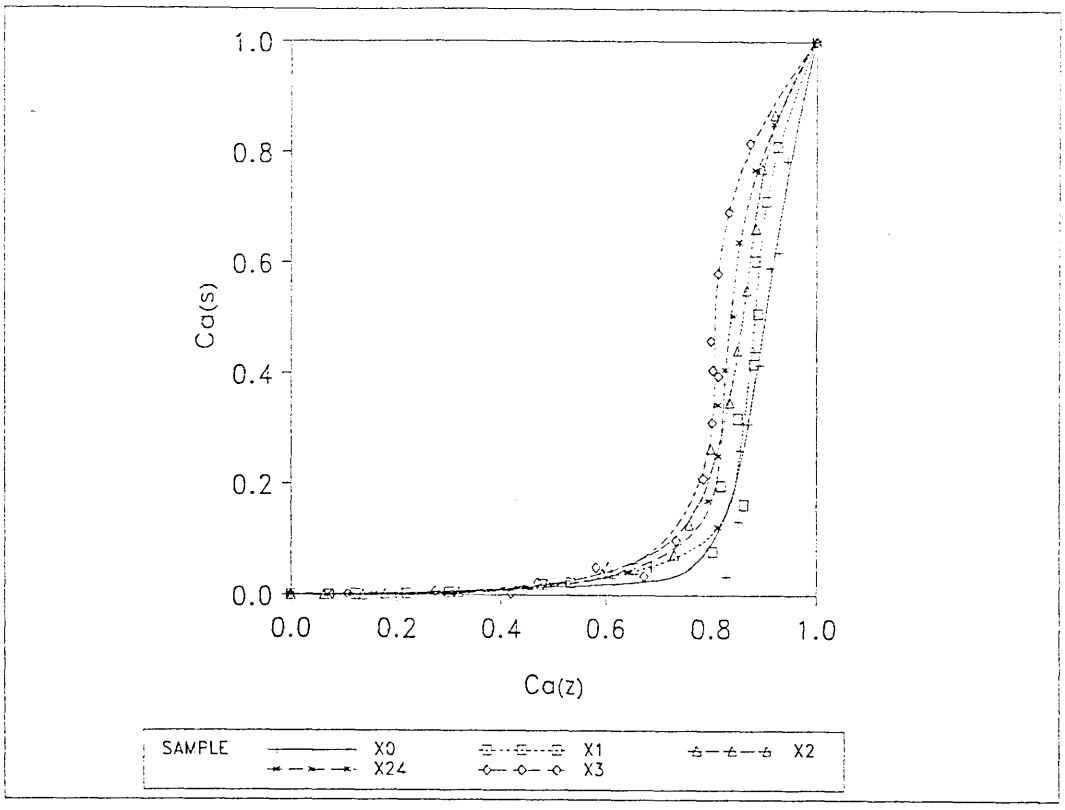

The sodium-calcium ion exchange isotherms for the zeolite X type samples also show good selectivity for the ingoing ion (calcium), although the selectivity is not as good as that shown by the zeolite A type samples. There is a clear decrease in selectivity for calcium as the gel reaction time increases, although this trend reverses as zeolite X crystallises and the isotherm for sample X24 lies between those of samples X2 and X3.

A similar situation exists for the sodium-magnesium ion exchange isotherms, shown in Figure 4.6. With the exception of samples X3, X4 and X6 the selectivity for the ingoing ion (magnesium) appears to be good. Again, there is a decrease in selectivity with increasing gel reaction time, and again this trend reverses as zeolite X crystallises. In this case, the ion exchange isotherm for the totally crystalline sample X24 lies between those of samples X1 and X2.

As with the zeolite A type gels, it is interesting to note that sample X4, which has been shown to consist of purely amorphous material, and sample X6, which contains a significant proportion of crystalline material, both exhibit identical

sodium-calcium and sodium-magnesium ion exchange isotherms to each other, although the selectivity to magnesium is extremely poor.

Figure 4.6. Sodium-Magnesium Ion Exchange Isotherms for Zeolite X type Samples

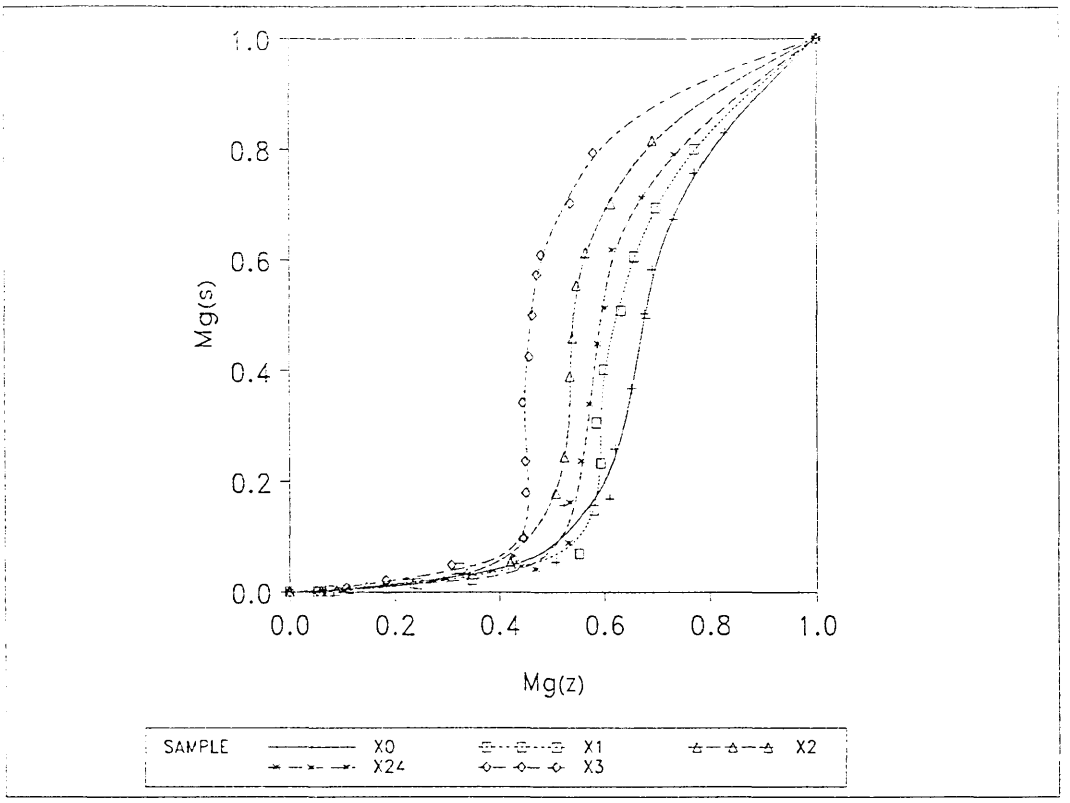

For uni-divalent ion exchanges such as sodium-calcium exchange, the corrected selectivity coefficient (K_c) can be calculated from the isotherm points using the following expression:

$$K_c = \frac{Ca_{(z)} \cdot (Na_{(s)})^2}{Ca_{(s)} \cdot (Na_{(z)})^2} \cdot 2N \cdot \Gamma$$

where N is the total solution normality and:

$$\Gamma = \frac{\gamma_{\pm}^{4}{}_{NaCl}}{\gamma_{\pm}^{3}{}_{CaCl_2}}$$

Similar expressions can be used for calculating the corrected selectivity coefficients for sodium-magnesium exchange. These data can then be used to generate a plot of $\log_{10}K_c$ against $Ca_{(z)}$ or $Mg_{(z)}$, the so called Kielland plot.

Evaluation of this expression, however, requires that the ion activity coefficients in mixed dilute solution are known. For sodium-calcium exchange, mean molal activity coefficients in the concentration range of interest can be obtained from the literature[6]. Glueckauf's equation[7] or the data of Moore and Ross[8] can be used to calculate values of Γ. For sodium-magnesium exchange, there are no literature data available, but it has been shown that values of γ_{MgCl_2} are remarkably similar to values of γ_{CaCl_2} and, therefore, that it is reasonable to use the same values of Γ for sodium-magnesium exchange as for sodium-calcium exchange[9].

In Figure 4.7 two plots of Γ as a function of $Ca_{(s)}$ are shown. The first of these has been determined using Glueckauf's equations, the second using the data of Moore and Ross. Clearly, these two approaches to calculating Γ produce very different results. Glueckauf's equations produce a straight line of the following form:

$$\Gamma = 1.43 + 0.1043Ca_{(s)}$$

The data of Moore and Ross, however, produces a curve which can be described by the following equation:

$$\Gamma = 1.64 - 0.40Ca_{(s)} + 0.19Ca_{(s)}^2 - 0.04Ca_{(s)}^3$$

For this study the data of Moore and Ross was used to calculate Γ. The same values of Γ were used for both sodium-calcium and sodium-magnesium ion exchange. However, because of the discrepancy between Glueckauf's equations and the data of Moore and Ross, $\log_{10}K_c$ was calculated for sodium-magnesium exchange in sample A0 using both methods. These results are shown in Figure 4.8 and indicate that the choice of method used for calculating Γ is relatively arbitrary. Clearly, there is very little difference between the values of $\log_{10}K_c$ when Γ is calculated using Glueckauf's equations and those calculated using the data of Moore and Ross. This discrepancy is even less important when the scatter of the experimental data is considered.

Figure 4.7. Γ as a Function of $Ca_{(s)}$

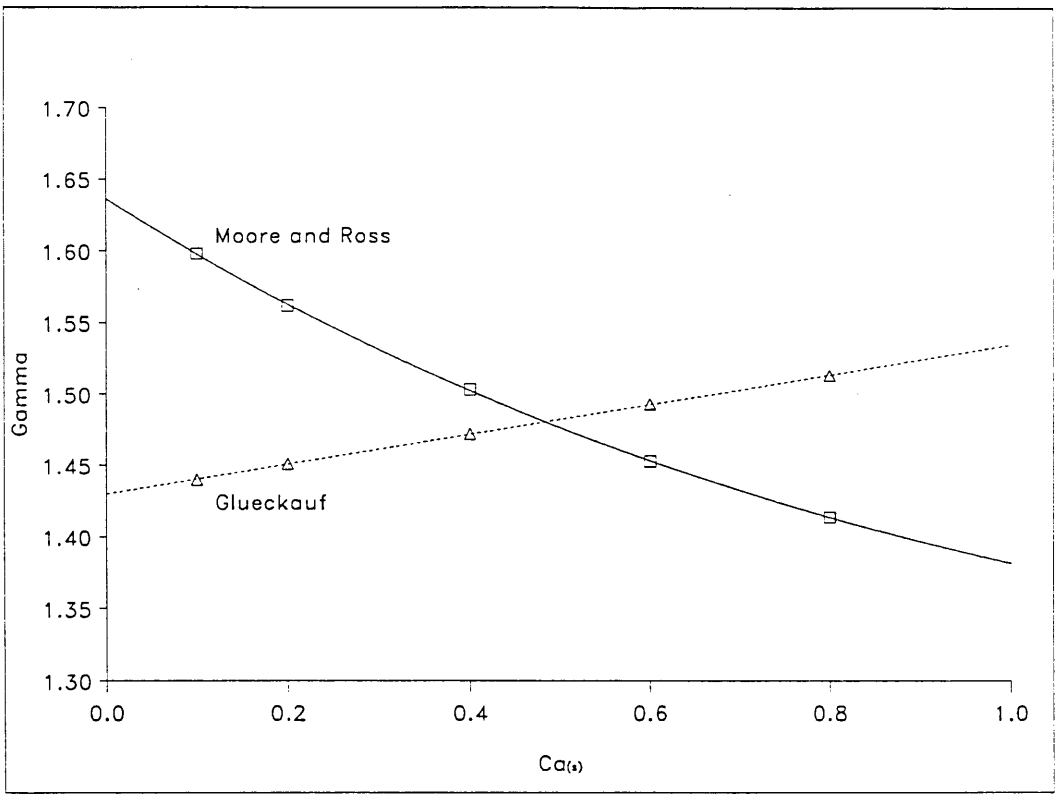

Having obtained plots of $\log_{10}K_c$ as a function of $Ca_{(z)}$ or $Mg_{(z)}$ it is possible to fit polynomial expressions of the following form to the experimental data:

$$\log_{10}K_c = B_0 + B_1Ca_{(z)} + B_2Ca_{(z)}^2 + B_3Ca_{(z)}^3 + \ldots$$

These polynomial expressions can then be used to calculate the thermodynamic selectivity coefficient, K_a, and the standard free energy of the ion exchange reaction, ΔG^θ according to the following equations:

$$\ln K_a = (z_b - z_a) + \int_0^1 \ln K_c dCa_{(z)}$$

$$\Delta G^\theta = - \frac{RT}{z_a z_b} \ln K_a$$

Similar expressions are used for sodium-magnesium exchange.

$Log_{10}K_c$ plots for sodium-calcium and sodium-magnesium exchange in the zeolite A type samples are shown in Figures 4.9 and 4.10 respectively. The points on these diagrams represent the experimental data and the lines represent

Figure 4.8. The Effect on Plots of $Log_{10}K_c$ vs $Mg_{(z)}$ of Using Glueckauf's Equations or the Data of Moore and Ross to Calculate Γ (Sample A0 Sodium-Magnesium Exchange)

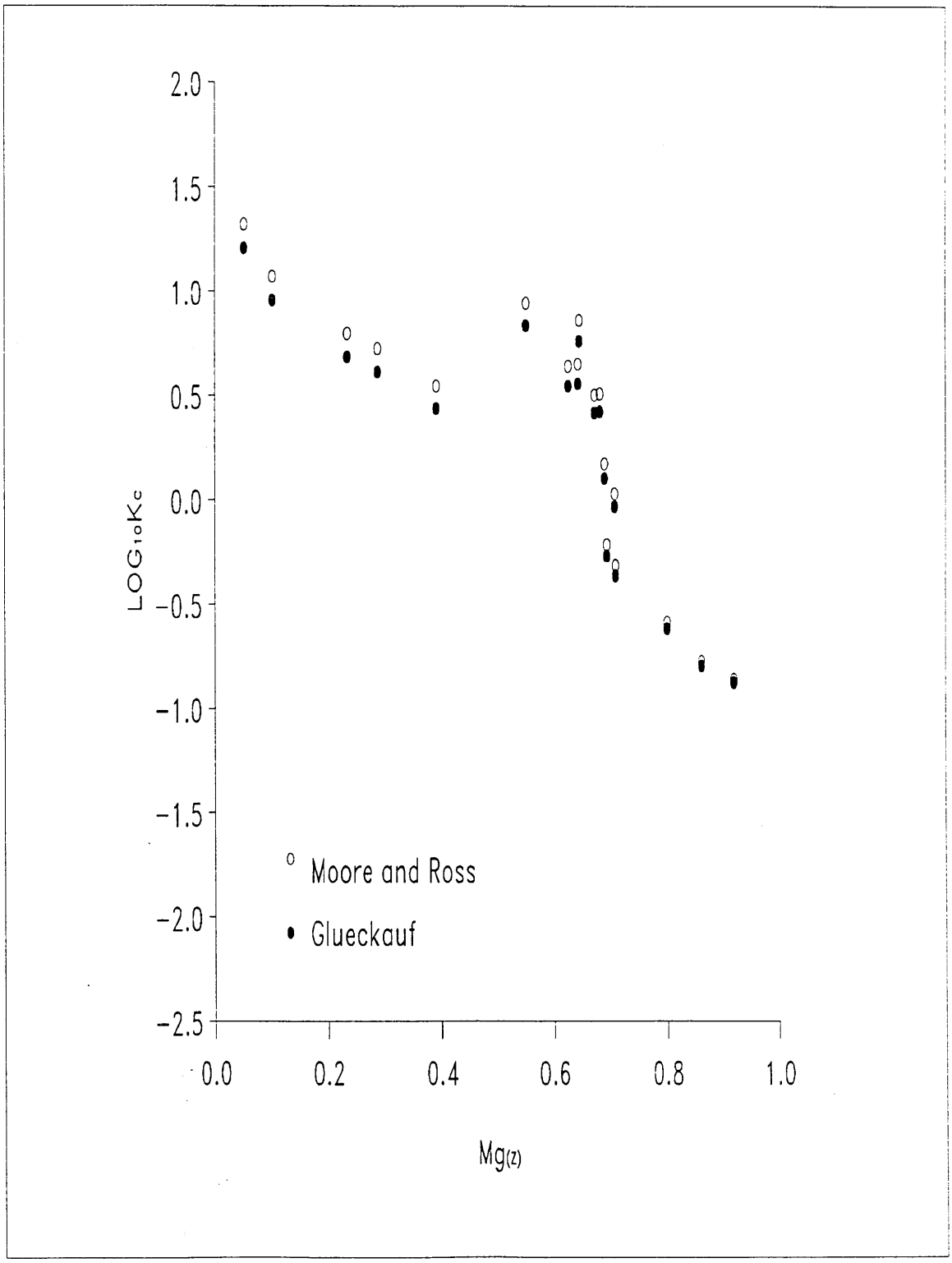

the polynomial expressions that best describe the data. These polynomials were determined using a least squares fitting routine (using the SAS statistical analysis computer package[10,11]). Linear, quadratic and cubic polynomials were fitted to the experimental data and an "R" factor determined. This factor is defined as follows:

$$R = \sum \frac{(\log_{10}K_{c\ (observed)} - \log_{10}K_{c\ (predicted)})^2}{M - N - 1}$$

where M is the number of data points used in the calculation and N is the order of the equation. R is, therefore, a measure of how well the polynomial expression fits the experimental data and can be used as a selection criterion for determining the best polynomial fit.

The $\log_{10}K_c$ plots for sodium-calcium exchange in the zeolite A type samples (Figure 4.9) again emphasise the decrease in selectivity for calcium (the ingoing ion) as the gel reaction time increases, although at low values of $Ca_{(z)}$ sample A0 exhibits the poorest selectivity.

It is evident that there is a lot of scatter on the experimental data. This is, at least partially, due to the fact that the expression relating $\log_{10}K_c$ to $Ca_{(z)}$ contains terms in $(Na_{(s)})^2$ and $(Na_{(z)})^2$. As a result, small errors in the determination of the isotherm points can give rise to relatively large errors in the calculation of $\log_{10}K_c$. This is especially true at very low values of $Ca_{(z)}$. Because these samples exhibit good selectivity towards calcium, low $Ca_{(z)}$ values correspond to very low $Ca_{(s)}$ values and the concentration of calcium in the equilibrium solution can be as low as 10^{-6}M. Despite the use of atomic absorption spectrophotometry for determining isotherm points at these low values, it is likely that significant errors exist.

As a consequence of the large scatter on the data, difficulty was encountered in fitting reasonable polynomials to the data. Fourth and fifth order polynomials gave very good fits to the data, but produced complex curves exhibiting maxima and minima and generally showing a sharp increase in $\log_{10}K_c$ at values of $Ca_{(z)}$ around 0.9. For this reason, polynomial fits were restricted to linear, quadratic or cubic equations.

Figure 4.9. $Log_{10}K_c$ vs $Ca_{(z)}$ Plots for Sodium-Calcium Exchange in Zeolite A Type Samples

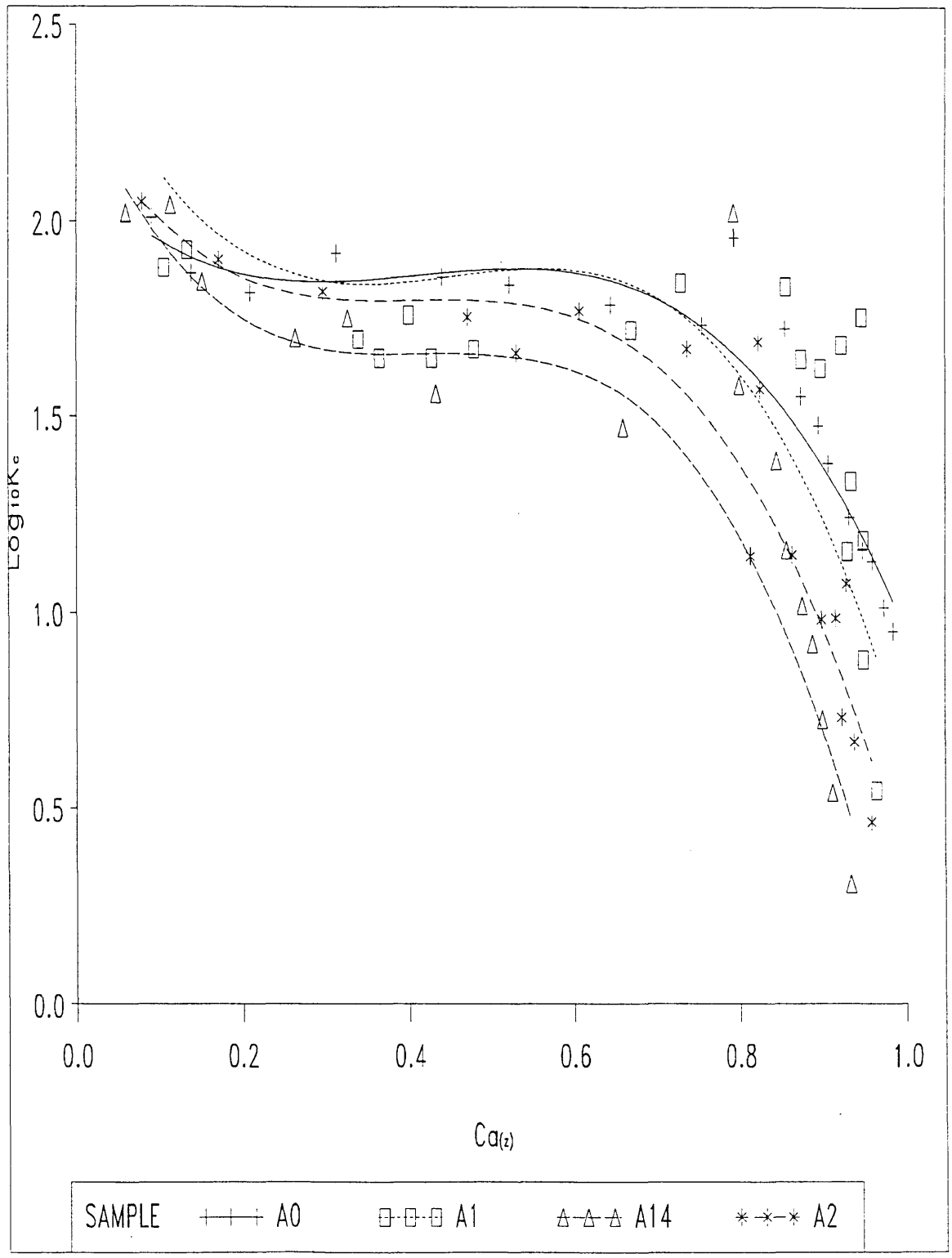

Polynomial fits for sodium-calcium exchange in the zeolite A type samples, together with their associated R values are shown in Table 4.3. In each case, the cubic expression was found to have the lowest R value and, therefore to provide the best fit to the data. These expressions have been used to evaluate K_a and ΔG^θ (in KJ/g equivalent), which are also given in Table 4.3

Table 4.3. Polynomial Fits for Sodium-Calcium Exchange in the Zeolite A Type Samples

Sample	Polynomial Equation	R	K_a	ΔG^θ
A0	$\log_{10}K_c = 2.15 - 0.85Ca_{(z)}$	0.05		
	$\log_{10}K_c = 1.84 + 0.97Ca_{(z)} - 1.72Ca_{(z)}^2$	0.03		
	$\log_{10}K_c = 2.13 - 2.38Ca_{(z)} + 6.30Ca_{(z)}^2 - 5.10Ca_{(z)}^3$	0.01	58.11	-5.03
A1	$\log_{10}K_c = 2.35 - 1.27Ca_{(z)}$	0.13		
	$\log_{10}K_c = 2.03 + 0.65Ca_{(z)} - 1.81Ca_{(z)}^2$	0.16		
	$\log_{10}K_c = 2.51 - 4.39Ca_{(z)} + 11.45Ca_{(z)}^2 - 8.43Ca_{(z)}^3$	0.12	59.13	-5.06
A2	$\log_{10}K_c = 2.37 - 1.50Ca_{(z)}$	0.08		
	$\log_{10}K_c = 1.87 + 1.15Ca_{(z)} - 2.50Ca_{(z)}^2$	0.06		
	$\log_{10}K_c = 2.28 - 3.63Ca_{(z)} + 8.95Ca_{(z)}^2 - 7.28Ca_{(z)}^3$	0.03	42.68	-4.65
A14	$\log_{10}K_c = 2.31 - 1.79Ca_{(z)}$	0.20		
	$\log_{10}K_c = 1.82 + 1.15Ca_{(z)} - 2.78Ca_{(z)}^2$	0.18		
	$\log_{10}K_c = 2.33 - 4.88Ca_{(z)} + 11.68Ca_{(z)}^2 - 9.19Ca_{(z)}^3$	0.09	30.51	-4.24

The values for ΔG^θ indicate that for, sodium-calcium exchange, the zeolite A type samples exhibit good overall selectivity for calcium and that the selectivity increases in the following order:

$$A0 = A1 > A2 > A14$$

Sherry and Walton[12] found ΔG^θ to be -3.06KJ/g equivalent for sodium-calcium exchange in zeolite A. Barri[9] reported a value of -2.68KJ/g equivalent. The value of -4.24KJ/g equivalent found here for the crystalline sample A14 is in reasonable agreement with these figures.

The $\log_{10}K_c$ plots for sodium-magnesium exchange in the zeolite A type samples (Figure 4.10) also confirm the decrease in selectivity for magnesium as the gel reaction time increases. However, at low values of $Mg_{(z)}$, this trend appears to reverse with sample A0 showing the poorest selectivity.

Polynomial equations have been fitted to this data and these are summarised in Table 4.4. Third order polynomials were again found to provide the best fits to the data, although in most cases there was very little difference between the values of R for linear, quadratic or cubic expressions.

Table 4.4. Polynomial Fits for Sodium-Magnesium Exchange in the Zeolite A Type Samples

Sample	Polynomial Equation	R	K_a	ΔG^θ
A0	$\log_{10}K_c = 1.46 - 2.20Mg_{(z)}$	0.17		
	$\log_{10}K_c = 0.98 + 1.01Mg_{(z)} - 3.46Mg_{(z)}^2$	0.10		
	$\log_{10}K_c = 1.38 - 4.06Mg_{(z)} + 9.95Mg_{(z)}^2 - 9.46Mg_{(z)}^3$	0.08	2.02	-0.87
A1	$\log_{10}K_c = 1.79 - 2.82Mg_{(z)}$	0.11		
	$\log_{10}K_c = 1.54 + 1.11Mg_{(z)} - 1.84Mg_{(z)}^2$	0.11		
	$\log_{10}K_c = 1.67 - 2.75Mg_{(z)} + 2.49Mg_{(z)}^2 - 3.06Mg_{(z)}^3$	0.11	1.18	-0.21
A2	$\log_{10}K_c = 1.86 - 3.68Mg_{(z)}$	0.11		
	$\log_{10}K_c = 1.70 - 2.59Mg_{(z)} - 1.17Mg_{(z)}^2$	0.11		
	$\log_{10}K_c = 1.50 - 0.03Mg_{(z)} - 7.95Mg_{(z)}^2 + 4.78Mg_{(z)}^3$	0.11	1.06	-0.08
A14	$\log_{10}K_c = 1.78 - 3.61Mg_{(z)}$	0.13		
	$\log_{10}K_c = 1.83 - 3.89Mg_{(z)} + 0.31Mg_{(z)}^2$	0.13		
	$\log_{10}K_c = 1.79 - 3.43Mg_{(z)} - 0.93Mg_{(z)}^2 + 0.87Mg_{(z)}^3$	0.13	0.97	+0.04

The values of ΔG^θ that have been obtained confirm that the order of selectivity for magnesium is:

$$A0 > A1 > A2 > A14$$

Figure 4.10. $Log_{10}K_c$ vs $Mg_{(z)}$ Plots for Sodium-Magnesium Exchange in Zeolite A Type Samples

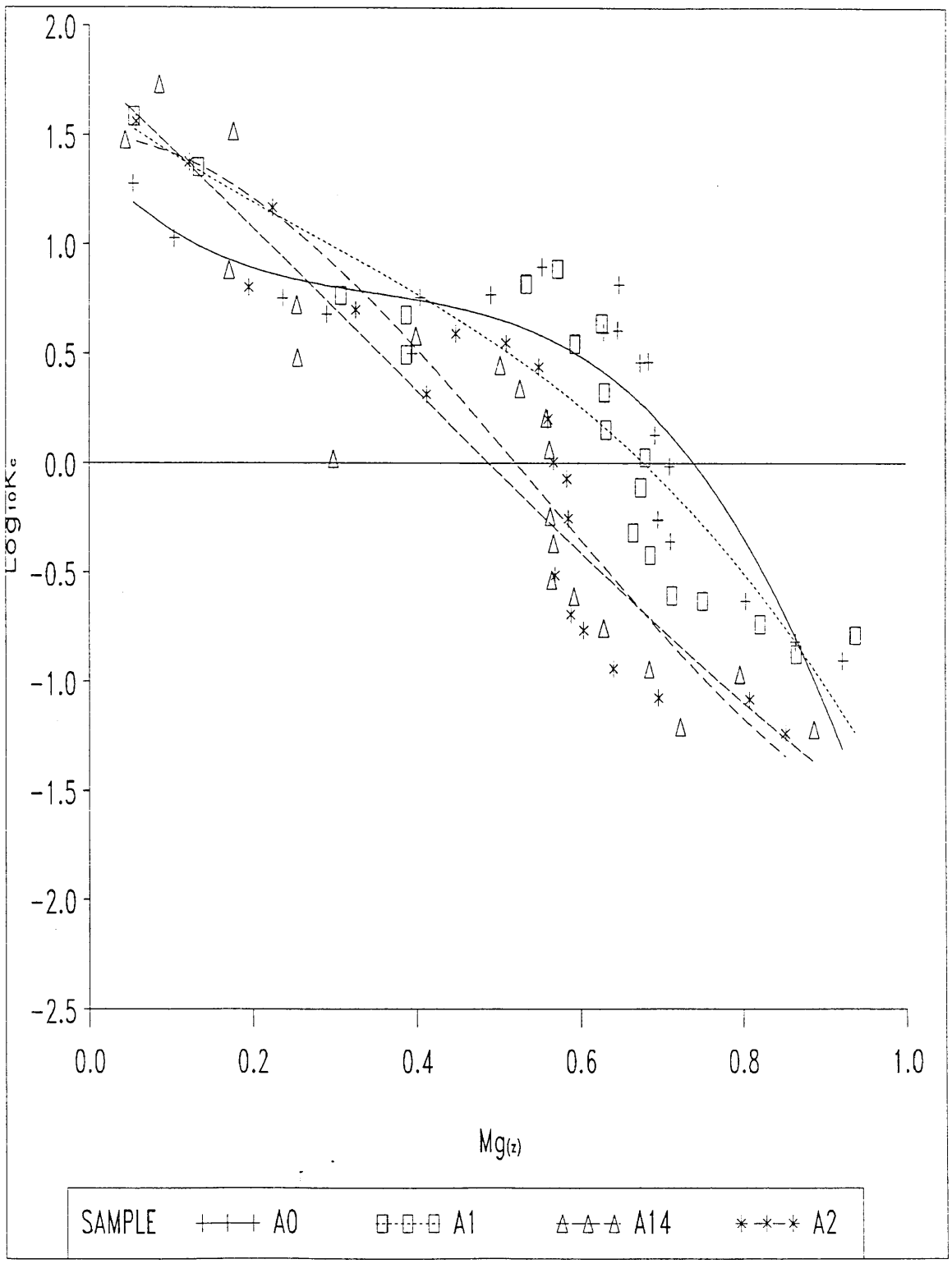

All the values of ΔG^{θ} are very small and sample A14 exhibits a small positive value (+0.04KJ/g equivalent) indicating that the overall selectivity of the exchange reaction is for sodium. This illustrates an important point. Examination of the sodium-magnesium ion exchange isotherm for this sample suggests that the overall selectivity is for magnesium. However, it has been shown[9] that, when $z_a \neq z_b$, the shape of the isotherm does not necessarily indicate the sign of ΔG^{θ}.

The value for ΔG^{θ} of +0.04KJ/g equivalent for the crystalline sample A14 is lower than that found by Barri[9] who reported a value of +3.26KJ/g equivalent for sodium-magnesium exchange in crystalline zeolite A.

$Log_{10}K_c$ plots for sodium-calcium and sodium-magnesium exchange in the zeolite X type samples are shown in Figures 4.11 and 4.12 respectively. Again, these diagrams show the experimental data as points and the fitted polynomial expressions as lines.

For sodium-calcium exchange in these samples (Figure 4.11), the change in selectivity for calcium with reaction time is clearly seen. As the gel reaction time increases, the selectivity for calcium decreases until zeolite X crystallises, where there is a reversal of this trend.

The polynomial equations that best describe the data, together with their associated R values are given in Table 4.5. Third order polynomials (cubic equations) were again found to provide the best fits to the data and these have been used to calculate K_a and ΔG^{θ}. As can be seen from this table, ΔG^{θ} increases from -3.54KJ/g equivalent for sample X0 to -2.13KJ/g equivalent for sample X3 then falls to -2.80KJ/g equivalent for sample X24. All of the samples show overall selectivity for calcium over sodium and the order of selectivity is:

$$X0 > X1 > X2 > X24 > X3$$

A similar change in selectivity with gel reaction time is observed for sodium-magnesium exchange in these samples, except that here the $log_{10}K_c$ plot for the crystalline sample X24 lies between those of samples X1 and X2 (Figure 4.12). Polynomial fits for the experimental data are given in Table 4.6.

Figure 4.11. $Log_{10}K_c$ vs $Ca_{(z)}$ Plots for Sodium-Calcium Exchange in Zeolite X Type Samples

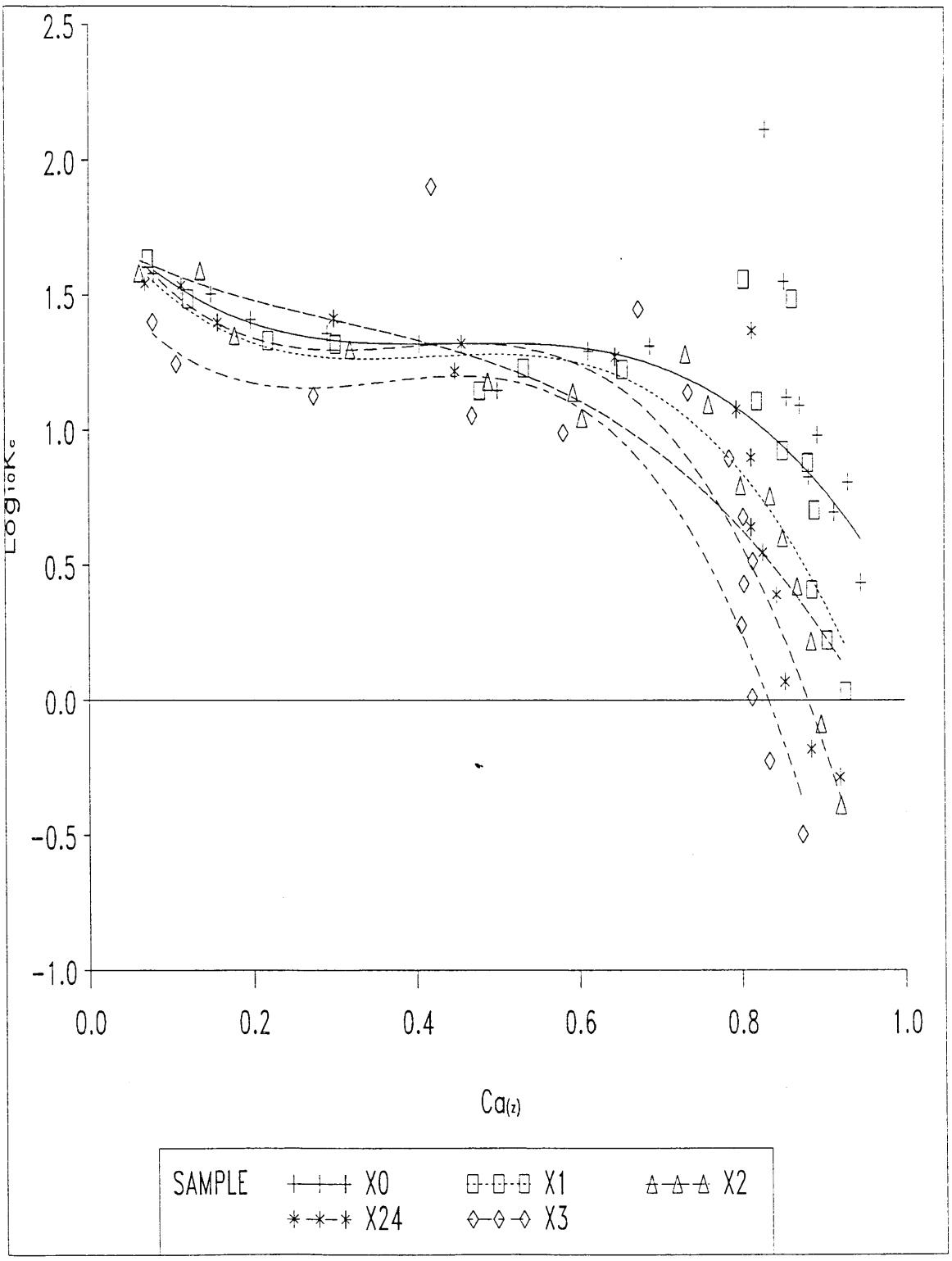

Table 4.5. Polynomial Fits for Sodium-Calcium Exchange in the Zeolite X Type Samples

Sample	Polynomial Equation	R	K_a	ΔG^θ
X0	$\log_{10}K_c = 1.68 - 0.91Ca_{(z)}$	0.15		
	$\log_{10}K_c = 1.53 + 0.08Ca_{(z)} - 0.99Ca_{(z)}^2$	0.16		
	$\log_{10}K_c = 1.81 - 3.46Ca_{(z)} + 7.90Ca_{(z)}^2 - 5.93Ca_{(z)}^3$	0.14	17.34	-3.54
X1	$\log_{10}K_c = 1.75 - 1.34Ca_{(z)}$	0.18		
	$\log_{10}K_c = 1.40 + 0.85Ca_{(z)} - 2.18Ca_{(z)}^2$	0.20		
	$\log_{10}K_c = 1.83 - 4.35Ca_{(z)} + 10.85Ca_{(z)}^2 - 8.69Ca_{(z)}^3$	0.15	12.54	-3.13
X2	$\log_{10}K_c = 1.87 - 1.64Ca_{(z)}$	0.13		
	$\log_{10}K_c = 1.55 + 0.41Ca_{(z)} - 2.05Ca_{(z)}^2$	0.09		
	$\log_{10}K_c = 1.73 - 1.76Ca_{(z)} + 3.41Ca_{(z)}^2 - 3.64Ca_{(z)}^3$	0.07	11.76	-3.05
X3	$\log_{10}K_c = 1.73 - 1.90Ca_{(z)}$	0.30		
	$\log_{10}K_c = 1.10 + 2.27Ca_{(z)} - 4.36Ca_{(z)}^2$	0.22		
	$\log_{10}K_c = 1.63 - 4.51Ca_{(z)} + 13.55Ca_{(z)}^2 - 12.60Ca_{(z)}^3$	0.15	5.56	-2.13
X24	$\log_{10}K_c = 1.95 - 2.01Ca_{(z)}$	0.22		
	$\log_{10}K_c = 1.81 + 2.01Ca_{(z)} - 4.02Ca_{(z)}^2$	0.27		
	$\log_{10}K_c = 1.89 - 5.04Ca_{(z)} + 13.68Ca_{(z)}^2 - 11.81Ca_{(z)}^3$	0.11	9.61	-2.80

For sodium-magnesium exchange in the zeolite X type samples, ΔG^θ rises from -0.07KJ/g equivalent for sample X0 to +4.80KJ/g equivalent for sample X3 then falls to +1.20KJ/g equivalent as zeolite X crystallises (sample X24). Thus, all samples, except sample X0, which exhibits a small negative value for ΔG^θ, show overall selectivity for sodium (the outgoing ion). This emphasises the fact that when $z_a \neq z_b$ the shape of the ion exchange isotherm does not necessarily reflect the sign of ΔG^θ. The order of selectivity for magnesium (the ingoing ion) is as follows:

$$X0 > X1 > X24 > X2 > X3$$

Figure 4.12. $Log_{10}K_c$ vs $Mg_{(z)}$ Plots for Sodium-Magnesium Exchange in Zeolite X Type Samples

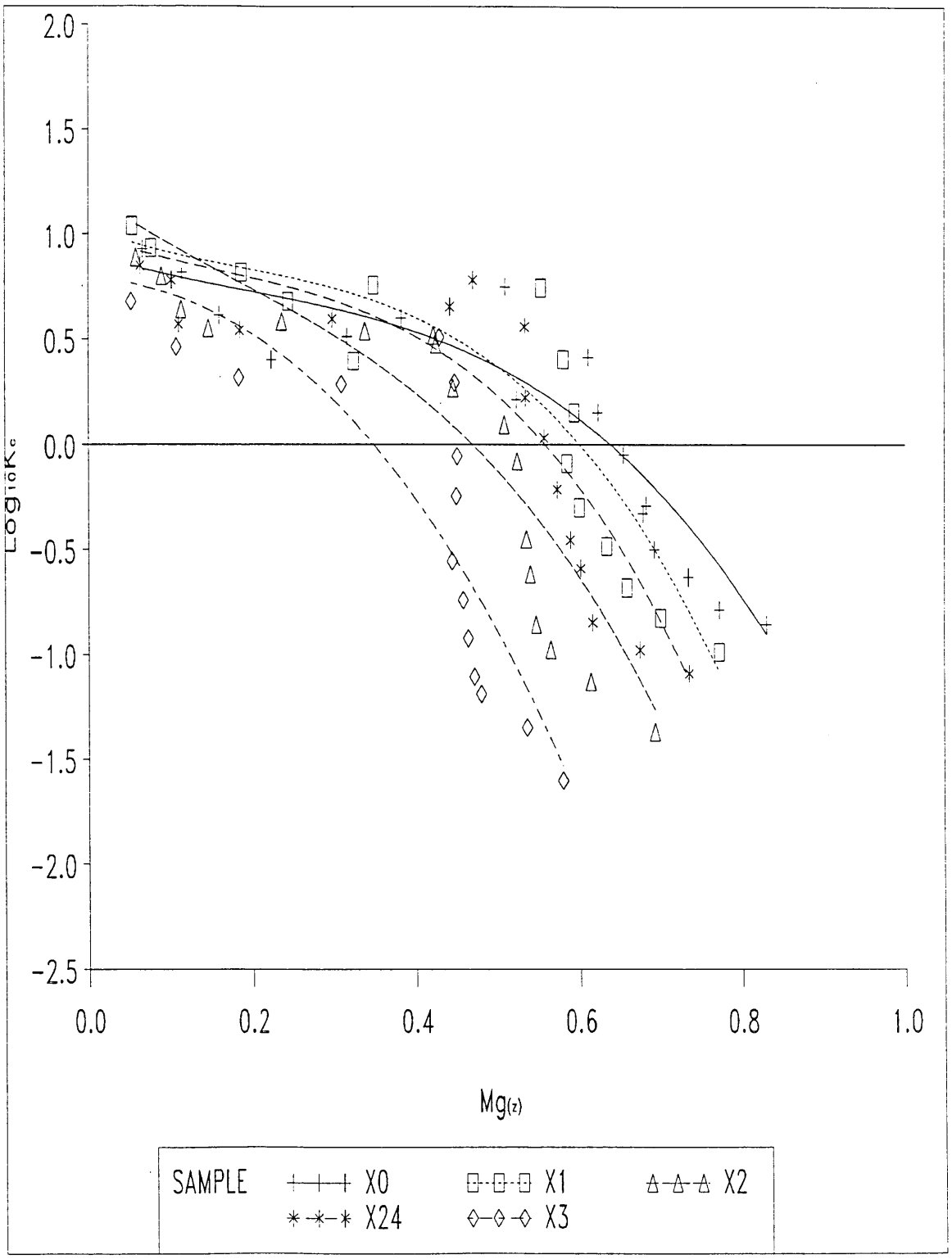

Table 4.6. Polynomial Fits for Sodium-Magnesium Exchange in the Zeolite X Type Samples

Sample	Polynomial Equation	R	K_a	ΔG^θ
X0	$\log_{10}K_c = 1.24 - 2.35Mg_{(z)}$	0.10		
	$\log_{10}K_c = 0.72 + 1.12Mg_{(z)} - 3.73Mg_{(z)}^2$	0.05		
	$\log_{10}K_c = 0.91 - 1.24Mg_{(z)} + 2.52Mg_{(z)}^2 - 4.41Mg_{(z)}^3$	0.05	1.06	-0.07
X1	$\log_{10}K_c = 1.38 - 2.72Mg_{(z)}$	0.13		
	$\log_{10}K_c = 0.81 + 1.62Mg_{(z)} - 5.22Mg_{(z)}^2$	0.09		
	$\log_{10}K_c = 1.03 - 1.52Mg_{(z)} + 4.03Mg_{(z)}^2 - 7.28Mg_{(z)}^3$	0.09	0.62	+0.59
X2	$\log_{10}K_c = 1.47 - 3.82Mg_{(z)}$	0.16		
	$\log_{10}K_c = 0.67 + 1.69Mg_{(z)} - 6.62Mg_{(z)}^2$	0.10		
	$\log_{10}K_c = 1.20 - 2.80Mg_{(z)} + 3.87Mg_{(z)}^2 - 7.18Mg_{(z)}^3$	0.10	0.20	+2.01
X3	$\log_{10}K_c = 1.38 - 5.08Mg_{(z)}$	0.38		
	$\log_{10}K_c = 0.50 + 1.97Mg_{(z)} - 9.49Mg_{(z)}^2$	0.20		
	$\log_{10}K_c = 0.80 - 0.39Mg_{(z)} + 4.31Mg_{(z)}^2 - 3.40Mg_{(z)}^3$	0.20	0.02	+4.80
X24	$\log_{10}K_c = 1.41 - 3.10Mg_{(z)}$	0.21		
	$\log_{10}K_c = 0.65 + 2.24Mg_{(z)} - 6.38Mg_{(z)}^2$	0.09		
	$\log_{10}K_c = 1.00 - 1.47Mg_{(z)} + 3.68Mg_{(z)}^2 - 7.63Mg_{(z)}^3$	0.09	0.38	+1.20

4.4 The Kinetics of Magnesium Ion Exchange

The kinetics of sodium-magnesium ion exchange were studied for samples A0, A1 and A14 and samples X0, X1 and X24. Detailed kinetic studies of the ion exchange reaction in zeolites are usually carried out using large crystals with a narrow particle size range, since the kinetics of ion exchange depend on crystal size. Thus, for small crystals, equilibrium is achieved relatively rapidly and a fast and accurate measurement technique is required. The crystalline samples studied here (samples A14 and X24) do not fulfil either of these requirements. Scanning electron microscopy (see section 3.4c) indicates that, for both these samples, crystal sizes are generally less than 5μm and that

both samples exhibit a wide range of particle sizes. For this reason, only a qualitative study of the kinetics of sodium-magnesium exchange has been carried out and diffusion coefficients have not been determined.

A sodium ion selective glass electrode with a calomel reference electrode was used to follow the kinetics of the sodium-magnesium ion exchange reaction. This electrode was calibrated immediately prior to use and was recalibrated after use. All calibration solutions were 0.05N in magnesium chloride in order to minimise any effects of magnesium ion interference. These solutions were also 10^{-4}N in sodium hydroxide, since this raised the solution pH to the optimum operating pH of the sodium selective electrode. After calibration, the electrodes were rinsed in distilled water, blotted dry with a tissue and transferred to a stirred beaker containing 100ml of a solution which was 0.05N in magnesium chloride and 10^{-4}N in sodium hydroxide. At time t=0, 0.1g of the sample under investigation was added to the beaker and the solution concentration of sodium followed for a period of ninety minutes, at which time the reaction was stopped.

Figure 4.13 shows the results for the zeolite A type samples (samples A0, A1 and A14). Numerical data is given in appendix 1. There is a clear decrease in the rate at which magnesium is exchanged for sodium as the gel reaction time increases. This effect is seen despite the larger particle sizes exhibited by sample A1 and A0 compared to sample A14 (see section 3.4f). This finding appears to confirm the view that aluminosilicate gels have a more open framework structure than their crystalline counterparts and, therefore, that (highly hydrated) magnesium ions can exchange more easily into these materials.

Similar results for the zeolite X type gels are shown in Figure 4.14 (numerical data appears in appendix 1), although the exchange reaction is considerably slower than for the zeolite A type samples. Here again there is a clear decrease in the rate of magnesium ion exchange as the gel reaction time increases, despite the larger particle sizes of the amorphous gels (samples X0 and X1). This can again be explained by the more open framework structures of the gel samples (samples X0 and X1) compared to that of the crystalline sample (sample X24). It is noticeable that there is a much smaller difference between the kinetics of exchange in sample X0 and those in sample X24 than there is for the corresponding zeolite A type samples. This probably arises because zeolite X has a more open framework structure than zeolite A and, therefore, magnesium ions can exchange more easily.

Figure 4.13. The Kinetics of Sodium-Magnesium Ion Exchange in the Zeolite A Type Samples

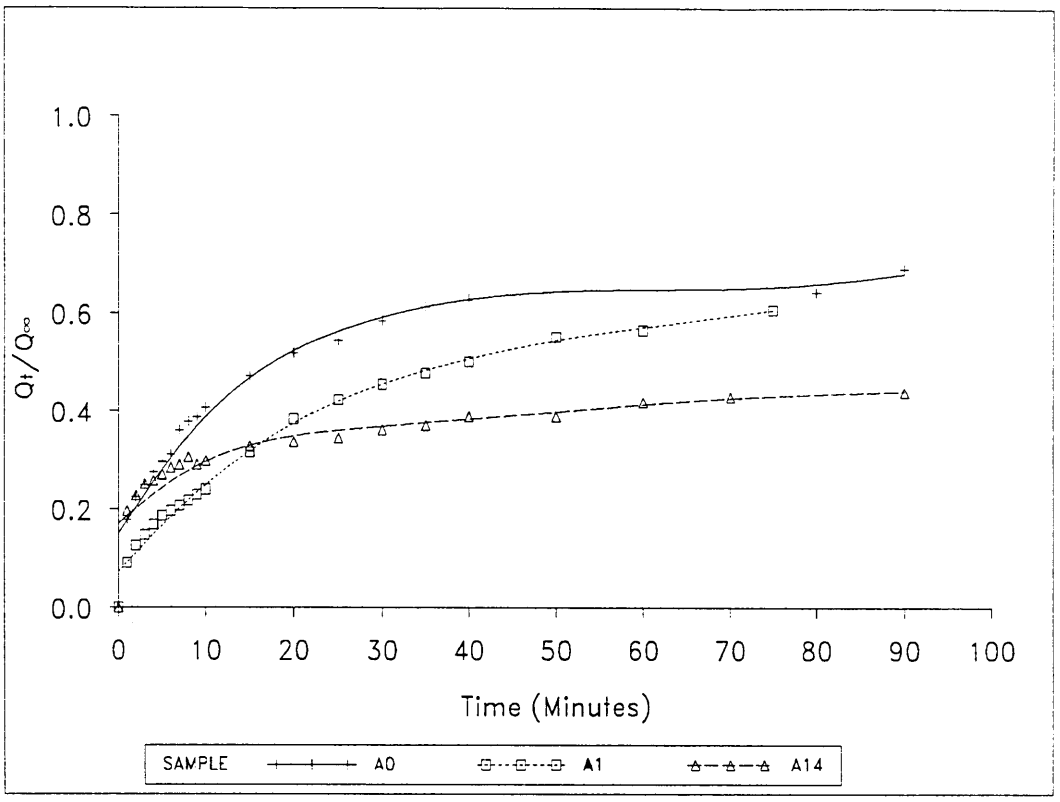

Figure 4.14. The Kinetics of Sodium-Magnesium Ion Exchange in the Zeolite X Type Samples

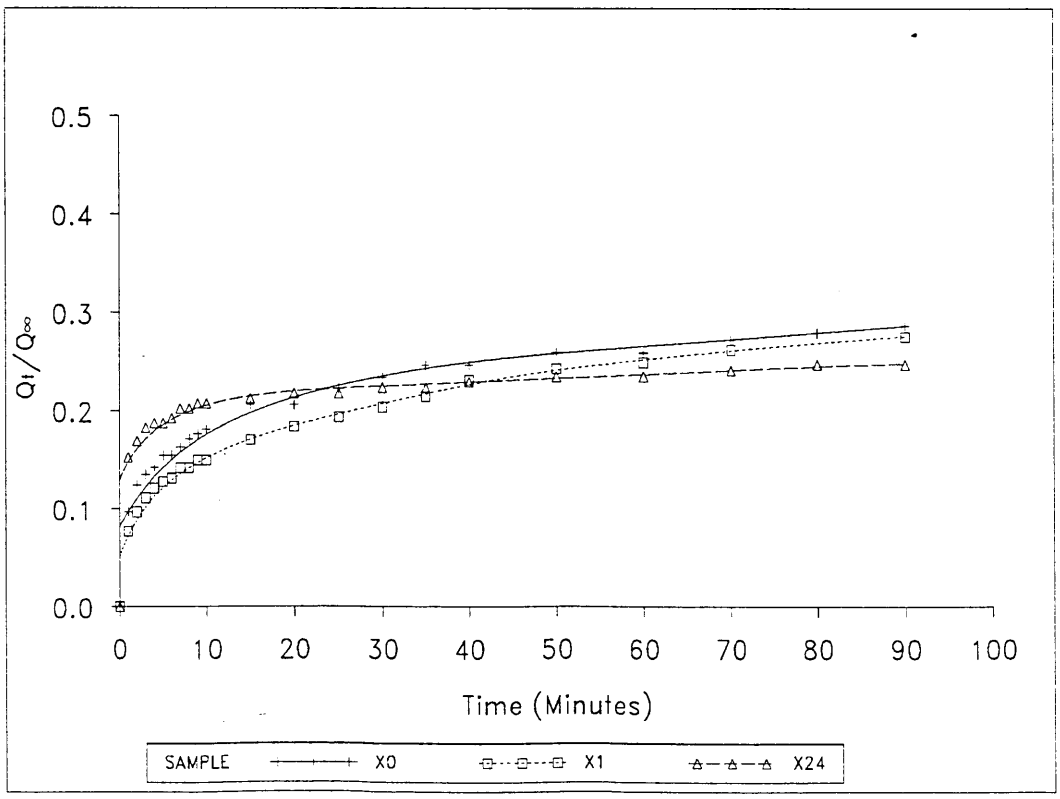

It is interesting to note that these results would appear to suggest that the kinetics of sodium-magnesium exchange in zeolite X are slower than in zeolite A. This is a surprising result in view of the more open framework structure of zeolite X. This anomaly can probably best be explained by differing crystal sizes in samples A14 and X24. Scanning electron microscopy (section 3.4c) indicates that the crystals of zeolite X (sample X24) that have been synthesised tend to be larger than the crystals of zeolite A (sample A14).

In the european front loading automatic washing machine, the timescale of a wash cycle (excluding the rinse cycles) may vary from 15 minutes to over an hour, depending on the machine type and the selected wash cycle. It is worth noting that, on this timescale, between 50% and 70% of the ion exchange capacity of sample A0 is used whereas for sample A14 only 30% to 40% of the capacity is used. In view of this, the lower ion exchange capacities of the amorphous aluminosilicate gels may not be a problem. A similar situation exists for the zeolite X type gels.

It must be noted that, in solutions containing a mixture of calcium and magnesium ions, the kinetics of exchange closely resemble those of sodium-calcium exchange and it can be concluded that little or none of the magnesium has exchanged[9]. Thus, although the amorphous aluminosilicate gels exhibit faster sodium-magnesium exchange kinetics than their crystalline counterparts, it must be remembered that it is the kinetics of exchange in mixed solution that are important. Unfortunately, the kinetics of exchange in mixed solution were not studied.

5.5 References

1. A. Llenado, Proc. 6th Int. Zeol. Conf., Butterworths, (1983), 940
2. Y. Tsurata, T. Satoh, T. Yoshida, O. Okumura and S. Ueda, Proc. 7th Int. Conf. Zeolites, Elsevier, Tokyo, (1986), 1001
3. K. R. Franklin and R. P. Townsend, J. Chem. Soc. Faraday Trans. 1, **81**, (1985), 3127
4. R. P. Townsend, Proc. 7th Int. Conf. Zeolites, Elsevier, Tokyo, (1986), 273
5. A. I. Vogel, "Textbook of Quantitative Inorganic Analysis", 4th Edition, Longmans, London, (1978)

6. R. A. Robinson and R. H. Stokes, "Electrolyte Solutions", Butterworths, (1955)
7. E. Glueckauf, Nature, **163**, (1949), 414
8. H. S. Moore and J. W. Ross, J. Appl. Physiology, **20**, (1965), 1332
9. S. A. I. Barri, PhD. Thesis, University of London
10. SAS Institute Inc., SAS User's Guide: Basics, Version 5 Edition, Cary North Carolina, (1985)
11. SAS Institute Inc., SAS User's Guide: Statistics, Version 5 Edition, Cary North Carolina, (1985)
12. H. S. Sherry and H. F. Walton, J. Phys. Chem, **71**, (1967), 1457

Chapter Five

Aluminosilicate Gels as Detergent Builders

5.1 Introduction

The aluminosilicate gels described in this thesis have been developed as potential replacements for the phosphate detergent builders currently used in detergent formulations. Whilst the work described in the previous two chapters (describing the synthesis, characterisation and ion exchange properties) provides valuable information, performance testing of these materials in a detergent formulation is essential to gain a view of their potential for this application. This chapter describes work carried out to assess the builder performance of selected gel samples. This work was carried out at the Procter and Gamble Newcastle Technical Centre. I am indebted to Procter and Gamble for the opportunity to carry out this work and to the staff of the Technical Centre for their considerable help.

Experimental detergent formulations can be tested in washing machines under controlled conditions using a variety of wash performance monitors. However, despite its relative mechanical simplicity, the washing machine is a complex chemical reactor. This is particularly true of the front loading automatic washing machine common throughout Europe. Thus, the results of machine testing can be complicated by factors which are beyond experimental control. For preliminary testing of experimental detergent formulations, this situation can be greatly simplified by the use of a launderometer.

The launderometer[1] consists of a thermostatted reservoir with a 15 gallon capacity. Inside the reservoir is a rotor which will hold up to 20 metal containers. This rotor is driven at a uniform speed of 42 r.p.m. The test formulations, wash liquor and appropriate wash performance monitors are sealed inside the metal pots and are rotated at a regulated temperature for a controlled period of time. The launderometer thus forms a greatly simplified model of a washing machine. It must, however, be stressed that there are significant differences between front loading automatic washing machines and launderometers, and that the results from launderometer testing may bear little

relationship to those obtained from machine testing. Thus, launderometers can only be used for preliminary screening exercises where they offer significant advantages of simplicity and degree of experimental control.

5.2 Launderometer Testing

The aim of this study was to assess the builder performance of selected aluminosilicate gel samples and to provide some comparison with the performance of current detergent builder options.

In order that performance differences could be discriminated more easily, the tests were designed to be as highly stressed as possible. The use of 30° hard water (4.29 x 10^{-3}M in total calcium and magnesium) throughout the tests ensured that the samples under test were working near the limits of their builder capacities. A calcium to magnesium ratio of 3:1 reflected conditions common in Europe. A low total product dosage (1% by weight) and the addition of soiling agents to the wash solution further stressed these tests.

Formulation details of the unbuilt detergent matrix used for this launderometer testing are given in Table 5.1. Although this is only a test formulation which is unavailable in the marketplace, it represents a typical current detergent formulation. It has an anionic/nonionic active mix, TAED/perborate bleach system and enzymes. The addition of 30.90 parts builder (i.e. the test samples) is required for the full formulation to be realised.

In real wash cycles, the wash liquor invariably contains dissolved and suspended soiling materials. Thus, in order to make these tests as realistic as possible, soiling agents were added to the wash solution. However, the use of natural soiling materials can be problematic and, consequently, it was decided to use artificial soils. These were air filter soil (AFS), clay, stearic acid, lauric acid and a 50:50 mixture of dirty motor oil (DMO) and tristearate.

As a result of the low product dosage used in these tests and the small size of the launderometer pots, only small amounts of detergent were required for each wash (2.5g). The weighing out of such small quantities of a detergent product may result in a serious and unnecessary experimental error due to large compositional variations. These arise because of the granular nature of the

product. These problems may be overcome by preparing a stock solution of the unbuilt detergent product and the soiling agents in water of the required hardness.

Table 5.1. Test Formulation for Launderometer Testing

Ingredient		Parts
SURFACTANT	: Linear Alkylbenzene Sulphonate	9.00
	: Nonionic Surfactant	4.71
BUILDER	: Polyacrylate	3.00
BUFFER	: Carbonate	10.00
	: Silicate	3.00
CHELANT	: EDTA	0.50
BLEACH	: Perborate Tetrahydrate	20.00
	: Tetra Acetyl Ethylene Diamine	2.00
ENZYME	:	0.80
MISCELLANEOUS	: Brightener	0.20
	: Antifoam Agent (Silicone)	0.30
	: Sulphate (to balance)	15.59
		69.10
BUILDER (not included)		30.90
		100.00

Wash performance can be measured by a variety of stained cloths and the selection of these monitors can be tailored to meet the needs of the test. In

these launderometer tests, tea, coffee, clay and DMO stains were used to monitor wash performance. Tea, coffee and clay stains were available as prestained cloths, but DMO stains had to be prepared by dropping a few drops of DMO onto clean cloths and leaving to dry overnight. Two types of clay stain were available, one prepared at the Newcastle Technical Centre (NTC clay) and the other at the European Technical Centre (ETC clay). Both were used. A whiteness monitor (a piece of clean white terry cotton) was also included to assess the redeposition of suspended and dissolved soils.

Wash performance is measured in terms of stain removal which can be visually or instrumentally assessed. Visual assessment has the advantage that it measures performance in the same way a housewife would do, whereas instrumental assessment does not. However instrumental assessment is less subjective and is more sensitive. In this study all stains except DMO stains were instrumentally assessed.

Stain removal is measured instrumentally using a Harrison Meter. This instrument measures the whiteness of a piece of cloth relative to that of a standard white tile. Measurements of the whitenesses of a piece of clean cloth and of the stained cloth both before and after washing allow percentage stain removal to be determined according to the following equation:

$$\text{Stain removal (\%)} = \frac{\text{after wash whiteness - before wash whiteness}}{\text{clean cloth whiteness - before wash whiteness}} \times 100$$

The Harrison Meter was also used to assess the deposition of soils onto the whiteness monitor. Here whiteness is calculated using the following equation:

$$\text{Whiteness (\%)} = \frac{\text{after wash whiteness}}{\text{before wash whiteness}} \times 100$$

5.3 Experimental Procedure

Two launderometer tests were carried out. The first of these examined the builder performance of selected zeolite X type aluminosilicate gels and the second assessed a selection of the zeolite A type gels. In both cases, sodium tripolyphosphate (STPP) and detergent grade zeolites were included as control samples. Table 5.2 provides details of the samples included in both tests.

Table 5.2. Samples Studied in Launderometer Testing

Test 1	Test 2
X0	A0
X1	A1
X2	A2
X3	A4
X4	A8
X6	
	X0 (comparison)
	X1 (comparison)
STPP (control)	STPP (control)
Zeolite A (control)	Zeolite A (control)
Zeolite X (control)	

The inclusion of samples X0 and X1 in the second test allowed comparison of the builder performance of zeolite A type aluminosilicate gels with that of these two zeolite X type gels. Direct comparison of the results from the two tests may be misleading because uncontrolled test to test variability can give rise to significant differences between tests.

A solution containing the unbuilt detergent matrix (6.91g/l), AFS (0.2g/l), clay (0.2g/l), stearic acid (0.4g/l) and lauric acid (0.4g/l) was prepared. This was immediately divided into 250ml portions in each launderometer pot. Two drops of a 50:50 mixture of DMO/tristearate was added to each pot together with nine wash monitors (2 x tea on cotton, 2 x coffee on cotton, 2 x DMO on cotton, 1 x NTC clay on knitted cotton, 1 x ETC clay on knitted cotton and 1 x clean cotton terry). The builder samples under investigation (0.77g) were then added to the launderometer pots to give a total product concentration of 1% by weight. Each sample was replicated twice. The pots were sealed and rotated in a launderometer for 20 minutes at 30°C. This treatment was followed by three five minute rinses in the launderometer using cold 30° hard water. The wash monitors were then removed from the launderometer pots, hand wrung and

dried overnight on absorbent paper. Harrison Meter reading were obtained for all wash monitors (with the exception of the DMO stains) both before and after washing. Clean pieces of cotton, knitted cotton and cotton terry were also measured.

5.4 Results

Visual examination of the DMO stains revealed only very small performance differences between the samples tested. The instrumental stain removal data for the remaining stains was generally in agreement with this, although some variation of builder performance with gel reaction time was seen. These effects are discussed in more detail below. Numerical data is given in appendix two.

Tea stain removal results are presented in Figures 5.1 (zeolite X type samples) and Figure 5.2 (zeolite A type samples). For each of the samples tested, four monitors were used (i.e. two monitors per launderometer pot, two replicates of each sample). These diagrams show both the mean and the range of stain removal exhibited by each sample. The horizontal reference lines indicate the mean stain removal exhibited by the control samples included in each test. For the zeolite X type gels (Figure 5.1), maximum stain removal was observed for a formulation built with a gel with a reaction time between one and two hours. All of the gel samples tested performed better than zeolite X and generally showed performance parity with STPP. However, the zeolite A built formulation exhibited the best performance.

In the case of the zeolite A type gels (Figure 5.2), maximum stain removal was observed for the formulation built with sample A2. Performance parity with STPP, zeolite A and sample X0 was generally observed, but the highest stain removal was seen for the formulation built with sample X1.

Coffee stain removal results for the zeolite X type samples are shown in Figure 5.3. All of the samples tested outperformed zeolite A, zeolite X and STPP built formulations. Maximum stain removal was observed for the formulation built with sample X2. The corresponding results for the zeolite A type gels are shown in Figure 5.4. As with the tea stain removal results, maximum stain removal was observed for sample A2, but even this was outperformed by sample X0.

NTC clay stain removal results are shown in Figure 5.5 (zeolite X type samples) and Figure 5.6 (zeolite A type samples). Of the zeolite X type samples tested (Figure 5.5), sample X1 showed the best performance. All of these samples performed better than zeolite X, but, with the exception of sample X1, were generally beaten by both zeolite A and STPP. For the zeolite A type gels (Figure 5.6), sample A2 performed well, but was again outperformed by sample X1.

Figure 5.7 (zeolite X type samples) and Figure 5.8 (zeolite A type samples) show stain removal performance for ETC clay stains. All of the zeolite X type samples that were tested (Figure 5.7) performed better than zeolite A, zeolite X and STPP. Maximum stain removal was observed for samples X1 and X2. Of the zeolite A type samples tested, sample A2 performed extremely well and, in this case, performed better than sample X1. In general, the zeolite A type samples performed better than both STPP and sample X0.

In general, the differences in performance between the samples tested (including both test and control samples) were small. Because of the small size of these differences, it is not clear whether they were due to genuine performance differences between the gel samples or to experimental error. The importance of random experimental error can be minimised by calculating average stain removal (Figures 5.9 and 5.10), although it must be stressed that this approach does not eliminate systematic experimental error and, indeed, may enhance it. Average stain removal results for the zeolite X type samples (Figure 5.9) indicated a more or less random variation of builder performance with gel reaction time, although there appeared to be a trend towards decreasing builder performance with increasing reaction time. For the zeolite A type gels (Figure 5.10), average stain removal results suggested that there was a dependence of builder performance on gel reaction time. Maximum performance was observed for a sample with a reaction time around two hours.

Post wash whiteness results are plotted in Figure 5.11 and Figure 5.12. For the zeolite X type gels (Figure 5.11), these were all around 90% and showed little differentiation between the samples tested (including controls). For the zeolite A type gels (Figure 5.12), results were generally around 89% except for sample A2 which gave a post wash whiteness of 93%. This was equalled by sample X1.

Figure 5.1. Tea Stain Removal - Zeolite X Type Samples

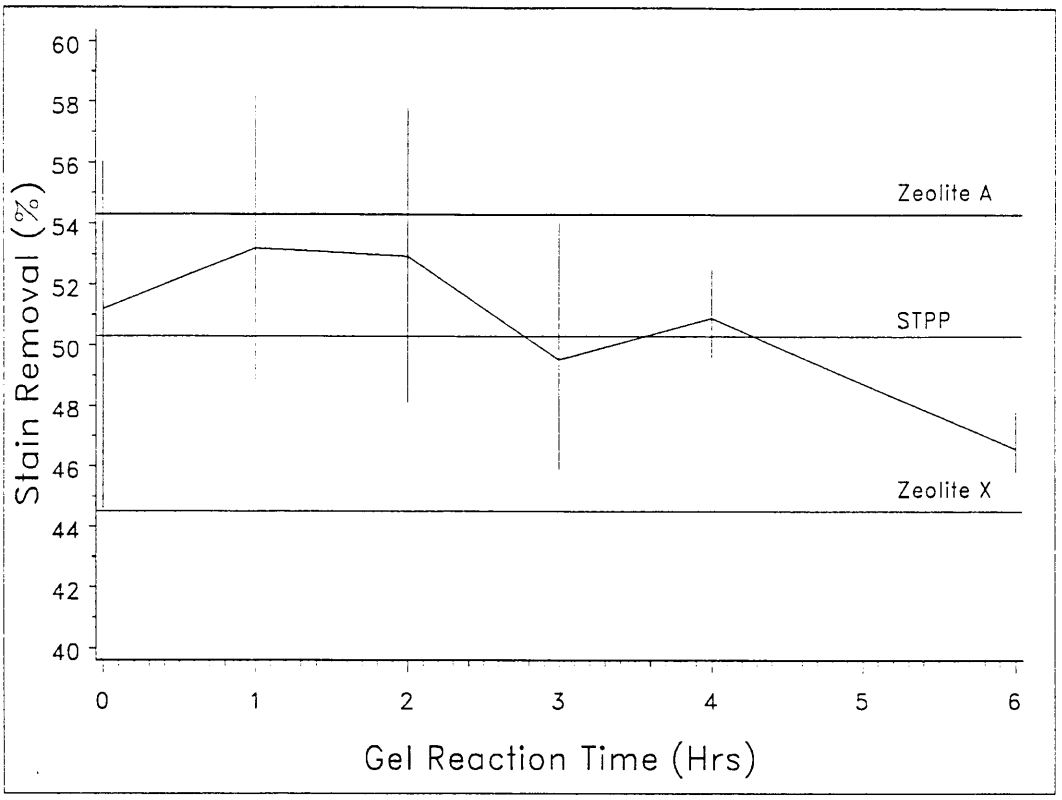

Figure 5.2. Tea Stain Removal - Zeolite A Type Samples

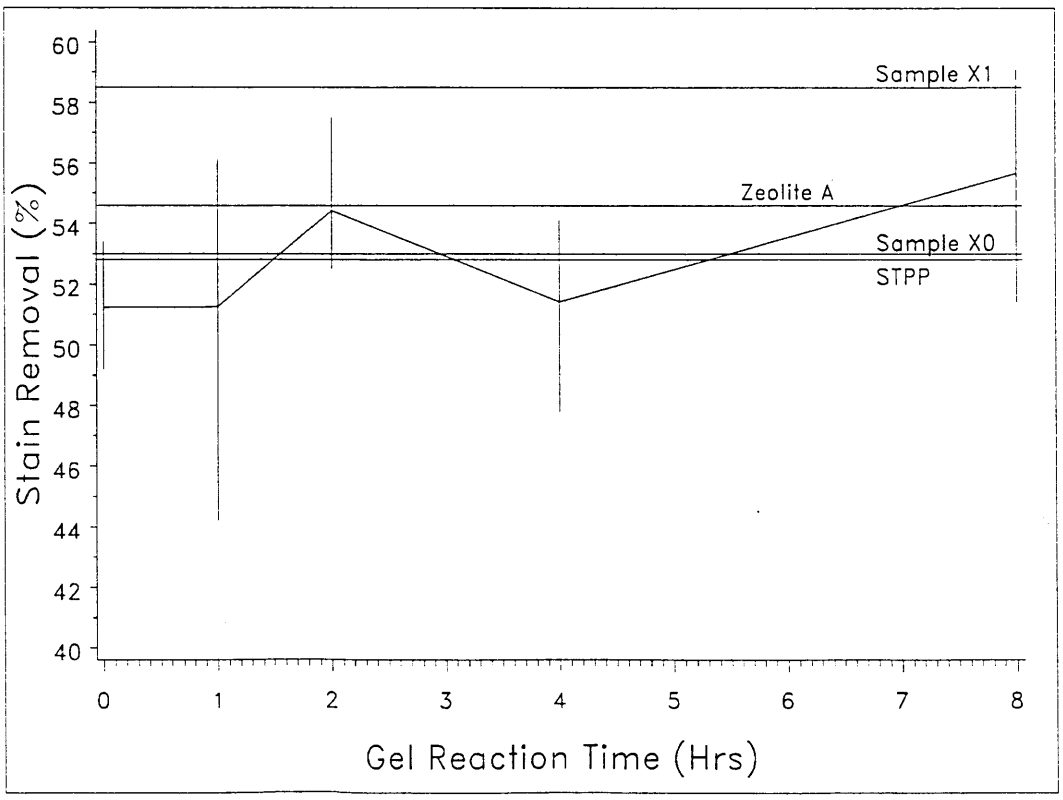

Figure 5.3. Coffee Stain Removal - Zeolite X Type Samples

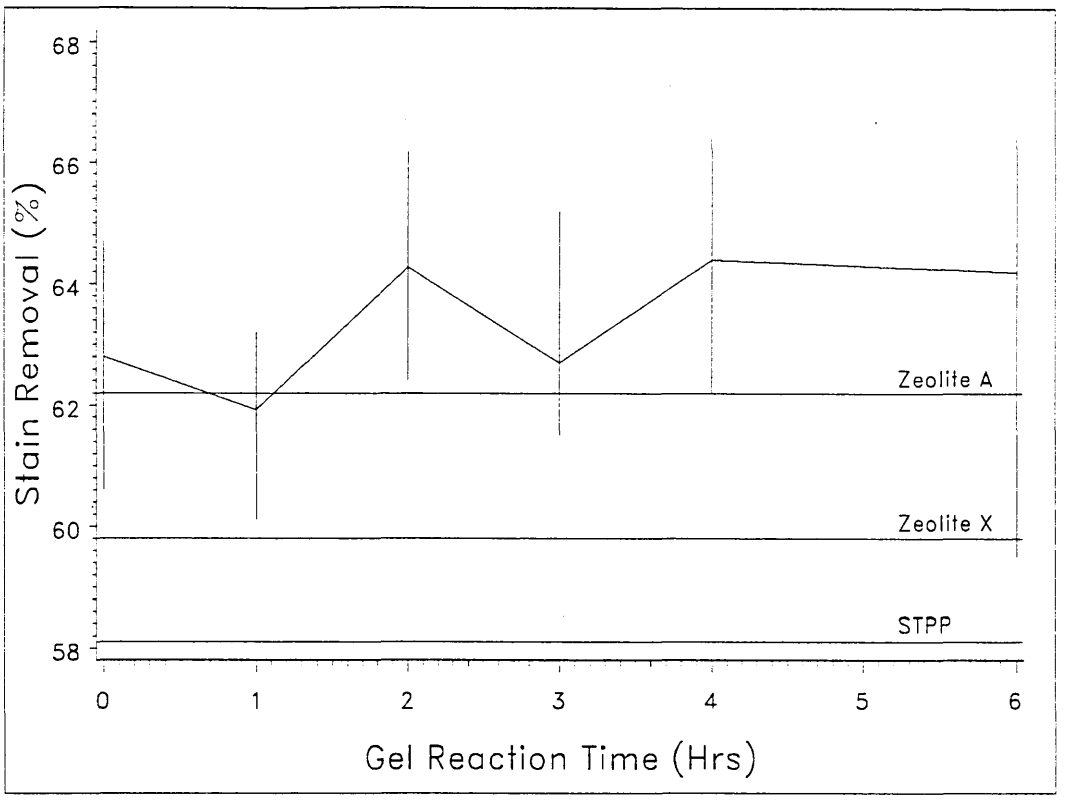

Figure 5.4. Coffee Stain Removal - Zeolite A Type Samples

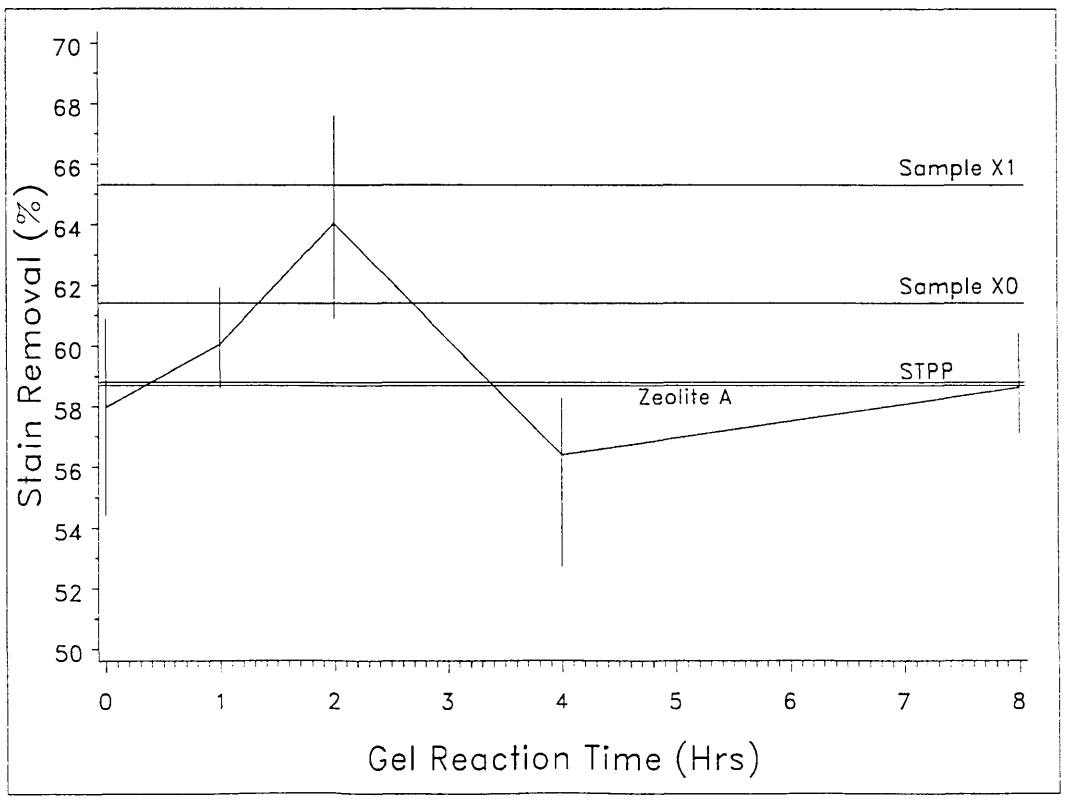

Figure 5.5. NTC Clay Stain Removal - Zeolite X Type Samples

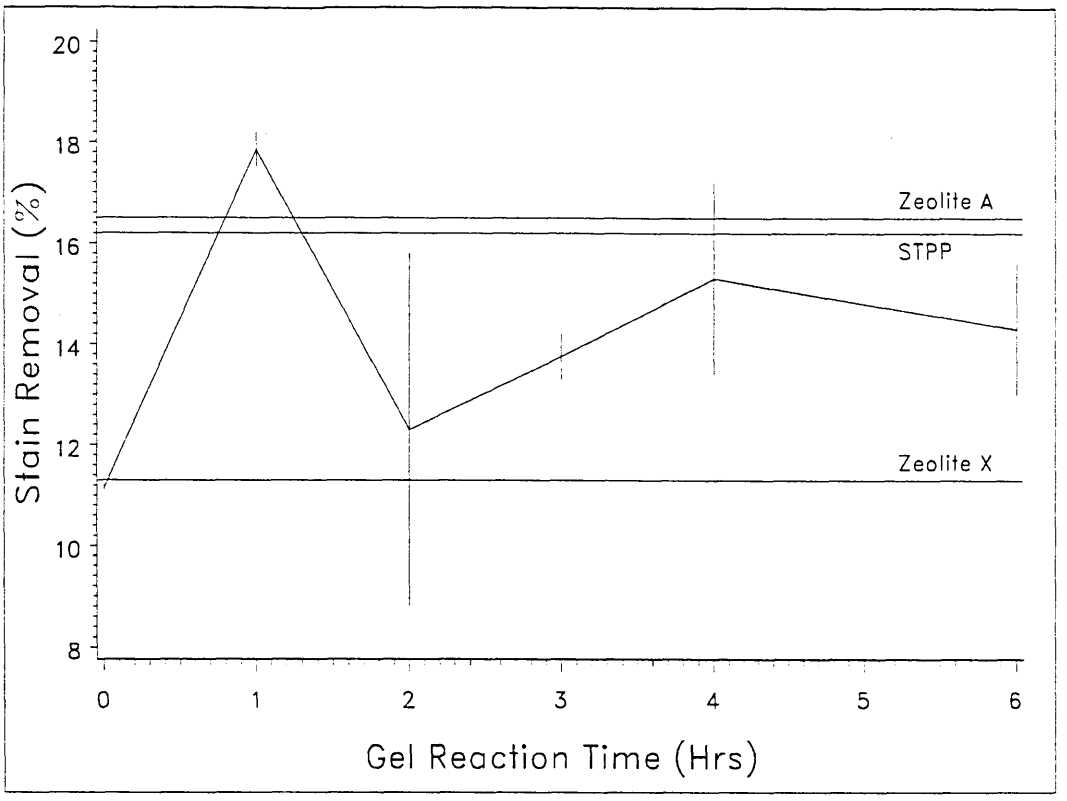

Figure 5.6. NTC Clay Stain Removal - Zeolite A Type Samples

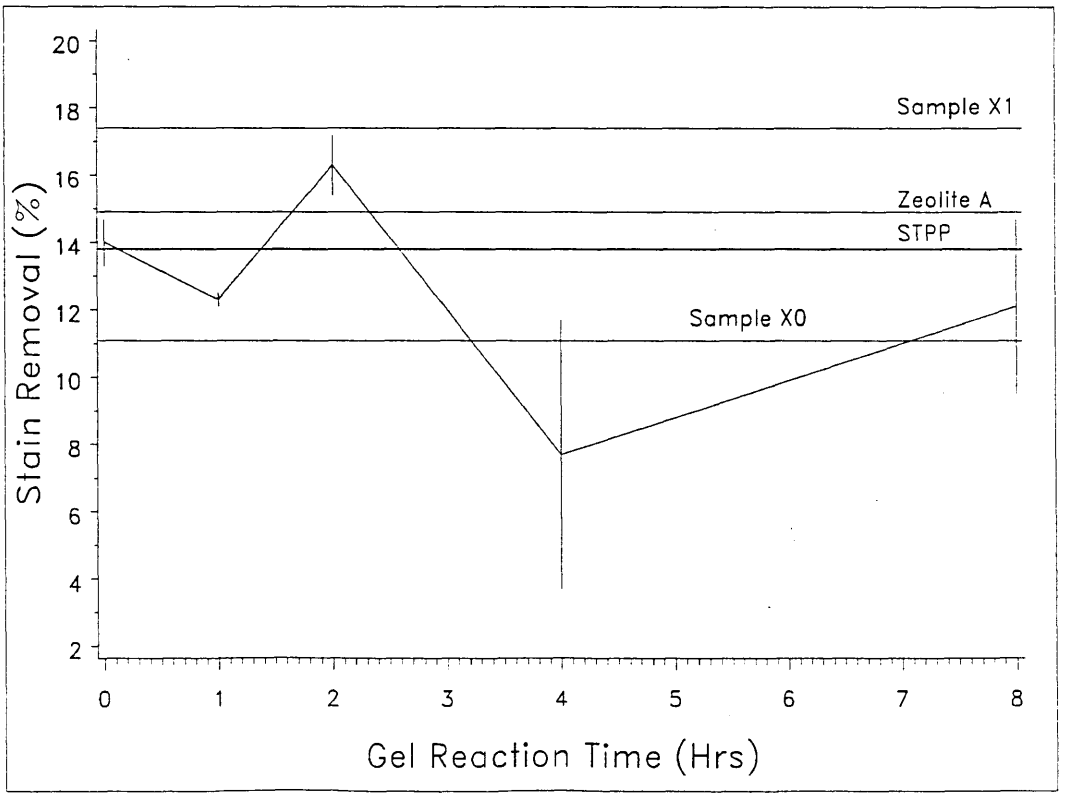

Figure 5.7. ETC Clay Stain Removal - Zeolite X Type Samples

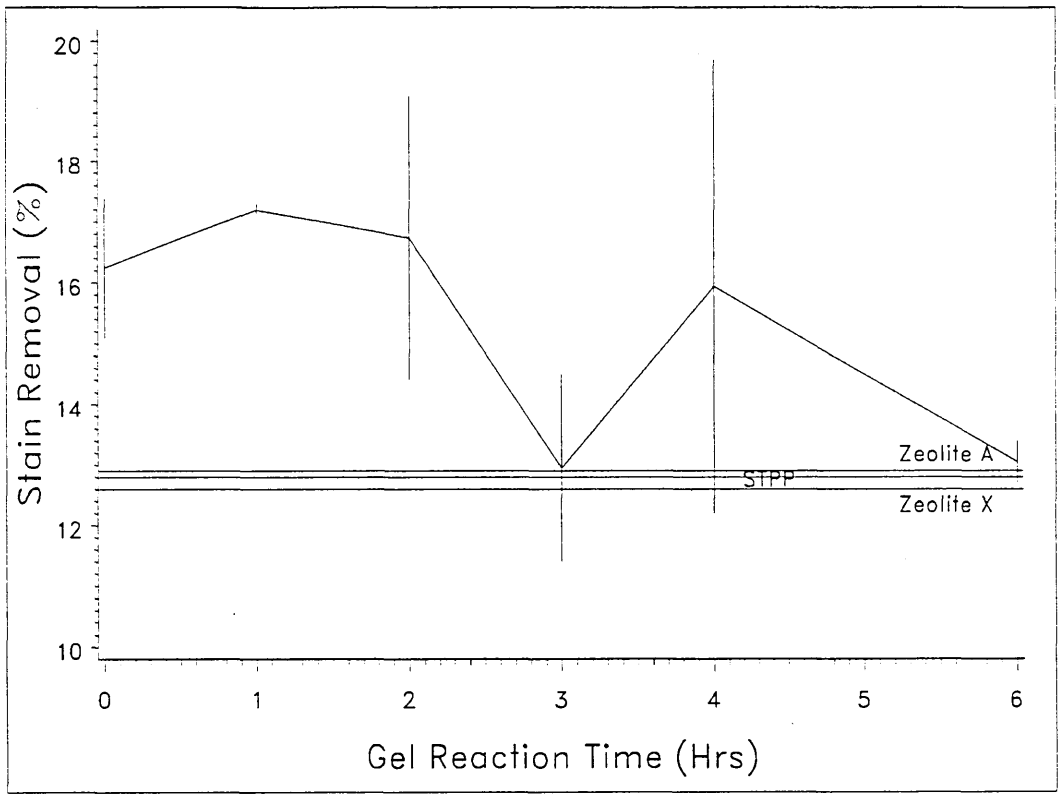

Figure 5.8. ETC Clay Stain Removal - Zeolite A Type Samples

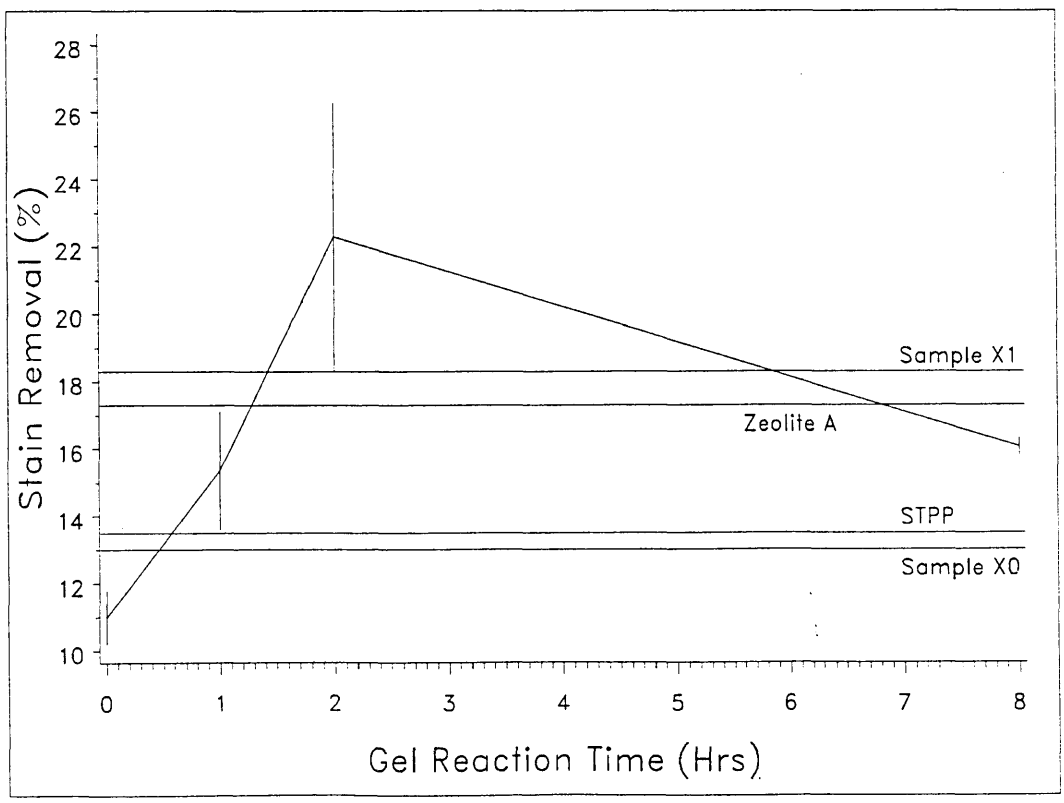

Figure 5.9. Average Stain Removal - Zeolite X Type Samples

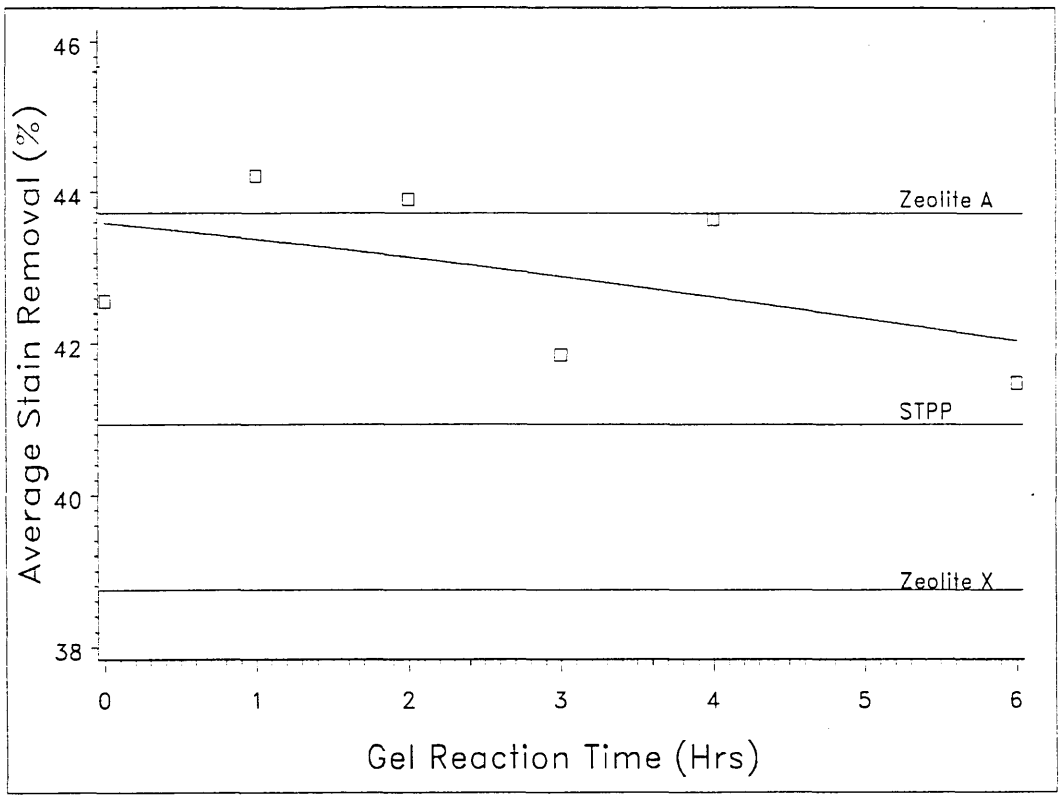

Figure 5.10. Average Stain Removal - Zeolite A Type Samples

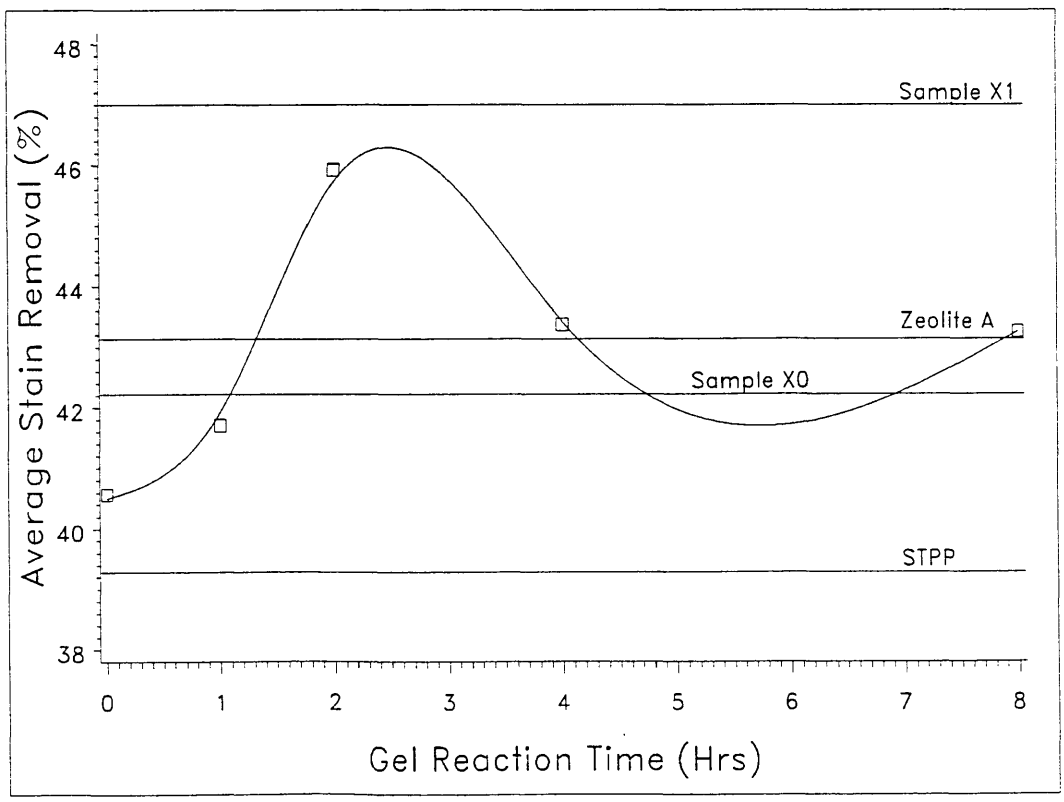

Figure 5.11. Post Wash Whiteness - Zeolite X Type Samples

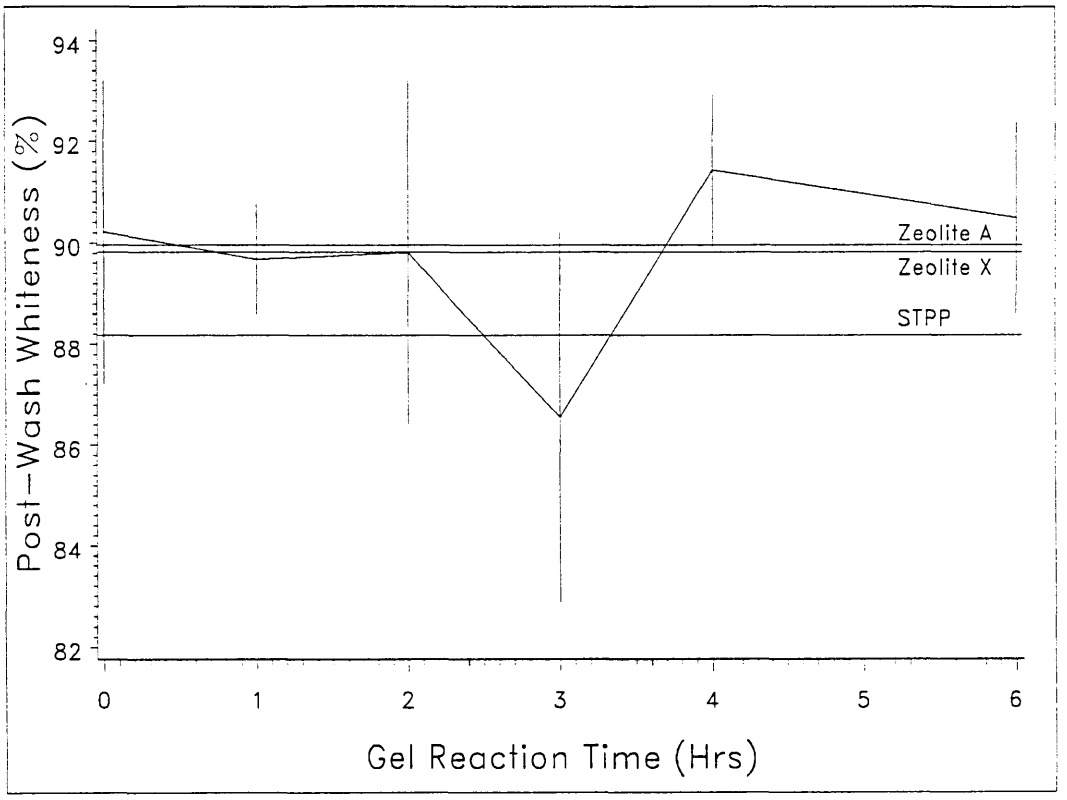

Figure 5.12. Post Wash Whiteness - Zeolite A Type Samples

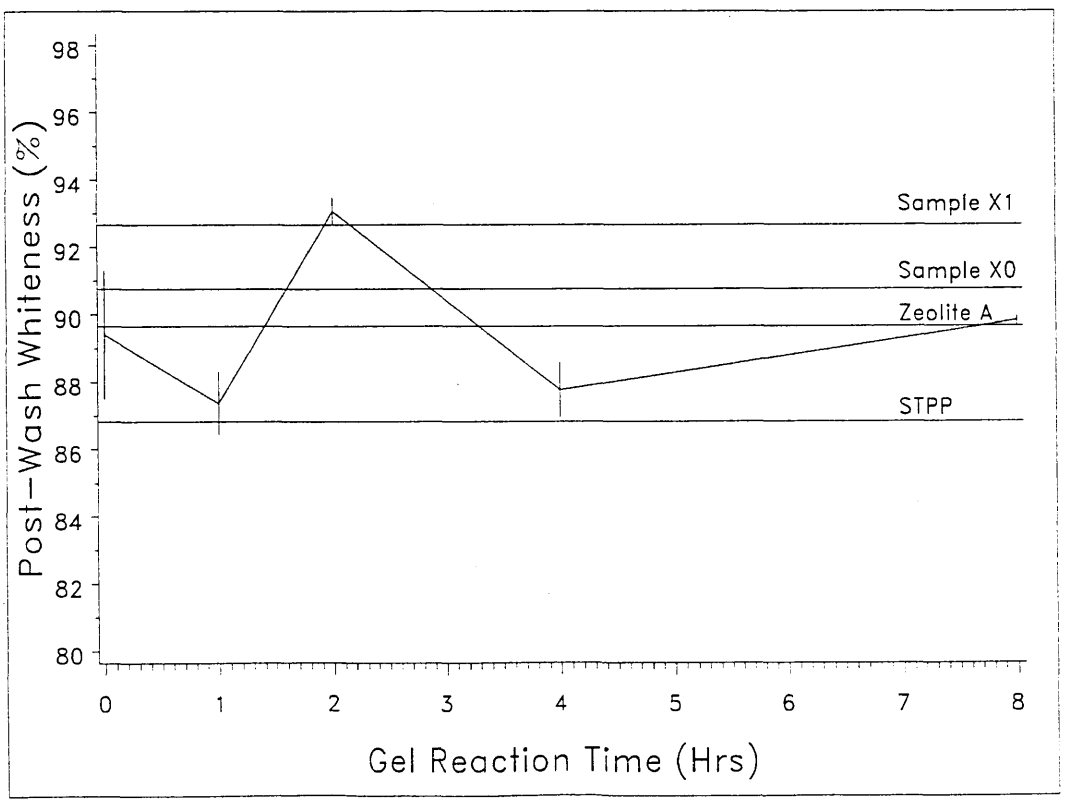

Generally, formulations containing amorphous aluminosilicate gels as builders outperformed STPP built formulations. Indeed, the average stain removal data indicated that, all of the samples tested performed better overall than STPP. In view of the fact that STPP is universally regarded as the preferred builder, this poor performance was unexpected. This may be an indication that the wash conditions were too harsh and that, in reality, all of the builders tested were performing equally poorly. Crystalline zeolite X was consistently outperformed by the zeolite X type gels. Zeolite A, however, performed better than STPP and was only outperformed by samples A2 and X1. Again, it must be pointed out that these differences were small and never exceeded 5% stain removal.

The inclusion of samples X0 and X1 in the second launderometer test allowed comparison of the performance of these two samples with that of the zeolite A type gels. Sample X1 showed comparable and, in many cases, better performance than sample A2, but sample X0 fared less well. This was consistent with the results from the first launderometer test in which the performance of the zeolite X type gels was investigated.

These results are encouraging, although, at this stage, it would be unwise to attach too much significance to them. Samples A2 and X1, in particular, appear worthy of further investigation. It is worth noting at this stage that the builder level in these experiments was constant at 30.90 parts (weight %) for all of the samples investigated. It is more usual for zeolite built detergents to contain a higher level of builder than their phosphate built counterparts to take account of the lower weight efficiency of the zeolites. If this approach had been adopted here, and the gel samples had been added to the test formulation at levels which reflected their ion exchange capacities (and, therefore, weight efficiencies), then the results might be expected to be more favourable towards the amorphous aluminosilicates.

5.5 References

1. "Detergency - Theory and Test Methods", Surfactant Science Series, Vol. 5 Part 1, W. G. Cutler and R. C. Davis (Editors), Marcel Dekker Inc., New York, (1972), Pages 415-417.

Chapter Six

Conclusions

Under the conditions of synthesis used in this work, zeolite A first appears after three hours, and the product is fully crystalline after four hours. For the synthesis of zeolite X, crystals first appear after six hours and the product is fully crystalline after ten hours, although only a small amount of amorphous material remains after eight hours.

It should be noted that Khatami and Flanigen[1] have reported the crystallisation of zeolite X in the absence of any liquid phase. It might, therefore, be expected that further crystallisation would have been observed in the amorphous aluminosilicate gels prepared using the zeolite X synthetic method. This does not, however, appear to be the case. Many of the characterisation procedures were carried out a considerable time after the synthesis of these samples and there is no evidence to suggest the existence of any crystalline material in samples X0, X1, X2, X3 or X4.

The ion exchange properties of the aluminosilicate gels clearly depend on gel reaction time. Although the amorphous gels exhibit relatively good ion exchange capacities, these are generally lower than for corresponding crystalline zeolites. The selectivities of the gel samples for calcium and magnesium ions are better than those for the crystalline samples, although this trend reverses as zeolite X crystallises, and the kinetics of sodium-magnesium exchange decrease with increasing gel reaction time (despite the larger particle sizes of the gel samples).

These changes in ion exchange properties as gel reaction time increases can all readily be explained by changes in the gel structure as the reaction proceeds. The fact tnat the kinetics of sodium-magnesium exchange slow down as the gel reaction time increases supports the view that amorphous gels have more open frameworks than their crystalline counterparts and that as the reaction proceeds, the size of the pores allowing entry to the channel system decreases. The changes in ion exchange capacities and selectivities can be explained by a redistribution of aluminium in the solid phase.

It is tempting to speculate that these results, particularly those for the zeolite A type samples, can best be explained by a solid phase crystallisation mechanism. After an induction period, zeolites crystallise fairly rapidly and, for a solution phase crystallisation mechanism, it might be expected that there would be a step change in ion exchange properties. This is possibly the case for the zeolite X type samples and would explain the reversal of the trends in ion exchange selectivities as zeolite X crystallises. However, the zeolite A type samples show a gradual change in ion exchange properties as the reaction proceeds and this is consistent with a gradual structural reorganisation of the aluminosilicate gel. Indeed, Tsurata et al[2] have reported that aluminosilicate gels obtained from the synthesis of zeolite A have the structure of zeolite A without the long range ordering.

Amorphous aluminosilicate gels appear to show some promise as detergent builders, although on the basis of the preliminary launderometer testing described in chapter five, it would be unwise to draw any firm conclusions. Much more work is required to evaluate the performance of these materials as detergent builders. In particular, testing in washing machines under a variety of wash conditions is needed. In addition, there are other considerations such as the storage stability and processing of detergent powders containing aluminosilicate gels. However, the results from the launderometer testing tend to suggest that amorphous aluminosilicate gels (in particular samples A2 and X1) may offer at least equivalent and, possibly, slightly improved performance over current detergent builder options and are certainly worthy of further investigation. In addition, it should be noted that one important consideration in assessing the usefulness of any proposed detergent ingredient is cost. The achievement of equivalent performance at lower cost is considered to be a major benefit. Aluminosilicate gels should be significantly cheaper than crystalline zeolites. With their short reaction times they lend themselves to continuous processing (rather than the batch processing commonly used for manufacturing zeolites) and require a much lower energy input.

It is interesting that there is little correlation between the results from the launderometer testing and the ion exchange properties of the aluminosilicate gels. The results from chapter four suggest that samples A0 and X0 should provide the best detergent builder performance. In fact, samples A2 and X1 showed the best performance. Clearly, detergent builder performance is not only related to ion exchange characteristics, but also to other factors such

as the wettability of the sample and interactions with other detergent ingredients. It should be pointed out that the wash monitors used in the launderometer tests do not measure builder performance directly, but, in fact, monitor overall detergent performance. Therefore, it is the full formulation that is being tested and any interactions between the builder and other detergent ingredients will be important.

References

1. H. Khatami and E. M. Flanigen, Unpublished Work
2. Y. Tsurata, T. Satoh, T. Yoshida, O.Okumura and S. Ueda, Proc 7th Int.. Conf. Zeolites, Elsevier, Tokyo, (1986), 1001

Appendix One

Ion Exchange Results

The tables in this appendix give the results obtained from the ion exchange work described in Chapter 4.

Tables 1a to 4b give the results of the sodium-calcium and sodium-magnesium exchange studies for the zeolite A type samples (samples A0, A1, A2 and A14). The corresponding results for the zeolite X type samples (samples X0, X1, X2, X3 and X24) are given in Tables 5a to 9b.

The sodium-calcium and sodium-magnesium ion exchange results for the remaining samples are given in Tables 10 to 15 (samples A3 to A12) and in Tables 16 to 20 (samples X4 to X12).

Tables 21 and 22 give the results from the study of the kinetics of sodium-magnesium exchange.

Table 1a. Sodium-Calcium Exchange in Sample A0

$Ca_{(z)}$	$Ca_{(s)}$	K_c	$Log_{10}K_c$
0.090	0.00017	102.092	2.00899
0.138	0.00041	73.615	1.86697
0.209	0.00083	65.603	1.81692
0.312	0.00130	82.579	1.91687
0.440	0.00317	71.890	1.85667
0.522	0.00538	68.617	1.83643
0.643	0.01313	61.038	1.78560
0.793	0.03100	91.027	1.95917
0.754	0.03480	54.112	1.73330
0.854	0.09800	53.158	1.72557
0.873	0.16600	35.693	1.55258
0.894	0.23800	30.082	1.47830
0.906	0.31000	24.050	1.38112
0.931	0.46800	17.543	1.24410
0.947	0.58500	14.445	1.15971
0.959	0.66800	13.532	1.13135
0.973	0.79200	10.306	1.01308
0.984	0.87900	8.953	0.95198

Table 1b. Sodium-Magnesium Exchange in Sample A0

$Mg_{(z)}$	$Mg_{(s)}$	K_c	$Log_{10}K_c$
0.05342	0.00051	18.9393	1.27736
0.10400	0.00198	10.6365	1.02680
0.23600	0.01140	5.6559	0.75250
0.29000	0.01887	4.7797	0.67940
0.40400	0.03054	5.6852	0.75475
0.49100	0.04735	5.8746	0.76898
0.39400	0.04960	3.1585	0.49948
0.55300	0.05100	7.8981	0.89752
0.64700	0.10200	6.5545	0.81654
0.62800	0.13600	3.9466	0.59622
0.64500	0.14600	4.0415	0.60655
0.67300	0.21200	2.8725	0.45826
0.68300	0.22100	2.9025	0.46278
0.69100	0.34700	1.3485	0.12985
0.70900	0.42600	0.9677	-0.01426
0.69500	0.50000	0.5511	-0.25873
0.71000	0.55600	0.4376	-0.35890
0.80300	0.75500	0.2336	-0.63145
0.86400	0.85900	0.1516	-0.81944
0.92200	0.92600	0.1246	-0.90432

Table 2a. Sodium-Calcium Exchange in Sample A1

$Ca_{(z)}$	$Ca_{(s)}$	K_c	$Log_{10}K_c$
0.105	0.00028	76.0292	1.88098
0.133	0.00034	84.1344	1.92497
0.339	0.00254	49.7436	1.69674
0.399	0.00313	57.3685	1.75867
0.364	0.00328	44.5304	1.64866
0.427	0.00473	44.5144	1.64850
0.479	0.00606	47.0282	1.67236
0.668	0.01809	52.6101	1.72107
0.728	0.02200	69.6230	1.84275
0.855	0.08100	68.0350	1.83273
0.873	0.14200	44.3980	1.64736
0.896	0.19800	42.0580	1.62385
0.922	0.26300	48.2529	1.68352
0.946	0.35700	56.8628	1.75483
0.933	0.44300	21.6868	1.33620
0.929	0.49100	14.3689	1.15742
0.948	0.58200	15.3252	1.18541
0.948	0.68000	7.5761	0.87945
0.964	0.83300	3.5020	0.54432

Table 2b. Sodium-Magnesium Exchange in Sample A1

$Mg_{(z)}$	$Mg_{(s)}$	K_c	$Log_{10}K_c$
0.05441	0.00026	38.3630	1.58391
0.13300	0.00128	22.5183	1.35254
0.30700	0.01727	5.8245	0.76526
0.38700	0.03293	4.7478	0.67649
0.38700	0.04845	3.1123	0.49308
0.53400	0.05400	6.5811	0.81830
0.57200	0.05800	7.7073	0.88690
0.59300	0.12451	3.5005	0.54414
0.62600	0.12500	4.3539	0.63888
0.62900	0.21100	2.1013	0.32249
0.63100	0.26900	1.4175	0.15153
0.67900	0.37100	1.0608	0.02561
0.67300	0.41600	0.7725	-0.11211
0.66400	0.48300	0.4816	-0.31732
0.68500	0.54700	0.3792	-0.42115
0.71200	0.64200	0.2473	-0.60684
0.75000	0.69300	0.2338	-0.63122
0.82100	0.79900	0.1830	-0.73761
0.86500	0.86800	0.1334	-0.87481
0.93700	0.93200	0.1628	-0.78835

Table 3a. Sodium-Calcium Exchange in Sample A2

$Ca_{(z)}$	$Ca_{(s)}$	K_C	$Log_{10}K_C$
0.078	0.00013	111.943	2.04900
0.171	0.00051	79.608	1.90096
0.296	0.00148	65.895	1.81885
0.471	0.00479	56.819	1.75449
0.530	0.00839	45.931	1.66211
0.606	0.01059	58.867	1.76987
0.736	0.03393	47.140	1.67339
0.822	0.07300	49.096	1.69104
0.824	0.09400	37.159	1.57007
0.813	0.17700	13.968	1.14514
0.863	0.26900	14.064	1.14812
0.898	0.43200	9.623	0.98329
0.915	0.49400	9.694	0.98651
0.928	0.51700	11.884	1.07498
0.922	0.61200	5.403	0.73263
0.937	0.69100	4.674	0.66968
0.958	0.82300	2.911	0.46401

Table 3b. Sodium-Magnesium Exchange in Sample A2

$Mg_{(z)}$	$Mg_{(s)}$	K_c	$Log_{10}K_c$
0.05673	0.00029	36.2900	1.5598
0.12200	0.00109	23.7652	1.3759
0.22400	0.00409	14.7311	1.1682
0.19500	0.00761	6.3561	0.8032
0.32500	0.02219	5.0016	0.6991
0.44800	0.05441	3.9016	0.5912
0.41200	0.07887	2.0580	0.3134
0.50900	0.08100	3.5323	0.5481
0.54900	0.12100	2.7400	0.4377
0.56000	0.18800	1.5889	0.2011
0.56700	0.25600	1.0096	0.0041
0.58300	0.29800	0.8488	-0.0712
0.58500	0.36800	0.5568	-0.2543
0.56900	0.45000	0.3064	-0.5137
0.58800	0.53700	0.2028	-0.6930
0.60400	0.57900	0.1718	-0.7651
0.64000	0.67100	0.1145	-0.9413
0.69600	0.75600	0.0842	-1.0746
0.80800	0.84900	0.0826	-1.0829
0.85200	0.90200	0.0578	-1.2384

Table 4a. Sodium-Calcium Exchange in Sample A14

$Ca_{(z)}$	$Ca_{(s)}$	K_c	$Log_{10}K_c$
0.059	0.00010	104.954	2.02100
0.113	0.00021	109.898	2.04099
0.151	0.00049	69.977	1.84496
0.263	0.00157	50.216	1.70084
0.326	0.00207	56.336	1.75079
0.432	0.00598	36.172	1.55837
0.793	0.02700	105.479	2.02317
0.658	0.02907	29.642	1.47190
0.799	0.07200	38.036	1.58020
0.844	0.15800	24.535	1.38978
0.856	0.24900	14.457	1.16008
0.875	0.34700	10.435	1.01848
0.887	0.42000	8.323	0.92030
0.899	0.53200	5.325	0.72632
0.911	0.63600	3.460	0.53910
0.933	0.77000	2.024	0.30623

Table 4b. Sodium-Magnesium Exchange in Sample A14

$Mg_{(z)}$	$Mg_{(s)}$	K_c	$Log_{10}K_c$
0.04339	0.00026	30.0896	1.4784
0.08539	0.00031	53.6013	1.7292
0.17600	0.00128	32.9383	1.5177
0.17100	0.00526	7.6462	0.8834
0.25300	0.01363	5.2789	0.7225
0.25400	0.02343	3.0223	0.4803
0.39900	0.04313	3.7968	0.5794
0.29800	0.07887	1.0443	0.0188
0.50200	0.09500	2.7910	0.4458
0.52600	0.12900	2.1848	0.3394
0.55800	0.18500	1.6072	0.2061
0.56200	0.23200	1.1556	0.0628
0.56300	0.34100	0.5700	-0.2441
0.56700	0.39200	0.4288	-0.3677
0.56500	0.45400	0.2916	-0.5353
0.59200	0.51100	0.2451	-0.6107
0.62800	0.60000	0.1757	-0.7552
0.68400	0.71200	0.1140	-0.9431
0.72300	0.80600	0.0621	-1.2070
0.79600	0.81900	0.1078	-0.9675
0.88700	0.92400	0.0604	-1.2189

Table 5a. Sodium-Calcium Exchange in Sample X0

$Ca_{(z)}$	$Ca_{(s)}$	K_c	$Log_{10}K_c$
0.079	0.00040	37.929	1.57897
0.149	0.00106	31.834	1.50290
0.198	0.00196	25.633	1.40880
0.291	0.00413	22.728	1.35657
0.404	0.00877	20.800	1.31807
0.500	0.02220	14.016	1.14663
0.612	0.03162	19.572	1.29163
0.829	0.03300	130.389	2.11524
0.687	0.04992	20.498	1.31171
0.852	0.13100	35.566	1.55103
0.855	0.26000	13.213	1.12099
0.871	0.30900	12.355	1.09183
0.893	0.41500	9.631	0.98367
0.882	0.44000	6.730	0.82801
0.913	0.59100	4.964	0.69586
0.930	0.61900	6.444	0.80917
0.946	0.78400	2.732	0.43643

Table 5b. Sodium-Magnesium Exchange in Sample X0

$Mg_{(z)}$	$Mg_{(s)}$	K_c	$Log_{10}K_c$
0.066	0.00145	8.48895	0.92885
0.114	0.00358	6.58605	0.81862
0.159	0.00877	4.11213	0.61407
0.223	0.02282	2.51516	0.40057
0.315	0.03148	3.24824	0.51165
0.382	0.03780	3.97174	0.59898
0.508	0.05400	5.61643	0.74946
0.522	0.15700	1.63075	0.21239
0.610	0.16800	2.59955	0.41490
0.621	0.25900	1.41419	0.15051
0.653	0.36700	0.89443	-0.04845
0.681	0.49400	0.51226	-0.29051
0.677	0.50300	0.46992	-0.32798
0.691	0.58200	0.31635	-0.49984
0.733	0.67400	0.23285	-0.63292
0.771	0.75700	0.16284	-0.78823
0.829	0.83000	0.13887	-0.85740

Table 6a. Sodium-Calcium Exchange in Sample X1

$Ca_{(z)}$	$Ca_{(s)}$	K_c	$Log_{10}K_c$
0.072	0.00032	43.1496	1.63498
0.121	0.00084	30.5436	1.48492
0.219	0.00273	21.4149	1.33072
0.301	0.00481	20.7249	1.31649
0.478	0.01966	13.9605	1.14490
0.532	0.02232	16.9285	1.22862
0.653	0.04751	16.7480	1.22396
0.803	0.07800	36.2087	1.55881
0.862	0.16300	30.6373	1.48625
0.819	0.19700	12.7911	1.10691
0.850	0.31800	8.4257	0.92561
0.881	0.41700	7.5901	0.88025
0.889	0.50800	5.0659	0.70466
0.886	0.60400	2.5685	0.40968
0.905	0.71200	1.6688	0.22242
0.927	0.81100	1.0804	0.03358

Table 6b. Sodium-Magnesium Exchange in Sample X1

$Mg_{(z)}$	$Mg_{(s)}$	K_c	$Log_{10}K_c$
0.053	0.00088	10.9374	1.03892
0.076	0.00169	8.6065	0.93483
0.186	0.00687	6.5807	0.81827
0.243	0.01406	4.7808	0.67950
0.347	0.02218	5.7100	0.75663
0.323	0.04221	2.4804	0.39452
0.552	0.06900	5.5593	0.74502
0.579	0.14800	2.5317	0.40342
0.593	0.23200	1.4122	0.14989
0.584	0.30600	0.8118	-0.09052
0.599	0.40100	0.5003	-0.30073
0.632	0.50800	0.3277	-0.48458
0.657	0.60600	0.2075	-0.68293
0.699	0.69400	0.1491	-0.82658
0.771	0.80100	0.1026	-0.98875

Table 7a. Sodium-Calcium Exchange in Sample X2

$Ca_{(z)}$	$Ca_{(s)}$	K_C	$Log_{10}K_C$
0.062	0.00030	38.1047	1.58098
0.136	0.00077	38.8086	1.58893
0.178	0.00192	22.3256	1.34880
0.319	0.00562	19.7882	1.29641
0.488	0.01931	15.0987	1.17894
0.593	0.03893	13.7677	1.13886
0.604	0.05073	11.0567	1.04363
0.731	0.07300	19.1172	1.28142
0.759	0.12700	12.4501	1.09517
0.799	0.26400	6.2549	0.79622
0.835	0.34700	5.7149	0.75701
0.850	0.44100	3.9896	0.60093
0.868	0.55200	2.6498	0.42321
0.885	0.66300	1.6489	0.21720
0.897	0.77100	0.8151	-0.08879
0.921	0.86900	0.4080	-0.38931

Table 7b. Sodium-Magnesium Exchange in Sample X2

$Mg_{(z)}$	$Mg_{(s)}$	K_c	$Log_{10}K_c$
0.058	0.00138	7.74216	0.8889
0.089	0.00276	6.31994	0.8007
0.113	0.00529	4.38976	0.6424
0.146	0.00900	3.56485	0.5520
0.235	0.01652	3.83033	0.5832
0.337	0.03370	3.44677	0.5374
0.421	0.05503	3.28987	0.5172
0.424	0.06100	2.97806	0.4739
0.445	0.10100	1.84630	0.2663
0.507	0.17800	1.24292	0.0944
0.523	0.24400	0.83334	-0.0792
0.534	0.38900	0.35504	-0.4497
0.539	0.45800	0.24174	-0.6167
0.546	0.55400	0.13910	-0.8567
0.564	0.61300	0.10505	-0.9786
0.613	0.70200	0.07407	-1.1304
0.692	0.81600	0.04265	-1.3701

Table 8a. Sodium-Calcium Exchange in Sample X3

$Ca_{(z)}$	$Ca_{(s)}$	K_c	$Log_{10}K_c$
0.078	0.00060	25.0580	1.39895
0.107	0.00125	17.4935	1.24288
0.419	0.00253	79.9352	1.90274
0.274	0.00630	13.3147	1.12433
0.469	0.02289	11.2865	1.05256
0.673	0.03400	28.0303	1.44763
0.581	0.04949	9.7669	0.98976
0.734	0.09800	13.7643	1.13875
0.785	0.21000	7.8675	0.89584
0.802	0.31100	4.7681	0.67835
0.814	0.39500	3.2765	0.51541
0.803	0.40600	2.6969	0.43086
0.800	0.45900	1.8948	0.27756
0.813	0.58100	1.0231	0.00990
0.834	0.69200	0.5944	-0.22594
0.874	0.81700	0.3180	-0.49763

Table 8b. Sodium-Magnesium Exchange in Sample X3

$Mg_{(z)}$	$Mg_{(s)}$	K_c	$Log_{10}K_c$
0.052	0.00197	4.77307	0.6788
0.107	0.00745	2.89874	0.4622
0.183	0.02064	2.07394	0.3168
0.308	0.04893	1.92227	0.2838
0.428	0.05800	3.22885	0.5090
0.447	0.09700	1.96424	0.2932
0.450	0.17900	0.87909	-0.0560
0.449	0.23600	0.56708	-0.2464
0.444	0.34100	0.27768	-0.5565
0.457	0.42400	0.18131	-0.7416
0.463	0.49900	0.11918	-0.9238
0.471	0.57300	0.07809	-1.1074
0.479	0.60800	0.06468	-1.1892
0.535	0.70200	0.04478	-1.3489
0.579	0.79300	0.02495	-1.6030

Table 9a. Sodium-Calcium Exchange in Sample X24

$Ca_{(z)}$	$Ca_{(s)}$	K_c	$Log_{10}K_c$
0.069	0.00037	34.9117	1.54297
0.113	0.00068	34.2718	1.53494
0.157	0.00144	24.9376	1.39685
0.199	0.00382	25.8585	1.41260
0.456	0.01176	20.8807	1.31975
0.448	0.01412	16.5003	1.21749
0.644	0.04063	18.6502	1.27068
0.813	0.12200	23.3492	1.36827
0.794	0.17000	11.9224	1.07636
0.812	0.25100	7.9360	0.89960
0.812	0.34300	4.3874	0.64220
0.826	0.40700	3.5346	0.54834
0.843	0.50400	2.4614	0.39118
0.853	0.63800	1.1706	0.06840
0.885	0.76900	0.6583	-0.18157
0.920	0.85200	0.5185	-0.28526

Table 9b. Sodium-Magnesium Exchange in Sample X24

$Mg_{(z)}$	$Mg_{(s)}$	K_C	$Log_{10}K_C$
0.063	0.00165	7.09305	0.8508
0.101	0.00336	6.03460	0.7806
0.110	0.00603	3.71844	0.5704
0.184	0.01263	3.48059	0.5417
0.297	0.02371	3.93071	0.5945
0.469	0.04100	6.04413	0.7813
0.441	0.04608	4.50933	0.6541
0.532	0.08900	3.62752	0.5596
0.533	0.16200	1.66879	0.2224
0.556	0.23700	1.07385	0.0309
0.572	0.33900	0.61118	-0.2138
0.588	0.44800	0.35072	-0.4550
0.601	0.51300	0.25695	-0.5902
0.615	0.61800	0.14187	-0.8481
0.673	0.71200	0.10474	-0.9799
0.734	0.79100	0.08098	-1.0916

Table 10. Ion Exchange Results for Sample A3

$Ca_{(z)}$	$Ca_{(s)}$	$Mg_{(z)}$	$Mg_{(s)}$
0.738	0.036	0.472	0.038
0.808	0.112	0.504	0.099
0.844	0.191	0.505	0.153
0.861	0.287	0.553	0.215
0.880	0.323	0.539	0.331
0.882	0.389	0.576	0.401
0.867	0.420	0.562	0.520
0.895	0.465	0.593	0.536
0.904	0.521	0.575	0.597
0.906	0.620	0.625	0.621
0.904	0.663	0.624	0.696
0.935	0.751	0.706	0.774

Table 11. Ion Exchange Results for Sample A4

$Ca_{(z)}$	$Ca_{(s)}$	$Mg_{(z)}$	$Mg_{(s)}$
0.756	0.054	0.438	0.063
0.791	0.093	0.524	0.092
0.829	0.151	0.502	0.171
0.861	0.239	0.550	0.249
0.874	0.333	0.534	0.309
0.848	0.357	0.569	0.321
0.883	0.406	0.571	0.378
0.872	0.511	0.543	0.437
0.894	0.548	0.585	0.552
0.903	0.639	0.588	0.613
0.924	0.722	0.633	0.658
		0.649	0.749

Table 12. Ion Exchange Results for Sample A6

$Ca_{(z)}$	$Ca_{(s)}$	$Mg_{(z)}$	$Mg_{(s)}$
0.801	0.050	0.482	0.051
0.865	0.147	0.486	0.097
0.873	0.194	0.490	0.129
0.912	0.286	0.514	0.224
0.880	0.308	0.556	0.331
0.893	0.363	0.582	0.403
0.924	0.471	0.585	0.491
0.904	0.515	0.602	0.538
0.932	0.573	0.611	0.608
0.916	0.664	0.638	0.700
0.926	0.752	0.721	0.773
		0.778	0.840

Table 13. Ion Exchange Results for Sample A8

$Ca_{(z)}$	$Ca_{(s)}$	$Mg_{(z)}$	$Mg_{(s)}$
0.743	0.048	0.463	0.039
0.799	0.092	0.455	0.088
0.836	0.134	0.520	0.126
0.900	0.181	0.506	0.191
0.899	0.283	0.529	0.202
0.898	0.342	0.544	0.257
0.899	0.421	0.550	0.332
0.912	0.506	0.568	0.438
0.913	0.578	0.612	0.543
0.932	0.613	0.614	0.579
0.933	0.700	0.610	0.618
0.941	0.759	0.638	0.703
		0.704	0.781

Table 14. Ion Exchange Results for Sample A10

$Ca_{(z)}$	$Ca_{(s)}$	$Mg_{(z)}$	$Mg_{(s)}$
0.869	0.029	0.498	0.072
0.846	0.080	0.552	0.096
0.882	0.132	0.590	0.168
0.933	0.168	0.574	0.274
0.920	0.211	0.609	0.412
0.912	0.358	0.628	0.475
0.921	0.409	0.610	0.523
0.920	0.473	0.596	0.604
0.961	0.551	0.621	0.665
0.942	0.605	0.681	0.743
0.953	0.666	0.760	0.886
0.934	0.736		

Table 15. Ion Exchange Results for Sample A12

$Ca_{(z)}$	$Ca_{(s)}$	$Mg_{(z)}$	$Mg_{(s)}$
0.784	0.034	0.478	0.021
0.802	0.056	0.509	0.106
0.839	0.110	0.497	0.147
0.851	0.169	0.558	0.208
0.862	0.272	0.534	0.227
0.889	0.324	0.539	0.329
0.908	0.436	0.551	0.398
0.923	0.502	0.570	0.457
0.939	0.554	0.579	0.548
0.948	0.629	0.638	0.613
0.948	0.732	0.702	0.715
0.950	0.789	0.761	0.792

Table 16. Ion Exchange Results for Sample X4

$Ca_{(z)}$	$Ca_{(s)}$	$Mg_{(z)}$	$Mg_{(s)}$
0.658	0.053	0.296	0.106
0.667	0.092	0.302	0.180
0.736	0.112	0.308	0.224
0.795	0.149	0.354	0.289
0.824	0.233	0.313	0.350
0.818	0.334	0.341	0.422
0.783	0.401	0.353	0.518
0.807	0.415	0.392	0.609
0.811	0.557	0.397	0.656
0.871	0.649	0.462	0.758
0.877	0.726	0.560	0.813

Table 17. Ion Exchange Results for Sample X6

$Ca_{(z)}$	$Ca_{(s)}$	$Mg_{(z)}$	$Mg_{(s)}$
0.657	0.050	0.304	0.100
0.689	0.082	0.332	0.179
0.673	0.129	0.344	0.234
0.799	0.246	0.363	0.265
0.776	0.298	0.384	0.341
0.794	0.369	0.397	0.436
0.822	0.410	0.401	0.512
0.813	0.474	0.415	0.587
0.830	0.551	0.424	0.674
0.864	0.598	0.461	0.746
0.873	0.694	0.536	0.795
0.921	0.776		

Table 18. Ion Exchange Results for Sample X8

$Ca_{(z)}$	$Ca_{(s)}$	$Mg_{(z)}$	$Mg_{(s)}$
0.680	0.009	0.485	0.061
0.724	0.012	0.546	0.136
0.783	0.181	0.542	0.203
0.826	0.197	0.573	0.257
0.812	0.286	0.558	0.298
0.814	0.351	0.590	0.392
0.835	0.419	0.579	0.479
0.856	0.504	0.627	0.580
0.845	0.527	0.638	0.604
0.871	0.622	0.691	0.697
0.879	0.743	0.700	0.758

Table 19. Ion Exchange Results for Sample X10

$Ca_{(z)}$	$Ca_{(s)}$	$Mg_{(z)}$	$Mg_{(s)}$
0.702	0.023		
0.781	0.113		
0.812	0.161		
0.799	0.208		
0.809	0.307		
0.839	0.416		
0.860	0.482		
0.834	0.540		
0.771	0.558		
0.880	0.673		
0.876	0.759		

Table 20. Ion Exchange Results for Sample X12

$Ca_{(z)}$	$Ca_{(s)}$	$Mg_{(z)}$	$Mg_{(s)}$
		0.508	0.030
		0.584	0.121
		0.539	0.129
		0.606	0.206
		0.635	0.274
		0.631	0.396
		0.633	0.490
		0.582	0.517
		0.601	0.606
		0.689	0.652
		0.702	0.758
		0.753	0.813

Table 21. Kinetics of Sodium-Magnesium exchange in the Zeolite A Type Samples

	Sample A0		Sample A1		Sample A14	
Time (Min)	pNa	Q_t/Q	pNa	Q_t/Q	pNa	Q_t/Q
0	4.00	0.0000	4.00	0.0000	4.00	0.0000
1	3.06	0.1780	3.30	0.0895	2.93	0.1953
2	2.97	0.2243	3.18	0.1250	2.87	0.2269
3	2.93	0.2482	3.12	0.1469	2.83	0.2506
4	2.89	0.2743	3.07	0.1675	2.82	0.2568
5	2.86	0.2956	3.03	0.1858	2.80	0.2698
6	2.84	0.3106	3.01	0.1957	2.78	0.2834
7	2.78	0.3601	2.99	0.2059	2.77	0.2904
8	2.76	0.3781	2.97	0.2167	2.75	0.3050
9	2.75	0.3875	2.95	0.2280	2.77	0.2904
10	2.73	0.4068	2.93	0.2398	2.76	0.2976
15	2.67	0.4705	2.82	0.3153	2.72	0.3281
20	2.63	0.5182	2.74	0.3836	2.71	0.3361
25	2.61	0.5437	2.70	0.4228	2.70	0.3444
30	2.58	0.5842	2.67	0.4546	2.68	0.3615
35	2.56	0.6128	2.65	0.4771	2.67	0.3703
40	2.55	0.6277	2.63	0.5006	2.65	0.3886
50			2.59	0.5511	2.65	0.3886
60			2.58	0.5645	2.62	0.4177
70					2.61	0.4279
75			2.55	0.6064		
80	2.54	0.6428				
90	2.51	0.6905			2.60	0.4383

Table 22. Kinetics of Sodium-Magnesium exchange in the Zeolite X Type Samples

	Sample X0		Sample X1		Sample X24	
Time (Min)	pNa	Q_t/Q_∞	pNa	Q_t/Q_∞	pNa	Q_t/Q_∞
0	4.00	0.0000	4.00	0.0000	4.00	0.0000
1	3.31	0.0962	3.34	0.0767	3.06	0.1523
2	3.22	0.1241	3.26	0.0966	3.02	0.1689
3	3.19	0.1347	3.21	0.1110	2.99	0.1824
4	3.17	0.1422	3.18	0.1205	2.98	0.1871
5	3.14	0.1542	3.16	0.1272	2.98	0.1871
6	3.14	0.1542	3.15	0.1306	2.97	0.1919
7	3.12	0.1626	3.12	0.1415	2.95	0.2019
8	3.10	0.1714	3.12	0.1415	2.95	0.2019
9	3.09	0.1760	3.10	0.1492	2.94	0.2070
10	3.08	0.1807	3.10	0.1492	2.94	0.2070
15	3.03	0.2057	3.05	0.1700	2.93	0.2123
20	3.03	0.2057	3.02	0.1837	2.92	0.2177
25	3.00	0.2222	3.00	0.1934	2.92	0.2177
30	2.98	0.2339	2.98	0.2035	2.91	0.2233
35	2.96	0.2461	2.96	0.2141	2.91	0.2233
40	2.96	0.2461	2.93	0.2310	2.90	0.2289
50	2.94	0.2588	2.91	0.2429	2.89	0.2347
60	2.94	0.2588	2.90	0.2491	2.89	0.2347
70	2.92	0.2722	2.88	0.2618	2.88	0.2406
80	2.91	0.2791			2.87	0.2467
90	2.90	0.2862	2.86	0.2752	2.87	0.2467

Appendix Two

Launderometer Testing Results

The tables in this appendix give the numerical data obtained from the launderometer testing described in chapter five.

Tables 1 to 4 show the results for tea, coffee, NTC clay and ETC clay stains respectively. In each of these tables, the stain removal results for each wash monitor and the mean stain removal for each of the samples tested are listed.

Average stain removal data, over all instrumentally assessed stains (i.e. tea, coffee, NTC clay and ETC clay stains), are shown in table 5 for each of the samples tested.

The results from the whiteness monitors included in each launderometer pot are given in table 6.

Table 1. Tea Stain Removal

Launderometer Test 1			Launderometer test 2		
Sample	Stain Removal (%)	Mean Stain Removal (%)	Sample	Stain Removal (%)	Mean Stain Removal (%)
STPP	48.9 52.2 51.1 48.9	50.28	STPP	52.9 53.2 39.4 37.4	45.73
A	50.8 53.0 58.1 55.3	54.30	A	54.7 55.8 54.8 53.1	54.60
X	51.1 47.4 40.3 39.1	44.48	X1	62.1 60.3 56.3 55.4	58.53
X0	54.5 56.1 49.6 44.6	51.20	X0	54.1 53.6 53.0 51.1	52.95
X1	56.9 58.2 48.8 48.9	53.20	A0	49.2 50.8 51.5 53.4	51.23
X2	50.0 48.1 57.8 55.8	52.93	A1	56.1 44.2 52.5 52.2	51.25
X3	49.6 54.1 48.5 45.9	49.53	A2	57.5 54.8 52.9 52.5	54.43
X4	49.6 52.5 51.5 50.0	50.90	A4	47.8 54.1 53.4 50.4	51.43
X6	46.2 46.5 47.8 45.8	46.58	A8	61.3 59.1 56.5 51.4	57.08

Table 2. Coffee Stain Removal

Launderometer Test 1			Launderometer test 2		
Sample	Stain Removal (%)	Mean Stain Removal (%)	Sample	Stain Removal (%)	Mean Stain Removal (%)
STPP	56.3 58.9 59.7 57.4	58.08	STPP	58.3 61.1 57.3 58.3	58.75
A	61.9 62.6 61.4 62.8	62.18	A	58.6 58.4 59.7 58.2	58.73
X	60.6 63.2 56.5 59.0	59.83	X1	67.1 63.7 62.1 68.1	65.25
X0	63.8 64.7 60.6 62.1	62.80	X0	60.9 62.7 58.3 63.8	61.43
X1	62.4 63.2 60.1 62.0	61.93	A0	54.4 56.8 59.8 60.9	57.98
X2	66.2 62.4 63.1 65.4	64.28	A1	61.9 58.6 59.7 60.0	60.05
X3	65.2 61.5 61.5 62.6	62.70	A2	60.9 62.3 65.4 67.6	64.05
X4	66.4 63.6 62.2 65.4	64.40	A4	58.3 58.2 52.7	56.40
X6	65.0 65.9 59.5 66.4	64.20	A8	58.3 58.7 60.4 57.1	58.63

Table 3. NTC Clay Stain Removal

Launderometer Test 1			Launderometer test 2		
Sample	Stain Removal (%)	Mean Stain Removal (%)	Sample	Stain Removal (%)	Mean Stain Removal (%)
STPP	12.3 20.0	16.15	STPP	16.3 11.2	13.75
A	17.4 15.6	16.50	A	19.1 10.7	14.90
X	9.2 13.5	11.35	X1	18.5 16.3	17.4
X0	11.2 11.1	11.15	X0	14.7 7.5	11.10
X1	18.2 17.5	17.85	A0	14.7 13.3	14.00
X2	8.8 15.8	12.30	A1	12.5 12.1	12.30
X3	13.3 14.2	13.75	A2	17.2 15.4	16.30
X4	13.4 17.2	15.30	A4	11.7 3.7	7.70
X6	13.0 15.6	14.30	A8	14.7 9.5	12.10

Table 4. ETC Clay Stain Removal

Launderometer Test 1			Launderometer test 2		
Sample	Stain Removal (%)	Mean Stain Removal (%)	Sample	Stain Removal (%)	Mean Stain Removal (%)
STPP	12.0 13.6	12.80	STPP	16.5 9.5	12.95
A	14.0 11.8	12.90	A	21.2 13.4	17.30
X	11.4 13.7	12.55	X1	19.1 17.4	18.25
X0	15.1 17.4	16.25	X0	16.4 10.5	13.45
X1	17.1 17.3	17.20	A0	11.8 10.2	11.00
X2	14.4 19.7	16.75	A1	17.1 13.6	15.35
X3	11.4 14.5	12.95	A2	18.3 26.3	22.30
X4	12.2 19.7	15.95	A4		
X6	12.7 13.4	13.05	A8	15.8 16.3	16.05

Table 5. Average Stain Removal

Launderometer Test 1		Launderometer test 2	
Sample	Mean Stain Removal (%)	Sample	Mean Stain Removal (%)
STPP	40.94	STPP	39.28
A	43.73	A	43.14
X	38.75	X1	47.20
X0	42.57	X0	42.22
X1	44.22	A0	40.57
X2	43.91	A1	41.71
X3	41.86	A2	45.93
X4	43.64	A4	43.37
X6	41.48	A8	43.26

Table 6. Post Wash Whitenesses

Launderometer Test 1			Launderometer test 2		
Sample	Whiteness (%)	Mean Whiteness (%)	Sample	Whiteness (%)	Mean Whiteness (%)
STPP	86.7 89.7	88.20	STPP	89.9 83.7	86.80
A	91.6 88.3	89.95	A	89.7 89.7	89.70
X	88.0 91.6	89.80	X1	93.2 92.1	92.65
X0	87.2 93.2	90.20	X0	90.2 91.3	90.75
X1	88.6 90.8	89.70	A0	87.5 91.3	89.40
X2	86.4 93.2	89.80	A1	86.4 88.3	87.35
X3	82.9 90.2	86.55	A2	92.7 93.5	93.10
X4	89.9 92.9	91.40	A4	87.0 88.6	87.80
X6	88.6 92.4	90.50	A8	89.7 89.9	89.8